

# LATTICE DYNAMICS FROM FIRST PRINCIPLES

---

## Dissertation

zur Erlangung des Doktorgrades der Naturwissenschaften  
(*Dr. rer. nat.*)

der

Naturwissenschaftlichen Fakultät II  
Chemie, Physik und Mathematik

der

MARTIN-LUTHER-UNIVERSITÄT  
HALLE-WITTENBERG

vorgelegt von

HERRN MARTIN HÖLZER

geboren am 07.09.1984 in Halle (Saale)

**Gutachter:**

1. PD Dr. Arthur Ernst, Max-Planck-Institut für Mikrostrukturphysik Halle
2. Prof. Dr. Wolfram Hergert, Martin-Luther-Universität Halle-Wittenberg
3. Prof. Dr. Vitalii Dugaev, Politechnika Rzeszowska, Polen

**Ort und Tag der Verteidigung:** Halle (Saale), 13. November 2015

# Abstract

This work studies a possible approach to the prediction of lattice vibrations in crystals by means of multiple scattering theory. The method of choice for the description of the electronic structure is the technique of Korring-Kohn-Rostoker (KKR) in its expression as Green function method. To begin with, the work elaborates on numerical models of lattice vibrations and continues with the basic principles of linear response theory as well as the outline of the KKR. In the following sections, equations for the calculation of phonon spectra are worked out, based on these methods and using a spherical approximation of the ionic Coulomb potential. It is shown that this approximation—commonly used in multiple scattering theory—is not sufficient for a quantitative description of lattice vibrations. As opposed to this, a treatment of the full potential is necessary. The second part of this work deals with the KKR description of electron-phonon interactions in superconducting thin films and their influence on the critical temperature.

Die Vorliegende Arbeit untersucht einen möglichen Ansatz, das Problem der Gitterschwingungen in Kristallen *ab initio* im Rahmen der Vielfachstreutheorie zu behandeln. Als methodischer Ansatz zur Beschreibung der Elektronenstruktur wurde hierfür die Korringa-Kohn-Rostoker-Methode (KKR) mit Greenschen Funktionen gewählt. Die Arbeit stellt zunächst grundlegende Verfahren zur Berechnung von Phononenspektren vor und geht danach auf die Details der KKR und der linearen Antworttheorie ein. Danach werden auf Basis dieser Methoden Gleichungen hergeleitet, mit welchen die Dispersionsrelationen der Gitterschwingungen berechnet werden können. Hierbei wurde insbesondere die effiziente Variante der KKR untersucht, in welcher die Potentiale der Ionenrümpfe als kugelsymmetrisch angenähert werden. Es wird gezeigt, dass dieses Modell nicht ausreicht, um die Spektren quantitativ vorherzusagen. Hingegen müssen in einem solchen Modell die asphärischen Komponenten der Potentiale berücksichtigt werden, was im Rahmen der Full-Potential-Methode geschehen kann. Im zweiten Teil der Arbeit wird der Einfluss der Elektron-Phonon-Wechselwirkung auf die Sprungtemperatur von Dünnschicht-Supraleitern untersucht.



# Contents

<b>1</b>	<b>Introduction</b>	<b>7</b>
<b>2</b>	<b>Lattice dynamics from first principles</b>	<b>9</b>
2.1	The problem of moving atoms . . . . .	9
2.2	Adiabatic approximation . . . . .	10
2.3	Lattice dynamics in the harmonic approximation . . . . .	12
2.4	Force constants from first principles . . . . .	14
2.4.1	Hellmann-Feynman theorem . . . . .	15
2.4.2	Direct methods . . . . .	16
2.4.3	Perturbation theory and linear response . . . . .	18
2.5	Contribution of bare ions . . . . .	19
<b>3</b>	<b>Linear response theory from first principles</b>	<b>25</b>
3.1	Introduction to linear response . . . . .	25
3.2	Electron density correlation function . . . . .	27
3.3	Time dependent density functional theory . . . . .	28
3.3.1	Hohenberg-Kohn theorems . . . . .	29
3.3.2	Kohn-Sham equations . . . . .	30
3.3.3	Exchange-correlation energy . . . . .	32
3.3.4	Generalization to time dependent problems . . . . .	32
3.4	Linear response DFT . . . . .	33
<b>4</b>	<b>The Korringa-Kohn-Rostoker Green function method</b>	<b>37</b>
4.1	Green functions . . . . .	37
4.2	The Korringa-Kohn-Rostoker method . . . . .	40
4.2.1	Single potential scattering . . . . .	40
4.2.2	Multiple scattering theory . . . . .	42
4.2.3	Self-consistent KKR scheme . . . . .	46
<b>5</b>	<b>Application to lattice dynamics</b>	<b>49</b>
5.1	Rigid-core model for force constants . . . . .	49
5.2	Contribution of valence electrons . . . . .	51
5.2.1	Perturbation of the valence charge density . . . . .	54
5.2.2	A Green function formulation of the non-interacting susceptibility . . . . .	57
5.2.3	Reciprocal space and angular momentum representation . . . . .	59
5.3	Implementation . . . . .	62
5.3.1	Test calculations . . . . .	65
5.3.2	Conclusion and Outlook . . . . .	73
<b>6</b>	<b>Electron-Phonon Interaction in superconducting metals</b>	<b>75</b>
6.1	Eliashberg function in rigid muffin-tin approximation . . . . .	78
6.2	Application to Pb/Cu(111) islands . . . . .	83
6.2.1	Quantum well states . . . . .	84
6.2.2	Phonon dispersion/Bulk calculations . . . . .	85
6.2.3	Surface and film calculations . . . . .	87

6.2.4 Summary and Outlook . . . . .	89
<b>7 Conclusion</b>	<b>91</b>
<b>A Coulomb potential</b>	<b>93</b>
A.1 Ewald summation technique . . . . .	93
A.2 Fourier transform of the Coulomb potential . . . . .	94
A.3 Derivatives . . . . .	96
<b>B Numerical Quadrature</b>	<b>97</b>
B.1 One-dimensional integration . . . . .	97
B.2 Angular integration . . . . .	97
<b>Bibliography</b>	<b>99</b>
<b>Eidesstattliche Versicherung</b>	<b>113</b>
<b>Danksagung</b>	<b>115</b>
<b>Curriculum Vitae</b>	<b>117</b>

# Introduction

Many properties of solids can only be understood if the model of a lattice of fixed ions is augmented by the picture of nuclei oscillating around their equilibrium positions. Only this degree of freedom allows to explain thermal expansion and phase transitions, heat capacity, thermal and acoustic conduction as well as electrical conductivity as functions of temperature. High-technology applications of phenomena such as superconductivity and thermoelectricity strongly depend on the electronic structure of the respective material as well as the vibrational spectrum of the ion lattice. Besides a fundamental understanding of these phenomena, a dedicated design of new materials requires detailed quantitative knowledge of both aspects of the problem for complex systems. With the beginning 20<sup>th</sup> century, first models of thermal conductivity including atomic motion appeared, one of the most prominent being Einstein's model [Ein07; SS06]. It starts from the assumption that atoms vibrate like independent harmonic oscillators at their lattice sites (even before the atomic structure of solids was proven) and describes their behaviour within the new quantum theory of radiation developed by Planck [Pla00]. Although this model reproduces the heat capacity at high temperatures well, it fails at low temperatures. The more advanced model of Debye [Deb12] solves this problem by assuming a monotone dispersion relation for two transverse and one longitudinal branch of lattice vibrations, but with a cut-off frequency (Debye frequency). In the same year, Born and v. Karman [BK12; BK13] presented the first analytical model of lattice vibrations based on harmonic forces between atoms arranged in a periodic lattice. Afterwards, the problem of predicting the lattice dynamics of real solids was reduced to the determination of inter-atomic forces which, apart from phenomenological models with adjustable parameters, soon became an assignment of the arising quantum mechanics.

Despite the emergence of ever-improving experimental methods for measurements of vibrational spectra of solids, it took a long time on the theory side to develop models capable of reproducing correct dispersion relations without external fitting parameters, which was mainly due to the complexity behind the different levels of abstraction of the problem. As always, the truth lies in reasonable simplification. Until today, with few exceptions, it is a standard procedure to describe the coupled vibrations of ions in a crystal potential by means of classical Newtonian mechanics. This ansatz allows the calculation of dispersion relations on the basis of force constants which parametrize the inter-atomic forces. A quantum-mechanical treatment of the phonons as quasiparticles<sup>1</sup> is only necessary, if the occupation of the available vibrational states is of interest or when interactions with other excitations, such as electrons or magnons are studied. But besides this classical level of abstraction, however, the crystal potential or the derived force constants need a more sophisticated model. They are, apart from simple ionic crystals, only assessable quantum-mechanically because they are determined by the dynamic distribution of the electron gas between the ions of the lattice.

With the development of density functional theory in the 1960s and 1970s, a new tool for the quantum-mechanical description of materials was born which, because of its efficiency, initiated a new age of computational physics and implied improved concepts for the ab-initio theory of lattice dynamics. The Korringa-Kohn-Rostoker (KKR) method used throughout this work is an all-electron model describing the electronic band structure of

---

<sup>1</sup>Throughout this work, the term 'phonon' is often used as synonym for the collective vibrations of atoms arranged in periodic lattice, without referring to its primary meaning of a quasiparticle.

crystals and, among many other numerical approaches, is able to make use of density functional theory to achieve more accurate results with less computational work. Its conception as a multiple-scattering theory as well as its reformulation as a Green function method makes it very attractive for the use with disordered or low-dimensional systems. These intrinsic properties, however, make the application of KKR to lattice dynamics a hard task. Therefore, a major objective of this work was to investigate the possibility to circumvent these problems by making use of linear response theory and thus extend the possible applications of KKR.

The second part of this work concentrates on the interactions between electrons and phonons and describes a model of this interplay using the rigid muffin tin approximation. The latter is augmented for use with the existing KKR formalism and is optimized for application on surfaces and layered systems. Both parts of this work have their origins in the permanent advancement of the in-house KKR code HUTSEPOT and can be seen as progress report of the ongoing developments. Therefore, this thesis is structured as follows: Chapters 2, 3 and 4 elaborate on an overview of the theoretical foundations of lattice dynamics, linear response theory and density functional theory, as well as an introduction to the concepts of the KKR Green function method. In Chapter 5, a rigid-ion model of lattice dynamics is developed, using the Green function of the electronic ground state to calculate the linear response of the electron gas upon lattice distortions. Chapter 6 describes in detail the formalism for the Eliashberg spectral function of electron-phonon coupling for layered systems and presents its application to inelastic tunnelling experiments. Finally, a short summary completes the thesis.

# Lattice dynamics from first principles

This chapter briefly outlines the present ab-initio methods (parameter-free quantum-mechanical models) for determination of lattice vibrational spectra of crystalline solids. The reader shall be introduced to the topic and the main goal of the work will become clear. For this purpose, the quantum-mechanical description of solids will be discussed initially and an approximation suitable for the investigation of lattice vibrations will be derived. Afterwards, the harmonic approximation to lattice dynamics will be introduced, which allows for a feasible solution of the equations of motion of the lattice atoms. The following section sheds some light on how the necessary potential can be determined using self-consistent electronic structure calculations. Additionally, the vibrational spectrum of a lattice of point charges will be examined, which makes an important contribution to the full spectrum of a real crystal lattice.

## 2.1 The problem of moving atoms

The goal of electronic structure theory lies in the correct description of the physical behaviour of quantum-mechanical systems containing electrons. More specifically, one is interested in the physical properties and time evolution of matter build up of atoms, including molecules and matter in all possible phases. Unless one is interested in hyperfine structure effects or high-energy phenomena such as radioactive decay or nuclear scattering, it is sufficient to assume the atomic nuclei as positive point charges with a fixed mass. Since the development of quantum mechanics in the late 1920s, it is known that, under neglect of relativistic effects and spin, such a system of  $N_n$  nuclei and  $N_e$  electrons can be completely described by a Schrödinger equation

$$\mathcal{H}\Psi(\{\mathbf{x}\}, \{\mathbf{R}\}, t) = i\partial_t\Psi(\{\mathbf{x}\}, \{\mathbf{R}\}, t), \quad (2.1)$$

the solution of which is the electron-nuclear wave function  $\Psi(\mathbf{x}, \mathbf{R}, t)$ . It is a function of the coordinates  $\{\mathbf{x}\}$  of the electrons, the positions  $\{\mathbf{R}\}$  of all nuclei and of time  $t$ . The system is defined by the Hamiltonian

$$\mathcal{H} = \hat{T}_n + \hat{T}_e + V_{ee}(\{\mathbf{x}\}) + \mathcal{V}(\{\mathbf{R}\}, \{\mathbf{x}\}) + V_{nn}(\{\mathbf{R}\}) + \Xi(t), \quad (2.2)$$

of which the first two terms are kinetic energy operators for nuclei and electrons,

$$\hat{T}_n = -\sum_l^{N_n} \frac{\hbar^2}{2M_l} \frac{\partial^2}{\partial \mathbf{R}_l^2} \quad \text{and} \quad \hat{T}_e = -\sum_i^{N_e} \frac{\hbar^2}{2m_e} \frac{\partial^2}{\partial \mathbf{x}_i^2} \quad (2.3)$$

with nuclear masses  $M_l$  and the electron mass  $m_e$ . The following terms describe the particle-particle interactions, beginning with the interelectronic Coulomb potential

$$V_{ee}(\{\mathbf{x}\}) = \frac{1}{2} \frac{1}{4\pi\epsilon_0} \sum_{i \neq j}^{N_e} \frac{e^2}{|\mathbf{x}_i - \mathbf{x}_j|}. \quad (2.4)$$

The second term quantifies the electron-nuclear interaction

$$\mathcal{V}(\{\mathbf{R}\}, \{\mathbf{x}\}) = -\frac{1}{4\pi\epsilon_0} \sum_l^{N_n} \sum_i^{N_e} \frac{e^2 Z_l}{|\mathbf{R}_l - \mathbf{x}_i|} \quad (2.5)$$

and is often referred to as external potential in electronic structure theory. This nomenclature reflects the fact that the potential of the atomic nuclei alone defines the electronic eigenstates. In contrast, the internal potential  $V_{ee}(\{\mathbf{x}\})$  depends on the distribution of electrons and thus only implicitly on the nuclear positions. The last contributions to the Hamiltonian are the Coulomb repulsion of the nuclei among each other,

$$V_{nn}(\{\mathbf{R}\}) = \frac{1}{2} \frac{1}{4\pi\epsilon_0} \sum_{l \neq l'} \frac{e^2 Z_l Z_{l'}}{|\mathbf{R}_l - \mathbf{R}_{l'}|}, \quad (2.6)$$

and a possible time-dependent external vector potential  $\Xi(t)$ , which might result from laser beams or other external perturbations. Apparently, there are two interacting kinds of particles with a fundamental difference: The electron's mass is at least  $1.84 \times 10^3$  [MTN12] smaller than the mass of the nuclei. This means, although the electromagnetic forces among these particles are of the same order of magnitude, the electrons will assume much higher velocities and respond more quickly to external perturbations. This behaviour motivates the assumption that the electrons move in a, possibly time-dependent, external potential defined by the distribution of positively charged nuclei and assume their ground state within a very short time compared to the time scale of nuclear motion. Since the Hamiltonian (2.2) is a sum, the decoupling of electronic and nuclear motion results in a product wave function

$$\Psi(\{\mathbf{x}\}, \{\mathbf{R}\}, t) = \chi(\{\mathbf{R}\}, t) \psi_{\{\mathbf{R}\}}(\{\mathbf{x}\}, t), \quad (2.7)$$

where  $\chi(\{\mathbf{R}\}, t)$  is a pure nuclear wave function and  $\psi_{\{\mathbf{R}\}}(\{\mathbf{x}\}, t)$  is a pure electronic wave function but depends implicitly on the nuclear positions, as indicated by the subscript  $\{\mathbf{R}\}$ . This ansatz has been used in approximate ways since the emergence of quantum mechanics and was first presented by Born and Oppenheimer [BO27], but only recently it was shown [Kha13; KMG12] that there exists an exact factorization of the kind of Eq. (2.7). Without going into details, it should be mentioned that this approach allows for an exact, yet numerically approximate, treatment of correlated electron-nuclear motion of arbitrary kind as is especially important in the study of strong external electromagnetic fields acting on molecules or condensed matter. Looking backwards, it is a good starting point for approximations. In many cases, the study of potential energy surfaces gives a deep insight into the physics. Here, the motion of the nuclei is often described classically or semi-classically as motion on a potential energy surface which is given by the instantaneous distribution of the electrons. The latter is recalculated by solving a purely electronic Schrödinger equation at every time step for the actual nuclear configuration.

In the case where no external time-dependent potential occurs or where the nuclear motion is slow, the adiabatic approximation of Born and Oppenheimer is still a very good method to obtain a simplified Schrödinger equation for the electronic system.

## 2.2 Adiabatic approximation

Because of its importance for the physics of condensed matter and since it is used in this work, the adiabatic approximation shall be discussed in more detail here. The term 'adiabatic' refers to the assumption that, because of the big mass difference between electrons and nuclei, no energy transfer occurs between both types of particles. This is equivalent to the picture of electrons moving in the static Coulomb potential of fixed nuclei. Assuming a time-independent scenario, Born and Oppenheimer divided the Hamiltonian

$$\mathcal{H} = \underbrace{\hat{T}_n + V_{nn}(\{\mathbf{R}\})}_{\mathcal{H}_n} + \underbrace{\hat{T}_e + V_{ee}(\{\mathbf{x}\}) + \mathcal{V}(\{\mathbf{R}\}, \{\mathbf{x}\})}_{\mathcal{H}_{\text{BO}}} \quad (2.8)$$

into a nuclear ( $\mathcal{H}_n$ ) and electronic part ( $\mathcal{H}_{\text{BO}}$ ) and assumed that the electronic wave functions  $\psi_i$  for a fixed set of nuclear positions  $\{\mathbf{R}\}$  obey the Schrödinger equation

$$\mathcal{H}_{\text{BO}}\psi_i(\{\mathbf{x}\}, \{\mathbf{R}\}) = \epsilon_i(\{\mathbf{R}\})\psi_i(\{\mathbf{x}\}, \{\mathbf{R}\}). \quad (2.9)$$

Under this assumption, the electronic eigenenergies  $\epsilon_i$  as well as the electronic eigenstates  $\psi_i$  are still functions of the nuclear coordinates, but for every set of  $\{\mathbf{R}\}$  the latter are being viewed as fixed. These solutions form a complete set of orthonormal functions, fulfilling

$$\int d\mathbf{x}_1 \dots d\mathbf{x}_{N_e} \psi_i^*(\{\mathbf{x}\}, \{\mathbf{R}\})\psi_j(\{\mathbf{x}\}, \{\mathbf{R}\}) = \delta_{ij} \quad (2.10)$$

and thus can be used to construct the electron-nuclear wave function

$$\Psi(\{\mathbf{x}\}, \{\mathbf{R}\}) = \sum_i \chi_i(\{\mathbf{R}\})\psi_i(\{\mathbf{x}\}, \{\mathbf{R}\}) = \sum_i \Psi_i \quad (2.11)$$

which fulfils the Schrödinger equation

$$\mathcal{H}\Psi(\{\mathbf{x}\}, \{\mathbf{R}\}) = \mathcal{E}\Psi(\{\mathbf{x}\}, \{\mathbf{R}\}). \quad (2.12)$$

Here,  $\mathcal{E}$  symbolises an eigenvalue of the electron-nuclear energy spectrum. Under these assumptions, the action of the full Hamiltonian onto the expansion coefficients of the total wave function yields

$$\begin{aligned} \mathcal{H}\Psi_i &= \hat{T}_n\Psi_i + \epsilon_i(\{\mathbf{R}\})\Psi_i + V_{\text{nn}}\Psi_i \\ &= \psi_i(\{\mathbf{x}\}, \{\mathbf{R}\}) \left[ \hat{T}_n + \epsilon_i(\{\mathbf{R}\}) + V_{\text{nn}} \right] \chi_i(\{\mathbf{R}\}) \\ &\quad - \sum_l^{N_n} \frac{\hbar^2}{2M_l} \left[ 2 \frac{\partial \chi_i(\{\mathbf{R}\})}{\partial \mathbf{R}_l} \frac{\partial \psi_i(\{\mathbf{x}\}, \{\mathbf{R}\})}{\partial \mathbf{R}_l} + \chi_i(\{\mathbf{R}\}) \frac{\partial^2 \psi_i(\{\mathbf{x}\}, \{\mathbf{R}\})}{\partial \mathbf{R}_l^2} \right] \\ &= \mathcal{E}\Psi_i \end{aligned} \quad (2.13)$$

The only non-adiabatic contributions, meaning terms which result from interactions between electronic and nuclear states, are the two in the third line of the above equation. They can be further examined by application of Eq. (2.10), giving

$$\begin{aligned} \mathcal{E}\chi_i &= \left[ \hat{T}_n + \epsilon_i(\{\mathbf{R}\}) + V_{\text{nn}} \right] \chi_i(\{\mathbf{R}\}) \\ &\quad - \sum_l^{N_n} \sum_j \left[ M_{ij} \frac{\partial \chi_i(\{\mathbf{R}\})}{\partial \mathbf{R}_l} + N_{ij} \chi_i(\{\mathbf{R}\}) \right] \end{aligned} \quad (2.14)$$

with the two matrix elements

$$M_{ij} = \frac{\hbar^2}{M_l} \int d\mathbf{x}_1 \dots d\mathbf{x}_{N_e} \psi_i^*(\{\mathbf{x}\}, \{\mathbf{R}\}) \frac{\partial \psi_j(\{\mathbf{x}\}, \{\mathbf{R}\})}{\partial \mathbf{R}_l} \quad (2.15)$$

$$N_{ij} = \frac{\hbar^2}{2M_l} \int d\mathbf{x}_1 \dots d\mathbf{x}_{N_e} \psi_i^*(\{\mathbf{x}\}, \{\mathbf{R}\}) \frac{\partial^2 \psi_j(\{\mathbf{x}\}, \{\mathbf{R}\})}{\partial \mathbf{R}_l^2} \quad (2.16)$$

As shown in [Sól09], partial integration reveals  $M_{ij}$  to be zero under particle conservation. The second expression is finite, but results in the expectation value of the kinetic energy of the electrons multiplied by a factor of  $m_e/M_n \approx 10^{-3} \dots 10^{-5}$ . Thus, it is a very small contribution to the total energy of the lattice and its neglect seems justified as long as

electron-phonon interaction is not under concern. Neglecting this term, it follows immediately that the total wave function can be written as single product of nuclear and electronic wave functions,

$$\Psi(\{\mathbf{x}\}, \{\mathbf{R}\}, t) = \chi(\{\mathbf{R}\}, t) \psi_{\{\mathbf{R}\}}(\{\mathbf{x}\}, t), \quad (2.17)$$

which are determined by the Schrödinger equations

$$[\mathcal{H}_n + \epsilon(\{\mathbf{R}\})] \chi(\{\mathbf{R}\}) = \mathcal{E} \chi(\{\mathbf{R}\}) \quad (2.18)$$

$$\mathcal{H}_{\text{BO}} \psi_{\{\mathbf{R}\}}(\{\mathbf{x}\}) = \epsilon(\{\mathbf{R}\}) \psi_{\{\mathbf{R}\}}(\{\mathbf{x}\}). \quad (2.19)$$

The first equation describes the movement of nuclei on the potential energy surface  $\epsilon(\{\mathbf{R}\})$  of the electrons which is determined by the second equation in which the nuclei are considered as fixed. This is the adiabatic or Born-Oppenheimer approximation. It is one of the basic principles that made electronic structure theory successful. In static cases, e. g. if the ground state of the lattice is of interest, the nuclear dynamics can be completely ignored and only the electronic Schrödinger equation has to be solved. Apart from the cases discussed in the beginning of this chapter, a classical treatment of the nuclear dynamics is often useful. In this case, the nuclear wave function is replaced by classical point masses obeying Newtonian dynamics, whereas the forces acting on these masses are still a result of the instantaneous electronic states. This treatment is successfully applied to lattice vibrations, as shown in the next section.

### 2.3 Lattice dynamics in the harmonic approximation

In the following, the theory of lattice dynamics of Born and v. Karman [BK12; BK13] is presented, following the derivations from standard textbooks like [Sri90; Zim92; Gon00; Sól07].

In order to construct a classical equation of motion for the atoms in a crystal, one needs a proper description of the potential in which the assumed point masses move. The potential energy of a crystal depends on the complex forces between the atoms composing it, that is, attractive and repulsive forces between all charged particles. However, for the purpose of deriving the equations of motion for the nuclei, it is not necessary to know the exact forces in the first place. Within the Born-Oppenheimer approximation it is sufficient to assume that the nuclei move on the potential energy surface defined by the ground state of the electronic system. Thus, the potential energy of the crystal  $\mathcal{U}$  can be written as a function of nuclear positions only. Here and in the following, the position of a single nucleus within a complex crystal will be written as

$$\mathbf{X}_{ni} = \mathbf{X}_{ni}^0 + \mathbf{u}(ni) = \mathbf{R}_n + \boldsymbol{\tau}_i + \mathbf{u}(ni), \quad (2.20)$$

where  $\mathbf{R}_n$  denotes the point of origin of the  $n$ th unit cell. Each cell contains  $1 \leq i \leq N$  ions with basis vectors  $\boldsymbol{\tau}_i$ , such that  $\mathbf{X}_{ni}^0$  denotes the equilibrium position of ion  $(ni)$ . Under neglect of lattice defects and at temperatures small compared to the melting point of the respective material, one can assume that the nuclei oscillate around their equilibrium positions. This time-dependent relative displacement is denoted by the vector  $\mathbf{u}(ni)$ . Since the equilibrium positions are fixed, the potential energy is a function of the  $\{\mathbf{u}\}$ ,

$$\mathcal{U} = \mathcal{U}(\{\mathbf{u}\}), \quad (2.21)$$

which has its minimum at  $\mathbf{u}(ni) = 0 \forall (n, i)$ . This potential energy can be expanded in a Taylor series

$$\begin{aligned} \mathcal{U} &= \mathcal{U}_0 + \mathcal{U}_1(\mathbf{u}) + \mathcal{U}_2(\mathbf{u}^2) + \dots \\ &= \mathcal{U}_0 + \sum_{ni\alpha} u_\alpha(ni) \left. \frac{\partial \mathcal{U}}{\partial u_\alpha(ni)} \right|_{\mathbf{u}=0} \\ &\quad + \frac{1}{2} \sum_{ni\alpha} \sum_{mj\beta} u_\alpha(ni) u_\beta(mj) \left. \frac{\partial^2 \mathcal{U}}{\partial u_\alpha(ni) \partial u_\beta(mj)} \right|_{\mathbf{u}=0} + \mathcal{O}(\mathbf{u}^3), \end{aligned}$$

which can be aborted after the quadratic term if the amplitudes  $\{\mathbf{u}\}$  are small ( $< 1\%$ ) compared to interatomic distances. The Greek letters denote vector components and can take the values  $\alpha \in \{x, y, z\}$ . The constant term  $\mathcal{U}_0$ , although it is the largest contribution to the total energy, does not contribute to the dynamics of the system and can be omitted in this context. The second, linear term is equivalent to the force resulting from a displacement and gives, by definition, zero at the equilibrium positions. Neglecting third- and higher order terms, the harmonic approximation of the crystal potential is defined as

$$\mathcal{U}_{\text{harm}} = \mathcal{U}_2 = \frac{1}{2} \sum_{ni\alpha} \sum_{mj\beta} \phi_{\alpha\beta}(ni|mj) u_\alpha(ni) u_\beta(mj) \quad (2.22)$$

with

$$\phi_{\alpha\beta}(ni|mj) = \left. \frac{\partial^2 \mathcal{U}}{\partial u_\alpha(ni) \partial u_\beta(mj)} \right|_{\mathbf{u}=0}. \quad (2.23)$$

The latter expression is also referred to as force constant matrix, since it is proportional to the force acting on atom  $(ni)$  in direction  $\alpha$  when atom  $(mj)$  is displaced along direction  $\beta$ . This also means that the force is linearly dependent on the respective atoms' distance from its equilibrium position, which is why a harmonic oscillation can be expected. In order to obtain the equation of motion of the particles, it is useful to use the Lagrange formalism. The Lagrange function, which is the difference between kinetic and potential energy of the system, reads

$$\mathbf{L} = \frac{1}{2} \sum_{ni\alpha} M_i \dot{u}_\alpha^2(ni) - \frac{1}{2} \sum_{ni\alpha} \sum_{mj\beta} \phi_{\alpha\beta}(ni|mj) u_\alpha(ni) u_\beta(mj), \quad (2.24)$$

where  $M_i$  denotes the mass of the atom at site  $i$  and the kinetic energy is the sum of the kinetic energies of all atoms. The derivative of  $\mathbf{L}$  with respect to a displacement, as well as the derivative with respect to a particle's velocity,

$$\frac{\partial \mathbf{L}}{\partial u_\alpha(ni)} = - \sum_{mj\beta} \phi_{\alpha\beta}(ni|mj) u_\beta(mj), \quad \frac{\partial \mathbf{L}}{\partial \dot{u}_\alpha(ni)} = M_i \dot{u}_\alpha(ni), \quad (2.25)$$

can then be used together with the Lagrange equations of the second kind

$$\frac{d}{dt} \left( \frac{\partial \mathbf{L}}{\partial \dot{u}_\alpha(ni)} \right) = \frac{\partial \mathbf{L}}{\partial u_\alpha(ni)} \quad (2.26)$$

to obtain the equation of motion describing the movement of all atoms of the system

$$M_i \ddot{u}_\alpha(ni) = - \sum_{mj\beta} \phi_{\alpha\beta}(ni|mj) u_\beta(mj). \quad (2.27)$$

Since this is an equation of motion of coupled harmonic oscillators, a reasonable ansatz for the solutions are plane waves

$$u_\alpha(ni) = \frac{A_\alpha(i, \mathbf{q})}{\sqrt{M_i}} e^{i(\mathbf{q} \cdot \mathbf{R}_n - \omega t)}, \quad (2.28)$$

where  $A_\alpha$  is the amplitude of the wave at site  $i$  for a given wave vector  $\mathbf{q}$ . This approach is also justified by a more general consideration [Fin03]: Obviously,  $A_\alpha(i, \mathbf{q})$  is a function with the periodicity of the lattice. Thus, a solution for a different lattice vector  $\mathbf{R}_n - \mathbf{R}_m$  is given by

$$u_\alpha(n - m, i) = \frac{A_\alpha(i, \mathbf{q})}{\sqrt{M_i}} e^{i(\mathbf{q} \cdot (\mathbf{R}_n - \mathbf{R}_m) - \omega t)}. \quad (2.29)$$

This is equivalent to the Bloch condition [Blo29] for electronic states in a periodic lattice. If this approach is correct, lattice waves can be described as Bloch waves, but instead of electronic Bloch functions, which depend on position in space, lattice Bloch waves depend on the basis atom  $i$ . In both cases, the solutions are a result of the periodicity of the lattice. Plugging in the functions  $u_\alpha(ni)$  into the equation of motion leads to the relation

$$\omega^2 A_\alpha(i, \mathbf{q}) = \sum_{mj\beta} \phi_{\alpha\beta}(ni|mj) \frac{A_\beta(j, \mathbf{q})}{\sqrt{M_i M_j}} e^{i\mathbf{q} \cdot (\mathbf{R}_m - \mathbf{R}_n)}. \quad (2.30)$$

In a perfect crystal with translational symmetry, the force constants do not depend on the absolute values of  $n$  and  $m$  but on the difference  $\mathbf{R}_n - \mathbf{R}_m$ . Thus,  $n$  can be set to zero and by defining

$$D_{\alpha\beta}^{ij}(\mathbf{q}) = \frac{1}{\sqrt{M_\alpha M_\beta}} \sum_m \phi_{\alpha\beta}(0i|mj) e^{i\mathbf{q} \cdot \mathbf{R}_m}, \quad (2.31)$$

Eq. (2.30) can be rewritten as

$$0 = \sum_{j\beta} \left[ D_{\alpha\beta}^{ij}(\mathbf{q}) - \omega^2 \delta_{\alpha\beta} \delta_{ij} \right] A_\beta(j, \mathbf{q}). \quad (2.32)$$

Non-trivial solutions for the Amplitudes  $A_\alpha(i, \mathbf{q})$  can only exist if

$$\det \left[ D_{\alpha\beta}^{ij}(\mathbf{q}) - \omega^2 \delta_{\alpha\beta} \delta_{ij} \right] = 0, \quad (2.33)$$

which is called the phonon secular equation. It provides the solutions  $\omega^2(\mathbf{q})$  and thus the phonon band structure. For a system with  $N$  atoms per unit cell, there exist  $3N$  solutions, since in three-dimensional space, the polarization vector  $\mathbf{A}$  may take three linearly independent directions (one longitudinal and two transverse). The lowest 3 frequencies belong to acoustical phonons with  $\omega \rightarrow 0$  for  $\mathbf{q} \rightarrow 0$  and the other  $3N - 3$  solutions are optical modes, approaching finite frequencies at the  $\Gamma$  point. The main problem in the theoretical description is the calculation of the *dynamical matrix*  $D(\mathbf{q})$ , which is a mass-reduced lattice Fourier transform of the force constants.

## 2.4 Force constants from first principles

Despite the fact that numerous phenomenological models of lattice dynamics have been developed since the fundamental paper of Born and v. Kármán [BK12; BK13], such as the rigid-ion-model, shell models or dipole models, all of them had two major drawbacks: None of them is valid for all types of solids and they depend on empiric parameters which do not necessarily relate to the physical nature of the problem [Sri90]. As a consequence, the

necessity of a full quantum-mechanical description became apparent in the early 1970s and first semi-phenomenological approaches have been presented [Sin69; Sha69; Sha74].

The calculation of phonon spectra requires on one side the treatment of the direct electrostatic, long-ranging nucleus-nucleus or ion-ion repulsion which gives rise to high phonon frequencies and can be evaluated analytically [Kel40]. This interaction, on the other hand, is screened by the electron gas, which itself rearranges upon every lattice distortion. Because of the adiabatic principle this rearrangement can be assumed as instantaneous process compared to the relatively slow movement of the ions. Thus, for every lattice geometry induced by a lattice vibration, the electron cloud assumes a new ground state which can be calculated by a quantum-mechanical method. The method of choice used throughout this work is the density functional theory (DFT), which will be presented in detail in the next chapter. It allows for the solution of the electronic Schrödinger equation (2.9), given a set of fixed nuclei, and delivers the electronic charge density  $n(\mathbf{x})$ . All ab-initio methods presented in the following rely on this tool.

### 2.4.1 Hellmann-Feynman theorem

A fundamental problem of quantum mechanics and especially for lattice or molecular dynamics is the calculation of derivatives of total energy with respect to parameters of the Hamilton operator. In the case of forces, this is necessary because a force acting on an ion in a molecule or solid is defined as

$$\mathbf{f} = -\nabla E, \quad (2.34)$$

where  $E$  is the total energy of the system, depending on the nuclear coordinates and the gradient is the slope of the energy at the position of the respective ion. This problem is addressed by the following theorem.

Consider a quantum-mechanical system described by a Hamiltonian  $\hat{H}(\lambda)$  which depends on a parameter  $\lambda$ . For a fixed  $\lambda$ , the system shall be in a stationary state  $\Psi_i(\lambda)$  with eigenenergies  $\epsilon_i(\lambda)$ . Let  $\hat{H}$  further be hermitian and let the states  $\Psi_i(\lambda)$  be normalized such that

$$\langle \Psi_i(\lambda) | \Psi_i(\lambda) \rangle = 1. \quad (2.35)$$

An example for this kind of Hamiltonian is the Born-Oppenheimer Hamiltonian introduced in section 2.2, which depends parametrically on the nuclear positions.

The slope of the function  $\epsilon_i(\lambda)$  can be determined by calculating its value directly for different values of  $\lambda$ , which is a very cumbersome task in the case of DFT calculations. Hellmann [Hel37] and later, independently Feynman [Fey39] showed that the same quantity can be obtained from a single total-energy calculation for a fixed  $\lambda$  by writing

$$\begin{aligned} \frac{d\epsilon_i(\lambda)}{d\lambda} &= \frac{d}{d\lambda} \langle \Psi_i(\lambda) | \hat{H}(\lambda) | \Psi_i(\lambda) \rangle \\ &= \left\langle \frac{d\Psi_i(\lambda)}{d\lambda} \middle| \hat{H}(\lambda) \middle| \Psi_i(\lambda) \right\rangle + \left\langle \Psi_i(\lambda) \middle| \frac{d\hat{H}(\lambda)}{d\lambda} \middle| \Psi_i(\lambda) \right\rangle \\ &\quad + \left\langle \Psi_i(\lambda) \middle| \hat{H}(\lambda) \middle| \frac{d\Psi_i(\lambda)}{d\lambda} \right\rangle. \end{aligned} \quad (2.36)$$

Applying  $\hat{H}(\lambda)\Psi_i(\lambda) = \epsilon_i(\lambda)\Psi_i(\lambda)$  and considering that  $\hat{H}$  is hermitian, this derivation can be continued as

$$\frac{d\epsilon_i(\lambda)}{d\lambda} = \epsilon_i(\lambda) \left\langle \frac{d\Psi_i(\lambda)}{d\lambda} \middle| \Psi_i(\lambda) \right\rangle + \left\langle \Psi_i(\lambda) \middle| \frac{d\hat{H}(\lambda)}{d\lambda} \middle| \Psi_i(\lambda) \right\rangle \quad (2.37)$$

$$+ \epsilon_i(\lambda) \left\langle \Psi_i(\lambda) \middle| \frac{d\Psi_i(\lambda)}{d\lambda} \right\rangle. \quad (2.38)$$

Using the normalization (2.35), it becomes clear that under conservation of the particle number during the variation of  $\lambda$ , the following statement holds:

$$\left\langle \frac{d\Psi_i(\lambda)}{d\lambda} \middle| \Psi_i(\lambda) \right\rangle + \left\langle \Psi_i(\lambda) \middle| \frac{d\Psi_i(\lambda)}{d\lambda} \right\rangle = \frac{d}{d\lambda} \langle \Psi_i(\lambda) | \Psi_i(\lambda) \rangle = 0, \quad (2.39)$$

which finally leads to the Hellmann-Feynman theorem

$$\frac{d\epsilon_i(\lambda)}{d\lambda} = \frac{d}{d\lambda} \langle \hat{H} \rangle_i = \left\langle \Psi_i(\lambda) \middle| \frac{d\hat{H}(\lambda)}{d\lambda} \middle| \Psi_i(\lambda) \right\rangle = \left\langle \frac{d\hat{H}}{d\lambda} \right\rangle_i. \quad (2.40)$$

To calculate the forces acting on atoms in a crystal or molecule, the theorem can be applied to the crystal Hamiltonian (2.2) or, within the adiabatic approximation, to the total energy of the crystal

$$E_{\text{tot}} = T_n + E_{\text{nn}}(\{\mathbf{u}\}) + E_{\text{BO}}(\{\mathbf{u}\}). \quad (2.41)$$

$E_{\text{BO}}(\{\mathbf{u}\})$  is the Born-Oppenheimer energy of the electronic system, depending parametrically on the positions of all atoms, or, as denoted here, on the displacements  $\mathbf{u}$  from their equilibrium positions and  $E_{\text{nn}}(\{\mathbf{u}\})$  is the instantaneous Coulomb energy of the nuclei as a function of the  $\{\mathbf{u}\}$ . The force acting on an atom at the  $i$ th site in cell  $n$  is then defined as

$$\begin{aligned} \mathbf{F}_n^i &= -\nabla_{\mathbf{u}(ni)} E_{\text{tot}} = -\nabla_{\mathbf{u}(ni)} E_{\text{nn}}(\{\mathbf{u}\}) - \nabla_{\mathbf{u}(ni)} E_{\text{BO}}(\{\mathbf{u}\}) \\ &= -\nabla_{\mathbf{u}(ni)} E_{\text{nn}}(\{\mathbf{u}\}) - \left\langle \Psi[n] \middle| \nabla_{\mathbf{u}(ni)} \left[ \hat{T}_e + V_{ee} + \mathcal{V}(\{\mathbf{u}\}) \right] \middle| \Psi[n] \right\rangle, \end{aligned} \quad (2.42)$$

where the second line is a result of the Hellmann-Feynman theorem. The kinetic energy of the nuclei does not enter the force equation since it does not depend explicitly on the positions of the nuclei. The same argument holds for the kinetic energy of the electrons as well as their pairwise Coulomb interaction. Thus, the resulting force reads

$$\begin{aligned} \mathbf{F}_n^i &= -\nabla_{\mathbf{u}(ni)} E_{\text{nn}}(\{\mathbf{u}\}) - \left\langle \Psi[n] \middle| \nabla_{\mathbf{u}(ni)} E_{\text{BO}}(\{\mathbf{u}\}) \middle| \Psi[n] \right\rangle \\ &= Z^i \left[ \sum_{l \neq n} \sum_{s \neq i} Z^s \frac{(\mathbf{R}_n + \boldsymbol{\tau}_i + \mathbf{u}(ni) - \mathbf{R}_l - \boldsymbol{\tau}_s - \mathbf{u}(ls))}{|\mathbf{R}_n + \boldsymbol{\tau}_i + \mathbf{u}(ni) - \mathbf{R}_l - \boldsymbol{\tau}_s - \mathbf{u}(ls)|^3} \right. \\ &\quad \left. - \int d\mathbf{x} n(\mathbf{x}) \frac{(\mathbf{R}_l + \boldsymbol{\tau}_i + \mathbf{u}(ni) - \mathbf{x})}{|\mathbf{R}_l + \boldsymbol{\tau}_i + \mathbf{u}(ni) - \mathbf{x}|^3} \right], \end{aligned} \quad (2.43)$$

an expression that is often referred to as electrostatic Hellmann-Feynman theorem because it is identical to the classical electrostatic force induced by a negative charge distribution and positive point charges.

One should note that this theorem is only valid if it is applied to the exact eigenfunctions of the Hamiltonian. Whereas deviations in the wave functions and thus the charge density enter the total energy in second order, the forces are influenced in first order by these kinds of errors [Fin03].

## 2.4.2 Direct methods

Among the first ab-initio methods for the treatment of lattice vibrations is the frozen phonon approach [WM78; WM79; Sri90]: A wave moving through a crystal causes the ions to displace from their equilibrium positions in a defined pattern, which is given by the amplitude vectors (Eq. (2.28)) of the respective ions. Within the adiabatic approximation, the electron gas assumes its ground state instantaneously at every point in time during the motion of the ions. Thus, the total energy of the system can be calculated self-consistently at every fixed

time and displacement. Such a 'frozen' vibrational mode is equivalent to a crystal lattice with reduced symmetry and increased total energy, compared to the undistorted ground state lattice. According to the harmonic approximation (Eq. (2.22)), the frequency  $\omega$  of a specific displacement pattern is given by

$$\frac{1}{2}\omega^2 \sum_s m_s |\mathbf{u}(s)|^2 = E_{\text{tot}}(\mathbf{u}) - E_{\text{tot}}(0), \quad (2.44)$$

in which the  $\mathbf{u}$  denote the displacements of the ions from their respective equilibrium positions and  $m_s$  refers to the ions' masses.  $E_{\text{tot}}$  denotes the total energy as sum of Born-Oppenheimer energy and ion-ion energy for the distorted and undistorted lattice, respectively. Due to the harmonic nature of the oscillation, total energy calculations for small  $\mathbf{u}$ ,  $-\mathbf{u}$  and  $2\mathbf{u}$  are sufficient to obtain the frequency of the mode.

In calculations using translational symmetry, the frozen mode is limited in wavelength by the size of the supercell. Thus, this method allows the calculation of vibrational frequencies only for a very limited set of  $\mathbf{q}$ -vectors. An illustration of a supercell configuration for a frozen phonon calculation is shown in Fig. 2.1 (a). An extension of this approach is the planar force constant method [KM82; Sri90], which allows the calculation of the phonon dispersion along distinct  $\mathbf{q}$  directions by introducing effective interplanar forces which affect the motion of planes of atoms perpendicular to  $\mathbf{q}$ . The respective force constants are equally determined via supercell calculations.

A more versatile approach was proposed by Kresse et al. [KFH95]: The displacement  $\mathbf{u}(ls)$  of an atom in a supercell, with  $l$  being the index of the respective unit cell and  $s$  denoting the position within the unit cell, induces forces  $\mathbf{F}_{ll'}^{ss'}$  between the displaced atom and all other atoms ( $l's'$ ) within the supercell. The resulting total force on ( $ls$ ) is

$$\mathbf{F}_s^l = \sum_{l's'} \mathbf{F}_{ll'}^{ss'}. \quad (2.45)$$

The force field  $\mathbf{F}_{ll'}^{ss'}$  resulting from a single displacement can be obtained from a self-consistent DFT calculation by making use of the Hellmann-Feynman theorem. By application of the symmetry operations of the lattice, the complete force field can be calculated

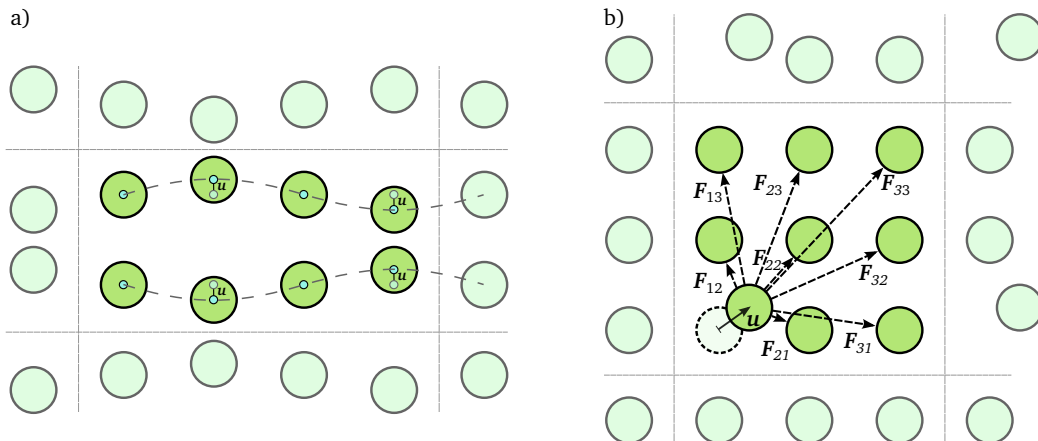


**Figure 2.1:** a) Frozen phonon method: A supercell of a two-dimensional lattice with an imprinted displacement pattern for a transverse vibrational mode with wavelength  $\lambda = 4a$  is shown. The corresponding undisturbed lattice would be simple quadratic with lattice constant  $a$ . b) Finite displacement method. The displacement amplitudes are exaggerated for the sake of clarity.

with a minimum of self-consistent calculations, each with a different displacement. Afterwards, the force constants are given by

$$\phi_{\alpha\beta}(ls|l's') = -\frac{\left(\mathbf{F}_{l'l}^{ss'}\right)_\beta}{u_\alpha(ls)}. \quad (2.46)$$

An important criterion for the convergence of Eq. (2.31), by which the dynamical matrix is calculated, is the size of the supercell. Its lattice constant has to be chosen big enough to obtain negligible contributions to the force field from atoms at greater distances. This can be a major drawback of the method, since the size of the supercells can be computationally very demanding in some cases, especially when long-wavelength effects are to be studied. The advantage of this method is that it can treat linear as well as non-linear effects and that it, in principle, can be used with every computer code capable of self-consistent electronic structure calculations.

### 2.4.3 Perturbation theory and linear response

To overcome the above mentioned disadvantages of supercell calculations, it is desirable to have a method available to calculate the dynamical matrix directly from the properties of the electronic ground state, without supercells and at arbitrary  $\mathbf{q}$ -vectors. Starting from Eq. (2.42), the total force on ion  $i$  in the  $n$ th unit cell is

$$\mathbf{F}_n^i = -\nabla_{\mathbf{u}(ni)} E'_{\text{tot}}, \quad (2.47)$$

where  $E'_{\text{tot}}$  is the total energy of the crystal minus the kinetic energy of the nuclei,

$$E'_{\text{tot}} = E_{\text{nn}} + E_{\text{BO}}. \quad (2.48)$$

Thus, the force constant matrix as the negative second derivative of the force with respect to the  $j$ th ion in cell  $m$  can be constructed out of two major contributions,

$$\phi_{\alpha\beta}(ni|mj) = \frac{\partial^2 E_{\text{nn}}}{\partial u_\alpha(ni) \partial u_\beta(mj)} + \frac{\partial^2 E_{\text{BO}}}{\partial u_\alpha(ni) \partial u_\beta(mj)} \quad (2.49)$$

$$= \phi_{\alpha\beta}^{\text{n}}(ni|mj) + \phi_{\alpha\beta}^{\text{e}}(ni|mj), \quad (2.50)$$

of which the first one results from the Coulomb interactions between ions only and the second one covers the contribution of the electronic states. From Eq. (2.42) it follows that the force resulting from the electron cloud is

$$\left(\mathbf{f}_n^i\right)_\alpha = -\nabla_{\mathbf{u}(ni)} E_{\text{BO}} = -\left\langle \Psi[n] \left| \nabla_{\mathbf{u}(ni)} \left[ \hat{T}_e + V_{\text{ee}} + \mathcal{V}(\{\mathbf{u}\}) \right] \right| \Psi[n] \right\rangle \quad (2.51)$$

and since the kinetic energy operator as well as the electron-electron interaction do not depend explicitly on nuclear coordinates,

$$\nabla_{\mathbf{u}(ni)} \left[ \hat{T}_e + V_{\text{ee}} \right] = 0 \quad (2.52)$$

and the remaining expression for the  $\alpha$ th vector component of the force, after evaluation the expectation value, becomes

$$\left(\mathbf{f}_n^i\right)_\alpha = - \int_{\Omega_{\text{cryst}}} d\mathbf{x} n(\mathbf{x}) \frac{\partial \mathcal{V}(\{\mathbf{u}\}, \mathbf{x})}{\partial u_\alpha(ni)}. \quad (2.53)$$

The negative derivative of this expression gives the desired element of the electronic force constant matrix

$$\phi_{\alpha\beta}(ni|mj) = - \frac{\partial}{\partial u_{\beta}(mj)} (\mathbf{f}_n^i)_{\alpha} \quad (2.54)$$

$$= \int_{\Omega_{\text{cryst}}} d\mathbf{x} \mathcal{K}_{m,\beta}^j(\mathbf{x}) \frac{\partial \mathcal{V}(\{\mathbf{u}\}, \mathbf{x})}{\partial u_{\alpha}(ni)} + \int_{\Omega_{\text{cryst}}} d\mathbf{x} n(\mathbf{x}) \frac{\partial^2 \mathcal{V}(\{\mathbf{u}\}, \mathbf{x})}{\partial u_{\alpha}(ni) \partial u_{\beta}(mj)}, \quad (2.55)$$

in which the quantity  $\mathcal{K}$  is defined as

$$\mathcal{K}_{m,\beta}^j(\mathbf{x}) = \frac{\partial n(\mathbf{x})}{\partial u_{\beta}(mj)}, \quad (2.56)$$

describing the rate of change of the electron density at position  $\mathbf{x}$  when ion ( $mj$ ) is displaced in direction  $\beta$ . This important result was first published in [DJ69; PCM70] and paved the way for modern first-principles lattice-dynamical methods. The different methods which have been developed since then mainly differ in the manner in which  $\mathcal{K}$  is determined. Since the density does not depend explicitly on the nuclear coordinates, but is a result of the Schrödinger equation for a given set of positions, a prediction for its response to external perturbations is needed.

One can apply traditional perturbation theory, which can be done in several ways. One of them is to linearize the electronic Schrödinger equation to obtain the Sternheimer equation [Ste54], which was originally developed for atomistic calculations and applied to lattice dynamics via a Green function method [Zei84; BGT87]. It is successfully used to calculate the first-order derivatives of the electronic wave functions with respect to nuclear coordinates. Another possible approach to this quantity is the Hylleraas variational principle [Hyl30], which was derived from the Reyleigh-Ritz principle. Reviews of these kinds of methods are given in [Gon95; Gon94; BGD01].

The focus in this work lies on the methods developed by Zangwill and Soven [ZS80], Stott and Zaremba [SZ80] and Mahan [Mah80], which are directly based on the linear response theory developed by Kubo (see Chap. 3). Here, the perturbation of the electronic charge density  $\delta n(\mathbf{x})$  due to an external force is given by the equation

$$\delta n(\mathbf{x}) = \int d\mathbf{x}' \chi(\mathbf{x}, \mathbf{x}') \delta \mathcal{V}(\{\mathbf{u}\}, \mathbf{x}'), \quad (2.57)$$

in which  $\delta \mathcal{V}$  is the perturbing external potential defining the electronic ground state and  $\chi(\mathbf{x}, \mathbf{x}')$  is the linear-order response function of the electron gas. The latter is a correlation function, which describes how strong the electron density  $n(\mathbf{x})$  is influenced when a perturbation at  $\mathbf{x}'$  occurs. In the context of lattice dynamics, the external perturbation  $\delta n(\mathbf{x})$  is given by the displacement of nuclei, resulting in

$$\mathcal{K}_{m,\beta}^j(\mathbf{x}) = \int d\mathbf{x}' \chi(\mathbf{x}, \mathbf{x}') \frac{\partial \mathcal{V}(\{\mathbf{u}\}, \mathbf{x}')}{\partial u_{\beta}(mj)}, \quad (2.58)$$

The path to the linear response function and thus to  $\mathcal{K}_{m,\beta}^j$  will be outlined in the following chapters. However, the contribution of the pure internuclear interaction  $E_{\text{nn}}$  to the phonon frequencies will be discussed first.

## 2.5 Contribution of bare ions

As shown in Eq. (2.50), the dynamical matrix of a crystal lattice can be written as sum of a pure nuclear part and a part containing all contributions from interactions with and

between electrons. Within the adiabatic approximation, the nuclear part  $\phi_{\alpha\beta}^n$  can be treated classically within high precision. The potential energy of the lattice upon the internuclear Coulomb repulsion is given by

$$E_{\text{nn}} = \frac{1}{2} \frac{e^2}{4\pi\epsilon_0} \sum_{ll'} \sum_{ss'}^{(ls) \neq (l's')} \frac{Z_s Z_{s'}}{|\mathbf{R}_l - \mathbf{R}_{l'} + \boldsymbol{\tau}_s - \boldsymbol{\tau}_{s'} + \mathbf{u}(ls) - \mathbf{u}(l's')|}. \quad (2.59)$$

In many cases (see chapter 5) it is useful to include strongly bound electrons into this classical treatment by assuming that these, together with the nuclei, compose non-polarizable ions with an effective charge  $Z_s^*$ . These ions can no longer be treated as point charges. Instead, one can assume a static charge density

$$n_{l_s}^{\text{ion}}(\mathbf{x}) = Z_s \delta(\mathbf{x} - \mathbf{R}_l - \boldsymbol{\tau}_s - \mathbf{u}(ls)) - n_{l_s}^c(\mathbf{x} - \mathbf{R}_l - \boldsymbol{\tau}_s - \mathbf{u}(ls)), \quad (2.60)$$

or

$$n_{l_s}^{\text{ion}}(\mathbf{r}) = Z_s \delta(\mathbf{r} - \mathbf{u}(ls)) - n_{l_s}^c(\mathbf{r} - \mathbf{u}(ls)) \quad (2.61)$$

in cell-centred coordinates (shifting the origin of the local coordinate to the center of the respective cell, such that  $\mathbf{x} = \mathbf{R}_l + \boldsymbol{\tau}_s + \mathbf{r}$ ).

Using Rydberg atomic units ( $e = \sqrt{2}$  and  $\epsilon_0 = 1/4\pi$ ) and introducing the definitions

$$\mathcal{V}_{ll'}^{ss'}(\mathbf{r}, \mathbf{r}') = \frac{2}{|\mathbf{R}_l - \mathbf{R}_{l'} + \boldsymbol{\tau}_s - \boldsymbol{\tau}_{s'} + \mathbf{u}(ls) - \mathbf{u}(l's') + \mathbf{r} - \mathbf{r}'|} \quad (2.62)$$

$$\mathring{\mathcal{V}}_{ll'}^{ss'}(\mathbf{r}, \mathbf{r}') = \frac{2}{|\mathbf{R}_l - \mathbf{R}_{l'} + \boldsymbol{\tau}_s - \boldsymbol{\tau}_{s'} + \mathbf{r} - \mathbf{r}'|}, \quad (2.63)$$

the ion-ion potential energy can be rewritten as

$$E_{\text{ii}} = \frac{1}{2} \sum_{ll'} \sum_{ss'}^{(ls) \neq (l's')} \int d\mathbf{r} \int d\mathbf{r}' n_s^{\text{ion}}(\mathbf{r}) \mathcal{V}_{ll'}^{ss'}(\mathbf{r}, \mathbf{r}') n_{s'}^{\text{ion}}(\mathbf{r}'). \quad (2.64)$$

where the dependence of the energy on the core positions is explicitly addressed by the Coulomb denominator  $\mathcal{V}_{ll'}^{ss'}(\mathbf{r}, \mathbf{r}')$ . The symbol  $\mathring{\mathcal{V}}$  defined in Eq. (2.63) denotes the Coulomb potential within a lattice in its ground state and is thus independent of the  $\{\mathbf{u}\}$ . Thus, the part of the force constants resulting only from the positively charged ionic cores reads

$$\begin{aligned} \phi_{\alpha\beta}^{\text{ion}}(mi|nj) &= \left. \nabla_{u_\beta(mi)} (\nabla_{u_\alpha(nj)} E_{\text{ii}}) \right|_{\mathbf{u}=0} \\ &= \int d\mathbf{r} \int d\mathbf{r}' n_i^{\text{ion}}(\mathbf{r}) \frac{1}{2} \left[ \delta_{mn} \delta_{ij} \sum_{l'} \sum_{s'} n_{s'}^{\text{ion}}(\mathbf{r}') \partial_{r_\alpha r'_\beta}^2 \mathring{\mathcal{V}}_{ml'}^{is'}(\mathbf{r}, \mathbf{r}') \right. \\ &\quad \left. - n_j^{\text{ion}}(\mathbf{r}') \partial_{r_\alpha r'_\beta}^2 \mathring{\mathcal{V}}_{mn}^{ij}(\mathbf{r}, \mathbf{r}') \right], \end{aligned} \quad (2.65)$$

where it was made use of the relations

$$\left. \nabla_{u(mi)_\alpha} \mathcal{V}_{mn}^{ij}(\mathbf{r}, \mathbf{r}') \right|_{\mathbf{u}=0} = \nabla_{r_\alpha} \mathring{\mathcal{V}}_{mn}^{ij}(\mathbf{r}, \mathbf{r}'), \quad (2.66)$$

$$\left. \nabla_{u(nj)_\beta} \mathcal{V}_{mn}^{ij}(\mathbf{r}, \mathbf{r}') \right|_{\mathbf{u}=0} = \nabla_{r'_\beta} \mathring{\mathcal{V}}_{mn}^{ij}(\mathbf{r}, \mathbf{r}') = -\nabla_{r_\beta} \mathring{\mathcal{V}}_{mn}^{ij}(\mathbf{r}, \mathbf{r}'). \quad (2.67)$$

The dynamical matrix resulting from the ion-ion interaction is the lattice Fourier transform of the above force constant matrix, normalized by the atomic masses (see Eq. (2.31))

$$\begin{aligned} {}^{\text{ion}}D_{\alpha\beta}^{ij}(\mathbf{q}) &= \frac{1}{\sqrt{M_i M_j}} \sum_n \phi_{\alpha\beta}^{\text{ion}}(0i|nj) e^{i\mathbf{q}\cdot\mathbf{R}_n} \\ &= \frac{1}{\sqrt{M_i M_j}} \int d\mathbf{r} \int d\mathbf{r}' n_i^{\text{ion}}(\mathbf{r}) \sum_n \left[ \delta_{0n} \delta_{ij} \sum_{l'} \sum_{s'} n_{s'}^{\text{ion}}(\mathbf{r}') \partial_{r_\alpha r'_\beta}^2 \mathring{\mathcal{V}}_{0l'}^{is'}(\mathbf{r}, \mathbf{r}') \right. \\ &\quad \left. - n_j^{\text{ion}}(\mathbf{r}') \partial_{r_\alpha r'_\beta}^2 \mathring{\mathcal{V}}_{0n}^{ij}(\mathbf{r}, \mathbf{r}') \right] e^{i\mathbf{q}\cdot\mathbf{R}_n}. \end{aligned} \quad (2.68)$$

The Fourier series above can be further developed as follows:

$$\begin{aligned} &\sum_n \left[ \delta_{0n} \delta_{ij} \sum_{l'} \sum_{s'} n_{s'}^{\text{ion}}(\mathbf{r}') \partial_{r_\alpha r'_\beta}^2 \mathring{\mathcal{V}}_{0l'}^{is'}(\mathbf{r}, \mathbf{r}') - n_j^{\text{ion}}(\mathbf{r}') \partial_{r_\alpha r'_\beta}^2 \mathring{\mathcal{V}}_{0n}^{ij}(\mathbf{r}, \mathbf{r}') \right] e^{i\mathbf{q}\cdot\mathbf{R}_n} \\ &= \sum_n \delta_{0n} \delta_{ij} \sum_{l'} \sum_{s'} n_{s'}^{\text{ion}}(\mathbf{r}') \partial_{r_\alpha r'_\beta}^2 \mathring{\mathcal{V}}_{0l'}^{is'}(\mathbf{r}, \mathbf{r}') e^{i\mathbf{q}\cdot\mathbf{R}_n} - n_j^{\text{ion}}(\mathbf{r}') \sum_n \partial_{r_\alpha r'_\beta}^2 \mathring{\mathcal{V}}_{0n}^{ij}(\mathbf{r}, \mathbf{r}') e^{i\mathbf{q}\cdot\mathbf{R}_n} \\ &= \delta_{ij} \sum_{l'} \sum_{s'} n_{s'}^{\text{ion}}(\mathbf{r}') \partial_{r_\alpha r'_\beta}^2 \mathring{\mathcal{V}}_{0l'}^{is'}(\mathbf{r}, \mathbf{r}') e^{i\mathbf{q}\cdot\mathbf{R}_0} - n_j^{\text{ion}}(\mathbf{r}') \sum_n \partial_{r_\alpha r'_\beta}^2 \mathring{\mathcal{V}}_{0n}^{ij}(\mathbf{r}, \mathbf{r}') e^{i\mathbf{q}\cdot\mathbf{R}_n} \\ &= \delta_{ij} \sum_{s'} n_{s'}^{\text{ion}}(\mathbf{r}') \sum_{l'} \partial_{r_\alpha r'_\beta}^2 \mathring{\mathcal{V}}_{0l'}^{is'}(\mathbf{r}, \mathbf{r}') e^{i0\cdot\mathbf{R}_{l'}} - n_j^{\text{ion}}(\mathbf{r}') \sum_n \partial_{r_\alpha r'_\beta}^2 \mathring{\mathcal{V}}_{0n}^{ij}(\mathbf{r}, \mathbf{r}') e^{i\mathbf{q}\cdot\mathbf{R}_n} \\ &= 2\delta_{ij} \sum_{s'} n_{s'}^{\text{ion}}(\mathbf{r}') C_{\alpha\beta}^{is'}(\mathbf{r}, \mathbf{r}', \mathbf{q} = 0) - 2n_j^{\text{ion}}(\mathbf{r}') C_{\alpha\beta}^{ij}(\mathbf{r}, \mathbf{r}', \mathbf{q}), \end{aligned} \quad (2.69)$$

where the second derivative of the lattice Fourier transform of the Coulomb potential was denoted as

$$C_{\alpha\beta}^{ij}(\mathbf{r}, \mathbf{r}', \mathbf{q}) = \frac{1}{2} \partial_{r_\alpha r'_\beta}^2 \sum_n \mathring{\mathcal{V}}_{0n}^{ij}(\mathbf{r}, \mathbf{r}') e^{i\mathbf{q}\cdot\mathbf{R}_n}. \quad (2.70)$$

The numerical evaluation of this quantity is described in appendix A.2. The resulting expression for the ion-ion dynamical Matrix is thus

$$\begin{aligned} {}^{\text{ion}}D_{\alpha\beta}^{ij}(\mathbf{q}) &= \frac{1}{\sqrt{M_i M_j}} \int d\mathbf{r} \int d\mathbf{r}' n_i^{\text{ion}}(\mathbf{r}) \times \\ &\quad \times \left[ \delta_{ij} \sum_s n_{s'}^{\text{ion}}(\mathbf{r}') C_{\alpha\beta}^{is}(\mathbf{r}, \mathbf{r}', \mathbf{q} = 0) - n_j^{\text{ion}}(\mathbf{r}') C_{\alpha\beta}^{ij}(\mathbf{r}, \mathbf{r}', \mathbf{q}) \right]. \end{aligned} \quad (2.71)$$

If the individual ionic densities are spherical and do not overlap, as is the case when only core electrons are included, their Coulomb interaction is equal to the Coulomb interaction of point charges  $n_i^{\text{ion}}(\mathbf{r}) = Z_i^* \delta(\mathbf{r})$  with an effective ion charge  $Z_i^*$ . In this case, Eq. (2.71) simplifies to

$${}^{\text{ion}}D_{\alpha\beta}^{ij}(\mathbf{q}) = \frac{Z_i^*}{\sqrt{M_i M_j}} \left[ \delta_{ij} \sum_s Z_s^* \tilde{C}_{\alpha\beta}^{is}(\mathbf{q} = 0) - Z_j^* \tilde{C}_{\alpha\beta}^{ij}(\mathbf{q}) \right]. \quad (2.72)$$

with

$$\tilde{C}_{\alpha\beta}^{ij}(\mathbf{q}) = -\frac{1}{2} \partial_{r_\alpha r'_\beta}^2 \sum_n \mathring{\mathcal{V}}_{0n}^{ij}(0, \mathbf{r}) e^{i\mathbf{q}\cdot\mathbf{R}_n} \Big|_{(\mathbf{r}=\mathbf{0})} = -\partial_{r_\alpha r'_\beta}^2 \sum_n \frac{e^{i\mathbf{q}\cdot\mathbf{R}_n}}{|\mathbf{R}_n + \boldsymbol{\tau}_i - \boldsymbol{\tau}_j - \mathbf{r}|} \Big|_{(\mathbf{r}=\mathbf{0})}. \quad (2.73)$$

The functions  $\tilde{C}(\mathbf{q})$  can not be evaluated directly from Eq. (2.70) due to the long-range nature of the unscreened Coulomb potential which causes a very slow convergence of the Fourier series. A way out of this problem lies in the application of the Ewald summation method [Ewa21; Ewa38; Zim92], by which the sum is split into two rapidly converging sums over real and reciprocal lattice vectors,

$$\sum_n \frac{e^{i\mathbf{q}\cdot\mathbf{R}_n}}{|\mathbf{R}_n - \mathbf{r}|} = \frac{4\pi}{\Omega_{\text{BZ}}} \sum_k \frac{e^{-|\mathbf{G}_k + \mathbf{q}|^2/4\eta}}{|\mathbf{G}_k + \mathbf{q}|^2} e^{i(\mathbf{G}_k + \mathbf{q})\cdot\mathbf{r}} + \sum_l \frac{\text{erfc}(\eta|\mathbf{R}_l - \mathbf{r}|)}{|\mathbf{R}_l - \mathbf{r}|} e^{i\mathbf{q}\cdot\mathbf{R}_l}. \quad (2.74)$$

The sums run over all reciprocal lattice vectors  $\mathbf{G}_k$  and real lattice vectors  $\mathbf{R}_n$ , respectively, arranged according to length. The summations are truncated only after complete shells of vectors to avoid symmetry-related errors. The factor  $e^{-|\mathbf{G}_k + \mathbf{q}|^2/4\eta}$  causes a fast convergence of the reciprocal sum with increasing  $\mathbf{G}_k$ . The same holds for the complementary Gaussian error function, which is defined [Bro+01] as

$$\text{erfc}(x) = 1 - \text{erf}(x) = 1 - \frac{2}{\sqrt{\pi}} \int_0^x dt e^{-t^2} \quad (2.75)$$

and approaches zero quickly for increasing arguments. The result of the two sums is independent of the Ewald parameter  $\eta$ , which is chosen such that both sums converge rapidly and can be aborted after few elements. The first correct result for the dynamical matrix of ion lattices was published by Kellermann [Kel40], for which a didactic approach can be found in [Brü82]. The resulting expression reads

$$\begin{aligned} \tilde{C}_{\alpha\beta}^{ij}(\mathbf{q}) &= \frac{4\pi e^2}{\Omega_{\text{UC}}} \sum_k \frac{(\mathbf{G}_k + \mathbf{q})_\alpha (\mathbf{G}_k + \mathbf{q})_\beta}{|\mathbf{G}_k + \mathbf{q}|^2} e^{-|\mathbf{G}_k + \mathbf{q}|^2/4\eta} e^{i\mathbf{G}_k \cdot (\boldsymbol{\tau}_i - \boldsymbol{\tau}_j)} \\ &\quad + e^2 \sum_n e^{i\mathbf{q}\cdot\mathbf{R}_n} f_{\alpha\beta}(\mathbf{R}_n + \boldsymbol{\tau}_i - \boldsymbol{\tau}_j), \end{aligned} \quad (2.76)$$

where the coefficients  $f_{\alpha\beta}$  result from the second derivative and are given by

$$\begin{aligned} f_{\alpha\beta}(\mathbf{x}) &= \frac{x_\alpha x_\beta}{|\mathbf{x}|^5} \left[ 3\text{erfc}(\sqrt{\eta}|\mathbf{x}|) + 2\sqrt{\frac{\eta}{\pi}} |\mathbf{x}| \left( 3 + 2\eta |\mathbf{x}|^2 \right) e^{-\eta|\mathbf{x}|^2} \right] \\ &\quad - \frac{\delta_{\alpha\beta}}{|\mathbf{x}|^3} \left[ \text{erfc}(\sqrt{\eta}|\mathbf{x}|) + 2\sqrt{\frac{\eta}{\pi}} |\mathbf{x}| e^{-\eta|\mathbf{x}|^2} \right], \end{aligned} \quad (2.77)$$

It is important to note that  $\tilde{C}_{\alpha\beta}^{ij}(\mathbf{q})$  is not defined for  $\mathbf{q} = 0$ , since the reciprocal sum contains a divergent term. This is a result from the pure electrostatic derivation of this expression. This weakness can be corrected by approaching the problem electrodynamically and taking into account the electromagnetic field which is generated by the oscillating ions [Kel40]. In this case, the formula for  $\mathbf{q} \neq 0$  stays unchanged, but one obtains the expression

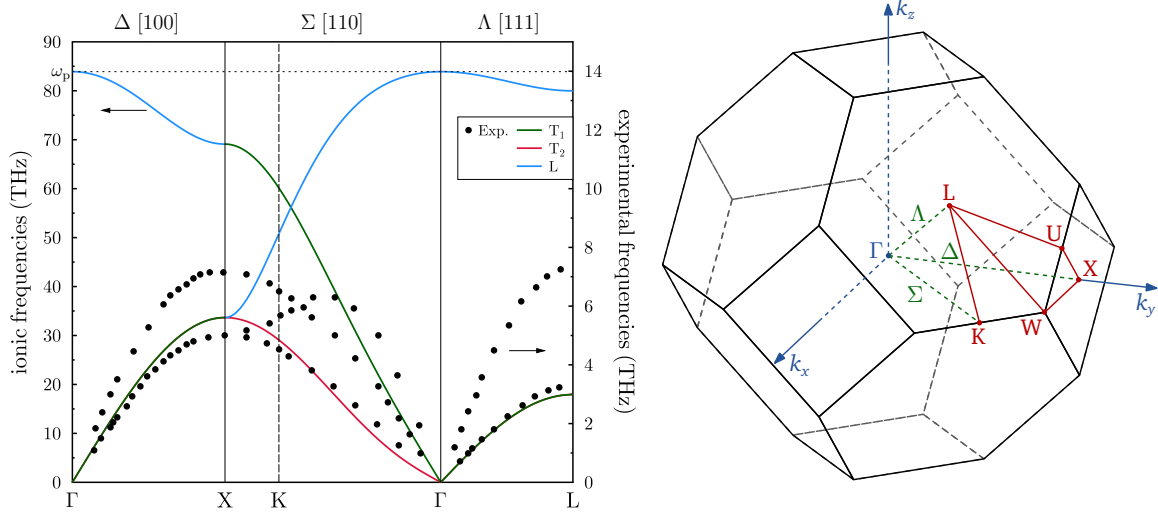
$$\begin{aligned} \tilde{C}_{\alpha\beta}^{ij}(\mathbf{q} = 0) &= \frac{4\pi e^2}{\Omega_{\text{UC}}} \sum_{\mathbf{G}_k \neq 0} \frac{(\mathbf{G}_k)_\alpha (\mathbf{G}_k)_\beta}{\mathbf{G}_k^2} e^{-\mathbf{G}_k^2/4\eta} \cos(\mathbf{G}_k \cdot (\boldsymbol{\tau}_i - \boldsymbol{\tau}_j)) \\ &\quad + e^2 \sum_n f_{\alpha\beta}(\mathbf{R}_n + \boldsymbol{\tau}_i - \boldsymbol{\tau}_j) \end{aligned} \quad (2.78)$$

for  $\mathbf{q} = 0$ .

It is most convenient to consider the above expression for ionic frequencies for the case of a monoatomic cubic crystal. In this case the dynamical matrix reduces to

$$\text{ion } D_{\alpha\beta}^{11}(\mathbf{q}) = \frac{(Z^*)^2}{M} \left[ \tilde{C}_{\alpha\beta}^{11}(\mathbf{q} = 0) - \tilde{C}_{\alpha\beta}^{11}(\mathbf{q}) \right]. \quad (2.79)$$

Fig. 2.2 (a) shows the lattice vibrational spectrum of a face-centred cubic (fcc) ion lattice along the high-symmetry lines  $\Delta$ ,  $\Sigma$  and  $\Lambda$  of the first Brillouin zone. This example represents a Cu crystal with ion charge  $Z^* = 11$  and without valence electrons. A scheme of the first Brillouin zone and the respective paths is shown in Fig. 2.2 (b).



(a) Comparison between calculated frequencies (solid lines) of a Cu ion lattice ( $Z^* = 11$ , face centred cubic lattice with a lattice parameter of  $6.83 a_0$ ) and experimental frequencies (black dots). The latter refer to the right hand frequency axis and are scaled by a factor of 6 to allow for better comparability.

(b) First Brillouin zone of the fcc lattice. Latin letters denote selected points of high symmetry and are connected by red lines for convenience. The three high-symmetry lines  $\Lambda$ ,  $\Sigma$  and  $\Delta$  correspond to the paths used in (a). Of line  $\Sigma$ , only the part  $\overline{K\Gamma}$  is shown. The remaining segment  $\overline{XK}$ , reaching into the neighbouring Brillouin Zone, is equivalent to  $\overline{XU}$ .

**Figure 2.2:** Lattice vibrational frequencies on high symmetry lines of a simple fcc lattice.

The discussion of lattice vibrational frequencies is most transparent for lines and points of high symmetry within the first Brillouin zone due to the existence of pure longitudinally and transversal polarized modes. As opposed to this, mixed modes occur in arbitrary propagation directions. Since the Ewald parameter  $\eta$  in  $\tilde{C}_{\alpha\beta}^{ij}$  has no influence on the converged result, it can be chosen sufficiently large that the sum over real lattice vectors vanishes. In case of a monoatomic lattice the phase factor  $e^{i\mathbf{G}\cdot(\boldsymbol{\tau}_i - \boldsymbol{\tau}_j)}$  equals 1 and it becomes clear that the matrix becomes diagonal in  $(\alpha, \beta)$  and reduces to

$${}^{\text{ion}}D_{\alpha\alpha}^{11}(\mathbf{q}) = \frac{4\pi(Z^*)^2 e^2}{M\Omega_{\text{UC}}} \left[ \sum_{\mathbf{G} \neq 0} \frac{G_\alpha^2}{G^2} - \sum_{\mathbf{G}} \frac{(\mathbf{G} + \mathbf{q})_\alpha^2}{|\mathbf{G} + \mathbf{q}|^2} \right] \quad (2.80)$$

In the following, the behaviour of the dynamical matrix on the  $\Delta$  line shall be briefly discussed. On this path, the  $\mathbf{q}$  vector can take values of  $(q_x, 0, 0)$  with  $q_x \in [0, \pi/a]$ , which means that the longitudinal mode with amplitude parallel to  $\mathbf{q}$  is represented by  $\alpha = x$ , and the parallel modes are represented by  $\alpha = y, z$ . In case of the latter, the matrix approaches

$$\lim_{\mathbf{q} \rightarrow 0} [{}^{\text{ion}}D_{\alpha\alpha}^{11}(\mathbf{q})] \propto \lim_{\mathbf{q} \rightarrow 0} \sum_{\mathbf{G} \neq 0} \frac{G_\alpha^2}{G^2} \left[ 1 - \frac{G^2}{(\mathbf{G} + \mathbf{q})^2} \right] = 0 \quad (2.81)$$

in the limit of long wavelength or small  $\mathbf{q}$ . Furthermore, the matrix elements approach the  $\Gamma$  point like  $q^2$ , resulting in a linear behaviour of the frequency. In contrast, the limit for the

longitudinal mode reads

$$\lim_{\mathbf{q} \rightarrow 0} [\text{ion} D_{\alpha\alpha}^{11}(\mathbf{q})] \propto \lim_{\mathbf{q} \rightarrow 0} \sum_{\mathbf{G} \neq 0} \left[ \left( \frac{G_{\alpha}^2}{G^2} - \frac{(\mathbf{G} + \mathbf{q})_{\alpha}^2}{(\mathbf{G} - \mathbf{q})^2} \right) - \frac{q_{\alpha}^2}{q^2} \right] = 1, \quad (2.82)$$

resulting in a finite frequency for long wavelengths. The reason for the long wavelength-behaviour of longitudinal modes can be understood as a result of the long-range Coulomb interaction in a positively charged ionic lattice, which behaves similar to a plasma of equally charged particles. Thus, the limiting frequency is given by the ion plasma frequency [Zim92]

$$\omega_p = \sqrt{\frac{Z^2 e^2}{\epsilon_0 \Omega_{UC} M}} \quad (\text{SI units}) \quad (2.83)$$

$$\omega_p = \sqrt{4\pi \frac{Z^2 e^2}{\Omega_{UC} M}} \quad (\text{ARU}). \quad (2.84)$$

The above described behaviour of different polarization branches is illustrated in Fig. 2.2 (a). Additionally, this plot shows the experimentally obtained phonon frequencies of Cu [Nic+67] (black dots). These are multiplied by a factor of 6 compared to the ionic frequencies and correspond to the right-hand scale. It becomes apparent that the behaviour of measured transverse modes, apart from their absolute values, is very similar to the respective ionic frequencies. This indicates that the presence of valence electrons effectively reduces the ion charge due to screening. The effect on longitudinal modes is different: Apart from scaling the frequencies, the valence electrons cause the longitudinal band to vanish at the  $\Gamma$  point similar to transverse modes. This effect can be understood by the electrostatic screening of the ion charge by the surrounding valence electrons and thus an effective range decrease of the ion-ion Coulomb interaction. In the limit of long wavelengths, neighbouring atoms are only weakly polarized and the effective forces between them vanish, and with them the frequency.

# Linear response theory from first principles

A widely used concept in physics is the assumption that a small external perturbation to a system near its equilibrium state causes a response which can well be described as proportional to the perturbation. Especially in the quantum mechanics of many-body systems, where exact solutions of the Schrödinger equation are impossible, this is, among other perturbative techniques, an important approach.

A modern method for solving the Schrödinger equation, which is very common in quantum chemistry and computational physics, is density functional theory. Instead of trying to solve the Schrödinger equation for every electron in its complex environment, it allows to determine the ground state electron density from an effective single-particle system in which the complex interactions between electrons are mapped onto effective potentials. This ab-initio method has been extended to time-dependent problems and can also be used in combination with linear response theory, allowing for the determination of excited states from ground state properties.

In this chapter, the basic principles of linear response theory are outlined and its application to electron densities is shown. Afterwards, an introduction to density functional theory (DFT) and its time-dependent generalization (TDDFT) is given. The last section shows how excitations induced by external fields can be treated by combining linear response and TDDFT.

## 3.1 Introduction to linear response

As first derived by R. Kubo in 1957 [Kub57; Kub66], the response to an external perturbation in linear response theory is given by the so called *Kubo formula*. The starting point for its derivation is a system in equilibrium state, described by the Hamiltonian  $\hat{H}_0$  with a complete set of eigenstates  $\{|n\rangle\}$  and eigenvalues  $\{E_n\}$ . As known from statistical quantum mechanics [BF04], the expectation value of an operator  $\hat{O}$  is given as

$$\langle \hat{O} \rangle = \frac{1}{Z_0} \text{Tr} [\hat{\rho}_0 \hat{O}] = \frac{1}{Z_0} \sum_n \langle n | \hat{O} | n \rangle e^{-\beta E_n}, \quad (3.1)$$

where  $Z_0 = \sum_n e^{-\beta E_n}$  is the canonical partition function and  $\beta = 1/k_B T$ . According to this, the equilibrium density operator  $\hat{\rho}_0$  is defined as

$$\hat{\rho}_0 = e^{-\beta \hat{H}_0} = \sum_n |n\rangle \langle n| e^{-\beta E_n}. \quad (3.2)$$

At  $t = t_0$  a small external perturbation  $V(t)$  is acting on the system, changing the Hamiltonian to

$$\hat{H}(t) = \hat{H}_0 + V(t)\theta(t - t_0). \quad (3.3)$$

For  $V(t)$  is small, it is reasonable to make use of the interaction picture representation  $|\hat{n}(t)\rangle$  which is related to the time-dependent state vector  $|n(t)\rangle$  by

$$|n(t)\rangle = e^{-i\hat{H}_0 t/\hbar} |\hat{n}(t)\rangle = e^{-i\hat{H}_0 t/\hbar} \hat{U}(t, t_0) |\hat{n}(t_0)\rangle = e^{-i\hat{H}_0 t/\hbar} \hat{U}(t, t_0) |n\rangle, \quad (3.4)$$

$$|\hat{n}(t_0)\rangle = e^{i\hat{H}_0 t_0/\hbar} |n(t_0)\rangle \quad (3.5)$$

with a unitary operator  $\hat{U}(t, t_0)$  describing the time evolution of the state  $|n\rangle$ . An application of the time-dependent Schrödinger equation  $i\hbar\partial_t|n(t)\rangle = H(t)|n(t)\rangle$  yields

$$\hat{U}(t, t_0) = 1 - \frac{i}{\hbar} \int_{t_0}^t dt' \underbrace{e^{i\hat{H}_0 t'/\hbar} V(t') e^{-i\hat{H}_0 t'/\hbar}}_{\hat{V}_I(t')} \hat{U}(t'), \quad (3.6)$$

which can be solved iteratively. The smallness of  $V_I(t)$  justifies the truncation of the resulting series after the linear term, giving

$$\hat{U}(t, t_0) = 1 - \frac{i}{\hbar} \int_{t_0}^t dt' \hat{V}_I(t'). \quad (3.7)$$

Plugging this result into Eq. (3.1) and considering only terms linear in  $\hat{V}_I(t)$ , one obtains the Kubo formula

$$\begin{aligned} \delta\langle\hat{O}(t)\rangle &= \langle\hat{O}(t)\rangle - \langle\hat{O}\rangle_0 = -\frac{i}{\hbar} \int_{t_0}^t dt' \langle[\hat{O}_I(t), \hat{V}_I(t')]\rangle_0 \\ &= \int_{t_0}^{\infty} dt' \chi_{\hat{O}\hat{V}}(t, t') \end{aligned} \quad (3.8)$$

which gives the linear response of the equilibrium quantity  $\langle\hat{O}\rangle$  to an external perturbation  $V(t)$  in form of a retarded correlation function

$$\chi_{\hat{O}_I\hat{V}_I}(t, t') = -\frac{i}{\hbar} \theta(t - t') \langle[\hat{O}_I(t), \hat{V}_I(t')]\rangle_0 \quad (3.9)$$

which is often referred to as generalized susceptibility. In the common case where the external perturbation can be expressed a product  $\hat{V}(t) = \hat{P}f(t)$  of a time-independent operator and an ordinary function of time, the susceptibility can be rewritten as

$$\chi_{\hat{O}\hat{P}}(t, t') = \chi_{\hat{O}\hat{P}}(t - t')f(t'), \quad (3.10)$$

giving rise to a modification of (3.8) as

$$\delta\langle\hat{O}(t)\rangle = \int_{-\infty}^{\infty} dt' \chi_{\hat{O}\hat{P}}(t - t')f(t'). \quad (3.11)$$

In this expression it was further assumed that the external potential  $\hat{V}$  was switched on at a moment  $t_0$  so long ago that the system has reached a new steady state. This assumption would be inappropriate when the description of such a switching process itself was of interest. The above equation has the form of a convolution and thus has the simple Fourier transform

$$\delta\langle\hat{O}(\omega)\rangle = \chi_{\hat{O}\hat{P}}(\omega)f(\omega), \quad (3.12)$$

which shows that the frequency of the linear response is equal to the frequency of the external perturbation.

The above description was limited to homogeneous systems with spatially independent perturbations. Assuming instead a perturbing operator of the form

$$\hat{V}(t) = \int d\mathbf{x} f(\mathbf{x}, t)\hat{P}(\mathbf{x}), \quad (3.13)$$

Eq. (3.10) still holds and because of the linearity of the Kubo formula the following set of equations is obtained:

$$\delta\langle\hat{O}(\mathbf{x}, t)\rangle = \int d\mathbf{x} \int_{t_0}^{\infty} dt' \chi(\mathbf{x}t, \mathbf{x}'t') f(\mathbf{x}, t') \quad (3.14)$$

$$\chi(\mathbf{x}t, \mathbf{x}'t') = \chi_{\hat{O}(\mathbf{x})\hat{P}(\mathbf{x}')} (t - t') = -\frac{i}{\hbar}\theta(t - t') \left\langle \left[ \hat{O}_I(\mathbf{x}, t), \hat{P}_I(\mathbf{x}', t') \right] \right\rangle_0.$$

The following section will shed some light on the practical use of these equations when applied to an ensemble of electrons in an external potential.

### 3.2 Electron density correlation function

One of the most important applications of linear response theory lies in the study of excitations in electronic systems induced by weak external forces. It is useful to describe such a system of interacting fermions in terms of quantum field operators. The unperturbed Hamiltonian reads [FW71]

$$\begin{aligned} \hat{H}_0 = & \sum_{\alpha=\uparrow\downarrow} \int d\mathbf{x} \psi_{\alpha}^{\dagger}(\mathbf{x}) \frac{1}{2m_e} \left( \frac{\hbar}{i} \nabla \right)^2 \psi_{\alpha}(\mathbf{x}) \\ & + e \int d\mathbf{x} \hat{n}(\mathbf{x}) \mathcal{V}(\mathbf{x}) \\ & + \frac{1}{2} \sum_{\alpha=\uparrow\downarrow} \sum_{\beta=\uparrow\downarrow} \int d\mathbf{x} \int d\mathbf{x}' \psi_{\alpha}^{\dagger}(\mathbf{x}) \psi_{\beta}^{\dagger}(\mathbf{x}') \psi_{\beta}(\mathbf{x}') \psi_{\alpha}(\mathbf{x}) V(\mathbf{x}, \mathbf{x}'), \end{aligned} \quad (3.15)$$

in which  $V(\mathbf{x}, \mathbf{x}')$  defines the Coulomb repulsion of two particles at places  $\mathbf{x}$  and  $\mathbf{x}'$ . The scalar, time-independent external potential  $\mathcal{V}(\mathbf{x})$  which is assumed to be diagonal in spin space couples to the system by means of the density operator

$$\hat{n}(\mathbf{r}) = \sum_{\alpha=\uparrow\downarrow} \psi_{\alpha}^{\dagger}(\mathbf{r}) \psi_{\alpha}(\mathbf{r}). \quad (3.16)$$

$\mathcal{V}$  is responsible for the electronic properties of the system. For instance, in a solid this can be the periodic potential of the atomic nuclei. An important question is how the electronic density is influenced if a small additional potential  $\delta\mathcal{V}(\mathbf{x}, t)$  is applied. By making use of Eq. (3.13), it becomes clear that the time-dependent operator

$$H'(t) = \int d\mathbf{x} \delta\mathcal{V}(\mathbf{x}, t) \hat{n}(\mathbf{x}) \quad (3.17)$$

has to be added to the Hamiltonian  $\hat{H}_0$ . In analogy to Eqs. (3.14), the linear response of the electron density is found to be

$$\delta\langle\hat{n}(\mathbf{x}, t)\rangle = \int d\mathbf{x} \int_{t_0}^{\infty} dt' \chi(\mathbf{x}t, \mathbf{x}'t') \delta\mathcal{V}(\mathbf{x}, t') \quad (3.18)$$

$$\chi(\mathbf{x}t, \mathbf{x}'t') = \chi_{\hat{n}(\mathbf{x})\hat{n}(\mathbf{x}')} (t - t') = -\frac{i}{\hbar}\theta(t - t') \left\langle \left[ \hat{n}_I(\mathbf{x}, t), \hat{n}_I(\mathbf{x}', t') \right] \right\rangle_0.$$

Again, causality is ensured by the Heavyside step function which ensures that only values of  $\delta\mathcal{V}(\mathbf{x}, t')$  for  $t' < t$  determine the evolution of  $\delta\langle\hat{n}(\mathbf{x}, t)\rangle$ . By application of Eq. (3.1) one

obtains

$$\chi(\mathbf{x}, \mathbf{x}', t - t') = -\frac{i}{\hbar} \theta(t - t') \sum_j \frac{e^{-\beta E_j}}{Z_0} \left[ \langle \Psi_j | \hat{n}_I(\mathbf{x}, t) \hat{n}_I(\mathbf{x}', t') | \Psi_j \rangle - \langle \Psi_j | \hat{n}_I(\mathbf{x}', t') \hat{n}_I(\mathbf{x}, t) | \Psi_j \rangle \right] \quad (3.19)$$

and inserting the completeness relation

$$\sum_{i=1}^{\infty} |\Psi_i\rangle \langle \Psi_i| = \hat{1} \quad (3.20)$$

yields

$$\chi(\mathbf{x}, \mathbf{x}', t - t') = -\frac{i}{\hbar} \theta(t - t') \left[ \sum_{ij} \frac{e^{-\beta E_j}}{Z_0} \langle \Psi_j | \hat{n}_H(\mathbf{x}) | \Psi_i \rangle \langle \Psi_i | \hat{n}_H(\mathbf{x}') | \Psi_j \rangle - \sum_{ji} \frac{e^{-\beta E_j}}{Z_0} \langle \Psi_i | \hat{n}_H(\mathbf{x}) | \Psi_j \rangle \langle \Psi_j | \hat{n}_H(\mathbf{x}') | \Psi_i \rangle \right]. \quad (3.21)$$

By a permutation of the summation indices in the second sum as well as making use of the occupation numbers  $f_i = e^{-\beta E_i} / Z_0$ , the response function can be written as

$$\begin{aligned} \chi(\mathbf{x}, \mathbf{x}', t - t') &= -\frac{i}{\hbar} \theta(t - t') \sum_{ij} (f_j - f_i) \langle \Psi_j | \hat{n}_H(\mathbf{x}) | \Psi_i \rangle \langle \Psi_i | \hat{n}_H(\mathbf{x}') | \Psi_j \rangle, \\ &= -\frac{i}{\hbar} \theta(t - t') \sum_{ij} (f_j - f_i) \langle \Psi_j | \hat{n}(\mathbf{x}) | \Psi_i \rangle \langle \Psi_i | \hat{n}(\mathbf{x}') | \Psi_j \rangle e^{-\frac{i}{\hbar} (E_j - E_i)(t - t')}, \end{aligned} \quad (3.22)$$

while in the last step the definition of the Heisenberg operators was used. This expression is often referred to as Lehmann or spectral representation [Käl52; Leh54]. By means of a Fourier transform, the susceptibility can be written in frequency space as

$$\chi(\mathbf{x}, \mathbf{x}', \omega) = \lim_{\eta \rightarrow 0^+} \int_0^{\infty} dt \chi(\mathbf{x}, \mathbf{x}', t) e^{i(\omega + i\eta)t} \quad (3.23)$$

$$= \lim_{\eta \rightarrow 0^+} \sum_{ij} (f_j - f_i) \frac{\langle \Psi_j | \hat{n}(\mathbf{x}) | \Psi_i \rangle \langle \Psi_i | \hat{n}(\mathbf{x}') | \Psi_j \rangle}{E_j - E_i - \hbar\omega - i\hbar\eta} \quad (3.24)$$

where the complex frequency  $\omega + i\eta$  has been introduced to ensure convergence of the Fourier integral. This picture has a clear physical interpretation: The density correlation function has poles at frequencies where transitions between occupied and unoccupied states occur and thus delivers information about excited states calculated from the ground state eigenfunctions of the unperturbed Hamiltonian.

### 3.3 Time dependent density functional theory

The goal of modern electronic structure theory is to describe an ensemble of electrons and nuclei whose behaviour is defined by the Hamiltonian (2.2). As discussed in section 2.2, it is sufficient in most cases to consider only those parts of the operator which act on electronic coordinates, resulting in the solution of Schrödinger equation for an inhomogeneous

electron gas in an external potential. The solution of this equation is the many-particle wave function of the  $N_e$  electrons populating the system and thus still a very complicated object.  $\Psi$  is a function of  $2 \cdot 3N_e$  electronic coordinates, each of which in a numerical calculation has to be represented on a mesh of  $p$  points. This results in  $p^{6N_e}$  floating point values which have to be stored during a calculation, making such a calculation a hard task even for single atoms. In contrast, the electron density, which for a normalized many-particle wave function  $\Psi$  is given by

$$n(\mathbf{x}) = N_e \sum_{\sigma, \sigma_2 \dots \sigma_{N_e}} \int d\mathbf{x}_2 \cdots \int d\mathbf{x}_{N_e} |\Psi(\mathbf{x}\sigma, \mathbf{x}_2\sigma_2 \cdots \mathbf{x}_{N_e}\sigma_{N_e})|^2, \quad (3.25)$$

is a simple function of space and often contains all physically relevant informations about the system under consideration. The first theory which dealt with the density as basic variable was proposed by Thomas and Fermi [Tho27; Fer28] but was only of limited predictive power, mainly due to the neglect of exchange and correlation effects. Modern density functional theory includes both in form of an effective potential acting on non-interacting auxiliary particles. The following description of basic DFT closely follows the expositions in [Gon00] and [GM12].

### 3.3.1 Hohenberg-Kohn theorems

In what follows, the description of electronic systems, defined by the Born-Oppenheimer Hamiltonian

$$\mathcal{H}_{\text{BO}} = \hat{T}_e(\{\mathbf{x}\}) + V_{\text{ee}}(\{\mathbf{x}\}) + \mathcal{V}(\{\mathbf{R}\}) \quad (3.26)$$

shall be of interest. The external potential  $\mathcal{V}(\{\mathbf{R}\})$  is not necessarily limited to Coulomb interactions, but in many applications it is given by the Coulomb potential of atomic nuclei of the system under concern. In all cases, this potential defines the system and determines its electronic structure. The fact that this relation is invertible is one of the keys to DFT. In their important paper from 1964 [HK64], Hohenberg and Kohn proved two theorems which laid the foundation of modern DFT:

First, the external potential acting on the electrons in their ground state is, up to an additive constant, defined by the electron density. Thus, the total energy can be written as a functional of the electron density as opposed to the wave function:

$$\begin{aligned} E_0 &= \langle \Psi_0 | \mathcal{H}_{\text{BO}} | \Psi_0 \rangle = E[n_0] = T[n_0] + U_{\text{ee}}[n_0] + \mathcal{V}[n_0] \\ &= F[n_0] + \int d\mathbf{r} n_0(\mathbf{x}) \mathcal{V}(\mathbf{x}). \end{aligned} \quad (3.27)$$

$F[n]$  is a universal functional of the density because it is independent of the external potential and is composed of

$$F[n] = T_e[n] + U_{\text{ee}}[n], \quad (3.28)$$

where the functional  $T_e[n]$  gives the kinetic energy of the fully interacting electron gas and  $U_{\text{ee}}[n]$  represents the energy contributed by all other interelectronic interactions. The latter can be further decomposed into

$$U_{\text{ee}}[n] = U_{\text{H}}[n] + K[n] = \frac{1}{2} \frac{e^2}{4\pi\epsilon_0} \int d\mathbf{x} \int d\mathbf{x}' \frac{n(\mathbf{x})n(\mathbf{x}')}{|\mathbf{x} - \mathbf{x}'|} + K[n], \quad (3.29)$$

with the first term being the classical Hartree energy and the functional  $K[n]$  containing all remaining contributions arising from the Pauli principle as well as the correlated motion of the electrons.  $\mathcal{V}[n_0]$  denotes the expectation value of the external potential as a functional

of the ground state density. The potential  $\mathcal{V}(\mathbf{x})$  in Eq. (3.27) is the external potential at point  $\mathbf{x}$ . In case of a periodic crystal, it reads

$$\mathcal{V}(\mathbf{x}) = \frac{1}{4\pi\epsilon_0} \sum_{ls} \frac{Z_s e}{|\mathbf{R}_l + \tau_s - \mathbf{x}|}, \quad (3.30)$$

where the sums run over all lattice vectors  $\mathbf{R}_l$  and site indices  $s$  within the unit cell.

The second theorem implies that the ground state density minimizes the energy functional under the constraint of fixed particle number and the condition

$$E_0 \leq E[n]. \quad (3.31)$$

In analogy to the Reyleigh-Ritz principle [No106] for wave functions, the density satisfies a variational principle

$$\delta \tilde{E}[n(\mathbf{x})] = \delta \left\{ E[n] - \mu \int d\mathbf{x} n(\mathbf{x}) - N \right\} = 0 \quad (3.32)$$

where the chemical potential  $\mu$  enters as Lagrange parameter which, together with Eq. (3.27), is defined as

$$\mu = \mathcal{V}(\mathbf{x}) + \frac{\delta F[n]}{\delta n(\mathbf{x})}. \quad (3.33)$$

This scheme, in principle, offers a way to obtain the exact ground state density. A direct numerical implementation is, however, a difficult task and turns out to be limited in accuracy.

### 3.3.2 Kohn-Sham equations

Kohn and Sham [KS65] presented an efficient numerical method at the cost of reintroducing wave functions. They defined a reference system of non-interacting electrons obeying the single particle Schrödinger equation  $\hat{h}_s \phi_i = \epsilon_i \phi_i$  and

$$\hat{h}_s = -\frac{\hbar^2}{2m_e} \nabla^2 + v_s(\mathbf{x}). \quad (3.34)$$

The spin orbitals  $\phi_i$  are then exactly given by linear combinations of Slater determinants. Furthermore, they are assumed to represent a unique decomposition of the exact ground state density via

$$n(\mathbf{x}) = \sum_i \theta(\mu - \epsilon_i) |\phi_i(\mathbf{x})|^2. \quad (3.35)$$

The kinetic energy is given by

$$T_s = \sum_i \langle \phi_i | -\frac{\hbar^2}{2m_e} \nabla^2 | \phi_i \rangle, \quad (3.36)$$

which is different from the kinetic energy functional  $T[n]$  of the interacting system. The universal functional  $F[n]$  can now be rewritten as

$$F[n] = T_s[n] + U_H + E_{xc}[n], \quad (3.37)$$

where the *exchange-correlation energy* is defined as

$$E_{XC}[n] = T[n] - T_s[n] + U_{ee} - U_H, \quad (3.38)$$

containing all contributions which arise from the many-particle nature of the interacting system. Still, an approximation for  $E_{xc}$  has to be found, while  $T_s$  is exactly known in terms

of spin orbitals. This is useful because  $T_s$  is a much larger quantity than  $E_{xc}$ . Apart from that,  $T_s$  mainly accounts for density oscillations which are well described within the Kohn-Sham scheme [PK03].

With the above definition of the universal functional  $F[n]$ , Eq. (3.33) becomes in the single-particle picture

$$\mu_s = v_{\text{eff}}(\mathbf{x}) + \frac{\delta T_s[n]}{\delta n(\mathbf{x})}, \quad (3.39)$$

where the effective Kohn-Sham potential is defined as

$$\begin{aligned} v_{\text{eff}}(\mathbf{x}) = v_s(\mathbf{x}) &= \mathcal{V}(\mathbf{x}) + \frac{\delta U_H[n]}{\delta n(\mathbf{x})} + \frac{\delta E_{xc}[n]}{\delta n(\mathbf{x})} \\ &= \mathcal{V}(\mathbf{x}) + \frac{1}{4\pi\epsilon_0} \int d\mathbf{x}' \frac{n(\mathbf{x}')}{|\mathbf{x} - \mathbf{x}'|} + v_{xc}(\mathbf{x}). \end{aligned} \quad (3.40)$$

Assuming that the chemical potentials  $\mu$  and  $\mu_s$  are identical under the constraint of particle number conservation, the solutions of the single-particle Schrödinger equation

$$\left[ -\frac{\hbar^2}{2m_e} \nabla^2 + v_{\text{eff}}(\mathbf{x}) \right] \phi_i(\mathbf{x}) = \epsilon_i \phi_i(\mathbf{x}) \quad (3.41)$$

yield the exact ground state density

$$n(\mathbf{r}) = \sum_i^{\text{occ}} |\phi_i(\mathbf{r})|^2. \quad (3.42)$$

Eqns. (3.40) to (3.42) are called the Kohn-Sham equations and have to be solved in a self-consistent procedure. The starting point for this iterative procedure usually is an educated guess (e.g. a sum of atomic densities) for  $n(\mathbf{x})$  from which the effective potential is calculated. In the next step, a solution of Eq. (3.41) is achieved, whence a new density follows via Eq. (3.42). This procedure is repeated and finalizes after  $m$  steps when  $\|n_m(\mathbf{x}) - n_{m-1}(\mathbf{x})\|$  is smaller than a predefined convergence parameter (see also Fig. 4.3 on p. 47).

The Kohn-Sham procedure was later generalized to the treatment of spin-dependent systems by von Barth and Hedin [BH72]. In the case of collinear magnetism, in which all magnetic moments are aligned parallel, the spin-dependent density can be expressed as

$$n^\sigma(\mathbf{x}) = \sum_i^{\text{occ}} |\phi_i^\sigma(\mathbf{x})|^2 \quad (3.43)$$

where the spin index can take the two states  $\sigma = \uparrow, \downarrow$ . The total density  $n(\mathbf{x})$  and the magnetization density  $m(\mathbf{x})$  are expressed as

$$n(\mathbf{x}) = n^\uparrow(\mathbf{x}) + n^\downarrow(\mathbf{x}) \quad (3.44)$$

$$m(\mathbf{x}) = n^\uparrow(\mathbf{x}) - n^\downarrow(\mathbf{x}). \quad (3.45)$$

According to this description, the spin-dependent Kohn-Sham potential takes the form

$$v_{\text{eff}}^\sigma(\mathbf{x}) = V^{\text{ext}}(\mathbf{x}) + \frac{1}{4\pi\epsilon_0} \int d\mathbf{x}' \frac{n(\mathbf{x}')}{|\mathbf{x} - \mathbf{x}'|} + \frac{\delta E_{XC}[n^\uparrow(\mathbf{x}), n^\downarrow(\mathbf{x})]}{\delta n^\sigma(\mathbf{x})} \quad (3.46)$$

and defines the spin-dependent Kohn-Sham equations

$$\left[ -\frac{\hbar^2}{2m_e} \nabla^2 + v_{\text{eff}}^\sigma(\mathbf{x}) \right] \phi_i^\sigma(\mathbf{x}) = \epsilon_i^\sigma \phi_i^\sigma(\mathbf{x}), \quad (3.47)$$

where the eigenvalues are spin-dependent, too. However, in this work only non-spin-polarized systems are under concern.

### 3.3.3 Exchange-correlation energy

Up to this point, the Kohn-Sham method is, in principle, exact. For a practical application of the presented theory, however, an explicit expression of the exchange-correlation energy functional  $E_{xc}$  is needed. This is only possible in an approximative scheme, which makes the results of DFT calculations mainly dependent on the choice of the model functional, of which a great variety has been presented until today [SS05].

The simplest and still most frequently used in computational solid state physics has been already proposed by Kohn and Sham and originates from Thomas-Fermi theory. The *local density approximation* (LDA) foosts on the assumption that the exchange-correlation energy of a spatially slowly varying, interacting electron gas can be approximated by the respective value of a uniform one. It is defined as

$$E_{xc}^{\text{LDA}}[n] = \int d\mathbf{x} n(\mathbf{x}) \epsilon_{xc}^{\text{hom}}(n(\mathbf{x})), \quad (3.48)$$

where the *function*  $\epsilon_{xc}^{\text{hom}}(n)$  is the exchange-correlation energy per particle of a homogeneous electron gas of density  $n$ . Consequently, the LDA exchange-correlation potential reads

$$v_{xc}^{\text{LDA}} = \frac{\delta E_{xc}^{\text{LDA}}[n]}{\delta n(\mathbf{x})} = \epsilon_{xc}^{\text{hom}}(n(\mathbf{x})) + n(\mathbf{x}) \left. \frac{d}{dn} \epsilon_{xc}^{\text{hom}}(n) \right|_{n=n(\mathbf{x})}. \quad (3.49)$$

The function  $\epsilon_{xc}(n)$  can be separated into an exchange and a correlation part [Lev96; Zel06],

$$\epsilon_{xc}^{\text{hom}}(n) = \epsilon_x(n) + \epsilon_c(n), \quad (3.50)$$

of which the first can be derived analytically to

$$\epsilon_x(n) = -\frac{3}{4} e^2 \left( \frac{3}{\pi} \right)^{1/3} n^{1/3}, \quad (3.51)$$

being identical to the corresponding Hartree-Fock result. For the correlation part, only limiting cases can be expressed analytically. Very often, the Monte Carlo results of Ceperley and Alder [CA80] have been used for parametric representations of  $\epsilon_c(n)$ , such as the approximation of Perdew and Wang [PW92] which was used in this work.

Surprisingly, this approximation has proven as accurate enough for many systems, especially crystals, even though their density is highly inhomogeneous [JG89]. The first approximations beyond LDA have been developed in form of *generalized gradient approximations* (GGA) [PW86; PW89; PBE96; PBE97] which are also local but include expansions of the gradient of the density. Further improvements have been achieved in recent years [Mat02] by introducing hybrid functionals [Bec93] and using the Jacobs Ladder [PS01] scheme to construct better functionals.

### 3.3.4 Generalization to time dependent problems

Time dependent density functional theory (TDDFT) is the natural generalization of static DFT to time-dependent problems. As DFT can be seen as an alternative formulation of steady-state quantum mechanics, TDDFT is an alternative to the time-dependent Schrödinger equation as it allows the treatment of arbitrary time-dependent problems and excitations. The first time-dependent Kohn-Sham calculations appeared more than a decade after the introduction of standard DFT, such as [And77; ZS80], and demonstrated the power of the method for photoabsorption calculations. However, the existence of a time-dependent Hohenberg-Kohn theorem was assumed, but for a long time unproven. A formal proof, which built the foundation of modern TDDFT, was given by Runge and Gross in 1984

[RG84]. Later, the theory was also extended to spin-polarized systems [LV89]. The principal statement of the Runge-Gross theorem is that there exists a one-to-one correspondence between an external, time-dependent potential  $\mathcal{V}(\mathbf{x}, t)$  and the density  $n(\mathbf{x}, t)$  for a many-body system evolving from a fixed initial state  $\Psi_0$ , which is not necessarily the ground state. The proof is more complicated than for the Hohenberg-Kohn theorem because the total energy is not a conserved quantity and thus no variational principle exists.

Practical use of TDDFT can be made by introducing time-dependent Kohn-Sham equations. One seeks for the solutions of the time-dependent single-particle Schrödinger equation

$$i\frac{\partial}{\partial t}\phi_i(\mathbf{x}, t) = \left[ -\frac{\hbar^2}{2m}\nabla^2 + v_{\text{eff}}(\mathbf{x}, t) \right] \phi_i(\mathbf{x}, t), \quad (3.52)$$

yielding the density

$$n(\mathbf{x}, t) = \sum_i^{\text{occ}} |\phi_i(\mathbf{x}, t)|^2. \quad (3.53)$$

The effective potential is, in analogy to Eq. (3.40), defined as

$$v_{\text{eff}}(\mathbf{x}, t) = \mathcal{V}(\mathbf{x}, t) + \int d\mathbf{x}' \frac{n(\mathbf{x}', t)}{|\mathbf{x} - \mathbf{x}'|} + v_{\text{xc}}(\mathbf{x}, t). \quad (3.54)$$

Since these time-dependent equations represent an initial value problem, the solutions depend on the initial states  $\phi_i(\mathbf{x}, t_0)$ .

Due to causality, the exchange-correlation potential  $v_{\text{xc}}(\mathbf{x}, t)$  does not only depend on the density at time  $t$ , but also on the initial interacting state  $\Psi_0$  as well as on the initial non-interacting Kohn-Sham functions. This makes the construction of exchange-correlation functionals for TDDFT much more difficult than in the case of static DFT. It was shown [Lee98; MG04] that the exchange-correlation potential can be written as the functional derivative

$$v_{\text{xc}}(\mathbf{x}, t) = \left. \frac{\delta A_{\text{xc}}[n]}{\delta n(\mathbf{x}, \tau)} \right|_{n=n(\mathbf{x}, t)} \quad (3.55)$$

where  $A_{\text{xc}}$  is a quantum-mechanical action functional, derived from the Keldysh formalism [Kel65], and  $\tau$  is the Keldysh time contour parameter. However, approximations to  $v_{\text{xc}}$  have to be made for practical uses.

A simple way to use the functionals already known from ground state DFT is the adiabatic approximation [MG03], which takes the density  $n(\mathbf{x}, t)$  as input function for a ground-state exchange-correlation potential

$$v_{\text{xc}}^{\text{adiabatic}}(\mathbf{x}, t) = v_{\text{xc}}^{\text{DFT}}[n] \Big|_{n=n(\mathbf{x}, t)}. \quad (3.56)$$

This is a crucial approximation because it is local in time and does not take into account the history of the system. A widely used flavour of this scheme is the adiabatic local density approximation (ALDA),

$$v_{\text{xc}}^{\text{ALDA}}(\mathbf{x}, t) = v_{\text{xc}}^{\text{LDA}}[n] \Big|_{n=n(\mathbf{x}, t)} \quad (3.57)$$

which uses the LDA exchange-correlation functional discussed above, adding the drawbacks of this approximation to the time-locality problem. Nevertheless, it delivers good results for excitation energies and many related applications.

### 3.4 Linear response DFT

If the time-dependent external potential  $\mathcal{V}(\mathbf{r}, t)$  differs only by a small amount from the external potential  $\mathcal{V}(\mathbf{r})$  of the unperturbed system, it is not always necessary to solve the

time-dependent Kohn-Sham equations. Often it is sufficient to treat the problem within the framework of linear response theory. In fact, the interacting linear response function can be described using the non-interacting Kohn-Sham eigensystem of the ground state [Str+12; GK85; GK86; PGG96]. The external potential can be written as

$$\mathcal{V}(\mathbf{x}, t) = \mathcal{V}(\mathbf{x}) + \Delta\mathcal{V}(\mathbf{x}, t)\theta(t - t_0), \quad (3.58)$$

where the weak perturbation  $\Delta\mathcal{V}(\mathbf{x}, t)$  is switched on at  $t = t_0$ . At that point in time, the system is in its ground state with its corresponding density  $n(\mathbf{x})$ , the linear response of which takes the form

$$\Delta n(\mathbf{x}, t) = \int d\mathbf{x}' \int dt' \chi(\mathbf{x}, \mathbf{x}', t - t') \Delta\mathcal{V}(\mathbf{x}, t'). \quad (3.59)$$

The response function  $\chi(\mathbf{x}, \mathbf{x}', t - t')$  is equal to the interacting susceptibility from Eq. (3.22). Despite the fact that this quantity is calculated from pure ground state wave functions, it is hard to achieve from perturbation theory. Since the density can be constructed from non-interacting Kohn-Sham orbitals, its linear response can be written equivalently as

$$\Delta n(\mathbf{x}, t) = \int d\mathbf{x}' \int dt' \chi_{\text{KS}}(\mathbf{x}, \mathbf{x}', t - t') \Delta v_{\text{eff}}(\mathbf{x}', t'), \quad (3.60)$$

with

$$\Delta v_{\text{eff}}(\mathbf{x}, t) = \Delta\mathcal{V}(\mathbf{x}, t) + \int d\mathbf{x}' \frac{\Delta n(\mathbf{x}, t)}{|\mathbf{x} - \mathbf{x}'|} + \Delta v_{\text{xc}}(\mathbf{x}, t) \quad (3.61)$$

being the effective potential arising from the density perturbation  $\Delta n(\mathbf{r}, t)$ . The change in the exchange-correlation potential, using the chain rule for functional derivatives, can be written as

$$\Delta v_{\text{xc}}[n](\mathbf{x}, t) = \int dt' \int d\mathbf{x} f_{\text{xc}}[n_{\text{GS}}](\mathbf{x}t, \mathbf{x}'t') \Delta n(\mathbf{x}', t') \quad (3.62)$$

where the so-called *exchange-correlation kernel*  $f_{\text{xc}}$  is defined via a functional derivative of the exchange-correlation potential with respect to the density, taken at the ground-state density  $n_{\text{GS}}$  [Str+12],

$$f_{\text{xc}}[n_{\text{GS}}](\mathbf{x}t, \mathbf{x}'t') = \left. \frac{\delta v_{\text{xc}}[n](\mathbf{x}, t)}{\delta n(\mathbf{x}', t')} \right|_{n=n_{\text{GS}}}. \quad (3.63)$$

The advantage of this description clearly lies in the use of the correlation function  $\chi_{\text{KS}}$ , which delivers the linear response of the non-interacting system to a change in the Kohn-Sham potential and which is, using Eq. (3.24), given in terms of ground-state Kohn-Sham orbitals as

$$\chi_{\text{KS}}(\mathbf{r}, \mathbf{r}', \omega) = \lim_{\eta \rightarrow 0^+} \sum_{ij} (f_j - f_i) \frac{\phi_j(\mathbf{x}) \phi_j^*(\mathbf{x}') \phi_i(\mathbf{x}') \phi_i(\mathbf{x})^*}{\epsilon_j - \epsilon_i - \hbar\omega - i\hbar\eta} \quad (3.64)$$

Identifying Eq. (3.59) with Eq. (3.60) and plugging in the definition of  $\Delta v^{\text{eff}}(\mathbf{r}, t)$  results, after careful reordering, in

$$\begin{aligned} \chi(\mathbf{x}t, \mathbf{x}'t') = & \chi_{\text{KS}}(\mathbf{x}t, \mathbf{x}'t') + \int d\mathbf{x}_1 \int dt_1 \int d\mathbf{x}_2 \int dt_2 \chi_{\text{KS}}(\mathbf{x}t, \mathbf{x}_1t_1) \\ & \left[ f_{\text{xc}}(\mathbf{x}_1t_1, \mathbf{r}_2t_2) + \frac{\delta(t_1 - t_2)}{|\mathbf{x}_1 - \mathbf{x}_2|} \right] \chi(\mathbf{x}_2t_2, \mathbf{x}'t') \end{aligned} \quad (3.65)$$

or, in frequency space,

$$\chi(\mathbf{x}, \mathbf{x}', \omega) = \chi_{\text{KS}}(\mathbf{x}, \mathbf{x}', \omega) + \int d\mathbf{r}_1 \int d\mathbf{x}_2 \chi_{\text{KS}}(\mathbf{x}, \mathbf{x}_1, \omega) \left[ f_{\text{xc}}(\mathbf{x}_1, \mathbf{x}_2, \omega) + \frac{1}{|\mathbf{x}_1 - \mathbf{x}_2|} \right] \chi(\mathbf{x}_2, \mathbf{x}', \omega). \quad (3.66)$$

This equation allows to compute the fully interacting density-density response function, using the non-interacting response function of the Kohn-Sham reference system. According to its characteristic form, it is often referred to as *susceptibility Dyson equation*.

As opposed to the *random phase approximation*, which does not include exchange and correlation, but relies on a proper reference susceptibility [FW71; BF04; Buc09], this equation is formally exact. The only approximation lies in the choice of the exchange-correlation kernel. In the static case  $\omega \rightarrow 0$ , the kernel reduces to

$$f_{\text{xc}}^{\text{static}}[n_{\text{GS}}](\mathbf{x}, \mathbf{x}') = \lim_{\omega \rightarrow 0} (\mathbf{x}, \mathbf{x}', \omega) = \frac{\delta E_{\text{xc}}[n]}{\delta n(\mathbf{x}) \delta n(\mathbf{x}')} \Big|_{n=n_{\text{GS}}}, \quad (3.67)$$

which is the most frequently used adiabatic approximation today [GM12]. In the LDA, it takes the form

$$f_{\text{xc}}^{\text{ALDA}}[n_{\text{GS}}](\mathbf{x}, \mathbf{x}') = \delta(\mathbf{x} - \mathbf{x}') \frac{d^2}{dn^2} \left[ n \epsilon_{\text{xc}}^{\text{hom}}(n) \right] \Big|_{n=n_{\text{GS}}(\mathbf{x})}. \quad (3.68)$$



# The Korringa-Kohn-Rostoker Green function method

For a practical implementation of electronic structure calculations using DFT, many different numerical techniques have been developed over the past decades [Blü06]. One of the most commonly used is the expansion of the single-electron wave functions into plane waves in combination with pseudopotentials [HSC79; Van90; Laa+91]. This method replaces the  $1/r$  singularity of the nuclear potential by an artificial soft potential which satisfies certain boundary conditions, such that the correct charge density is obtained. Modern pseudopotentials include pre-calculated pseudo wave functions which describe the core electrons and which are not changed during the self-consistent calculation of the valence charge density. This method is computationally very efficient and delivers accurate results for a wide range of materials. Nevertheless, in every single case it has to be checked carefully whether the chosen pseudopotential is appropriate for the respective task.

In contrast, all-electron methods allow for the self-consistent calculation of the core charge density, too. In general, these methods provide a more accurate description of the electronic structure of a material, especially in the case of 3d and 4f electrons as well as in the description of magnetic properties [Blü06].

A common all-electron approach is the Korringa-Kohn-Rostoker Green function method (KKR). Opposed to most other methods, Green function techniques do not solve the Kohn-Sham equations directly, but in terms of a resolvent which is called the Green function. Once this quantity is calculated, the charge density and other observables of the system can be extracted from it. Some advantages of Green function methods are their ability to treat systems with reduced symmetry, such as impurities and surfaces, elegantly without the need to construct supercells. Another typical usage of Green function methods are disordered materials like alloys. For these reasons, the KKR is the method of choice in this work.

This chapter is organized as follows: The first section will give a short overview on the general properties of Green functions and which kind of information about the system under concern they can provide. The second part is entirely devoted to an introduction to the Korringa-Kohn-Rostoker (KKR) Green function method. This short overview will help the reader unfamiliar with this method to understand the subsequent chapters.

## 4.1 Green functions

The Green function method is a general approach to solutions of inhomogeneous differential equations. Originally developed by George Green [Gre28] for electrostatic and magnetic boundary value problems, it has also become an important tool in quantum field theories and solid state physics. It is especially useful at solving problems which differ from a simpler, already solved problem by a small external perturbation. In quantum mechanics, the Green function is defined as resolvent of the Schrödinger equation

$$\left[ i\partial_t - \hat{H} \right] \psi(\mathbf{r}, t) = 0 \quad (4.1)$$

by rewriting it as

$$\left[ i\partial_t - \hat{H} \right] G(t) = \delta(t). \quad (4.2)$$

While the formal solution of (4.1) reads  $\psi(t) = e^{-i\hat{H}t}\psi(0)$  with  $\psi(0)$  being the solution of the stationary Schrödinger equation  $\hat{H}\psi = E\psi$ , the Green function solves (4.2) as

$$G(t) = -i\theta(t)e^{-i\hat{H}t}. \quad (4.3)$$

This is the *retarded* Green function which propagates the wave function forward in time via

$$\psi(t) = iG(t-t')\psi(t'). \quad (4.4)$$

The *advanced* Green function, which corresponds to the opposite direction of time, shall not be further discussed in this thesis. Given the case, that the Green function  $G_0$  for the Hamiltonian  $\hat{H}_0$  is known, the Green function  $G$  for the Hamiltonian  $\hat{H}_1 = \hat{H}_0 + \Delta V$  is given by the Dyson equation [Dys49]

$$G_1(t) = G_0(t) + \int_0^t dt' G_0(t-t')\Delta V G_1(t'). \quad (4.5)$$

Thus, the Green function of an electron interacting with a potential  $\Delta V$  can be computed by iteration of (4.5), only requiring the green function of a free electron and the potential  $\Delta V$ . In analogy, the propagation of its wave function is given by the Lippmann-Schwinger equation [LS50; GG53]

$$\psi_1(t) = \psi_0(t) + \int_{-\infty}^t dt' G_0(t-t')\Delta V \psi_1(t'). \quad (4.6)$$

In the stationary case, the Green function can be defined as the operator

$$\mathcal{G}(z) = (z - \hat{H})^{-1}, \quad z = E + i\eta. \quad (4.7)$$

It is clearly seen that  $\mathcal{G}(z)$  is not defined on the real axis where  $z$  coincides with the eigenvalues  $\epsilon_i$  of  $\hat{H}$ . In particular within the discrete spectrum of  $\hat{H}$  it has poles, but is analytical for all energies and  $\eta \neq 0$ . The above expression can also be obtained directly via a Fourier transform of  $G(t)$ , where the imaginary energy  $i\eta$  has to be introduced to ensure the convergence of the integral. For a complete set of eigenfunctions  $\psi_i(\mathbf{r})$  given in real space notation, the Green function has the Lehmann representation

$$\mathcal{G}(\mathbf{r}, \mathbf{r}', z) = \sum_i \frac{\psi_i(\mathbf{r})\psi_i^*(\mathbf{r}')}{z - \epsilon_i}. \quad (4.8)$$

For  $\mathbf{r} = \mathbf{r}'$  it can be rewritten as

$$\mathcal{G}(\mathbf{r}, \mathbf{r}, z) = \sum_i |\psi_i(\mathbf{r})|^2 \left( \frac{E - \epsilon_i}{(E - \epsilon_i)^2 + \eta^2} - i \frac{\eta}{(E - \epsilon_i)^2 + \eta^2} \right), \quad (4.9)$$

where the imaginary part approaches  $\pi\delta(E^+ - \epsilon_i)$  in the limit of vanishing  $\eta$ . From this equation it can be seen that the local density of states can be expressed in terms of the Green function via

$$d(\mathbf{r}, E) = -\frac{1}{\pi} \text{Im} \mathcal{G}(\mathbf{r}, \mathbf{r}, E^+). \quad (4.10)$$

The superscript of  $E^+$  denotes that  $\mathcal{G}$  in the limit of  $\eta \rightarrow 0^+$  is taken. By integration of (4.10), two important quantities can be obtained. An integral over space results in the total density of states,

$$d(E) = \int d\mathbf{r}' d(\mathbf{r}', E) = -\frac{1}{\pi} \text{Im} \text{Tr} \mathcal{G}(E). \quad (4.11)$$

The usage of the trace operator stresses that the Green function does not have to be given in its spatial basis. By integration over the Energy up to the Fermi level, the particle density

$$n(\mathbf{r}) = \int_{-\infty}^{\infty} dE f(E - \mu) d(\mathbf{r}, E) = -\frac{1}{\pi} \text{Im} \int_{-\infty}^{\infty} dE f(E - \mu) \text{Tr} [\hat{r} \mathcal{G}(E)] \quad (4.12)$$

is obtained, while the position operator  $\hat{r} = |\mathbf{r}\rangle \delta(\mathbf{r} - \mathbf{r}') \langle \mathbf{r}'|$  and the Fermi distribution function  $f$  were used. In fact, it can be shown that a similar relation holds for all observables of the system:

$$\langle \hat{O} \rangle = -\frac{1}{\pi} \text{Im} \int_{-\infty}^{\infty} dE f(E - \mu) \text{Tr} [\hat{O} \mathcal{G}(E)], \quad (4.13)$$

which confirms that the Green function contains all the information of the system that can be extracted from the wave function. For the case  $T = 0$ , the convolution with the Fermi function can be replaced by an energy integration up to  $E = \epsilon_F$ . This also makes the energy integration an important numerical process when quantum mechanical systems are to be described using the Green function technique. A direct integration along the real energy axis is not possible since  $\mathcal{G}(z)$  has its poles at discrete eigenenergies of the Hamiltonian. Instead, one uses the fact that the Green function is analytical for energies with non-vanishing imaginary part  $\eta$ .

From Eq. (4.7), it follows for the Green functions of the unperturbed and the perturbed system that

$$\begin{aligned} \mathcal{G}_0(z)^{-1} &= z - H_0 \\ \mathcal{G}_1(z)^{-1} &= z - (H_0 + \Delta V). \end{aligned} \quad (4.14)$$

Thus, for the connection of the two,

$$\mathcal{G}_1(z)^{-1} = \mathcal{G}_0(z)^{-1} - \Delta V \quad (4.15)$$

is obtained. By rearrangement, the Dyson equation for the two Green functions is found to be

$$\mathcal{G}_1(z) = \mathcal{G}_0(z) + \mathcal{G}_0(z) \Delta V \mathcal{G}_1(z), \quad (4.16)$$

which, via iteration, can be expanded into the Born series

$$\mathcal{G}_1(z) = \mathcal{G}_0(z) + \mathcal{G}_0(z) \Delta V \mathcal{G}_0(z) + \mathcal{G}_0(z) \Delta V \mathcal{G}_0(z) \Delta V \mathcal{G}_0(z) + \dots \quad (4.17)$$

Here, the first term gives the contribution of the unperturbed particle, the second term resembles the contribution of single scattering process at the perturbing potential  $\Delta V$  and the third term a two-fold scattering event. Thus, this equation represents a general way to find approximations to the Green function  $\mathcal{G}_1$  which contains all possible scattering events. The exact form of (4.17) depends on the basis in which  $\mathcal{G}$  is chosen to be represented. This equation becomes more convenient by introducing the transition operator or  $T$ -matrix:

$$\mathcal{G}_1(z) = \mathcal{G}_0(z) + \mathcal{G}_0(z) T(z) \mathcal{G}_0(z), \quad (4.18)$$

which represents all possible scattering events and is defined as

$$T(z) = \Delta V + \Delta V \mathcal{G}_0(z) \Delta V + \Delta V \mathcal{G}_0(z) \Delta V \mathcal{G}_0(z) \Delta V + \dots \quad (4.19)$$

In a similar fashion, the Lippmann-Schwinger equation for the corresponding unperturbed and scattered wave functions reads

$$\begin{aligned} |\psi_1\rangle &= |\psi_0\rangle + \mathcal{G}_0(z) \Delta V |\psi_1\rangle \\ &= |\psi_0\rangle + \mathcal{G}_0(z) \Delta V |\psi_0\rangle + \mathcal{G}_0(z) \Delta V \mathcal{G}_0(z) \Delta V |\psi_0\rangle + \dots \\ &= |\psi_0\rangle + \mathcal{G}_0(z) T(z) |\psi_0\rangle. \end{aligned} \quad (4.20)$$

## 4.2 The Korringa-Kohn-Rostoker method

The Korringa-Kohn-Rostoker (KKR) method is a computational scheme to calculate the electronic structure of ordered and disordered solids. In its original form, first presented by Korringa [Kor47] and later, independently by Kohn and Rostoker [KR54], it was a method to solve the Schrödinger equation by making use of multiple scattering theory:

Electrons are treated as Bloch-waves moving through the crystal, where they are scattered at periodically distributed nuclear potentials. During a single scattering process, the wave experiences a phase shift and a change of momentum. This effect can be quantified as an energy-dependent scattering matrix. Multiple scattering events of many waves with different energies result in a specific distribution of the electrons. The general scattering behaviour of a lattice (the *structure constants*) can be calculated without knowledge of the single-scattering matrix. This separation of the influences of the atomic type on one side and the geometry of the crystal on the other promised to make electronic structure calculations very efficient.

Nevertheless, the numerical effort was huge before the KKR method was reintroduced as a Green function method [Bee67], in which the crystal Green function is connected to the Green function of the free electron by means of a Dyson equation. This advancement made KKR calculations much more efficient and thus attractive. Another branch of efficient computational schemes, the LMTO-related (linear muffin-tin orbital) methods emerged from the original KKR method through the use of energy-independent eigenfunctions [And75; AJ84]. Nevertheless, the KKR-GF method has been further improved by introducing methods to describe disordered [Kor58; Bee64; Sov67; Tay67] and low-dimensional systems [DLZ06], transport properties, the ability to use the full potential instead of the muffin-tin approximation [Zel87; Dri91; Ded+91] and screened structure constants [Szu+94; BL94] for an even better performance.

As for many other electronic-structure methods, the introduction of density functional theory improved the results of KKR calculations significantly by replacing the Schrödinger equation by the effective Kohn-Sham equations. In order to give an introduction to electronic structure calculations with the KKR-GF method, Both single-atom and multiple-site scattering are discussed in the following.

### 4.2.1 Single potential scattering

For the description of scattering processes of electrons at a single perturbing potential it is suggestive to use free space as reference System. The Green function of the free electron can be obtained by using the spectral representation. The Schrödinger equation of the free particle reads

$$\hat{H}|\mathbf{k}\rangle = \epsilon|\mathbf{k}\rangle, \quad \hat{H} = -\nabla^2, \quad (4.21)$$

and its solutions in real space representation are plane waves

$$\psi_{\mathbf{k}}(\mathbf{r}) = \langle \mathbf{r} | \mathbf{k} \rangle = \frac{1}{(2\pi)^{3/2}} e^{i\mathbf{k}\cdot\mathbf{r}}, \quad (4.22)$$

which are characterized by the momentum quantum numbers  $\mathbf{k}$  and a continuous eigenvalue spectrum  $\epsilon(\mathbf{k}) = \mathbf{k}^2 = k^2$ . For the corresponding spectral representation it follows

$$\mathcal{G}_f(\mathbf{r}, \mathbf{r}', E) = \langle \mathbf{r} | \mathcal{G}_f(E^+) | \mathbf{r}' \rangle \quad (4.23)$$

$$= \lim_{\eta \rightarrow 0^+} \sum_{\mathbf{k}} \frac{\langle \mathbf{r} | \mathbf{k} \rangle \langle \mathbf{k} | \mathbf{r}' \rangle}{k_0^2 + i\eta - k^2} \quad (4.24)$$

$$= \frac{1}{(2\pi)^3} \lim_{\eta \rightarrow 0^+} \int d\mathbf{k} \frac{e^{i\mathbf{k}\cdot(\mathbf{r}-\mathbf{r}')}}{k_0^2 - k^2 + i\eta}, \quad (4.25)$$

where  $E = k_0^2$  was defined. The integral over  $\mathbf{k}$ -space can be reformulated into a contour integral in the complex plane and solved by making use of the residue theorem. The final result for the free-particle propagator [Gon00] is obtained as

$$\mathcal{G}_f(\mathbf{r}, \mathbf{r}', E) = -\frac{1}{4\pi} \frac{e^{ik_0|\mathbf{r}-\mathbf{r}'|}}{|\mathbf{r}-\mathbf{r}'|} \quad (4.26)$$

and depends only on  $|\mathbf{r}-\mathbf{r}'|$ . Direction and absolute position are irrelevant because the constant potential of free space is invariant under rotation and translation.

When single as well as multiple scattering at central potentials comes into play, the expansion of the Green function into eigenfunctions of the angular momentum operator has proven to be very useful. In the case of free electrons, it can be constructed by using the angular momentum expansion of a plane wave,

$$e^{i\mathbf{k}\cdot\mathbf{r}} = 4\pi \sum_{\ell=0}^{\infty} \sum_{m=-\ell}^{\ell} i^{\ell} j_{\ell}(kr) Y_{\ell m}(\theta(\mathbf{r}), \phi(\mathbf{r})) Y_{\ell m}(\theta(\mathbf{k}), \phi(\mathbf{k})) \quad (4.27)$$

$$= 4\pi \sum_L i^{\ell} j_{\ell}(kr) Y_L(\hat{\mathbf{r}}) Y_L(\hat{\mathbf{k}}). \quad (4.28)$$

$j_{\ell}$  is the spherical Bessel function and the  $Y_{\ell m}(\theta, \phi)$  are spherical harmonics. In the second line, the combined index  $L = (\ell, m) \forall |m| \leq \ell$  of the angular momentum and magnetic quantum numbers has been introduced and the sum runs over all possible combinations of them. Additionally, the short form  $\hat{\mathbf{r}}$  for the angles  $(\theta, \phi)$  connected to the vector  $\mathbf{r}$  in spherical coordinates, was introduced. Using this expansion, the Green function can be expressed as

$$\mathcal{G}_f(\mathbf{r}, \mathbf{r}', E) = \sum_L g_L(r, r', E) Y_L(\hat{\mathbf{r}}) Y_L(\hat{\mathbf{r}}') \quad (4.29)$$

were

$$g_L(r, r', E) = -i\sqrt{E} j_{\ell}(\sqrt{E}r_{<}) h_{\ell}(\sqrt{E}r_{>}). \quad (4.30)$$

Here,  $h_{\ell} = j_{\ell} + in_{\ell}$  is the spherical Hankel function and  $n_{\ell}$  the spherical Neumann function.  $r_{<}$  means the smaller of the two values  $r$  and  $r'$ , and vice versa. Being a result of the diverging character of the Hankel function, this distinction is strictly necessary to ensure convergence of the series [Gon00].

By means of this representation, the discussion of the scattering process at a spherically symmetric potential becomes feasible, because the angular momentum is a conserved quantity during the process and the angular momentum components of the scattered wave can be treated individually [Gon92]. Additionally, the following considerations shall be restricted to potentials with a limited range  $a$ , which are given by

$$V(\mathbf{r}) = \begin{cases} V(r) & r \leq a \\ 0 & r > a. \end{cases} \quad (4.31)$$

The radial wave function  $u_{\ell}(r, E)$  resulting from this type of potential is determined by the radial Schrödinger equation

$$\left[ -\frac{1}{r} \nabla^2 r + \frac{\ell(\ell+1)}{r^2} + V(r) - E \right] u_{\ell}(r, E) = 0. \quad (4.32)$$

This equation has two linearly independent solutions which are often referred to as regular and irregular solution due to their behaviour at the origin of the potential. For  $r > a$ , both solutions can be determined from the free-space solutions using the Lippmann-Schwinger

equation. Inside the potential region, the Schrödinger equation is solved numerically, whereby the boundary conditions are defined by the solutions for  $r > a$ .

The regular solution outside the potential is given by the Lippmann-Schwinger equation

$$\bar{R}_\ell(r, E) = j_\ell(\sqrt{E}, r) + \int_0^a dr' r'^2 g_L(r, r', E) V(r') \bar{R}_\ell(r', E), \quad (4.33)$$

which, using the angular momentum representation (4.30), can be rewritten as

$$\bar{R}_\ell(r, E) = j_\ell(\sqrt{E}, r) - i h_\ell(\sqrt{E}, r) \sqrt{E} \int_0^a dr' r'^2 j_\ell(\sqrt{E}, r') V(r') \bar{R}_\ell(r', E). \quad (4.34)$$

Comparing this equation to (4.20), it follows that

$$\bar{R}_\ell(r, E) = j_\ell(\sqrt{E}, r) - i \sqrt{E} t_\ell(E) h_\ell(\sqrt{E}, r) \quad (4.35)$$

with the single-scattering  $t$ -matrix in angular momentum representation

$$t_\ell(E) = \int_0^a dr' r'^2 j_\ell(\sqrt{E}, r') V(r') \bar{R}_\ell(r', E). \quad (4.36)$$

The numerical integration of Eq. (4.32) from  $r = 0$  to  $r = a$  yields  $\bar{R}_\ell(r, E)$  inside the potential, which has to be normalized to match the scattering solution at  $r = a$ . This function behaves like  $r^{l+1}$  for  $r \rightarrow 0$ . The second, irregular solution behaves like

$$\bar{H}_\ell(r, E) = -i \sqrt{E} h_\ell(\sqrt{E}, r) \quad (4.37)$$

outside the potential region. Its counterpart inside the potential can be calculated by integrating Eq. (4.32) inwards and behaves like  $r^{-\ell}$  as  $r$  approaches 0.

The angular-dependent solutions of the Schrödinger equation are spherical harmonics, which allow to construct the full solutions of the single potential scattering Problem as

$$\begin{aligned} R_L(\mathbf{r}, E) &= \sum_L \frac{\bar{R}_\ell(r, E)}{r} Y_L(\hat{\mathbf{r}}) = \sum_L R_\ell(r, E) Y_L(\hat{\mathbf{r}}), \\ H_L(\mathbf{r}, E) &= \sum_L \frac{\bar{H}_\ell(r, E)}{r} Y_L(\hat{\mathbf{r}}) = \sum_L H_\ell(r, E) Y_L(\hat{\mathbf{r}}). \end{aligned} \quad (4.38)$$

The functions  $R$  and  $H$  of the right side will be used subsequently. The Green function of the single scattering problem can now be constructed via the Dyson equation, using the Green function of free space (4.29) and the  $t$ -matrix (4.36) as

$$\mathcal{G}_S(\mathbf{r}, \mathbf{r}', z) = -\sqrt{z} \sum_L R_\ell(r_<, z) H_\ell(r_>, z) Y_L(\hat{\mathbf{r}}) Y_L(\hat{\mathbf{r}}'). \quad (4.39)$$

## 4.2.2 Multiple scattering theory

Multiple scattering theory is the natural generalization of single potential scattering to an array of scatterers. In case of crystalline solids, these are atoms arranged in a Bravais lattice. In order to discuss the scattering properties of a crystal, it is intuitively accessible to consider first the Green function of a free particle in empty space, which shall be divided into disjunct cells, as shown in Fig. (4.1). Every cell is identified by an index  $n$  and its point of origin by

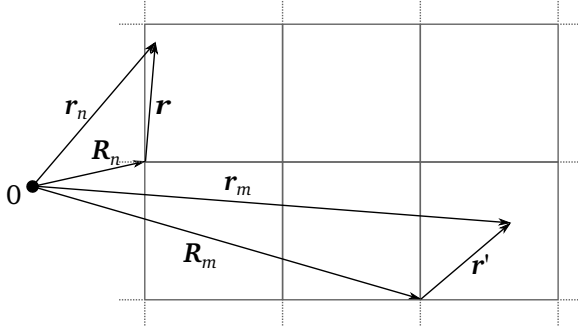


**Figure 4.1:** Division of space into disjunct cells arranged in a periodic 2-dimensional lattice.  $\mathbf{R}_n$  and  $\mathbf{R}_m$  denote lattice vectors,  $\mathbf{r}$  and  $\mathbf{r}'$  are points within the cells, positioned relative to their respective origins.  $\mathbf{r}_n$  denotes the total vector  $\mathbf{R}_n + \mathbf{r}$ .

a lattice vector  $\mathbf{R}_n$ . A point within a cell is denoted by the relative vector  $\mathbf{r}$  and the absolute position  $\mathbf{r}_n = \mathbf{R}_n + \mathbf{r}$ . The Green function of free space  $\mathcal{G}_f(\mathbf{r}_n, \mathbf{r}_{n'}, z)$  can now be written in terms of cellular coordinates. If the two vectors point into the same cell ( $n = n'$ ), Eq. (4.29) can be written as a single center expansion

$$\mathcal{G}_{f,S}^n(\mathbf{r}, \mathbf{r}', z) = \mathcal{G}_{f,S}(\mathbf{r}_n, \mathbf{r}_n, z) = -ik \sum_L Y_L(\hat{\mathbf{r}}) j_\ell^n(kr_<) h_\ell^n(kr_>) Y_L(\hat{\mathbf{r}}'), \quad (4.40)$$

where the superscripts of the Bessel and Hankel functions indicate that their points of origin are identical to their respective cell's origin. In case the two spatial arguments of the free particle propagator point in different cells  $n$  and  $n'$ , it can be written as a two-center expansion

$$\mathcal{G}_{f,M}^{nn'}(\mathbf{r}, \mathbf{r}', z) = \sum_{LL'} Y_L(\hat{\mathbf{r}}) j_\ell^n(kr) g_{f,LL'}^{nn'}(z) j_{\ell'}^{n'}(kr') Y_{L'}(\hat{\mathbf{r}}'). \quad (4.41)$$

This expression was obtained by expanding the Hankel functions as

$$h_\ell^{n'}(\sqrt{z} |\mathbf{R}_{nn'} + \mathbf{r}'|) Y_L(\widehat{\mathbf{R}_{nn'} + \mathbf{r}'}) = \frac{i}{\sqrt{z}} \sum_{L'} g_{LL'}^{nn'}(z) j_\ell^{n'}(\sqrt{z} r') Y_{L'}(\hat{\mathbf{r}}') \quad (4.42)$$

where the real-space structure constants of free space have been introduced as

$$g_{LL'}^{nn'}(z) = -4\pi i (1 - \delta_{nn'}) \sum_{L''} i^{-\ell + \ell' - \ell''} h_{\ell''}(\sqrt{z} |\mathbf{R}_{nn'}|) Y_{L''}(\hat{\mathbf{R}}_{nn'}) C_{LL'}^{L''} \quad (4.43)$$

using the Gaunt coefficients

$$C_{LL'}^{L''} = \int d\hat{\mathbf{r}} Y_L(\hat{\mathbf{r}}) Y_{L'}(\hat{\mathbf{r}}) Y_{L''}(\hat{\mathbf{r}}). \quad (4.44)$$

All information about the lattice is contained in the structure constants, which depend on the relative position  $\mathbf{R}_{nn'}$  of pairs of cells. The Green function can now be written as

$$\mathcal{G}_f(\mathbf{r}_n, \mathbf{r}_{n'}, z) = \delta_{nn'} \mathcal{G}_{f,S}^n(\mathbf{r}, \mathbf{r}', z) + \mathcal{G}_{f,M}^{nn'}(\mathbf{r}, \mathbf{r}', z). \quad (4.45)$$

For the description of multiple scattering of electrons in a crystal, the latter is divided into disjunct space-filling cells in a way that every atom is centred in one cell. This is usually achieved by a Voronoi construction [FH08], which in the case of mono-atomic lattices is equivalent to Wigner-Seitz cells. The three common approximations for the single scattering potentials in such a lattice are shown in Fig. 4.2. For the sake of simplicity, only crystals with single atoms per unit cell shall be discussed here.

In the muffin-tin approximation [Sla53] (Fig. 4.2 a), the single scattering potentials  $V^n(\mathbf{r}) = V(\mathbf{r}_n)$  equal the spherical atomic potentials  $V(r)$  inside a sphere with a radius  $R_{MT}$  which is chosen such that the muffin-tin sphere coincides with every side of the Wigner-Seitz

cell at most in one point, respectively. The potential outside the spheres is chosen to be constant and equal to  $V(R_{MT})$ . Consequently, besides the well-known spherical potential within the spheres, an interstitial region between them remains and has to be considered separately when integrals over the cell are taken. This approximation was used in the original derivation of the KKR method.

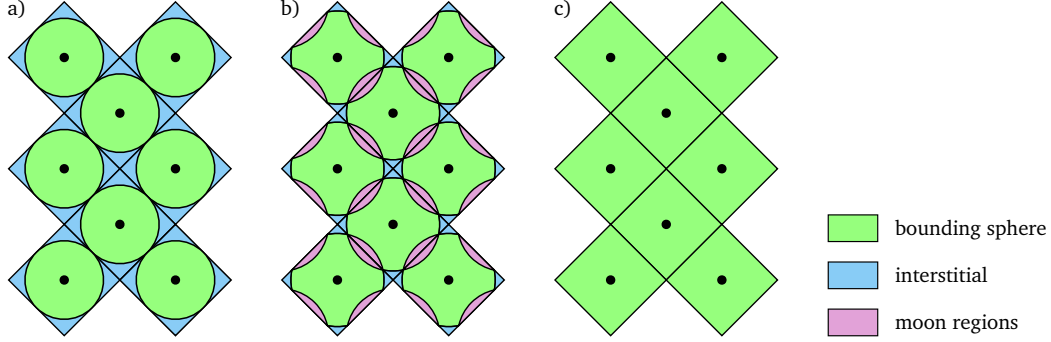


**Figure 4.2:** Different approximations for single scattering potentials arranged in a crystalline solid: a) Muffin-tin approximation, b) atomic sphere approximation, c) full-potential method.

In contrast, the atomic sphere approximation (ASA, Fig. 4.2 b) assumes a spherical potential confined by a sphere with a Wigner-Seitz radius  $R_{WS}$  which is defined [AM05] such that the volume of the sphere coincides with the total volume of the cell. Thus, the interstitial region becomes small and can be neglected, while the integration of the Green function over the sphere often yields good results for the total charge and density of states. As a drawback, the spheres overlap, what makes this approximation advisable only in the case of slowly varying potentials and densities at the cell boundary, which is often the case for metals.

For systems with highly anisotropic densities, the full potential method is appropriate, since it takes into account the non-spherical symmetry of an atom due to its neighbouring scatterers. All components of the single scattering potential  $V(\mathbf{r}) = \sum_L V_L(r)Y_L(\hat{\mathbf{r}})$  are included and it is no longer assumed to be of spherical symmetry. Likewise, it is limited in range only by the boundaries of the Wigner-Seitz cell (Fig. 4.2 c). Full-potential calculations are computationally more expensive but result in a very accurate description of the electronic structure.

For the sake of simplicity, the following description of multiple scattering theory is restricted to the MT approximation. The Green function of an array of scattering potentials  $V^n(r)$  is defined by

$$[-\nabla^2 + V^n(r) - z] \mathcal{G}(\mathbf{r}_n, \mathbf{r}'_{n'}, z) = -\delta_{nn'} \delta(\mathbf{r} - \mathbf{r}'). \quad (4.46)$$

For  $n \neq n'$ , the Schrödinger equation becomes homogeneous, which implicates that  $\mathcal{G}$  can be expanded in terms of the regular solutions in analogy to Eq. (4.41). For  $n = n'$ , Eq. (4.46) yields the inhomogeneous equation which describes the single scatter and its Green function can be expanded in regular and irregular Solutions. Thus,

$$\begin{aligned} \mathcal{G}(\mathbf{r}_n, \mathbf{r}'_{n'}, z) &= \delta_{nn'} \mathcal{G}_S(\mathbf{r}_n, \mathbf{r}'_{n'}, z) + \mathcal{G}_M(\mathbf{r}_n, \mathbf{r}'_{n'}, z) \\ &= -i\sqrt{z} \delta_{nn'} \sum_L R_L^n(\mathbf{r}_{<}, z) H_L^n(\mathbf{r}_{>}, z) + \sum_{LL'} R_L^n(\mathbf{r}, z) G_{LL'}^{nn'}(z) R_{L'}^n(\mathbf{r}', z), \end{aligned} \quad (4.47)$$

where the abbreviations  $R_L^n(\mathbf{r}) = R_\ell^n(r)Y_L(\hat{\mathbf{r}})$  and  $H_L^n(\mathbf{r}) = H_\ell^n(r)Y_L(\hat{\mathbf{r}})$  for the regular and irregular solutions have been introduced. The  $G_{LL'}^{nn'}(z)$  are the structure constants of

the crystal, which can be calculated from their free space pendants by setting up a Dyson equation which relates the Green functions of both systems via the scattering potentials,

$$\mathcal{G}(\mathbf{r}_n, \mathbf{r}'_{n'}, z) = \mathcal{G}_f(\mathbf{r}_n, \mathbf{r}'_{n'}, z) + \sum_{n''} \int d\mathbf{r}'' \mathcal{G}_f(\mathbf{r}_n, \mathbf{r}''_{n''}, z) V^{n''}(\mathbf{r}'') \mathcal{G}(\mathbf{r}''_{n''}, \mathbf{r}'_{n'}, z). \quad (4.48)$$

Through algebraic conversions, using the definition of the  $t$ -matrix (4.36) and the Lippmann-Schwinger equation (4.34), the structure constants are given by

$$G_{LL'}^{nn'}(z) = g_{LL'}^{nn'}(z) + \sum_{n''} \sum_{L''} g_{LL''}^{nn''}(z) t_{L''}^{n''}(z) G_{L''L'}^{n''n'}(z) \quad (4.49)$$

and written in a matrix form, a solution can be obtained via a matrix inversion

$$\mathbf{G}(z) = [\mathbf{g}^{-1}(z) - \mathbf{t}(z)]^{-1}, \quad (4.50)$$

where all quantities are matrices in  $(nn')$  and  $(LL')$  and

$$\{\mathbf{t}(z)\}_{LL'}^{nn'} = t_{\ell}^{nn'}(z) \delta_{nn'} \delta_{LL'}. \quad (4.51)$$

The inversion becomes cumbersome for large matrices in  $(nn')$ . In order to accelerate this procedure, the translational symmetry of the lattice can be used to achieve a representation in reciprocal space via lattice Fourier transforms of the form

$$g_{LL'}(\mathbf{k}, z) = \sum_n g_{LL'}^{nn'}(z) e^{i\mathbf{k} \cdot \mathbf{R}_{nn'}}, \quad (4.52)$$

where  $n'$  can be chosen arbitrarily, because  $g_{LL'}^{nn'}(z)$  only depends on the difference vector  $\mathbf{R}_{nn'}$ . The inverse transformation is given by

$$g_{LL'}^{nn'}(z) = \frac{1}{\Omega_{\text{BZ}}} \int_{\text{BZ}} d\mathbf{k} g_{LL'}(\mathbf{k}, z) e^{-i\mathbf{k} \cdot \mathbf{R}_{nn'}}, \quad (4.53)$$

where  $\Omega_{\text{BZ}}$  denotes the volume of the first Brillouin zone and the integral is taken right there. In practice, the structure constants  $g_{f,LL'}(\mathbf{k}, z)$  are calculated using an Ewald summation technique so that convergence is reached after summing over a finite cluster of scatterers. The real space structure constants are then obtained by a matrix inversion and transformation into real space as

$$G_{LL'}^{nn'}(z) = \frac{1}{\Omega_{\text{BZ}}} \int_{\text{BZ}} d\mathbf{k} e^{-i\mathbf{k} \cdot \mathbf{R}_{nn'}} \left\{ \left[ \hat{\mathbf{I}} - \mathbf{g}(\mathbf{k}, z) \mathbf{t}(z) \right]^{-1} \mathbf{g}(\mathbf{k}, z) \right\}_{LL'}, \quad (4.54)$$

so that only a matrix in  $(LL')$  needs to be inverted. Its dimensions are limited since the  $t$ -matrix vanishes for angular momentum indices above  $\ell_{\text{max}} = 2 \dots 4$ , depending on the system.

The reciprocal space representation is also important in a different context: An important part of electronic structure theory is the band structure given as the electronic eigenenergies  $\epsilon(\mathbf{k})$  as function of a vector within the first Brillouin zone. This quantity can be obtained by introducing the scattering path operator  $\tau_{nn'}$ . The  $T$ -operator given in Eq. (4.19) is

$$\begin{aligned} T(z) &= V + V\mathcal{G}(z)V \\ &= V + V\mathcal{G}_f(z)T(z), \end{aligned} \quad (4.55)$$

where in the second line the free particle propagator was used. Instead of using the total potential  $V = \sum_n V_n$  of the crystal lattice, this equation can be written in terms of single scattering potentials as

$$\begin{aligned} T(z) &= \sum_n (V_n + V_n \mathcal{G}_f(z) T(z)) \\ &= \sum_{nn'} \tau_{nn'}(z). \end{aligned} \quad (4.56)$$

The scattering path operator introduced in the second line is connected to the single scattering  $t$ -matrices via

$$\begin{aligned} \tau_{nn'}(z) &= t^n(z) \delta_{nn'} + t^n(z) \mathcal{G}_f t^{n'}(z)^\top (1 - \delta_{nn'}) \\ &\quad + \sum_{n''} t^n(z) \mathcal{G}_f(z) t^{n'}(z)^\top (1 - \delta_{nn'}) \mathcal{G}_f(z) t^{n''}(z)^\top (1 - \delta_{n'n''}) + \dots, \end{aligned} \quad (4.57)$$

which shows vividly that  $\tau_{nn'}$  describes all possible scattering events which can occur for a particle travelling from cell  $n$  to cell  $n'$ . Using the formerly introduced matrix notation, the last expression can be written as

$$\boldsymbol{\tau}(z) = [\mathbf{t}^{-1}(z) - \mathbf{G}_f(z)]^{-1}. \quad (4.58)$$

This equation gives the fundamental insight that all scattering processes and thus the motion of electrons in a crystal are determined by the scattering properties of the single atoms, given by the  $t$ -matrix, and the spatial arrangement of the latter, represented by the free particle propagator  $\mathbf{G}_f$ . Using again a Fourier representation of  $\tau_{LL'}^{nn'}(z)$  and  $\mathcal{G}_{fLL'}^{nn'}(z)$  and restricting  $z$  to real energies, it can be found that

$$\boldsymbol{\tau}(\mathbf{k}, \epsilon) = [\mathbf{t}^{-1}(\epsilon) - \mathbf{G}_f(\mathbf{k}, \epsilon)]^{-1} \quad (4.59)$$

where again all objects are matrices in  $(LL')$ . This equation provides non-trivial scattering solutions only if

$$\det [\mathbf{t}^{-1}(\epsilon) - \mathbf{G}_f(\mathbf{k}, \epsilon)] = 0, \quad (4.60)$$

the latter being called the KKR secular equation because of its importance for the electronic band structure  $\epsilon(\mathbf{k})$  which can be obtained by variation of  $\mathbf{k}$  for constant energy or vice versa.

### 4.2.3 Self-consistent KKR scheme

The full performance of the KKR Green function method is exploited when it is used together with DFT. To do so, the radial Schrödinger equation (4.32) is replaced by a radial Kohn-Sham equation, which means that the atomic potential is replaced by the effective Kohn-Sham potential. Therefore, the following working scheme for practical electronic structure calculations is implemented: Initially, a guess for the effective potential  $V_{\text{in}}(\mathbf{r})$  within the cells is provided for which often the potential resulting from a self-consistent single-atom DFT calculation is used. With this potential, the radial Kohn-Sham equation is solved to obtain the regular  $R_L(\mathbf{r}, z)$  and the irregular  $H_L(\mathbf{r}, z)$ , as well as the  $t$ -matrix. The latter is calculated only for the valence electrons, since the core wave functions are highly localized and a multiple scattering description is not necessary. The same, in a later step, holds for the Green function. These quantities are evaluated for typically around 30 values of  $z$  on a complex energy contour. The most demanding part of the calculation is the evaluation of the structure constants, which is done via a Brillouin zone integration using Eq. (4.54).

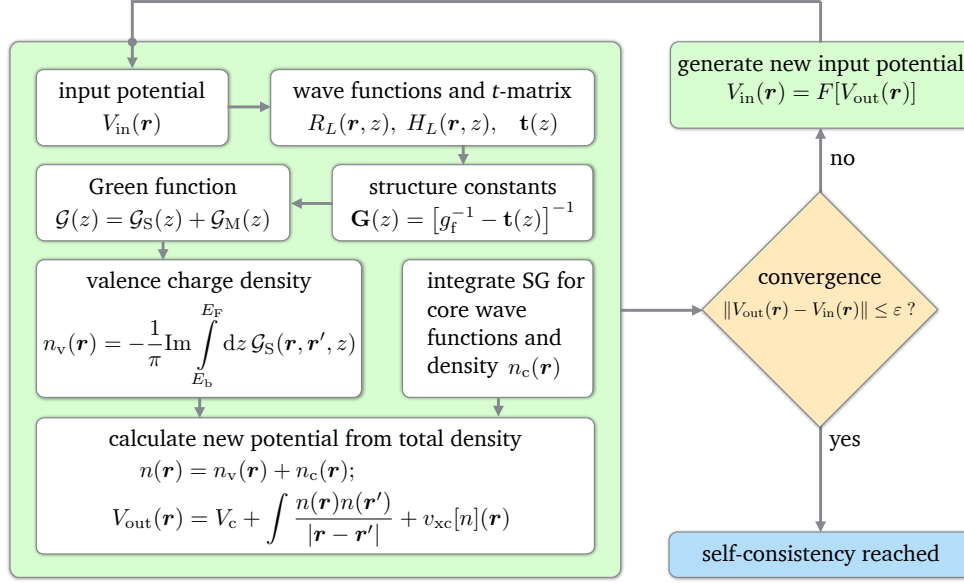


**Figure 4.3:** A typical algorithm for self-consistent calculations using the KKR-GF method. The effective Kohn-Sham potential is updated and mixed from step to step. Alternatively, the old and new charge density can be mixed and used as input for the next iteration. The one of the most frequently used mixing algorithm is Broyden's Method [Bro65].

The number of  $\mathbf{k}$ -points needed for this procedure depends mainly on the imaginary part of the complex energy  $z$  at which it is done. At large distances from the real axis, the structure constants as well as the Green function are smooth and less  $\mathbf{k}$ -points are necessary. Afterwards, all necessary quantities for constructing the Green function via Eq. (4.47) are at hand. First, the density of states can be calculated using Eq. (4.11). Using this information, the Fermi level can be determined by integration of the density of states,

$$N_e = \int_{-\infty}^{E_t} dE d(E). \quad (4.61)$$

If  $N_e$  equals the core charge  $Z$ , then  $E_t = \epsilon_F$ . Afterwards, a complex contour integration of

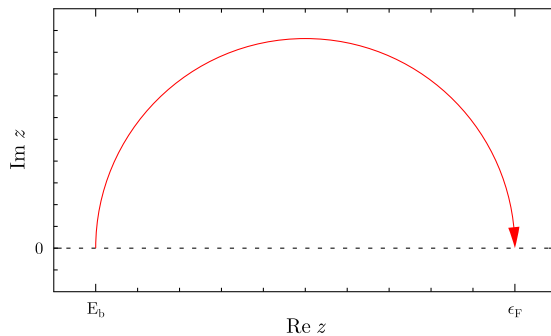


**Figure 4.4:** Typical circular integration path for the evaluation of the valence charge density using Eq. (4.62). For optimal performance, the structure constants for the Green function at integration points far away from the real axis can be calculated with less  $\mathbf{k}$ -points than in the vicinity of it.

the Green function from the bottom of the valence band  $E_b$  up to the Fermi energy,

$$n_v(\mathbf{r}) = -\frac{1}{\pi} \text{Im} \int_C^{[E_b, \epsilon_f]} dz \mathcal{G}(\mathbf{r}, \mathbf{r}, z), \quad (4.62)$$

is performed to obtain the valence charge density  $n_v(\mathbf{r})$ . The integration contour  $C$  is chosen such that the majority of integration points are located far away from the real axis where the Green function is smooth. The choice of this kind of integration path allows to reduce the necessary number of integration points from several 1000 near the real axis to typically 20-30 [MP06].

The core charge density  $n_c(\mathbf{r})$  is obtained separately by summing over the squares of the absolute values of the core wave functions. Finally, the obtained total charge density  $n(\mathbf{r}) = n_c(\mathbf{r}) + n_v(\mathbf{r})$  is used to calculate the potential via the Poisson equation. The complete Kohn-Sham potential  $V_{\text{out}}(\mathbf{r})$  is obtained by adding the exchange-correlation potential as functional of the density. This potential is used to construct a new input potential for the algorithm. Only when  $\|V_{\text{out}}(\mathbf{r}) - V_{\text{in}}(\mathbf{r})\| \leq \varepsilon$ , where  $\varepsilon$  is a predefined convergence parameter, the procedure finalizes and the potential is self-consistent up to an accuracy determined by  $\varepsilon$ . A summary of the described procedure is given in Fig. (4.3).

The converged Green function of a material is the basis for the calculation of response functions. The next chapter describes how it can be used to determine the response of an electron gas to a perturbation in the external potential.

## Application to lattice dynamics

Methods for the calculation of phonon dispersions within the scope of DFT exist since the late 1970s (see Chap. 2). However, it was not until the 1990s that the required evaluation of forces with the necessary precision became available as part of the KKR method. The so far used and in many applications very successful ASA and MT approximations in which atomic potential as well as valence charge density are assumed to be of spherical symmetry allow for good band structure calculations, but their simplifications are too crude to obtain the necessary accuracy required for lattice relaxations and force calculations with direct methods.

The crucial breakthrough was the development of a KKR method for the full Wigner-Seitz cell, the Full-Potential (FP) method [Zel87; GZN88; Dri91], which on one side avoids the interstitial and moon regions of the spherical ASA and MT cells, and on the other incorporates the aspherical components of potentials and charge densities. This new method allowed, besides the lattice relaxation at impurities and vacancies, the calculation of phonon frequencies [Ded+91; Zel+98; Asa+99; PZD02]. The latter have been obtained, in analogy to the finite-displacement method using supercells, by the displacement of a single atom from its equilibrium position within a finite cluster and subsequent calculation of all resulting force constants. Due to the shift of the atom from the equilibrium position (usually the center) of its cell, the angular momentum cutoff ( $\ell_{\max}$ ) has to be chosen rather high. Additionally, the cluster has to be large enough to ensure a decay of the forces between the displaced atom and the other cluster atoms to negligible values at its boundary. This reduces the field of application of this method to very simple systems.

The idea behind the work in hand is to use the linear-response principle to circumvent the finite-displacement method and thus to avoid the problems connected with reduced symmetry and off-center expansions of densities and potentials, whereby for a start the FP method should be relinquished.

The chapter is structured as follows: In the first part, a first-principles rigid-ion model for the dynamical matrix is derived, which is independent of the KKR at the first place. Afterwards, the necessary formalism for the change of the valence charge density upon a periodic lattice distortion is developed using linear response theory and the KKR formalism. The last part focuses on details of the implementation, test calculations and an outlook for further developments based on the tests.

### 5.1 Rigid-core model for force constants

According to Eqs. (2.23) and (2.42), the harmonic force constants are given as the second derivative of the potential energy of the crystal with respect to the displacements of atomic nuclei. This energy can be written as the sum of the direct Coulomb repulsion of the nuclei

$$E_{\text{nn}} = \frac{1}{2} \sum_{ll'} \sum_{ss'}^{\overbrace{(ls) \neq (l's')}} Z_s Z_{s'} \mathcal{V}_{l's'}^{ls}(0, 0) \quad (5.1)$$

on one side, and the potential-energy part of the Born-Oppenheimer energy in cell-centred coordinates

$$E_{\text{BO}} = E_{\text{ee}} + E_{\text{ne}} + E_{\text{xc}}[n] \quad (5.2)$$

$$= \frac{1}{2} \sum_{ll'} \sum_{ss'} \int d\mathbf{r} \int d\mathbf{r}' n_{ls}(\mathbf{r}) \mathcal{V}_{ll'}^{ss'}(\mathbf{r}, \mathbf{r}') n_{l's'}(\mathbf{r}') \quad (5.3)$$

$$+ \sum_{ll'} \sum_{ss'} \int d\mathbf{r} \int d\mathbf{r}' Z_s \delta(\mathbf{r}) \mathring{\mathcal{V}}_{ll'}^{ss'}(\mathbf{r} + \mathbf{u}(ls), \mathbf{r}') n_{l's'}(\mathbf{r}') + E_{\text{xc}}[n] \quad (5.4)$$

on the other. Here, the electron density at unit cell  $l$  and site  $s$  was denoted as

$$n_{ls}(\mathbf{r}) = n(\mathbf{R}_l + \boldsymbol{\tau}_s + \mathbf{r}) \quad (5.5)$$

and for the Coulomb interaction the definitions (2.62) and (2.63),

$$\mathcal{V}_{ll'}^{ss'}(\mathbf{r}, \mathbf{r}') = \frac{2}{|\mathbf{R}_l - \mathbf{R}_{l'} + \boldsymbol{\tau}_s - \boldsymbol{\tau}_{s'} + \mathbf{u}(ls) - \mathbf{u}(l's') + \mathbf{r} - \mathbf{r}'|}$$

$$\mathring{\mathcal{V}}_{ll'}^{ss'}(\mathbf{r}, \mathbf{r}') = \frac{2}{|\mathbf{R}_l - \mathbf{R}_{l'} + \boldsymbol{\tau}_s - \boldsymbol{\tau}_{s'} + \mathbf{r} - \mathbf{r}'|},$$

have been used. Again, the first quantity denotes the Coulomb potential experienced by two point charges with their respective coordinates given in cell-centred coordinates and which are displaced from their equilibrium positions by the displacement vectors  $\mathbf{u}$ . The second quantity denotes the potential of two particles in their equilibrium positions.

The first derivative of the energy expressions above with respect to an infinitesimal nuclear displacement  $\mathbf{u}(mi)$  results in the negative force acting on the nucleus at position  $\mathbf{R}_m + \boldsymbol{\tau}_i$ . According to the Hellmann-Feynman theorem, only terms which are explicitly dependent on  $\mathbf{u}(mi)$  survive in the force, resulting in Eq. (2.43).

To overcome the problems which are related to an aspherical distortion of the core electrons, a rigid-core model in which the core electrons move rigidly with the nuclei and are not polarizable upon external perturbations is used. For this purpose, the electron density is divided into valence and core parts,

$$n(\mathbf{x}) = n^c(\mathbf{x}) + n^v(\mathbf{x}), \quad (5.6)$$

where the core density  $n_c(\mathbf{x})$  is made up of deep-lying and strongly localized states. By definition,  $n_c$  vanishes at the cell boundary. Additionally, only spherical contributions to the density shall be included in  $n_c(\mathbf{x})$ , which is common for KKR calculations. Which electrons can be treated as core or valence states must be decided according to these conditions for every material under concern.

To be able to cope with the problems associated with the calculation of forces mentioned in Sec. 2.4.1, the core electron density and the nucleus can be combined into an ionic core, the density of which is given by

$$n_{ls}^{\text{ion}}(\mathbf{r} - \mathbf{u}(ls)) = Z_s \delta(\mathbf{r} - \mathbf{u}(ls)) - n_s^c(\mathbf{r} - \mathbf{u}(ls)). \quad (5.7)$$

In this model, often referred to as rigid-ion or rigid-core model, the core electrons are assumed to move rigidly together with the nucleus as it moves around its equilibrium position. This dependence on the nuclear coordinates is explicitly expressed by the appearance of the displacement vector in the above expression and has to be taken into account in the application of the Hellmann-Feynman theorem. For the calculation of forces which occur when the nucleus moves out of its equilibrium position it is, under the above assumptions, sufficient

to calculate the forces on the ion core as a whole. Forces between the nucleus and its surrounding core electrons are treated as internal forces and do not have to be evaluated. The advantage of this method lies in the fact that big errors in the force exerted on the nucleus due to an inaccurate description of the core density are avoided [Zec01]. The total charge of the core is given by

$$\int_{\Omega_{\text{cell}}} d\mathbf{r} n_{l_s}^{\text{ion}}(\mathbf{r}) = Z_s^*. \quad (5.8)$$

Using the above definitions, the potential energy of the crystal can be written as

$$E_{\text{tot}} = E_{\text{ion-ion}} + E_{\text{BO}}^{\text{ion}}, \quad (5.9)$$

in which the first term denotes the direct Coulomb repulsion of the non-overlapping ion cores, consisting of the positive nuclei and the rigidly bound core electrons. Its contribution to the dynamical matrix has already been discussed in sect. 2.5.

## 5.2 Contribution of valence electrons

The second term in Eq. (5.9) is the rigid-ion version of the Born-Oppenheimer energy which, due to the separation of the density, consists of four terms:

$$\begin{aligned} E_{\text{BO}}^{\text{ion}} &= E_{\text{nv}} + E_{\text{cv}} + E_{\text{vv}} + E_{\text{xc}}[n^{\text{c}} + n^{\text{v}}] \\ &= - \sum_{ll'} \sum_{ss'} \int d\mathbf{r} \int d\mathbf{r}' Z_s \delta(\mathbf{r} - \mathbf{u}(ls)) \mathring{\mathcal{V}}_{ll'}^{ss'}(\mathbf{r}, \mathbf{r}') n_{l's'}^{\text{v}}(\mathbf{r}') \\ &\quad + \sum_{ll'} \sum_{ss'} \int d\mathbf{r} \int d\mathbf{r}' n_s^{\text{c}}(\mathbf{r} - \mathbf{u}(ls)) \mathring{\mathcal{V}}_{ll'}^{ss'}(\mathbf{r}, \mathbf{r}') n_{l's'}^{\text{v}}(\mathbf{r}') \\ &\quad + \frac{1}{2} \sum_{ll'} \sum_{ss'} \int d\mathbf{r} \int d\mathbf{r}' n_{l_s}^{\text{v}}(\mathbf{r}) \mathring{\mathcal{V}}_{ll'}^{ss'}(\mathbf{r}, \mathbf{r}') n_{l's'}^{\text{v}}(\mathbf{r}') \\ &\quad + \sum_{ls} \int d\mathbf{r} [n_s^{\text{c}}(\mathbf{r} - \mathbf{u}(ls)) + n_{l_s}^{\text{v}}(\mathbf{r})] \epsilon_{\text{xc}}^{\text{hom}}(n_s^{\text{c}}(\mathbf{r} - \mathbf{u}(ls)) + n_{l_s}^{\text{v}}(\mathbf{r})). \end{aligned} \quad (5.10)$$

The first term denotes the direct Coulomb interaction between positive nuclei and valence electrons. Its dependence on the nuclear displacements is taken into account via the delta distribution which describes the spatial dependence of the nuclear charge. The second term describes the interaction energy between core and valence electrons. The following expression represents the classical Hartree energy of the valence electrons and does not depend explicitly on the nuclear coordinates. The last line represents the exchange-correlation energy of the electronic system. It is important to note that  $n^{\text{c}}$  and  $n^{\text{v}}$  are self-consistent solutions for the undisturbed crystal. The rigid-ion model assumes that the core electrons do not change their relative distribution but are shifted rigidly with their respective nuclei, which is why the core density depends explicitly on the displacement vector  $\mathbf{u}$ . This assumption can not be made for the valence electrons, which will assume a new minimum-energy configuration according to the perturbed crystal lattice. This adiabatic change has to be calculated self-consistently using linear response theory. Thus, the ground state of the valence electrons does not depend explicitly on the nuclear coordinates, but implicitly.

The interaction among the valence electrons (third line) is not explicitly dependent on the nuclear coordinates and subsequently will not contribute to the forces after application of the Hellmann-Feynman theorem. Therefore, after evaluating the delta distribution, the

terms of the effective electronic contribution to the total energy relevant for force calculations can be written as

$$\begin{aligned}
 E_{\text{BO}}^{\text{ion}} = & - \sum_{l'} \sum_{ss'} Z_s \int d\mathbf{r}' \dot{\mathcal{V}}_{ll'}^{ss'}(\mathbf{u}(ls), \mathbf{r}') n_{l's'}^{\text{v}}(\mathbf{r}') \\
 & + \sum_{l'} \sum_{ss'} \int d\mathbf{r} \int d\mathbf{r}' n_s^{\text{c}}(\mathbf{r} - \mathbf{u}(ls)) \dot{\mathcal{V}}_{ll'}^{ss'}(\mathbf{r}, \mathbf{r}') n_{l's'}^{\text{v}}(\mathbf{r}') \\
 & + \sum_{ls} \int d\mathbf{r} [n_s^{\text{c}}(\mathbf{r} - \mathbf{u}(ls)) + n_{ls}^{\text{v}}(\mathbf{r})] \epsilon_{\text{xc}}^{\text{hom}} [n_s^{\text{c}}(\mathbf{r} - \mathbf{u}(ls)) + n_{ls}^{\text{v}}(\mathbf{r})].
 \end{aligned} \tag{5.11}$$

The first derivative with respect to a displacement of ion  $i$  in cell  $m$  in direction  $\alpha$ ,  $u_\alpha(im)$ , gives the respective component of the force acting on the same ion. Using the Hellmann-Feynman theorem, one obtains

$$\begin{aligned}
 -F_\alpha^{\text{el}}(mi) = & Z_i \sum_{ls} \int d\mathbf{r} \left[ \partial_{r_\alpha} \dot{\mathcal{V}}_{ml}^{is}(\mathbf{u}(mi), \mathbf{r}) \right] n_{ls}^{\text{v}}(\mathbf{r}) \\
 & - \sum_{ls} \int d\mathbf{r} \int d\mathbf{r}' [\partial_{r_\alpha} n_i^{\text{c}}(\mathbf{r} - \mathbf{u}(mi))] \dot{\mathcal{V}}_{ml}^{is}(\mathbf{r}, \mathbf{r}') n_{ls}^{\text{v}}(\mathbf{r}') \\
 & - \int d\mathbf{r} [\partial_{r_\alpha} n_i^{\text{c}}(\mathbf{r} - \mathbf{u}(mi))] v_{\text{xc}}^{\text{hom}} [n_i^{\text{c}}(\mathbf{r} - \mathbf{u}(mi)) + n_{mi}^{\text{v}}(\mathbf{r})],
 \end{aligned} \tag{5.12}$$

where in the first line relation (2.67) was used to use  $\mathbf{r}$  as differentiation variable. In order to avoid the numerical derivation of the nuclear charge density, the second term can also be rewritten as

$$\begin{aligned}
 {}^{(2)}F_\alpha^{\text{el}}(mi) = & \sum_{ls} \int d\mathbf{r} \int d\mathbf{r}' [\partial_{r_\alpha} n_i^{\text{c}}(\mathbf{r} - \mathbf{u}(mi))] \dot{\mathcal{V}}_{ml}^{is}(\mathbf{r}, \mathbf{r}') n_{ls}^{\text{v}}(\mathbf{r}') \\
 = & \sum_{ls} \int d\mathbf{r} \int d\mathbf{r}' \partial_{r_\alpha} \left[ n_i^{\text{c}}(\mathbf{r} - \mathbf{u}(mi)) \dot{\mathcal{V}}_{ml}^{is}(\mathbf{r}, \mathbf{r}') \right] n_{ls}^{\text{v}}(\mathbf{r}') \quad (*) \\
 & - \sum_{ls} \int d\mathbf{r} \int d\mathbf{r}' n_i^{\text{c}}(\mathbf{r} - \mathbf{u}(mi)) \left[ \partial_{r_\alpha} \dot{\mathcal{V}}_{ml}^{is}(\mathbf{r}, \mathbf{r}') \right] n_{ls}^{\text{v}}(\mathbf{r}').
 \end{aligned} \tag{5.13}$$

Writing all three components of the force in vector form, the first term (\*) reads

$$(*) = \sum_{ls} \int d\mathbf{r}' n_{ls}^{\text{v}}(\mathbf{r}') \int d\mathbf{r} \nabla_{\mathbf{r}} \left[ n_i^{\text{c}}(\mathbf{r} - \mathbf{u}(mi)) \dot{\mathcal{V}}_{ml}^{is}(\mathbf{r}, \mathbf{r}') \right]$$

which, according to Gauss's divergence theorem, can be rewritten in form of a surface integral over the boundary of the Wigner-Seitz cell,

$$(*) = \sum_{ls} \int d\mathbf{r}' n_{ls}^{\text{v}}(\mathbf{r}') \int d\mathbf{S} \left[ n_i^{\text{c}}(\mathbf{r}(\mathbf{S}) - \mathbf{u}(mi)) \dot{\mathcal{V}}_{ml}^{is}(\mathbf{r}(\mathbf{S}), \mathbf{r}') \right] = 0. \tag{5.14}$$

This expression gives zero because the core charge density vanishes at the surface by definition. Thus,

$$\begin{aligned}
 -F_\alpha^{\text{el}}(mi) = & Z_i \sum_{ls} \int d\mathbf{r} \left[ \partial_{r_\alpha} \dot{\mathcal{V}}_{ml}^{is}(\mathbf{u}(mi), \mathbf{r}) \right] n_{ls}^{\text{v}}(\mathbf{r}) \\
 & + \sum_{ls} \int d\mathbf{r} \int d\mathbf{r}' n_i^{\text{c}}(\mathbf{r} - \mathbf{u}(mi)) \left[ \partial_{r_\alpha} \dot{\mathcal{V}}_{ml}^{is}(\mathbf{r}, \mathbf{r}') \right] n_{ls}^{\text{v}}(\mathbf{r}') \\
 & - \int d\mathbf{r} [\partial_{r_\alpha} n_i^{\text{c}}(\mathbf{r} - \mathbf{u}(mi))] v_{\text{xc}}^{\text{hom}} [n_i^{\text{c}}(\mathbf{r} - \mathbf{u}(mi)) + n_{mi}^{\text{v}}(\mathbf{r})].
 \end{aligned} \tag{5.15}$$

During the development of the numerical details of the method it turned out that the angular-momentum expansion of  $\partial_{r_\alpha} \mathring{\mathcal{V}}_{ml}^{is}(\mathbf{r}, \mathbf{r}')$  converges very slowly. For this reason, Eq. (5.12) will be used in the following, although it leads to a second derivative of the core charge density in the next step:

Continuing from this equation, the electronic contribution to the linear-order force constants are obtained by means of Eq. (2.23) and result in

$$\begin{aligned}
 \phi_{\alpha\beta}^{\text{ion}}(mi|nj) &= Z_i \sum_{ls} \int d\mathbf{r} \left[ \partial_{r_\alpha} \mathring{\mathcal{V}}_{ml}^{is}(0, \mathbf{r}) \right]_{\mathbf{u}=0} \mathcal{K}_{n,\beta}^j(\mathbf{r}, ls) \\
 &\quad - \delta_{mn} \delta_{ij} Z_i \sum_{ls} \int d\mathbf{r} \left[ \partial_{r_\alpha} \partial_{r_\beta} \mathring{\mathcal{V}}_{ml}^{is}(0, \mathbf{r}) \right]_{\mathbf{u}=0} n_{ls}^v(\mathbf{r}') \\
 &\quad \sum_{ls} \int d\mathbf{r} \int d\mathbf{r}' [\partial_{r_\alpha} n_i^c(\mathbf{r})] \mathring{\mathcal{V}}_{ml}^{is}(\mathbf{r}, \mathbf{r}') \mathcal{K}_{n,\beta}^j(\mathbf{r}', ls) \\
 &\quad - \delta_{mn} \delta_{ij} \sum_{ls} \int d\mathbf{r} \int d\mathbf{r}' [\partial_{r_\beta} \partial_{r_\alpha} n_i^c(\mathbf{r})] \mathring{\mathcal{V}}_{ml}^{is}(\mathbf{r}, \mathbf{r}') n_{ls}^v(\mathbf{r}') \\
 &\quad - \int d\mathbf{r} f_{xc}[n(\mathbf{r})] \partial_{r_\alpha} n^c(\mathbf{r}) \mathcal{K}_{n,\beta}^j(\mathbf{r}, mi) \\
 &\quad + \delta_{mn} \delta_{ij} \int d\mathbf{r} f_{xc}[n(\mathbf{r})] \partial_{r_\alpha} n^c(\mathbf{r}) \partial_{r_\beta} n^c(\mathbf{r}) \\
 &= \sum_{k=1}^6 \phi_{\alpha\beta}^{\text{el}(k)}(mi|nj)
 \end{aligned} \tag{5.16}$$

Here, the quantity  $\mathcal{K}$  denotes the derivative of the valence charge density with respect to a displacement of the ion at  $\mathbf{R}_n + \boldsymbol{\tau}_j + \mathbf{u}(nj)$ . Its approximation by linear response theory will be discussed in detail in the next section.

A lattice Fourier transform of the above expression leads to the electronic part of the dynamical matrix. How this can be achieved shall be illustrated for the first term of Eq. (5.16):

$$\begin{aligned}
 \text{el}^{(1)} \hat{D}_{\alpha\beta}^{ij}(\mathbf{q}) &= \sum_n \phi_{\alpha\beta}^{\text{el}(1)}(0i|nj) e^{i\mathbf{q} \cdot \mathbf{R}_n} \\
 &= Z_i \sum_n e^{i\mathbf{q} \cdot \mathbf{R}_n} \sum_{ls} \int d\mathbf{r} \left[ \partial_{r_\alpha} \mathring{\mathcal{V}}_{0l}^{is}(0, \mathbf{r}) \right] \mathcal{K}_{n,\beta}^j(\mathbf{r}, ls) e^{i\mathbf{q} \cdot \mathbf{R}_l} e^{-i\mathbf{q} \cdot \mathbf{R}_l}.
 \end{aligned}$$

The unit factor appended at the end will be useful to transform the two functions  $\partial \mathring{\mathcal{V}}$  and  $\mathcal{K}$  which depend on vectors between different lattice points:

$$\begin{aligned}
 \text{el}^{(1)} \hat{D}_{\alpha\beta}^{ij}(\mathbf{q}) &= Z_i \int d\mathbf{r} \underbrace{\sum_{ls} \left[ \partial_{r_\alpha} \mathring{\mathcal{V}}_{0l}^{is}(0, \mathbf{r}) \right] e^{i\mathbf{q} \cdot \mathbf{R}_l}}_{=\sum_s \mathcal{C}_\alpha^{is}(\mathbf{r}, \mathbf{q})} \underbrace{\sum_n \mathcal{K}_{n,\beta}^j(\mathbf{r}, ls) e^{i\mathbf{q} \cdot (\mathbf{R}_n - \mathbf{R}_l)}}_{=\mathcal{K}_\beta^j(\mathbf{r}', \mathbf{q}, s)},
 \end{aligned}$$

where the Fourier-transformed  $\mathcal{K}$  can be obtained as shown because the sum running over all lattice vectors  $\mathbf{R}_n$  is independent of the second lattice point  $l$ . The function  $\mathcal{C}(\mathbf{r}, \mathbf{q})$ , which is the derivative of the FT of the lattice potential, is derived in App. A. Thus,

$$\text{el}^{(1)} \hat{D}_{\alpha\beta}^{ij}(\mathbf{q}) = Z_i \int d\mathbf{r} \sum_s \mathcal{C}_\alpha^{is}(\mathbf{r}, \mathbf{q}) \mathcal{K}_\beta^j(\mathbf{r}', \mathbf{q}, s). \tag{5.17}$$

Similar transformations can be made with terms 3 and 5 of the force constants (5.16). The remaining terms 2, 4 and 6 are diagonal with respect to site and lattice point, which has the

consequence that their FT is not  $\mathbf{q}$ -dependent. Thus, the electronic part of the dynamical matrix can be summarized as

$${}^{\text{el}}D_{\alpha\beta}^{ij}(\mathbf{q}) = \frac{1}{\sqrt{M_i M_j}} \left[ {}^{\text{el}}\hat{D}_{\alpha\beta}^{ij}(\mathbf{q}) - \delta_{ij} {}^{\text{el}}\hat{D}_{\alpha\beta}^{ii}(\mathbf{q} = 0) \right], \quad (5.18)$$

which is very similar to the expression for the ionic contribution (2.72). The argument  $\mathbf{q} = 0$  shall symbolize that this function is independent of  $\mathbf{q}$ . The  $\mathbf{q}$ -dependent contribution reads

$${}^{\text{el}}\hat{D}_{\alpha\beta}^{ij}(\mathbf{q}) = Z_i \int d\mathbf{r} \sum_s \mathcal{C}_{\alpha}^{is}(\mathbf{r}, \mathbf{q}) \mathcal{K}_{\beta}^j(\mathbf{r}, \mathbf{q}, s) \quad (5.19)$$

$$+ \int d\mathbf{r} \int d\mathbf{r}' [\partial_{r_{\alpha}} n_i^c(\mathbf{r})] \sum_s \mathcal{V}_{ml}^{is}(\mathbf{r}, \mathbf{r}', \mathbf{q}) \mathcal{K}_{\beta}^j(\mathbf{r}', \mathbf{q}, s) \quad (5.20)$$

$$- \int d\mathbf{r} f_{\text{xc}}[n(\mathbf{r}, i)] \partial_{r_{\alpha}} n_i^c(\mathbf{r}) \mathcal{K}_{\beta}^j(\mathbf{r}, \mathbf{q}, i), \quad (5.21)$$

whereas the  $\mathbf{q}$ -independent part is given by

$${}^{\text{el}}\hat{D}_{\alpha\beta}^{ii}(\mathbf{q} = 0) = Z_i \int d\mathbf{r} \sum_s \left[ \partial_{r_{\alpha}} \partial_{r_{\beta}} \mathcal{V}_{\alpha}^{is}(0, \mathbf{r}) \right] n_s^v(\mathbf{r}) \quad (5.22)$$

$$+ \int d\mathbf{r} \int d\mathbf{r}' [\partial_{r_{\alpha}} \partial_{r_{\beta}} n_i^c(\mathbf{r})] \sum_s \mathcal{V}_{00}^{is}(\mathbf{r}, \mathbf{r}') n_s^v(\mathbf{r}') \quad (5.23)$$

$$- \int d\mathbf{r} f_{\text{xc}}[n(\mathbf{r}, i)] \partial_{r_{\alpha}} n_i^c(\mathbf{r}) \partial_{r_{\beta}} n_i^c(\mathbf{r}). \quad (5.24)$$

In practice, there is no need to calculate the  $\mathbf{q}$ -independent part since it is determined by the behaviour of the acoustic modes for long wavelengths: The transverse modes have to approach zero and the longitudinal modes have to approach the value of the ion plasma frequency, such that the total dynamical matrix approaches zero for  $\mathbf{q} \rightarrow 0$ .

Still, the missing piece is the response of the valence charge density to the displacement of an ion,  $\mathcal{K}$ . Its derivation is discussed in the following chapters.

### 5.2.1 Perturbation of the valence charge density

To implement TDDFT in its linear response version into a multiple scattering scheme, several adaptations are necessary. In this work, only the static response of the electronic system

$$\chi(\mathbf{x}, \mathbf{x}') = \chi(\mathbf{x}, \mathbf{x}', \omega = 0), \quad (5.25)$$

shall be under concern. The neglect of the frequency dependence of the susceptibility is crucial, but a good approximation for density perturbations on a time scale which is slow compared to relaxation times of the density. Lattice vibrations are an example for this kind of perturbation. The goal is to obtain a computationally feasible scheme for the calculation of the static interacting susceptibility, starting from the static Kohn-Sham susceptibility, hereafter being referred to as polarization function

$$\Pi(\mathbf{x}, \mathbf{x}') = \chi_{\text{KS}}(\mathbf{x}, \mathbf{x}', \omega = 0). \quad (5.26)$$

The above introduced quantity  $\mathcal{K}$  is defined as

$$\mathcal{K}_{n,\beta}^j(\mathbf{r}', l' s') = \frac{\partial n_{l' s'}^v(\mathbf{r}')}{\partial u_{\beta}(n_j)} \quad (5.27)$$

and describes the change of the valence charge density  $n^v(\mathbf{r}, l' s')$  in cell  $l'$  and place  $s'$  under an infinitesimal displacement of ion  $j$  in cell  $n$  in direction  $\beta$ .

According to section 3.4, the perturbation of the total charge density, induced by a small change of the potential, can be described using linear response theory and is given as

$$\delta n(\mathbf{x}) = \int d\mathbf{x}' \chi(\mathbf{x}, \mathbf{x}') \delta V^{\text{ext}}(\mathbf{x}') \quad (5.28)$$

in terms of the periodic nuclear potential  $V^{\text{ext}}$  and the electronic susceptibility which is defined by

$$\chi(\mathbf{x}, \mathbf{x}') = \Pi(\mathbf{x}, \mathbf{x}') + \int d\mathbf{x}_1 \Pi(\mathbf{x}, \mathbf{x}_1) \int d\mathbf{x}_2 F_{\text{xc}}(\mathbf{x}_1, \mathbf{x}_2) \chi(\mathbf{x}_2, \mathbf{x}'), \quad (5.29)$$

$$F(\mathbf{x}_1, \mathbf{x}_2) = f_{\text{xc}}^{\text{ALDA}}(\mathbf{x}_1, \mathbf{x}_2) + \frac{2}{|\mathbf{x}_1 - \mathbf{x}_2|}. \quad (5.30)$$

The variation of the charge density is the sum of the variations of both core and valence density. Likewise, the non-interacting Kohn-Sham susceptibility  $\chi_{\text{KS}}$  can be written as sum of the polarization functions of core and valence electrons, respectively,

$$\delta n(\mathbf{x}) = \delta n^c(\mathbf{x}) + \delta n^v(\mathbf{x}) \quad (5.31)$$

$$\Pi(\mathbf{x}, \mathbf{x}') = \Pi^c(\mathbf{x}, \mathbf{x}') + \Pi^v(\mathbf{x}, \mathbf{x}'), \quad (5.32)$$

where the latter division follows directly from the definition of the non-interacting susceptibility as a sum over states (Eq. (3.64)). Since the change of the core density is described as rigid shift, only the polarization function of the valence density is needed in the following. For the moment, it shall be assumed that this quantity is known. Sect. 5.2.2 describes in detail how it can be obtained from the single-particle Green function.

Under the assumption that the interacting susceptibility can be similarly written as sum  $\chi = \chi^c + \chi^v$  of a core and a valence part, the change of the valence charge density reads in linear order

$$\delta n^v(\mathbf{x}) = \int d\mathbf{x}' \chi^v(\mathbf{x}, \mathbf{x}') \delta V^{\text{ext}}(\mathbf{x}'). \quad (5.33)$$

The valence susceptibility  $\chi^v$  correctly incorporates the interaction with core electrons and is given by the Dyson-like equation

$$\chi^v(\mathbf{x}, \mathbf{x}') = \Pi^v(\mathbf{x}, \mathbf{x}') + \int d\mathbf{x}_1 \Pi^v(\mathbf{x}, \mathbf{x}_1) \int d\mathbf{x}_2 F(\mathbf{x}_1, \mathbf{x}_2) \chi(\mathbf{x}_2, \mathbf{x}') \quad (5.34)$$

Combining the last equation with Eqs. (5.33) and (5.27) and turning back to cell-centred coordinates

$$\Pi(\mathbf{x}, \mathbf{x}') = \Pi(\mathbf{R}_n + \tau_i + \mathbf{r}, \mathbf{R}_{n'} + \tau_j + \mathbf{r}') = \Pi_{nn'}^{ij}(\mathbf{r}, \mathbf{r}'), \quad (5.35)$$

this approach results in a change of the valence charge density given by

$$\begin{aligned} \mathcal{K}_{n,\beta}^j(\mathbf{r}', l' s') &= \frac{\partial n_{l' s'}^v(\mathbf{r}')}{\partial u_\beta(nj)} \\ &= \sum_{l' s'} \int d\mathbf{r}' \Pi_{ll'}^{s s'}(\mathbf{r}, \mathbf{r}') \frac{\partial V^{\text{ext}}(\mathbf{r}', l' s')}{\partial u_\beta(nj)} \\ &\quad + \sum_{l_1 s_1} \int d\mathbf{r}_1 \sum_{l_2 s_2} \int d\mathbf{r}_2 \Pi_{ll_1}^{s s_1}(\mathbf{r}, \mathbf{r}_1) F_{l_1 l_2}^{s_1 s_2}(\mathbf{r}_1, \mathbf{r}_2) \times \\ &\quad \times \sum_{l' s'} \int d\mathbf{r}' \chi_{l_2 l'}^{s_2 s'}(\mathbf{r}_2, \mathbf{r}') \frac{\partial V^{\text{ext}}(\mathbf{r}', l' s')}{\partial u_\beta(nj)}. \end{aligned} \quad (5.36)$$

By comparison with Eq. (5.28), it becomes apparent that the last line can be replaced by

$$\begin{aligned} \sum_{l's'} \int d\mathbf{r}' \chi_{l_2 l'}^{s_2 s'}(\mathbf{r}_2, \mathbf{r}') \frac{\partial V^{\text{ext}}(\mathbf{r}', l's')}{\partial u_\beta(nj)} &= \frac{\partial n_{l_2 s_2}(\mathbf{r}_2)}{\partial u_\beta(nj)} \\ &= \frac{\partial n_{l_2 s_2}^c(\mathbf{r}_2 - \mathbf{u}(nj))}{\partial u_\beta(nj)} + \mathcal{K}_{n,\beta}^j(\mathbf{r}_2, l_2 s_2), \end{aligned} \quad (5.37)$$

where the rigid-core approximation was used again for the derivative of the core charge density with respect to an ionic displacement. After careful reordering of indices, Eq. (5.36) can be turned in to a compact linear integral equation for the change of the valence charge density,

$$\mathcal{K}_{n,\beta}^j(\mathbf{r}, ls) = \mathcal{I}_{nl}^{js}(\mathbf{r}) + \sum_{l's'} \int d\mathbf{r}' A_{ll'}^{ss'}(\mathbf{r}, \mathbf{r}') \mathcal{K}_{n,\beta}^j(\mathbf{r}', l's'). \quad (5.38)$$

The inhomogeneity  $\mathcal{I}_{nl}^{js}(\mathbf{r})$  is the offspring of the polarization function in the susceptibility Dyson equation (5.34) and contains all terms which are independent of  $\mathcal{K}$ ,

$$\mathcal{I}_{nl}^{js}(\mathbf{r}) = \sum_{l's'} \int d\mathbf{r}' \Pi_{ll'}^{ss'}(\mathbf{r}, \mathbf{r}') \frac{\partial V^{\text{ext}}(\mathbf{r}', l's')}{\partial u_\beta(nj)} \quad (5.39)$$

$$+ \sum_{l's'} \int d\mathbf{r}' \Pi_{ll'}^{ss'}(\mathbf{r}, \mathbf{r}') \sum_{l''1s''} \int d\mathbf{r}'' F_{l'l''}^{s's''}(\mathbf{r}', \mathbf{r}'') \partial_{r_\beta} n_j^n(\mathbf{r}''). \quad (5.40)$$

The kernel of the equation is given by

$$A_{ll'}^{ss'}(\mathbf{r}, \mathbf{r}') = \sum_{l''s''} \int d\mathbf{r}'' \Pi_{ll''}^{ss''}(\mathbf{r}, \mathbf{r}'') F_{l''l'}^{s''s'}(\mathbf{r}'', \mathbf{r}') \quad (5.41)$$

and the potential  $F$ , using the respective coordinates, reads

$$F_{l'l''}^{s's''}(\mathbf{r}', \mathbf{r}'') = \hat{V}_{l'l''}^{s's''}(\mathbf{r}', \mathbf{r}'') + \delta_{l'l''} \delta_{s's''} \delta(\mathbf{r}' - \mathbf{r}'') f_{\text{xc}}^{\text{ALDA}}(\mathbf{r}', \mathbf{r}'', l's'). \quad (5.42)$$

$\mathcal{K}$  only depends on the relative positions of the displaced ion and the respective point  $\mathbf{R}_l + \boldsymbol{\tau}_s + \mathbf{r}$  at which the density is probed, allowing for the lattice Fourier transform

$$\mathcal{K}_\beta^j(\mathbf{r}, \mathbf{q}, s) = \sum_n \mathcal{K}_{n,\beta}^j(\mathbf{r}, ls) e^{i\mathbf{q} \cdot (\mathbf{R}_n - \mathbf{R}_l)} = \sum_n \mathcal{K}_{n,\beta}^j(\mathbf{r}, 0s) e^{i\mathbf{q} \cdot (\mathbf{R}_n)}. \quad (5.43)$$

Using this approach, a Fourier representation of the integral equation can be found in a way similar to the dynamical matrix (p. 53) and is given by

$$\mathcal{K}_\beta^j(\mathbf{r}, \mathbf{q}, s) = \mathcal{I}^{js}(\mathbf{r}, \mathbf{q}) + \sum_{s'} \int d\mathbf{r}' A^{ss'}(\mathbf{r}, \mathbf{r}', \mathbf{q}) \mathcal{K}_\beta^j(\mathbf{r}', \mathbf{q}, s') \quad (5.44)$$

with the respective inhomogeneity and kernel

$$\mathcal{I}^{js}(\mathbf{r}, \mathbf{q}) = \sum_{s'} \int d\mathbf{r}' \Pi^{ss'}(\mathbf{r}, \mathbf{r}', \mathbf{q}) \mathcal{C}_{\text{ext}}^{js'}(\mathbf{r}', \mathbf{q}) \quad (5.45)$$

$$- \sum_{s'} \int d\mathbf{r}' \Pi^{ss'}(\mathbf{r}, \mathbf{r}', \mathbf{q}) \int d\mathbf{r}'' \partial_{r_\beta} n_j^c(\mathbf{r}'') V^{s'j}(\mathbf{r}', \mathbf{r}'', \mathbf{q}) \quad (5.46)$$

$$- \int d\mathbf{r}' \Pi^{sj}(\mathbf{r}, \mathbf{r}', \mathbf{q}) \partial_{r_\beta} n_j^c(\mathbf{r}') f_{\text{xc}}[n(\mathbf{r}', s')] \delta_{sj} \quad (5.47)$$

$$A^{ss'}(\mathbf{r}, \mathbf{r}', \mathbf{q}) = - \sum_{s''} \int d\mathbf{r}'' \Pi^{ss''}(\mathbf{r}, \mathbf{r}'', \mathbf{q}) V^{s's''}(\mathbf{r}'', \mathbf{r}', \mathbf{q}) \quad (5.48)$$

$$+ \Pi^{ss'}(\mathbf{r}, \mathbf{r}', \mathbf{q}) f_{\text{xc}}[n(\mathbf{r}', s')]. \quad (5.49)$$

All quantities which enter this equation can be obtained from a self-consistent KKR calculation. While the calculation of the charge density was already discussed in chap. 4, the next section explains how the polarization function  $\Pi$  can be constructed from the KKR Green function. The Fourier transform of the Coulomb potential,  $V^{ss'}(\mathbf{r}, \mathbf{r}', \mathbf{q})$ , is described in App. A.2. The function  $C_{\text{ext}}^{js'}$  is the lattice Fourier transform of the derivative of the external potential with respect to an atomic displacement and is closely related to the derivative  $C^j$  used in the dynamical matrix (5.21). Both are discussed in App. A.3.

### 5.2.2 A Green function formulation of the non-interacting susceptibility

The solution of the self-consistent KKR equations results in the single-particle Green function of a crystal, describing the properties of single electrons moving in an effective potential. To obtain a corresponding representation of the polarization function, a good starting point is its description in terms of Kohn-Sham eigenfunctions in Eq. (3.64),

$$\begin{aligned} \Pi(\mathbf{x}, \mathbf{x}') &= \lim_{\eta \rightarrow 0^+} \left( \sum_{ij} f_i \frac{\phi_j(\mathbf{x}) \phi_j^*(\mathbf{x}') \phi_i(\mathbf{x}') \phi_i(\mathbf{x})^*}{\epsilon_i - \epsilon_j - \hbar\omega - i\hbar\eta} \right. \\ &\quad \left. - \sum_{ij} f_j \frac{\phi_j(\mathbf{x}) \phi_j^*(\mathbf{x}') \phi_i(\mathbf{x}') \phi_i(\mathbf{x})^*}{\epsilon_i - \epsilon_j - \hbar\omega - i\hbar\eta} \right) \\ &= \Pi_A(\mathbf{x}, \mathbf{x}') + \Pi_B(\mathbf{x}, \mathbf{x}'). \end{aligned} \quad (5.50)$$

The susceptibility has been split into two terms again because they have to be treated separately. Following [Gon00], the Residue theorem can be used to obtain the auxiliary formula

$$\frac{1}{\epsilon_i - \epsilon_j + 2i\eta} = \frac{1}{2\pi i} \oint_C \frac{dz}{(z - \epsilon_i - i\eta)(z - \epsilon_j + i\eta)}, \quad (5.51)$$

where the integral is taken on a closed contour  $C$  within the complex energy plane. Using this result and keeping in mind that the limit  $\eta \rightarrow 0$  is taken, the first part of Eq. (5.50) can be expressed as

$$\begin{aligned} \Pi_A(\mathbf{x}, \mathbf{x}') &= \lim_{\eta \rightarrow 0^+} \sum_{ij} f_i \frac{\phi_j(\mathbf{x}) \phi_j^*(\mathbf{x}') \phi_i(\mathbf{x}') \phi_i(\mathbf{x})^*}{\epsilon_i - \epsilon_j - \hbar\omega - i\hbar\eta} \\ &= \frac{1}{2\pi i} \lim_{\eta \rightarrow 0^+} \sum_{ij} f_i \oint_C dz \frac{\phi_j(\mathbf{x}) \phi_j^*(\mathbf{x}') \phi_i(\mathbf{x}') \phi_i(\mathbf{x})^*}{(z - \epsilon_i - i\eta)(z - \epsilon_j + i\eta)}. \end{aligned} \quad (5.52)$$

The actual shape of the contour can be chosen accordingly to match certain boundary conditions. Since the response function of the valence electron density shall be obtained, the integration can be restricted to an energy interval between the bottom of the valence band  $E_b$  and the Fermi level  $E_f$ . Now summation and integration can be exchanged, giving

$$\Pi_A(\mathbf{x}, \mathbf{x}') = \frac{1}{2\pi i} \lim_{\eta \rightarrow 0^+} \oint_{c_1}^{[E_b, E_f]} dz \sum_{ij} \frac{\phi_j(\mathbf{x}) \phi_j^*(\mathbf{x}') \phi_i(\mathbf{x}') \phi_i(\mathbf{x})^*}{(z - \epsilon_i - i\eta)(z - \epsilon_j + i\eta)}. \quad (5.53)$$

The integration only includes occupied states of the valence band, which is why the occupation numbers  $f_i$  can be omitted. A schematic view of the integration contour  $c_1$  used here, lying within the upper half of the complex plane, is given in Fig. 5.1 (left panel).

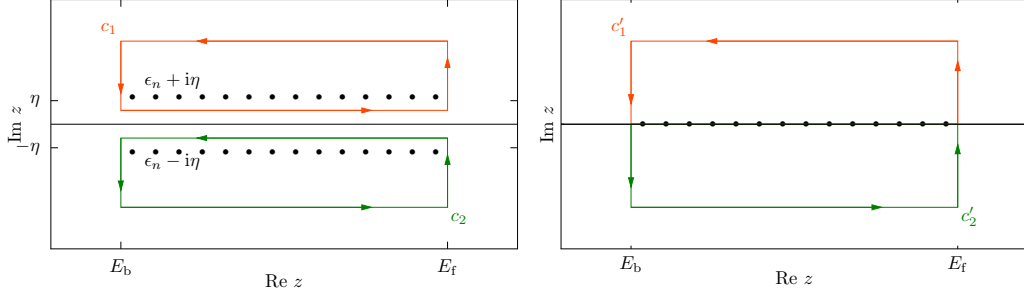


**Figure 5.1:** Different contours for complex energy integration. Diagram adapted from [Gon00].

Comparing this to the spectral representation of the Green function in terms of Kohn-Sham orbitals,

$$\mathcal{G}(\mathbf{x}, \mathbf{x}', z) = \sum_i \frac{\phi_i(\mathbf{x})\phi_i^*(\mathbf{x}')}{z - \epsilon_i}. \quad (5.54)$$

the first part of the static response function is obtained as

$$\Pi_A(\mathbf{x}, \mathbf{x}') = \frac{1}{2\pi i} \lim_{\eta \rightarrow 0^+} \oint_{c_1}^{[E_b, E_f]} dz \mathcal{G}(\mathbf{x}, \mathbf{x}', z - i\eta) \mathcal{G}(\mathbf{x}', \mathbf{x}, z + i\eta). \quad (5.55)$$

In a similar fashion, the second term of Eq. (5.50) can be written as

$$\begin{aligned} \Pi_B(\mathbf{x}, \mathbf{x}') &= - \lim_{\eta \rightarrow 0^+} \sum_{ij} f_j \frac{\phi_j(\mathbf{x})\phi_j^*(\mathbf{x}')\phi_i(\mathbf{x}')\phi_i(\mathbf{x})^*}{\epsilon_i - \epsilon_j - \hbar\omega - i\hbar\eta} \\ &= \frac{1}{2\pi i} \lim_{\eta \rightarrow 0^+} \oint_{c_2}^{[E_b, E_f]} dz \sum_{ij} \frac{\phi_j(\mathbf{x})\phi_j^*(\mathbf{x}')\phi_i(\mathbf{x}')\phi_i(\mathbf{x})^*}{(-z + \epsilon_i + i\eta)(z - \epsilon_j + i\eta)}, \end{aligned} \quad (5.56)$$

where the negative sign was absorbed by the denominator and the integration contour  $c_2$ , as shown in Fig. 5.1 (left panel), was used. Summing up, the total valence susceptibility reads

$$\begin{aligned} \Pi(\mathbf{x}, \mathbf{x}') &= \frac{1}{2\pi i} \lim_{\eta \rightarrow 0^+} \left( \oint_{c_1}^{[E_b, E_f]} dz \mathcal{G}(\mathbf{x}, \mathbf{x}', z - i\eta) \mathcal{G}(\mathbf{x}', \mathbf{x}, z + i\eta) \right. \\ &\quad \left. + \oint_{c_2}^{[E_b, E_f]} dz \mathcal{G}(\mathbf{x}, \mathbf{x}', z - i\eta) \mathcal{G}(\mathbf{x}', \mathbf{x}, z + i\eta) \right). \end{aligned} \quad (5.57)$$

Taking the limit  $\eta \rightarrow 0^+$  reshapes the contours such that the opposed branches near the real axis cancel each other. Thus, the integrals can now be taken over the open contours  $c_1'$  and  $c_2'$ , as sketched in Fig. 5.1 (right panel),

$$\Pi(\mathbf{x}, \mathbf{x}') = \frac{1}{2\pi i} \left( \int_{c_1'}^{[E_b, E_f]} dz \mathcal{G}(\mathbf{x}, \mathbf{x}', z) \mathcal{G}(\mathbf{x}', \mathbf{x}, z) + \int_{c_2'}^{[E_b, E_f]} dz \mathcal{G}(\mathbf{x}, \mathbf{x}', z) \mathcal{G}(\mathbf{x}', \mathbf{x}, z) \right). \quad (5.58)$$

To make the contours symmetric with respect to the real axis,  $c'_1$  can be reversed under change of the sign of the first integral,

$$\Pi(\mathbf{x}, \mathbf{x}') = -\frac{1}{2\pi i} \left( \int_{-c'_1}^{[E_b, E_f]} dz \mathcal{G}(\mathbf{x}, \mathbf{x}', z) \mathcal{G}(\mathbf{x}', \mathbf{x}, z) - \int_{c'_2}^{[E_b, E_f]} dz \mathcal{G}(\mathbf{x}, \mathbf{x}', z) \mathcal{G}(\mathbf{x}', \mathbf{x}, z) \right). \quad (5.59)$$

The second integration can be done, without changing its value, using the contour  $-c'_1$  when the complex conjugate of the energy argument of the Green function is used. Additionally, using the relation [Zab+05]

$$\mathcal{G}(\mathbf{x}, \mathbf{x}', z) = \mathcal{G}(\mathbf{x}', \mathbf{x}, z^*)^* \quad (5.60)$$

gives

$$\begin{aligned} \Pi(\mathbf{x}, \mathbf{x}') &= -\frac{1}{2\pi i} \int_{-c'_1}^{[E_b, E_f]} dz [\mathcal{G}(\mathbf{x}, \mathbf{x}', z) \mathcal{G}(\mathbf{x}', \mathbf{x}, z) - \mathcal{G}(\mathbf{x}, \mathbf{x}', z) \mathcal{G}(\mathbf{x}', \mathbf{x}, z)^*] \\ &= \frac{i}{\pi} \int_{-c'_1}^{[E_b, E_f]} dz \text{Im} \{ \mathcal{G}(\mathbf{x}, \mathbf{x}', z) \mathcal{G}(\mathbf{x}', \mathbf{x}, z) \} \end{aligned} \quad (5.61)$$

This expression is valid for the real-space representation of  $\Pi$ . The next section shows how the corresponding reciprocal-space expression needed for Eq. (5.44) as well as its angular momentum expansion is derived.

### 5.2.3 Reciprocal space and angular momentum representation

In order to account for the crystal lattice structure, the arbitrary vector  $\mathbf{x}$  is replaced by cell-centered coordinates

$$\mathbf{x} = \mathbf{R}_n + \tau_x + \mathbf{r} \quad (5.62)$$

where  $\mathbf{R}_n$  denotes a lattice vector pointing to cell  $n$  and  $\tau_s$  represents coordinates of ion sites indexed by  $s$  within every unit cell.  $\mathbf{r}$  then is a vector relative to the center of the respective cell and, within the atomic sphere approximation (ASA), is limited in its length by the Wigner-Seitz radius  $R_{\text{WS}}(i)$  of each ion. Using this representation,  $\Pi$  can be transformed into its reciprocal space representation via the Bloch-Fourier transform

$$\Pi^{ss'}(\mathbf{r}, \mathbf{r}', \mathbf{q}) = \sum_n \Pi_{nn'}^{ss'}(\mathbf{r}, \mathbf{r}') e^{i\mathbf{q} \cdot \mathbf{R}_{nn'}} = \sum_n \Pi_{nn'}^{ss'}(\mathbf{r}, \mathbf{r}') e^{i\mathbf{q} \cdot \mathbf{R}_n}, \quad (5.63)$$

where the second cell index  $n'$  has been set to zero because  $\Pi_{nn'}^{ss'}$  depends only on the difference  $\mathbf{R}_{nn'}$  rather than on the coordinates of the individual cells. Defining the Green function products

$$P_{nn'}^{ss'}(\mathbf{r}, \mathbf{r}', z) = \mathcal{G}_{nn'}^{ss'}(\mathbf{r}, \mathbf{r}', z) \mathcal{G}_{n'n}^{s's}(\mathbf{r}', \mathbf{r}, z), \quad (5.64)$$

$$\bar{P}_{nn'}^{ss'}(\mathbf{r}, \mathbf{r}', z) = \mathcal{G}_{nn'}^{ss'}(\mathbf{r}, \mathbf{r}', z) \mathcal{G}_{n'n}^{s's}(\mathbf{r}', \mathbf{r}, z)^*, \quad (5.65)$$

Eq. (5.61) in cell-centred coordinates reads

$$\Pi_{nn'}^{ss'}(\mathbf{r}, \mathbf{r}') = \frac{i}{2\pi} \int_{-c_1}^{[E_b, E_f]} dz \left[ P_{nn'}^{ss'}(\mathbf{r}, \mathbf{r}', z) - \bar{P}_{nn'}^{ss'}(\mathbf{r}, \mathbf{r}', z) \right] \quad (5.66)$$

For the lattice Fourier transformation of this equation, the following convolution theorem [Buc12a] for two lattice-periodic functions  $f_1$  and  $f_2$ ,

$$\sum_n f_1(\mathbf{R}_n) f_2(-\mathbf{R}_n) e^{i\mathbf{q} \cdot \mathbf{R}_n} = \frac{1}{\Omega_{\text{BZ}}} \int d\mathbf{k} f_1(\mathbf{k}) f_2(\mathbf{k} - \mathbf{q}), \quad (5.67)$$

comes in useful to transform the first term in the square brackets of Eq. (5.66) and yields

$$P^{ss'}(\mathbf{r}, \mathbf{r}', z, \mathbf{q}) = \int_{\Omega_{\text{BZ}}} \frac{d\mathbf{k}}{\Omega_{\text{BZ}}} \mathcal{G}^{ss'}(\mathbf{r}, \mathbf{r}', z, \mathbf{k}) \mathcal{G}^{s's}(\mathbf{r}', \mathbf{r}, z, \mathbf{k} - \mathbf{q}), \quad (5.68)$$

where the lattice Fourier transform of the Green function is given by

$$\mathcal{G}^{ss'}(\mathbf{r}, \mathbf{r}', z, \mathbf{k}) = \sum_{n'} \mathcal{G}_{nn'}^{ss'}(\mathbf{r}, \mathbf{r}', z) e^{i\mathbf{k} \cdot \mathbf{R}_{n'}} \Big|_{n=0}. \quad (5.69)$$

The lattice point index  $n$  on the right side can be chosen arbitrarily because  $\mathcal{G}_{nn'}$  depends only on the difference  $\mathbf{R}_n - \mathbf{R}_{n'}$ . The direct transformation of the second term reads

$$\begin{aligned} \bar{P}^{ss'}(\mathbf{r}, \mathbf{r}', z, \mathbf{q}) &= \sum_{n'} \mathcal{G}_{0n'}^{ss'}(\mathbf{r}, \mathbf{r}', z)^* \mathcal{G}_{n'0}^{s's}(\mathbf{r}', \mathbf{r}, z)^* e^{i\mathbf{q} \cdot \mathbf{R}_{n'}} \\ &= \sum_{n'} \mathcal{G}(\mathbf{r} + \boldsymbol{\tau}_s, \mathbf{r}' + \boldsymbol{\tau}_{s'} + \mathbf{R}_{n'}, z)^* \mathcal{G}(\mathbf{r}' + \boldsymbol{\tau}_{s'} + \mathbf{R}_{n'}, \mathbf{r} + \boldsymbol{\tau}_s, z)^* e^{i\mathbf{q} \cdot \mathbf{R}_{n'}}, \end{aligned} \quad (5.70)$$

which, due to inversion symmetry<sup>1</sup>, is equivalent to

$$\bar{P}^{ss'}(\mathbf{r}, \mathbf{r}', z, \mathbf{q}) = \sum_{n'} \mathcal{G}(\mathbf{r} + \boldsymbol{\tau}_s, \mathbf{r}' + \boldsymbol{\tau}_{s'} - \mathbf{R}_{n'}, z)^* \mathcal{G}(\mathbf{r}' + \boldsymbol{\tau}_{s'} - \mathbf{R}_{n'}, \mathbf{r} + \boldsymbol{\tau}_s, z)^* e^{-i\mathbf{q} \cdot \mathbf{R}_{n'}}. \quad (5.71)$$

Furthermore, the inversion symmetry of the Green function

$$\mathcal{G}(\mathbf{x}, \mathbf{x}', z) = \mathcal{G}(-\mathbf{x}, -\mathbf{x}', z), \quad (5.72)$$

gives rise to the relations [Win13]

$$\begin{aligned} \bar{P}^{ss'}(\mathbf{r}, \mathbf{r}', z, \mathbf{q}) &= \sum_{n'} \mathcal{G}(-\mathbf{r} - \boldsymbol{\tau}_s, -\mathbf{r}' - \boldsymbol{\tau}_{s'} + \mathbf{R}_{n'}, z)^* \times \\ &\quad \times \mathcal{G}(-\mathbf{r}' - \boldsymbol{\tau}_{s'} + \mathbf{R}_{n'}, -\mathbf{r} - \boldsymbol{\tau}_s, z)^* e^{-i\mathbf{q} \cdot \mathbf{R}_{n'}} \\ &= \sum_{n'} [\mathcal{G}(-\mathbf{r} - \boldsymbol{\tau}_s, -\mathbf{r}' - \boldsymbol{\tau}_{s'} + \mathbf{R}_{n'}, z) \times \\ &\quad \times \mathcal{G}(-\mathbf{r}' - \boldsymbol{\tau}_{s'} + \mathbf{R}_{n'}, -\mathbf{r} - \boldsymbol{\tau}_s, z) e^{i\mathbf{q} \cdot \mathbf{R}_{n'}}]^* \\ &= P(-\mathbf{r} - \boldsymbol{\tau}_s, -\mathbf{r}' - \boldsymbol{\tau}_{s'}, z, \mathbf{q})^* \\ &= P^{ss'}(-\mathbf{r}, -\mathbf{r}', z, \mathbf{q})^*. \end{aligned} \quad (5.73)$$

<sup>1</sup>The requirement of inversion symmetry is, in principle, not necessary but allows for a more condensed notation of the formalism. Within the scope of the materials tested in the following, the assumption is valid without restrictions.

Using the Fourier representation has the advantage that spatial integrals over the polarization function or related quantities, which are taken over the whole crystal, can be transformed into integrals over the first Brillouin zone. According to Eq. (4.47), (4.52) and (5.62), the Fourier transformed Green function for a complex lattice is given by

$$\begin{aligned} \mathcal{G}^{ss'}(\mathbf{r}, \mathbf{r}', z, \mathbf{k}) = & -i\sqrt{z}\delta_{ss'} \sum_L R_L^s(\mathbf{r}_<, z) H_L^s(\mathbf{r}_>, z) \\ & + \sum_{LL'} R_L^s(\mathbf{r}, z) G_{LL'}^{ss'}(z, \mathbf{k}) R_{L'}^{s'}(\mathbf{r}', z), \end{aligned} \quad (5.74)$$

or equally

$$\mathcal{G}^{ss'}(\mathbf{r}, \mathbf{r}', z, \mathbf{k}) = \sum_{LL'} Y_L(\hat{\mathbf{r}}) \mathcal{G}_{LL'}^{ss'}(r, r', z, \mathbf{k}) Y_{L'}(\hat{\mathbf{r}}'), \quad (5.75)$$

using the expansion coefficients

$$\mathcal{G}_{LL'}^{ss'}(r, r', z, \mathbf{k}) = -i\sqrt{z}\delta_{ss'}\delta_{LL'} R_\ell^s(r_<, z) H_\ell^s(r_>, z) + R_\ell^s(r, z) G_{LL'}^{ss'}(z, \mathbf{k}) R_{\ell'}^{s'}(r', z) \quad (5.76)$$

which can be obtained by using  $\sum_L f_{LL} = \sum_{LL'} f_{LL'} \delta_{LL'}$  in the single-site term of  $\mathcal{G}$ . The functions  $P^{ss'}(\mathbf{r}, \mathbf{r}', z, \mathbf{q})$  which have been defined in Eq. (5.68) can thus be written as

$$\begin{aligned} P^{ss'}(\mathbf{r}, \mathbf{r}', z, \mathbf{q}) = & \int_{\Omega_{\text{BZ}}} \frac{d\mathbf{k}}{\Omega_{\text{BZ}}} \sum_{L_1 L_1'} Y_{L_1}(\hat{\mathbf{r}}) \mathcal{G}_{L_1 L_1'}^{ss'}(r, r', z, \mathbf{k}) Y_{L_1'}(\hat{\mathbf{r}}') \times \\ & \times \sum_{L_2 L_2'} Y_{L_2}(\hat{\mathbf{r}}') \mathcal{G}_{L_2 L_2'}^{s's}(r', r, z, \mathbf{k} - \mathbf{q}) Y_{L_2}(\hat{\mathbf{r}}), \end{aligned} \quad (5.77)$$

where the site indices ( $s, s'$ ) above the wave functions account for the different atomic types within the unit cell. By making use of the relation

$$Y_{L'}(\hat{\mathbf{r}}) Y_{L''}(\hat{\mathbf{r}}) = \sum_L Y_L(\hat{\mathbf{r}}) C_{L'L''}^L \quad (5.78)$$

where  $C_{L'L''}^L$  are Gaunt coefficients, defined by an integral over the unit sphere

$$C_{L'L''}^L = \int d\hat{\mathbf{r}} Y_L(\hat{\mathbf{r}}) Y_{L'}(\hat{\mathbf{r}}) Y_{L''}(\hat{\mathbf{r}}), \quad (5.79)$$

the  $P$  can be expanded in spherical harmonics via

$$\begin{aligned} P^{ss'}(\mathbf{r}, \mathbf{r}', z, \mathbf{q}) = & \sum_{LL'} Y_L(\hat{\mathbf{r}}) Y_{L'}(\hat{\mathbf{r}}') \left[ \sum_{L_1 L_1'} \sum_{L_2 L_2'} C_{L_1 L_2}^L C_{L_1' L_2'}^{L'} \times \right. \\ & \times \left. \int_{\Omega_{\text{BZ}}} \frac{d\mathbf{k}}{\Omega_{\text{BZ}}} \mathcal{G}_{L_1 L_1'}^{ss'}(r, r', z, \mathbf{k}) \mathcal{G}_{L_2 L_2'}^{s's}(r', r, z, \mathbf{k} - \mathbf{q}) \right] \\ = & \sum_{LL'} Y_L(\hat{\mathbf{r}}) P_{LL'}^{ss'}(r, r', z, \mathbf{q}) Y_{L'}(\hat{\mathbf{r}}'), \end{aligned} \quad (5.80)$$

where the summation within the square brackets is finite because the Gaunt coefficients  $C_{L'L''}^L$  are non-zero only for  $|\ell' - \ell''| \leq \ell \leq \ell' + \ell''$  [MP06]. The coefficients  $P_{LL'}^{ss'}$  are then

given by

$$\begin{aligned}
 P_{LL'}^{ss'}(\mathbf{r}, \mathbf{r}', z, \mathbf{q}) = & \left[ \delta_{L_1 L_1'} \delta_{L_2 L_2'} \delta_{ss'} z R_{\ell_1}^s(r_{<}, z) H_{\ell_1'}^{s'}(r_{>}, z) R_{\ell_2}^{s'}(r_{<}, z) H_{\ell_2}^s(r_{>}, z) \right. \\
 & + \delta_{L_1 L_1'} \delta_{ss'} \sqrt{z} R_{\ell_1}^s(r_{<}, z) H_{\ell_1}^s(r_{>}, z) R_{\ell_2}^s(r', z) R_{\ell_2'}^s(r, z) \int \frac{d\mathbf{k}}{\Omega_{\text{BZ}}} G_{L_2 L_2'}^{ss}(z, \mathbf{k}) \\
 & + \delta_{L_2 L_2'} \delta_{ss'} \sqrt{z} R_{\ell_2}^s(r_{<}, z) H_{\ell_2}^s(r_{>}, z) R_{\ell_1}^s(r, z) R_{\ell_1'}^s(r', z) \int \frac{d\mathbf{k}}{\Omega_{\text{BZ}}} G_{L_1 L_1'}^{ss}(z, \mathbf{k}) \\
 & \left. + R_{\ell_1}^s(r, z) R_{\ell_1'}^{s'}(r', z) R_{\ell_2}^{s'}(r', z) R_{\ell_2}^s(r, z) \int \frac{d\mathbf{k}}{\Omega_{\text{BZ}}} G_{L_1 L_1'}^{ss'}(z, \mathbf{k}) G_{L_2 L_2'}^{s's}(z, \mathbf{k} - \mathbf{q}) \right]. \quad (5.81)
 \end{aligned}$$

All required quantities for the calculation of these coefficients can be obtained from a self-consistent KKR calculation.

Using relation (5.73) and the symmetry relations of spherical harmonics, the angular momentum expansion of Eq. (5.71) is obtained as

$$\begin{aligned}
 \bar{P}^{ss'}(\mathbf{r}, \mathbf{r}', z, \mathbf{q}) &= P^{s's}(-\mathbf{r}, -\mathbf{r}', z, \mathbf{q})^* \\
 &= \sum_{LL'} Y_L(-\hat{\mathbf{r}}) P_{LL'}^{s's}(r, r', z, \mathbf{q})^* Y_{L'}(-\hat{\mathbf{r}}') \\
 &= \sum_{LL'} (-1)^{\ell+\ell'} Y_L(\hat{\mathbf{r}}) P_{LL'}^{s's}(r, r', z, \mathbf{q})^* Y_{L'}(\hat{\mathbf{r}}'). \quad (5.82)
 \end{aligned}$$

Combining the formulas derived above leads to the handy expansion of the polarization function

$$\Pi^{ss'}(\mathbf{r}, \mathbf{r}', \mathbf{q}) = \sum_{LL'} Y_L(\hat{\mathbf{r}}) \Pi_{LL'}^{ss'}(r, r', \mathbf{q}) Y_{L'}(\hat{\mathbf{r}}') \quad (5.83)$$

with expansion coefficients

$$\Pi_{LL'}^{ss'}(r, r', \mathbf{q}) = \frac{i}{2\pi} \int_{-c_1}^{[E_b, E_t]} dz \left[ P_{LL'}^{ss'}(r, r', z, \mathbf{q}) - (-1)^{\ell+\ell'} P_{LL'}^{s's}(r, r', z, \mathbf{q}) \right]. \quad (5.84)$$

### 5.3 Implementation

The implementation of the above presented equations was done as part of the permanent enhancement and improvement of the in-house screened KKR code HUTSEPOT, which has been developed in Halle since 2000 and is a collection of contributions of many developers<sup>2</sup> (hence the name). It allows an efficient, full-relativistic treatment of complex magnetic systems, including strong correlations, self-interaction correction and dynamic spin excitations. Traditionally, the potentials are described using ASA and MT approximations, but also the treatment of potentials of arbitrary shape has been made possible recently. The module PHON, developed as part of this work, uses the self-consistently calculated Green function of HUTSEPOT in AS approximation as input and computes the Fourier-transformed polarization function from it. The latter is then used, together with the Fourier-transformed lattice potential, to solve the Susceptibility Dyson Equation. For this purpose, initially an efficient Broyden scheme was implemented to solve the equation iteratively, but turned out to be unstable under certain conditions. In the present version, the discretised equation is solved by matrix inversion. These and other details of the implementation will be elaborated on on the following pages.

<sup>2</sup>[Lüd+01], [Lüd+05], [Hug+07], [Buc+09], [Kha+09]

### Angular momentum representation of the dynamical matrix

In order to perform efficient numerical calculations of the electronic part of the dynamical matrix, it is necessary to introduce spherical coordinates and to expand all involved quantities as linear combinations of spherical harmonics. The change of the valence charge density, as well as the bare Coulomb potential can be written as

$$\mathcal{K}_\beta^j(\mathbf{r}s, \mathbf{q}) = \sum_L \mathcal{K}_{\beta,L}^j(r, s, \mathbf{q}) Y_L(\hat{\mathbf{r}}), \quad (5.85)$$

$$V^{is}(\mathbf{r}, \mathbf{r}', \mathbf{q}) = \sum_{LL'} V_{LL'}^{is}(r, r', \mathbf{q}) Y_L(\hat{\mathbf{r}}) Y_{L'}(\hat{\mathbf{r}}'), \quad (5.86)$$

$$(5.87)$$

The calculation of the first quantity is discussed below, whereas the second one is discussed in appendix A.2. The adiabatic exchange-correlation kernel is expanded in a similar fashion,

$$f_{xc}[n(\mathbf{r}, i)] = \sum_L f_{xc,L}^i(r) Y_L(\hat{\mathbf{r}}). \quad (5.88)$$

In this case, the expansion coefficients are given by

$$f_{xc,L}^i(r) = \int d\hat{\mathbf{r}} Y_L(\hat{\mathbf{r}}) f_{xc}[n(\mathbf{r}, \hat{\mathbf{r}}, i)] \quad (5.89)$$

and have to be approximated numerically using a combination of radial and angular integration methods (see App. B).

Analogously, the valence charge density is expanded as

$$n_i^v(\mathbf{r}) = \sum_L n_L^v(r, i) Y_L(\hat{\mathbf{r}}), \quad (5.90)$$

opposed to the spherical core electron density, which can be written as

$$n_i^c(\mathbf{r}) = n_0^c(r, i) Y_0(\hat{\mathbf{r}}). \quad (5.91)$$

Since  $Y_0(\hat{\mathbf{r}}) = 1/\sqrt{4\pi}$  is a constant, the gradient of a spherical symmetric function is given by

$$\nabla_{\mathbf{r}} n_i^c(\mathbf{r}) = \frac{\hat{\mathbf{r}}}{\sqrt{4\pi}} \frac{d}{dr} n_0^c(r, i). \quad (5.92)$$

The unit vector  $\hat{\mathbf{r}}$  can be represented as

$$\hat{\mathbf{r}} = \frac{\mathbf{r}}{r} = \sqrt{\frac{4\pi}{3}} \begin{pmatrix} Y_{11}(\hat{\mathbf{r}}) \\ Y_{1-1}(\hat{\mathbf{r}}) \\ Y_{10}(\hat{\mathbf{r}}) \end{pmatrix}, \quad (5.93)$$

leading to a component of the gradient

$$\partial_{r_\alpha} n_i^c(\mathbf{r}) = \frac{1}{\sqrt{3}} \frac{d}{dr} n_0^c(r, i) Y_{L_\alpha}(\hat{\mathbf{r}}), \quad L_\alpha = \begin{cases} (1, 1), & \alpha = 1 \\ (1, -1), & \alpha = 2 \\ (1, 0), & \alpha = 3 \end{cases} \quad (5.94)$$

where  $L_\alpha$  refers to the angular momentum index combination for the respective direction  $\alpha$ . Using the relations given above, the  $\mathbf{q}$ -dependent part of the electronic contribution to

the dynamical matrix (Eq. (5.21)) in terms of angular momentum eigenfunctions is given by

$$\text{el} \hat{D}_{\alpha\beta}^{ij}(\mathbf{q}) = Z_i \int dr r^2 \sum_s \sum_L C_{\alpha,L}^{is}(rr, \mathbf{q}) \mathcal{K}_{\beta L}^j(rs, \mathbf{q}) \quad (5.95)$$

$$+ \frac{1}{\sqrt{3}} \int dr r^2 \left[ \frac{d}{dr} n_i^c(r) \right] \int dr' r'^2 \sum_s \sum_L V_{L\alpha,L}^{is}(r, r', \mathbf{q}) \mathcal{K}_{\beta L}^j(r's, \mathbf{q}) \quad (5.96)$$

$$- \frac{1}{\sqrt{3}} \int dr r^2 \sum_{LL'} f_{xc,L}^i(r) \left[ \frac{d}{dr} n_i^c(r) \right] \mathcal{K}_{\beta L'}^j(ri, \mathbf{q}) C_{LL'}^{L\alpha}. \quad (5.97)$$

### Susceptibility Dyson equation

In a similar fashion, the Dyson equation which describes the variation of the valence charge density can be expanded in terms of spherical harmonics. Then, the angular momentum components of  $\mathcal{K}$  are given by

$$\mathcal{K}_{\beta,L}^j(rs, \mathbf{q}) = \mathcal{I}_L^{js}(r, \mathbf{q}) + \sum_{s'} \sum_{L'} \int_0^{R_{\text{ASA}}} dr' r'^2 A_{LL'}^{ss'}(rr', \mathbf{q}) \mathcal{K}_{\beta,L'}^j(r's', \mathbf{q}) \quad (5.98)$$

with the inhomogeneity

$$\begin{aligned} \mathcal{I}_L^{js}(r, \mathbf{q}) &= \sum_{s'} \int_0^{R_{\text{ASA}}} dr' r'^2 \sum_{L'} \Pi_{LL'}^{ss'}(rr', \mathbf{q}) \mathcal{C}_{\text{ext},L'}^{js'}(r', \mathbf{q}) \\ &- \frac{1}{\sqrt{3}} \sum_{s'} \int_0^{R_{\text{ASA}}} dr' r'^2 \sum_{L'} \Pi_{LL'}^{ss'}(rr', \mathbf{q}) \int_0^{R_{\text{ASA}}} dr'' r''^2 V_{L'L\beta}^{s'j}(r'r'', \mathbf{q}) \frac{d}{dr''} n_i^c(r'') \\ &- \frac{1}{\sqrt{3}} \int_0^{R_{\text{ASA}}} dr' r'^2 \sum_{L'} \Pi_{LL'}^{sj}(rr', \mathbf{q}) \sum_{L''} C_{L'L''}^{L\beta} f_{xc,L''}^j(r') \frac{d}{dr'} n_j^c(r') \end{aligned} \quad (5.99)$$

and kernel

$$A_{LL'}^{ss'}(rr', \mathbf{q}) = - \sum_{s''} \sum_{L''} \int_0^{R_{\text{ASA}}} dr'' r''^2 \Pi_{LL''}^{ss''}(rr'', \mathbf{q}) F_{L''L'}^{s''s'}(r''r', \mathbf{q}), \quad (5.100)$$

using

$$F_{L''L'}^{s''s'}(r''r', \mathbf{q}) = V_{L''L'}^{s''s'}(r''r', \mathbf{q}) + \delta_{s's''} \delta(r' - r'') \sum_{L_1} f_{xc,L_1}^{s'}(r') C_{L'L''}^{L_1}. \quad (5.101)$$

Additionally, the radial coordinate has to be discretised in a practical calculation. Thus,  $r \in [0, R_{\text{ASA}}]$  is replaced by  $N_r$  values of  $r_a$  with  $a \in \{1 \dots N_r\}$  which satisfy Eq. (B.4). Using this discrete mesh, all radial integrations can be approximated via the Gauss-Legendre method described above and replaced by weighted sums. The discretised Dyson equation reads

$$\mathcal{K}_{\beta,L}^j(r_a, s, \mathbf{q}) = \mathcal{I}_L^{js}(r_a, \mathbf{q}) + \sum_{s'} \sum_{L'} \sum_{b=1}^{N_r} r_b^2 w_b A_{LL'}^{ss'}(r_a r_b, \mathbf{q}) \mathcal{K}_{\beta,L'}^j(r_b s', \mathbf{q}) \quad (5.102)$$

with Gaussian integration weights  $w_b$ . By further introducing general indices  $\mu = (s, L, a)$  and  $\nu = (s', L', b)$  ( $\mu, \nu \in [1, N]$  and  $N = N_{\text{site}} \cdot L_{\text{max}} \cdot N_r$ ), all quantities can be written in vector or matrix representation as follows:

$$\mathcal{K}_{\beta, L}^j(r_a s, \mathbf{q}) = \mathcal{K}_\mu(j\beta, \mathbf{q}) = [\mathcal{K}(j\beta, \mathbf{q})]_\mu \quad (5.103)$$

$$\mathcal{I}_L^j(r_a s, \mathbf{q}) = \mathcal{I}_\mu(j, \mathbf{q}) = [\mathcal{I}(j, \mathbf{q})]_\mu \quad (5.104)$$

$$A_{LL'}^{ss'}(r_a r_b, \mathbf{q}) r_b^2 w_b = A_{\mu\nu}(\mathbf{q}) = [\mathbf{A}(\mathbf{q})]_{\mu\nu} \quad (5.105)$$

This way, Eq. (5.102) can be written in the form

$$\mathcal{K}_\mu(j\beta, \mathbf{q}) = \mathcal{I}_\mu(j, \mathbf{q}) + \sum_{\nu=1}^N A_{\mu\nu}(\mathbf{q}) \mathcal{K}_\nu(j\beta, \mathbf{q}) \quad (5.106)$$

or, in matrix notation, as

$$\mathcal{K}(j\beta, \mathbf{q}) = \mathcal{I}(j, \mathbf{q}) + \mathbf{A}(\mathbf{q}) \cdot \mathcal{K}(j\beta, \mathbf{q}). \quad (5.107)$$

The latter equation shows that  $\mathcal{K}(j\beta, \mathbf{q})$  is the solution of the linear equation system

$$\mathcal{I}(j, \mathbf{q}) = [\mathbf{1} - \mathbf{A}(\mathbf{q})] \cdot \mathcal{K}(j\beta, \mathbf{q}), \quad (5.108)$$

in which  $\mathbf{1}$  is the identity matrix. Systems of this type can be efficiently solved using LAPACK [Ang+90] routines.

### 5.3.1 Test calculations

#### Polarization function

To test the correct computation of the polarization function, a sum rule introduced by Terakura [AT79; Ter+82; SW85] comes in handy. It states, that the density of valence states at the Fermi energy can be obtained from a spatial integration of the polarization function,

$$\int d\mathbf{r}' \Pi(\mathbf{r}, \mathbf{r}', \mathbf{q} = 0) = -d^V(\mathbf{r}, \epsilon_F). \quad (5.109)$$

A proof of this expression [SW85; Buc12a] shall be given in real space, starting from Eq. (5.61)

$$\int d\mathbf{x}' \Pi(\mathbf{x}, \mathbf{x}') = -\frac{1}{2\pi i} \int_{-c_1}^{[E_b, E_f]} dz \int d\mathbf{x}' [\mathcal{G}(\mathbf{x}, \mathbf{x}', z) \mathcal{G}(\mathbf{x}', \mathbf{x}, z) - \mathcal{G}^*(\mathbf{x}, \mathbf{x}', z) \mathcal{G}^*(\mathbf{x}', \mathbf{x}, z)].$$

Using the Lehmann representation of the Green function, it can be written in terms of Kohn-Sham orbitals  $\psi_i$ ,

$$\mathcal{G}(\mathbf{x}, \mathbf{x}', z) = \sum_i \frac{\phi_i(\mathbf{x}) \phi_i(\mathbf{x}')^*}{z - \epsilon_i}. \quad (5.110)$$

As a result of the orthonormality of the KS orbitals, the space integral of the product of two Green functions can be evaluated as

$$L(\mathbf{x}, z) = \sum_i \frac{\phi_i(\mathbf{x}) \phi_i(\mathbf{x})^*}{(z - \epsilon_i)^2}, \quad (5.111)$$

such that Eq. (5.110) can be written as

$$\int d\mathbf{x}' \Pi(\mathbf{x}, \mathbf{x}') = -\frac{1}{2\pi i} \int_{-c_1}^{[E_b, E_f]} dz [L(\mathbf{x}, z) - L(\mathbf{x}, z)^*]. \quad (5.112)$$

As  $L$  is identical to the energy derivative of the Green function,

$$L(\mathbf{x}, z) = -\frac{d}{dz} \mathcal{G}(\mathbf{x}, \mathbf{x}, z), \quad (5.113)$$

the integral can be easily evaluated to

$$\begin{aligned} \int d\mathbf{r}' \Pi(\mathbf{x}, \mathbf{x}', \mathbf{q} = 0) &= \frac{1}{2\pi i} [-\mathcal{G}(\mathbf{x}, \mathbf{x}, \epsilon_F) + \mathcal{G}(\mathbf{x}, \mathbf{x}, \epsilon_F)^* + \mathcal{G}(\mathbf{x}, \mathbf{x}, E_b) - \mathcal{G}(\mathbf{x}, \mathbf{x}, E_b)^*] \\ &= -\frac{1}{\pi} \text{Im} \mathcal{G}(\mathbf{x}, \mathbf{x}, \epsilon_F), \end{aligned} \quad (5.114)$$

which is the local density of states at  $\epsilon_F$ . This sum rule can be implemented into a test calculation by plugging in the angular momentum expansion of the susceptibility. For the total valence DOS, one obtains

$$\begin{aligned} d^v(\epsilon_F) &= - \int d\mathbf{r} \int d\mathbf{r}' \Pi(\mathbf{r}, \mathbf{r}', \mathbf{q} = 0) \\ &= - \int d\mathbf{r} \int d\mathbf{r}' \sum_{LL'} \Pi_{LL'}(r, r', \mathbf{q} = 0) Y_L(\hat{\mathbf{r}}) Y_{L'}(\hat{\mathbf{r}}') \\ &= - \int_0^{R_{ASA}} dr r^2 \int_0^{R_{ASA}} dr' r'^2 \sum_{LL'} \Pi_{LL'}(r, r', \mathbf{q} = 0) \int d\hat{\mathbf{r}} Y_L(\hat{\mathbf{r}}) \int d\hat{\mathbf{r}}' Y_{L'}(\hat{\mathbf{r}}') \\ &= -\frac{1}{4\pi} \int_0^{R_{ASA}} dr r^2 \int_0^{R_{ASA}} dr' r'^2 \Pi_{00}(r, r', \mathbf{q} = 0). \end{aligned} \quad (5.115)$$

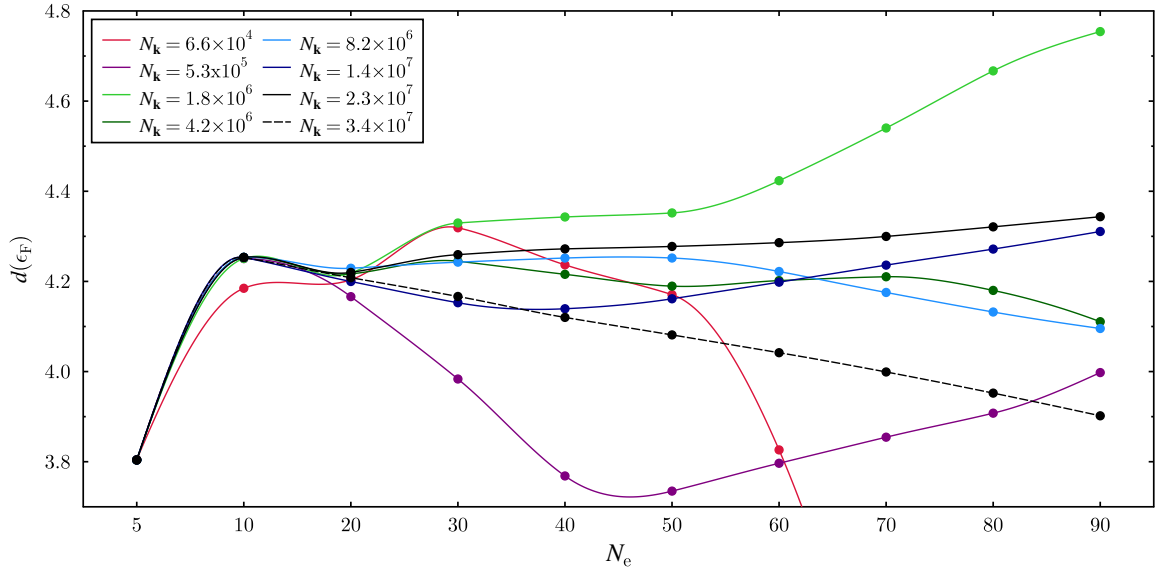


**Figure 5.2:** Total density of states of Cu at  $E = \epsilon_F$  depending on the number of energy integration points  $N_E$ . Points of different colors correspond to  $\mathbf{k}$ -meshes of increasing density (the lines are guides to the eye).

Interestingly, the value for the total DOS depends only on the coefficient with  $\ell = \ell' = 0$ .

Fig. 5.2 shows resulting values for different  $\mathbf{k}$ -meshes as function of the number of energy points  $N_E$ . All calculations used the same semicircular integration contour with gaussian weights and the highest density of integration points near the real axis. While using only 5 points leads to identical results for all  $\mathbf{k}$ -meshes, the values of  $d(\epsilon_F)$  varied quite remarkably with increasing  $N_E$ . The most stable results have been achieved with  $N_{\mathbf{k}} = 2.3 \times 10^7$  (black), while the deviations from the almost linear run seen here become strongest for the sparse  $\mathbf{k}$ -meshes. This behaviour obviously is a consequence of the analytical properties of the Green function. As described in section 4.2.3, the Green function shows more features near the real axis and is smooth far away from it. At the same time, for the exact evaluation of its run at small imaginary energies, the Brillouin zone integration in Eq. (5.82) has to be performed on a much denser mesh of integration points to obtain a converged result at a specific complex energy. The more energy points are used on the contour, the more energy points lie in the region near the real axis and the Brillouin zone integration becomes more important.

This test indicates that a very dense  $\mathbf{k}$ -mesh is needed to obtain a converged polarization function at high  $N_E$ , but it only allows to draw conclusions about the integrated  $\ell = 0$  component of it. A better evaluation of its spatial dependence can be obtained using the Terakura formula for the local density of states:

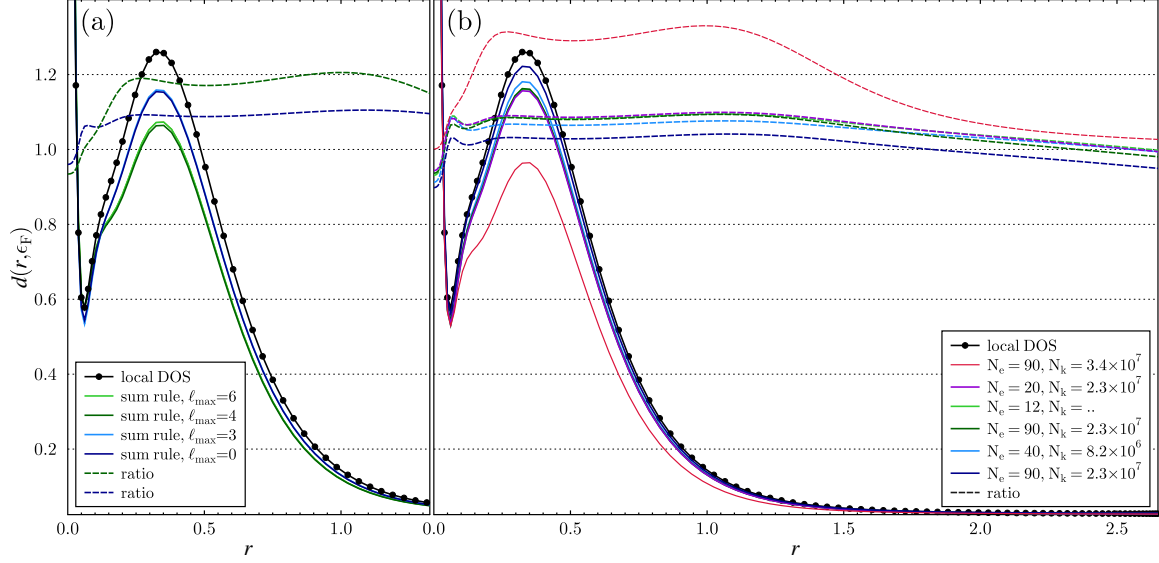
$$\begin{aligned}
 d^N(\mathbf{r}, \epsilon_F) &= - \int d\mathbf{r}' \Pi(\mathbf{r}, \mathbf{r}', \mathbf{q} = 0) \\
 &= - \int d\mathbf{r}' \sum_{LL'} \Pi_{LL'}(r, r', \mathbf{q} = 0) Y_L(\hat{\mathbf{r}}) Y_{L'}(\hat{\mathbf{r}}') \\
 &= - \int_0^{R_{\text{ASA}}} dr' r'^2 \sum_{LL'} \Pi_{LL'}(r, r', \mathbf{q} = 0) Y_L(\hat{\mathbf{r}}) \int d\hat{\mathbf{r}}' Y_{L'}(\hat{\mathbf{r}}') \\
 &= - \frac{1}{\sqrt{4\pi}} \int_0^{R_{\text{ASA}}} dr' r'^2 \sum_L \Pi_{L0}(r, r', \mathbf{q} = 0) Y_L(\hat{\mathbf{r}}). \tag{5.116}
 \end{aligned}$$

Fig. 5.3 shows results for Cu on a line from  $r = 0$  to  $r = r_{\text{WS}}$  linking two next neighbours. As a reference, the local DOS (black dots) has been calculated from the Green function using Eq. (4.10). In order to obtain the correct value on the real axis, an analytic continuation scheme has been used (formula 25.2.67 in [AS72]). The results obtained from the sum rule are plotted as coloured lines. The left panel shows results for  $N_E = 12$  with different values of  $\ell_{\text{max}}$  in different colours. The ratios between exact DOS and sum rule are plotted as dashed lines in the respective colours. The curves are very similar for  $\ell_{\text{max}} \in [0 \dots 3]$  (green) as well as  $\ell_{\text{max}} \in [4 \dots 6]$  (blue). The only major dependence on  $\ell_{\text{max}}$  appears at the step from  $\ell_{\text{max}} = 3$  to  $\ell_{\text{max}} = 4$ , where the deviation from the exact density is reduced by 50%. This is still true for polarization functions obtained with higher numbers of energy points, shown in the right panel (always using  $\ell_{\text{max}} = 4$ ). The smallest deviation ( $< 5\%$ ) is achieved using  $N_E = 90$  and  $N_{\mathbf{k}} = 2.3 \times 10^7$ , whereas an even larger number of  $\mathbf{k}$ -points (red curve) leads to a large error in the polarization function, in conformity with Fig. 5.2.

### Charge density response

The response of the charge density upon a wave-like perturbation of the external potential was defined as

$$\mathcal{K}_{\beta}^j(\mathbf{r}, \mathbf{q}, s) = \sum_n \mathcal{K}_{n,\beta}^j(\mathbf{r}, 0s) e^{i\mathbf{q} \cdot (\mathbf{R}_n)} = \sum_n e^{i\mathbf{q} \cdot (\mathbf{R}_n)} \frac{\partial n_{s' \neq s}^v(\mathbf{r}')}{\partial u_{\beta}(nj)}. \tag{5.117}$$



**Figure 5.3:** Local density of states of Cu at  $E = \epsilon_F$ . The black line has been calculated directly from the Green function by means of Eq. (4.10), using an extrapolation formula to obtain the value on the real axis (see text). (a) Coloured lines denote the local DOS obtained from the Terakura sum rule, Eq. (5.116), for different values of  $\ell_{\max}$  used in the expansion of the polarization function. The dashed lines denote the ratio between the reference DOS and the Terakura value for  $\ell_{\max} = 6$ . The curves from  $\ell = 4$  to  $\ell = 6$  differ by less than 1%. (b) Different colours denote variable densities of the  $\mathbf{k}$ -mesh and energy points (see key). All curves have been evaluated using  $\ell = 4$ .

In the limit  $\mathbf{q} \rightarrow 0$ , the charge density experiences a perturbation of infinite wavelength, which corresponds to a displacement of all ions in the same direction and thus to a shift of the whole crystal. In that case,  $\mathcal{K}(\mathbf{r}, \mathbf{q} \rightarrow 0)$  must become equal to the gradient of the ground state valence charge density,

$$\lim_{\mathbf{q} \rightarrow 0} \mathcal{K}(\mathbf{r}, \mathbf{q}) = \frac{d}{d\mathbf{r}} n^v(\mathbf{r}). \quad (5.118)$$

This relation allows to check the result of the susceptibility Dyson equation. Fig. 5.4 shows this comparison for different metals on a line from nucleus to WS radius in (001) direction. All calculations have been performed using 200 radial mesh points and  $\ell_{\max} = 4$ , such that the result was converged with respect to these parameters. The number of energy integration points was  $N_E = 90$  and a  $\mathbf{k}$ -mesh of  $2.3 \times 10^7$  points was used. In all cases, the derivative of the charge density is plotted black and  $\mathcal{K}(\mathbf{r}, \mathbf{q} \rightarrow 0)$  is shown as red curve. The qualitative agreement between the two curves is good, indicating that the presented formalism, in principle, delivers reasonable results. Nevertheless, deviations from the ideal curve, depending on radius and element type, are obvious. Extrema of  $\mathcal{K}(\mathbf{r}, \mathbf{q} \rightarrow 0)$  differ in height and position compared to  $\nabla n^v(\mathbf{r})$ . Although the difference between both curves becomes small at large radii compared to intermediate radii, the relative deviation is largest for  $r \rightarrow R_{WS}$ . The ratio between both values,

$$\Delta_{WS} = \frac{\mathcal{K}(\mathbf{R}_{WS}, \mathbf{q} \rightarrow 0)}{\nabla n^v(\mathbf{R}_{WS})} \quad (5.119)$$

is given next to each graph, respectively. The strongest deviations are found for the alkali metals Li and K with  $\Delta_{WS} \approx 24$  and  $\Delta_{WS} \approx -48$ , whereas in the case of the tested 3d elements  $\mathcal{K}(\mathbf{R}_{WS}, \mathbf{q} \rightarrow 0)$  is always smaller than the respective  $\nabla n^v(\mathbf{R}_{WS})$  with a best value of  $\Delta_{WS} \approx 0.77$  for Cu.

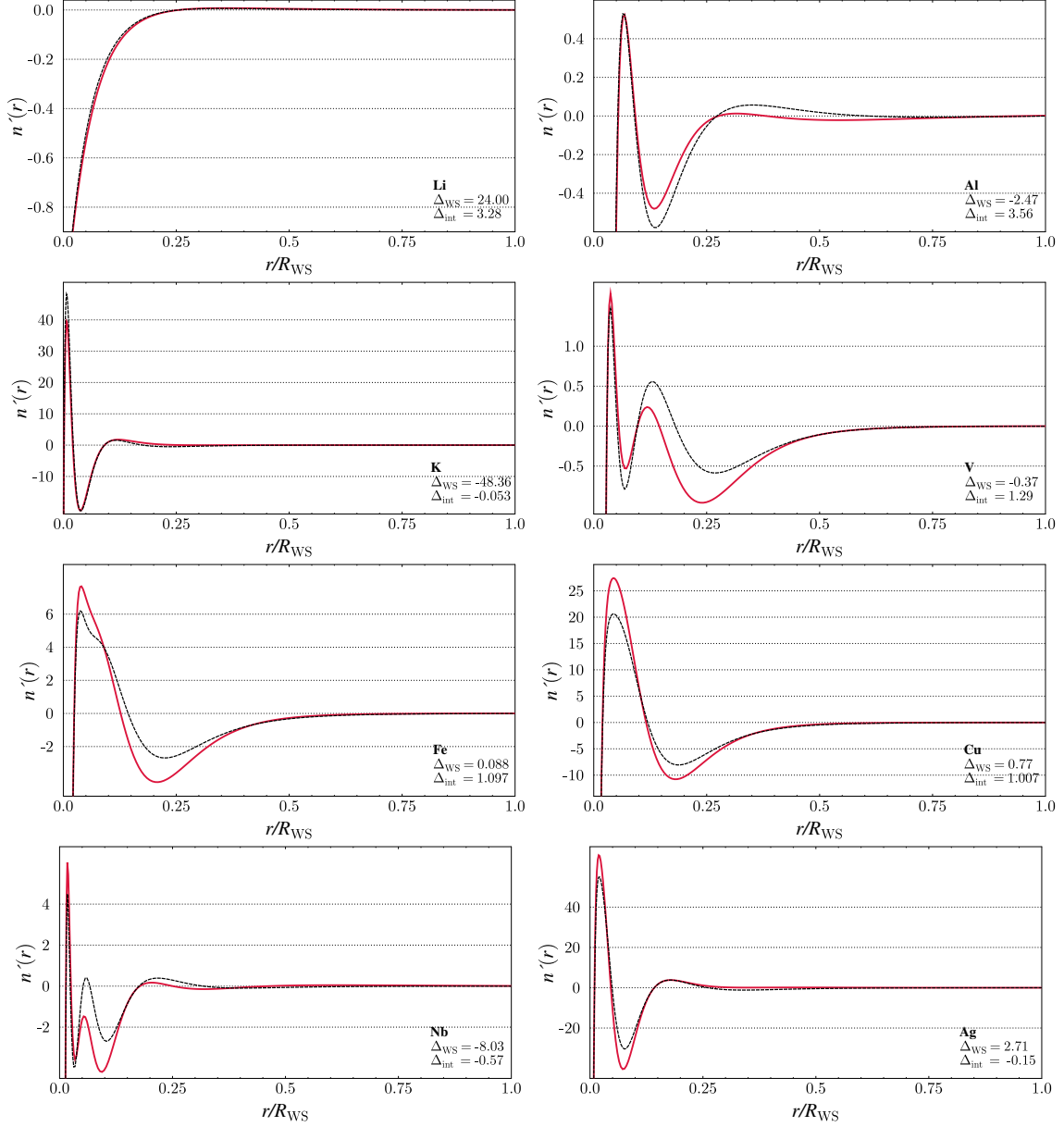


**Figure 5.4:** Comparison between exact gradient of the valence charge density (black lines) and extrapolation of  $\mathcal{K}$  to  $q = 0$  (red lines) for different metals. Qualitatively, the runs of both respective functions are similar. For small and large radii, both curves are almost indistinguishable. At medium radii, the curves show the same characteristic features, but with slightly different peak positions and heights. At a closer look, it turns out that the ratio between both curves is largest at the Wigner-Seitz radius (denoted as  $\Delta_{WS}$ ). The ratio of the integrated quantities (see text) is given as  $\Delta_{int}$ .

The deviation in this region is important because the values at large radii give the biggest contribution in volume integrals over the Wigner-Seitz cell.  $\mathcal{K}(r, q)$  enters the dynamical matrix as a factor and thus even small deviations have a crucial influence on the resulting phonon frequencies. Thus, the influence on the exchange-correlation part of the dynamical matrix (Eq. 5.97) is expected to be small, since the gradient of the core charge density quickly approaches zero for large radii, opposed to the other terms (5.96 and 5.95) in which the integrals are taken over products of coulomb terms and  $\mathcal{K}(r, q)$ . Due to the integral form of the dynamical matrix, it seems also useful to compare the integrated values

of  $\mathcal{K}(\mathbf{r}, \mathbf{q})$ . The resulting ratio,

$$\Delta_{\text{int}} = \frac{\int_0^{R_{\text{WS}}} dr r^2 \mathcal{K}(r, \mathbf{q} \rightarrow 0)}{\int_0^{R_{\text{WS}}} dr r^2 \nabla n^v(r)}, \quad (5.120)$$

is also given in Fig. 5.4. In this case, Cu and Fe show ratios of  $\approx 1.0$  and also V has a reasonable  $\Delta_{\text{int}}$  of 1.29. Opposed to this, the light elements Li, K, and Al show far worse values of this ratio. This contrast possibly originates in the fact that the valence bands of these elements are dominated by weakly localized s and p states, whereas the 3d elements are dominated by strongly localized valence states. Basically, the KKR method is better suited for the description of localized states, especially when used with ASA and MT approximation. Nevertheless, the ratio  $\Delta_{\text{WS}}$  is more important for the quality of the resulting dynamical matrix. The fact, that the ratio between  $\nabla n(\mathbf{r})$  and  $\mathcal{K}(\mathbf{r}, \mathbf{q})$  is worst at large radii indicates that the used approximation for the scattering potential (ASA) is problematic since at large radii, the exact potential and density differ widely from spherical symmetry.

### Phonon dispersions

The above presented test results show, on one side, that non-interacting susceptibilities are numerically manageable and can be improved through refinement of computational parameters. Apart from that, it is obvious that the result of the valence charge density response function  $\mathcal{K}$  is questionable and its deviation from optimum depends on the respective material. The remaining question is, how strong this deviation affects the calculation of phonon frequencies. In the following, some example calculations are shown, beginning with the material which gave the best results, Copper. Fig. 5.5 (a) shows the eigenvalues of both

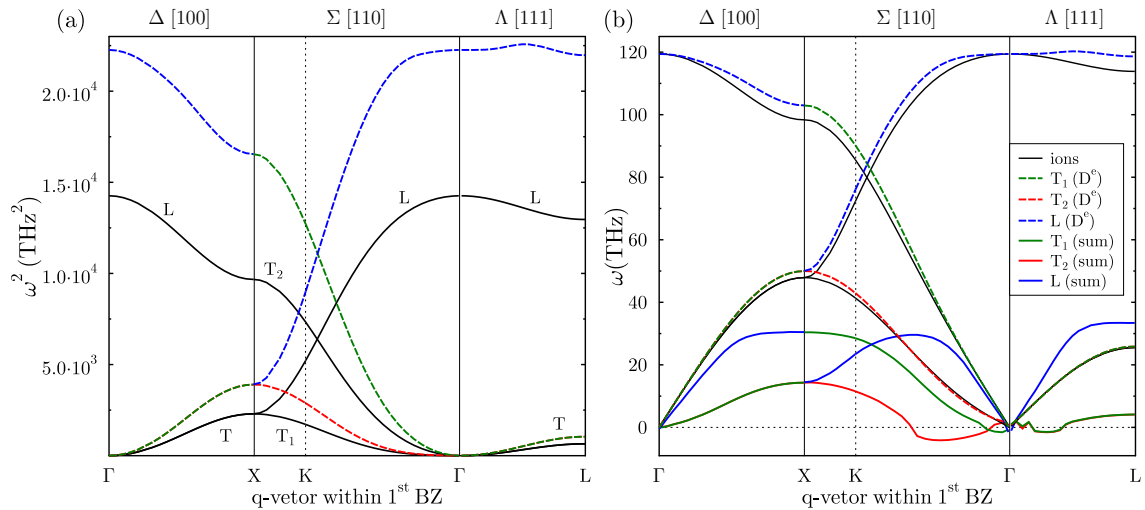


**Figure 5.5:** (a) The plot shows the eigenvalues of both ionic part (straight lines) and electronic part (dashed lines) of the dynamical matrix of Copper on high-symmetry lines of the fcc Brillouin zone. All values of the electronic part have been shifted such that the transverse branches approach zero at the  $\Gamma$  point. (b) The resulting frequencies as square root of the eigenvalues. The frequencies of the valence part have been reduced by a factor of 1.56 such that the longitudinal modes of both parts coincide at  $\Gamma$ . The residual frequencies, obtained from the difference of both dynamical matrices, are plotted as thick coloured lines.

parts of the dynamical matrix of a Cu bulk crystal

$$D_{\alpha,\beta}^{11}(\mathbf{q}) = {}^{\text{ion}} D_{\alpha,\beta}^{11}(\mathbf{q}) - {}^{\text{el}} D_{\alpha,\beta}^{11}(\mathbf{q}), \quad (5.121)$$

as a function of  $\mathbf{q}$ -vectors on selected high-symmetry lines of the first Brillouin zone of the fcc lattice. The solid lines denote the eigenvalues of the ion part  ${}^{\text{ion}} D_{\alpha,\beta}^{11}(\mathbf{q})$ , which are basically the square of the vibrational frequencies of the bare ion lattice. The three branches are denoted by labels 'L' for longitudinal and, respectively, 'T<sub>1</sub>' or 'T<sub>2</sub>' for the transverse branches. The latter are degenerate on the (100) and (111) lines.

The eigenvalues of the valence part  ${}^{\text{el}} D_{\alpha,\beta}^{11}(\mathbf{q})$  are plotted as coloured dashed lines, where blue denotes longitudinal modes and red as well as green transverse modes. Obviously the behaviour of the valence part is very similar to the ion part, but all eigenvalues seem enhanced by a nearly  $\mathbf{q}$ -independent factor. Ideally, ion and valence eigenvalues should coincide at  $\Gamma$  and run close to each other such that the eigenvalues of the resulting difference matrix provide the correct phonon dispersion. This is not the case, as the valence  $\omega_L^2$  at  $\Gamma$  is 56% larger than the respective ion value. Nevertheless, the general behaviour as well as the symmetry of the modes are correct.

In order to allow for a better comparison of both parts, the right panel (b) shows the resulting phonon frequencies. Black lines again represent the frequencies of the bare ion lattice and are obtained by taking the square root of the eigenvalues of the respective dynamical matrix  ${}^{\text{ion}} D_{\alpha,\beta}^{ij}(\mathbf{q})$ . To match the condition of the acoustic sum rule

$$\lim_{\mathbf{q} \rightarrow 0} D_{\alpha,\beta}^{ij}(\mathbf{q}) = 0, \quad (5.122)$$

${}^{\text{el}} D_{\alpha,\beta}^{ij}(\mathbf{q})$  has to coincide with the ion part at  $\Gamma$ . For this purpose, the valence part has been reduced by a factor of  $f \approx 0.64$ . Thus, the coloured dashed lines denote the frequencies of this augmented matrix. Now the frequencies are equal at the  $\Gamma$ -point, but the valence frequencies at finite  $\mathbf{q}$ -vectors are almost always higher than their ionic counterparts, although the opposite should be true. Thus, the resulting dynamical matrix

$${}^f D_{\alpha,\beta}^{11}(\mathbf{q}) = {}^{\text{ion}} D_{\alpha,\beta}^{11}(\mathbf{q}) - f \cdot {}^{\text{el}} D_{\alpha,\beta}^{11}(\mathbf{q}), \quad (5.123)$$

has the wrong sign. For the sake of clearness, the frequencies which result from the matrix  $-{}^f D_{\alpha,\beta}^{11}(\mathbf{q})$  are shown in Fig. 5.5 (b) as thick coloured lines.

The fact that the valence eigenvalues are bigger than the ionic ones essentially means that the scaling with a constant factor  $f$  is wrong. Indeed, the dynamical matrix needs a  $\mathbf{q}$ -dependent correction to match the vibronic properties of the electron gas. The large deviation at  $\Gamma$  can be directly related to the differences between  $\mathcal{K}(\mathbf{r}, \mathbf{q} = 0)$  and  $\nabla n^{\text{v}}(\mathbf{r})$  in Fig. 5.4.

Another 3d element with similar values of integrated  $\mathcal{K}(\mathbf{r}, \mathbf{q} = 0)$  and integrated gradient of the valence charge density is Fe. Fig. 5.6 (a) shows the eigenvalues of both parts of the dynamical matrix on high-symmetry lines within the BZ of the BCC crystal. As expected for this Bravais lattice, electronic as well as ionic eigenvalues are threefold degenerate at high-symmetry points H and P. While the ionic eigenvalues at both points are equal, the valence values in P are higher than in H. Thus, the resulting frequencies (Fig. 5.6 (b)) in P are lower than at H, in correspondence with the experimental results.

In the fashion of Cu, the run of the transverse modes of the valence matrix is very similar to the ionic values, but, besides the difference in overall scaling, several distinctions become apparent: the transverse valence mode on the  $\Delta$  line does not approach H like  $q^2$ , but approximately linear. Moreover, the transverse mode T<sub>1</sub> on the  $\Sigma$  line is too high compared to T<sub>2</sub> and to the respective ionic mode. Nevertheless, the greatest discrepancy appears in the longitudinal mode near the  $\Gamma$  point. The electronic eigenvalues assume maxima between

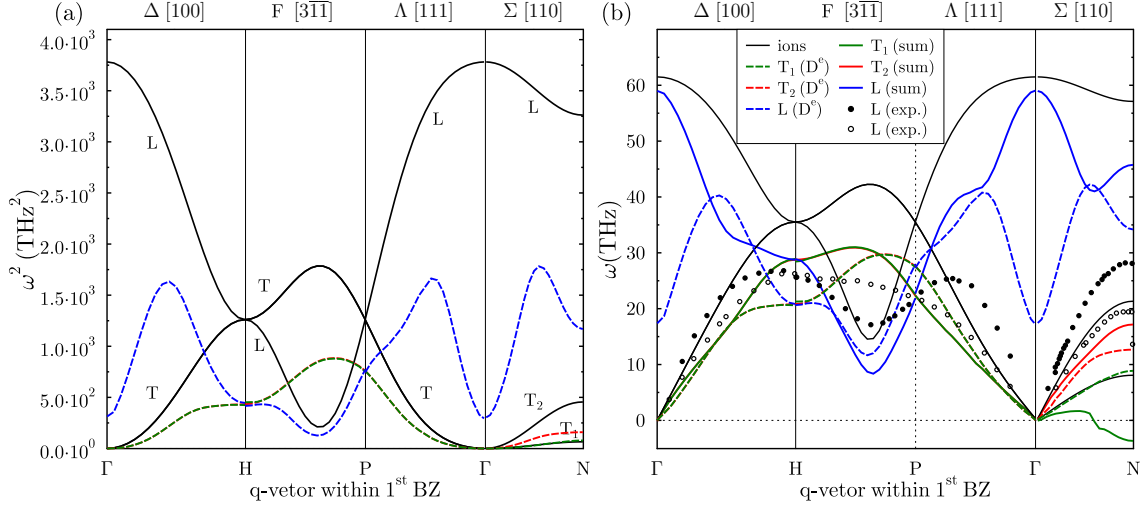


**Figure 5.6:** Fe. (a) Eigenvalues of both ionic and electronic parts of the dynamical matrix for Fe, similar to Fig. 5.5. (b) Resulting phonon frequencies. For comparison, neutron scattering data from [MSN67] are plotted as circles (Filled circles for longitudinal modes, empty circles for transverse modes. On the  $\Sigma$  line, only the  $T_2$  branch is shown.)

center and boundary of the BZ and thus decrease towards  $\Gamma$ , instead of approaching the ion plasma frequency. The resulting value at  $\Gamma$  is by a factor of appr. 12 smaller than the respective longitudinal ionic mode. For that reason it is not useful to scale the valence eigenvalues by a constant factor similar to Cu when it comes to plotting the phonon frequencies in panel (b) of Fig. 5.6. The plot shows ionic (black lines) and valence frequencies (dashed lines) as well as the resulting frequencies of the total dynamical matrix (straight coloured lines). For better comparison, experimentally measured frequencies, taken from [MSN67], are indicated by black dots. The latter are scaled by a factor of 3 for clearness and they indicate that the ab-initio frequencies show, at least far from the zone centre, correct behaviour.

The phonon dispersions obtained for other tested elements show, in principle, the same problem: The symmetry properties of the electronic part of the dynamical matrix is similar to the ionic one. Near the BZ boundary, the run of the modes is quite similar, although the absolute values of the electronic part are too small compared to the ionic part, causing too large values of the resulting phonon frequencies. In the long-wavelength limit, the longitudinal mode of electronic and ionic matrix differ largely, instead of both approaching the ion plasma frequency. This limit can be, to some extent, compared with the  $\mathbf{q} \rightarrow 0$  limit of  $\mathcal{K}$ . Table 5.1 shows the ratio between  $\mathcal{K}(\mathbf{q} \rightarrow 0, R_{WS})$  and  $\nabla n(R_{WS})$  on one side, and the ratio between the longitudinal eigenvalues of  ${}^{\text{ion}}D_{\alpha,\beta}^{11}(\mathbf{q})$  and  ${}^{\text{el}}D_{\alpha,\beta}^{11}(\mathbf{q})$  on the other. Especially for the smaller values of  $\Delta_{WS}$  a correlation with  $(\omega_{\Gamma}^{\text{el}}/\omega_{\Gamma}^{\text{ion}})^2$  is recognizable. Since  $\Delta_{WS}$  is only the deviation of  $\mathcal{K}$  at  $R_{WS}$  and does not include smaller radii, a more obvious correlation can not be expected. Particularly the large values of  $\Delta_{WS}$  in Nb, Li and K are clearly overestimating the deviation of the dynamical matrix at  $\Gamma$  (as already can be

Element	Fe	V	Cu	Al	Ag	Nb	Li	K
$ \Delta_{WS} $	0.088	0.37	0.77	2.47	2.71	8.03	24.00	48.36
$(\omega_{\Gamma}^{\text{el}}/\omega_{\Gamma}^{\text{ion}})^2$	0.079	0.384	1.56	1.08	3.35	1.92	4.248	2.454

**Table 5.1:** Comparison between  $\Delta_{WS}$  (see Eq. (5.119)) and the ratio between the eigenvalues of electronic and ionic part of the dynamical matrix for the longitudinal branch at the  $\Gamma$  point.

estimated from Fig. 5.4). This correlation is a significant hint to the discrepancies in  $\mathcal{K}$  being the reason for the errors in the phonon dispersions.

### 5.3.2 Conclusion and Outlook

The results shown here represent the status quo of an ongoing development. Much time was invested in development and testing of the formalisms for the linear response of the charge density and the dynamical matrix. So far, the results question the chosen methods, but if and how they can be improved becomes apparent on closer consideration of possible sources of errors:

**The choice of the exchange-correlation kernel.** The choice of LDA as approximation to the exchange-correlation potential may be questioned with respect to the validity of the Hellmann-Feynman-Theorem. Since LDA is, strictly speaking, only valid for a homogeneous electron gas, it does not lead to the exact ground state density which is a basis for the validity of the HFT. As shown in [Gon00], this is not a problem since the HFT holds exactly within the LDA. In the same sense, the choice of the simplest approximation for an exchange-correlation kernel  $f_{xc}$  is a possible source of errors. Its essential simplification lies in the assumption that the rate of change of the exchange-correlation potential is independent of the rate of change of the external potential. This limitation is indeed crucial when it comes to the description of numerous dynamic processes where the perturbation of the external potential is of high amplitude. Nevertheless, this adiabatic LDA kernel has proven very useful [BGD01] because lattice vibrations which can be described within the harmonic approximation live on time scales in which the electron gas can be regarded as static. Thus, it is unlikely that the use of a frequency-dependent kernel would improve the results.

**Geometric problem of ASA: Moon regions and interstitials** A fundamental property of the atomic sphere approximation is the overlap between neighbouring atomic spheres on one side and the interstitial regions on the other. In the current version of the formalism, both issues are not addressed. All integrals are taken over the Wigner-Seitz spheres and neglect the interstitial regions completely. Also the Moon regions cause a wrong assignment of integration regions and a double-counting of contributions from them. In order to eliminate these problems, one has to introduce near-field corrections into the formalism. Test calculations using the Muffin-Tin approximation with larger interstitial regions but without moon regions showed similar results to ASA. This indicates that the limitation of a spherical cell boundary is important, but not crucial for the observed results. In order to improve the numerical accuracy, it would be easier to augment the formalism for space-filling cells using shape functions instead of the introduction of near-field corrections. This solution also has the advantage to be applicable to the next point:

**Spherical density and spherical potential.** As mentioned before, the HFT is only valid for the exact ground-state wave function and thus the exact ground-state charge density. Errors in the charge density enter the HF forces in linear order. In the MT or ASA approximation, the charge density is always of spherical symmetry, and thus causes errors in the forces. Despite this fact, it still seems possible to obtain reasonable forces from KKR methods applying MT or ASA approximations [Zec01] if a rigid-ion model is used. The problem increases, when the derivative of the force is taken to calculate the harmonic force constants. Here, the linear response  $\mathcal{K}$  of the charge density to a lattice distortion enters and increases the errors caused by the spherical density. The errors in  $\mathcal{K}$  are most likely caused by the spherical density in combination with the non-spherical derivatives of the

core charge density (Eq. (5.94)) and the Coulomb potential (Eq. (2.70)). In the long-wavelength limit, these result in non-spherical contributions to  $\mathcal{K}$  which are not part of the derivative of the spherical valence density. This problem can not be avoided by cutting off the angular momentum summation in the susceptibility dyson equation at  $\ell = 0$  because of the almost vanishing spherical contributions of the above mentioned derivatives.

A promising solution for this problem is the implementation of the full-potential method which uses space-filling, non-overlapping cells as well as densities and potentials without spherical symmetry. An efficient self-consistent FP algorithm has been implemented into the HUTSEPOT code recently. Instead of spherically symmetric scattering centres it uses the full Wigner-Seitz cells, the complex boundary of which is taken into account via shape functions

$$\Theta(\mathbf{r}) = \begin{cases} 1; & \mathbf{r} \in \Omega_{\text{WS}} \\ 0; & \mathbf{r} \notin \Omega_{\text{WS}} \end{cases}. \quad (5.124)$$

By the expansion of those in terms of spherical harmonics

$$\Theta(\mathbf{r}) = \sum_L \Theta_L(r) Y_L(\hat{\mathbf{r}}), \quad (5.125)$$

all integrals over the Wigner-Seitz cell occurring in the dynamical matrix or the linear response formalism can be kept but have to be rewritten using shape functions and an the integration radius of the bounding sphere of the cell. By acknowledging aspherical expansion terms in the potential

$$V(\mathbf{r}) = \sum_L v_L(r) Y_L(\hat{\mathbf{r}}) \quad (5.126)$$

during the solution of the single site scattering problem, the representation of the respective non-spherically symmetric coefficients of regular and irregular solutions has to be augmented by an additional angular momentum expansion

$$R_L(\mathbf{r}, E) = \sum_{L'} R_{LL'}(r, E) Y_{L'}(\hat{\mathbf{r}}) \quad (5.127)$$

$$H_L(\mathbf{r}, E) = \sum_{L'} H_{LL'}(r, E) Y_{L'}(\hat{\mathbf{r}}). \quad (5.128)$$

As a consequence thereof, the representations of charge density and polarization function as well as  $\mathcal{K}$  have to be rewritten in terms of the additional indices, which can be done straightforwardly. This enhancement of the formalism will increase the computational effort needed for the evaluation of polarization function and subsequent quantities considerably. Parts of the additional costs may be decreased by using the full-charge-density approximation [VKS97] instead of the full-potential scheme. This approach still uses non-spherical densities and space-filling cells, but uses only the spherical component of the potential, as is done in MT and ASA. Benchmark calculations in [Asa+99] have shown that this simplified approach still generates results with extremely high accuracy.

# Electron-Phonon Interaction in superconducting metals

The interaction between electronic and vibrational states affects almost all physical properties of solids and has been studied since the 1920s. It plays an important role in the description of transport processes. The effect that an electron moving through a lattice of positive ions distorts this lattice has two important consequences: The momentum of the electron can be degraded due to energy dissipation into the lattice, which gives the main contribution to electrical resistivity at high temperatures. Opposed to this, at very low temperatures, the electron-phonon interaction can lead to an effective reduction of the Coulomb repulsion between two electrons, leading to the formation of Cooper pairs and thus reducing the electrical resistance to zero. Superconductivity, discovered in 1911 [DK10], was not understood on a microscopic scale until the 1950s, when Cooper, Bardeen and Schrieffer developed their theory based on electron-phonon interaction [Coo56; BCS57]. They considered an electron gas whose particles did not only interact via the screened coulomb interaction, but also exchanged virtual phonons (see Fig. 6.1). In a simple picture, one electron in state  $|k\rangle$  distorts the lattice and thus creates a phonon of frequency  $q$ . A second electron  $|k'\rangle$  responds to the resulting charge imbalance and annihilates the phonon [BK09] such that  $k - k' = q$ . The authors showed that these bound states become energetically favourable when the interaction is attractive for states near the Fermi level, opening an energy gap  $\Delta$  and creating a new ground state with fundamentally different properties than the Fermi gas. The BCS theory was able to predict the superconducting transition

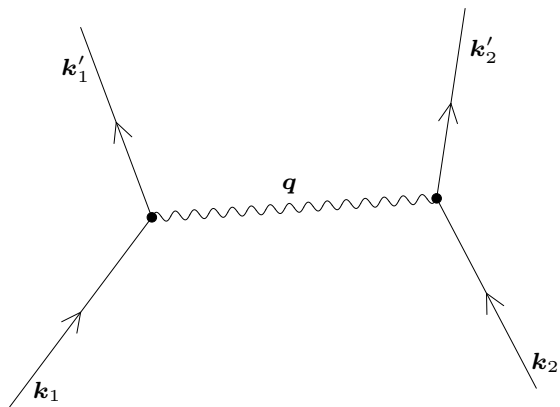


**Figure 6.1:** Feynman diagram of the electron-phonon interaction which induces the creation of a Cooper pair. Here, space and time are represented by the horizontal and vertical axis, respectively. The trajectory of both electrons  $k_1$  and  $k_2$  is changed due to the exchange of a virtual phonon with wave vector  $q$ , leading to an effective attraction between the electrons. Both scattering processes are considered elastic, such that  $q = k_1 - k_1' = k_2' - k_2$ .

temperature  $T_C$  as well as the gap for a wide range of metals. However, it failed for some heavy metals, such as Hg and Pb, because the theory was constructed without a detailed picture of the electron-phonon interaction. In particular, it ignored the retardation between emission and absorption of the virtual phonon as well as the limited lifetime of the cooper pairs.

These problems have been addressed by Eliashberg [Éli60; Éli61; Éli62] who developed self-consistent equations for the determination of  $\Delta$  and  $T_C$ . In his picture, which is based on Green function techniques, the electron-phonon interaction is described by a spectral function  $\alpha^2(\omega)F(\omega)$ , which is related to the interaction strength  $\lambda$  by

$$\lambda = 2 \int \frac{d\omega}{\omega} \alpha^2(\omega) F(\omega). \quad (6.1)$$

Here,  $F(\omega)$  is the phonon density of normal modes at frequency  $\omega$  and  $\alpha^2(\omega)$  is a weighting function describing the coupling strength to electronic states. An interesting way to derive this function named after Eliashberg, is the following (after [Gon00]):

An important effect of the electron-phonon interaction is that it slows down the electrons near the Fermi energy in a metal, without causing energy dissipation. In a physical picture, this reduction of velocity is caused by the local distortion of the lattice by the electrons moving through it, which causes higher forces between ions and electrons. For a metal with an approximate free electron dispersion, the Fermi velocity is given by  $v_F = \hbar k_F / m$  with  $m$  being the effective mass of an electron under neglect of the electron-phonon interaction. Since the Fermi momentum  $k_F$  remains unchanged, the effect can be interpreted as being caused by a larger effective mass of the electrons, and is related to the electron-phonon coupling constant via

$$m^* = m(1 + \lambda). \quad (6.2)$$

This effect is also connected to the density of states at the Fermi level, as

$$d(E) = \frac{\Omega_{UC}}{(2\pi)^3} \int dE \int_{S(E)} \frac{dS_{\mathbf{k}}(E)}{\hbar |\mathbf{v}_{\mathbf{k}}|}. \quad (6.3)$$

The effects on the electronic system caused by electron-phonon interaction can be better understood by examining the electronic self-energy. If the electronic states of a material can be described by the single-particle equation

$$\left[ -\frac{\hbar}{2m_e} \nabla_{\mathbf{r}}^2 + V_{\text{eff}}(\mathbf{r}) \right] \psi_{\mathbf{k}}(\mathbf{r}) = E_{\mathbf{k}} \psi_{\mathbf{k}}(\mathbf{r}), \quad (6.4)$$

in which  $V_{\text{eff}}(\mathbf{r})$  is the self-consistent and energy-independent effective single-particle potential in which the electron moves. The energy of the electron in state  $|\mathbf{k}\rangle$  is given by  $E_{\mathbf{k}}$ , but this is not equal to the difference between the total energy of the system  $E_{N_e}$  and an equal system without the electron  $|\mathbf{k}\rangle$ , or a system with an additional electron  $E_{N_e+1}$ . Instead, the system would relax into a different ground state. The energy difference can be written as

$$E_{N_e+1} - E_{N_e} = E_{\mathbf{k}} + \Sigma(\mathbf{k}, E), \quad (6.5)$$

where the additional term  $\Sigma(\mathbf{k}, E)$  is called the self-energy of the electron in state  $|\mathbf{k}\rangle$ .

The energy of an electron  $\mathbf{k}$  which is added to an electronic system in its ground state must lie above the Fermi level. If this electron emits a phonon and gets shifted to the state  $\mathbf{k}'$ , the self-energy related to this process is given by

$$\sum_{\mathbf{k}'} \sum_j \left| M_{\mathbf{k}\mathbf{k}'}^j \right|^2 \frac{1 - f_{\mathbf{k}'}}{E - E_{\mathbf{k}'} - \hbar\omega_{\mathbf{k}'-\mathbf{k}}^j}, \quad (6.6)$$

which is the golden-rule expression obtained from a perturbative treatment of this process [Sca69]. The factor  $(1 - f_{\mathbf{k}'})$  emerges from the condition that  $|\mathbf{k}'\rangle$  has to be unoccupied to allow the scattering to happen. The energy is quantified by the electron-phonon matrix element  $\left| M_{\mathbf{k}\mathbf{k}'}^j \right|^2$  which expresses the interaction energy of the two states which are coupled by a phonon of band/polarization index  $j$  and wave vector  $\mathbf{k}' - \mathbf{k}$ . Under consideration of the fact, that after the addition of  $|\mathbf{k}\rangle$  no more scattering from occupied states  $|\mathbf{k}'\rangle$  into  $|\mathbf{k}\rangle$  is allowed, the electron-phonon contribution to the self-energy in lowest order reads

$$\Sigma_{\text{ep}}(\mathbf{k}, E) = \sum_{\mathbf{k}'} \sum_j \left| M_{\mathbf{k}\mathbf{k}'}^j \right|^2 \left[ \frac{1 - f_{\mathbf{k}'}}{E - E_{\mathbf{k}'} - \hbar\omega_{\mathbf{k}'-\mathbf{k}}^j} - \frac{f_{\mathbf{k}'}}{E_{\mathbf{k}'} - E - \hbar\omega_{\mathbf{k}'-\mathbf{k}}^j} \right]. \quad (6.7)$$

In order to simplify the evaluation of this expression, it is useful to replace the sum over states by an integration over constant energy surfaces,

$$\sum_{\mathbf{k}} \rightarrow \int dE \sum_{\mathbf{k}} \delta(E - E_{\mathbf{k}}) = \int dE \frac{V_{\text{UC}}}{(2\pi)^3} \int_E \frac{dS_{\mathbf{k}}(E)}{\hbar v_{\mathbf{k}}}, \quad (6.8)$$

where  $dS_{\mathbf{k}}(E)$  is a surface element of the constant-energy surface related to  $E$ , oriented in direction  $\mathbf{k}$ . Adding an additional integration over  $\omega$  results in the expression

$$\begin{aligned} \Sigma_{\text{ep}}(\mathbf{k}, E) = & \int d\omega \int dE' \frac{V_{\text{UC}}}{(2\pi)^3} \int_{E'} \frac{dS_{\mathbf{k}}(E')}{\hbar v_{\mathbf{k}}} \sum_j \left| M_{\mathbf{k}\mathbf{k}'}^j \right|^2 \delta(\omega - \omega_{\mathbf{k}'-\mathbf{k}}^j) \times \\ & \times \left[ \frac{1 - f_{\mathbf{k}'}}{E - E' - \hbar\omega_{\mathbf{k}'-\mathbf{k}}^j} - \frac{f_{\mathbf{k}'}}{E' - E - \hbar\omega_{\mathbf{k}'-\mathbf{k}}^j} \right] \end{aligned} \quad (6.9)$$

The major contribution to the energy integration occurs around the region  $E \pm \hbar\omega$ . The phonon energy  $\hbar\omega$  varies in the range of meV, whereas the electronic eigenenergies occur in an interval of several eV. Thus, under the assumption that the electron-phonon matrix elements are constant near the Fermi surface, it is sufficient to evaluate the integrals there. Introducing the auxiliary quantity

$$\alpha_{\mathbf{k}}^2(\omega)F(\omega) = \frac{V_{\text{UC}}}{(2\pi)^3} \int_{\epsilon_{\text{F}}} \frac{dS_{\mathbf{k}}(\epsilon_{\text{F}})}{\hbar v_{\mathbf{k}}} \sum_j \left| M_{\mathbf{k}\mathbf{k}'}^j \right|^2 \delta(\omega - \omega_{\mathbf{k}'-\mathbf{k}}^j), \quad (6.10)$$

the electron-phonon self energy is obtained as

$$\Sigma_{\text{ep}}(\mathbf{k}, E) = \hbar \int d\omega \alpha_{\mathbf{k}}^2(\omega)F(\omega) \ln \left| \frac{E - \hbar\omega}{E + \hbar\omega} \right|. \quad (6.11)$$

The  $\mathbf{k}$ -dependent spectral function defined in (6.10) is a key value in the Eliashberg theory of electron-phonon coupling. It measures the scattering rate of electrons in state  $|\mathbf{k}\rangle$  with phonons of frequency  $\omega$ . It can be used to obtain the electron-phonon coupling constant  $\lambda$ : Using Eq. (6.2), the Fermi velocity renormalized due to electron-phonon coupling reads

$$v_{\mathbf{k}}^* = \hbar\mathbf{k}/m^* = v_{\mathbf{k}}/(1 + \lambda_{\mathbf{k}}) = \frac{1}{\hbar} \nabla_{\mathbf{k}} E_{\mathbf{k}}/(1 + \lambda_{\mathbf{k}}). \quad (6.12)$$

Together with Eq. (6.5) one obtains

$$\lambda_{\mathbf{k}} = \left. \frac{-\partial \Sigma_{\text{ep}}(\mathbf{k}, E)}{\partial E} \right|_{E=\epsilon_{\text{F}}}, \quad (6.13)$$

which results in the  $\mathbf{k}$ -dependent mass enhancement factor

$$\lambda_{\mathbf{k}} = 2 \int \frac{d\omega}{\omega} \alpha_{\mathbf{k}}^2(\omega)F(\omega). \quad (6.14)$$

The related  $\mathbf{k}$ -independent quantities from Eq. (6.1) can be obtained by averaging over the full Brillouin zone. The averaged  $\lambda$  can be used to determine the superconducting gap  $\Delta$  and the critical Temperature  $T_{\text{C}}$ , for which numerous approximation formulas exist [Car90]. Due to the decreased Fermi velocity, the electron-phonon interaction also influences the density of states at the Fermi level, which results in a similar expression for the effective mass:

$$d^*(\epsilon_{\text{F}}) = \sum_{\mathbf{k}} \delta(E_{\mathbf{k}} - \epsilon_{\text{F}}) = \frac{V_{\text{UC}}}{(2\pi)^3} \int_{\epsilon_{\text{F}}} \frac{dS_{\mathbf{k}}(\epsilon_{\text{F}})}{\hbar v_{\mathbf{k}}^*} \quad (6.15)$$

$$= d(\epsilon_{\text{F}})(1 + \lambda). \quad (6.16)$$

Both phenomena strongly depend on the electron-phonon coupling strength  $\lambda$ , the prediction of which by ab-initio methods is a challenging task until today. A general problem in this case is that the distortion of the lattice by an electron lies beyond the scope of the Born-Oppenheimer approximation [Gon00]. A possible way out of this dilemma is the development of a density functional theory of the superconducting state [OG88]. Nevertheless, it is possible to approximate  $\lambda$  using 'classical' band structure methods.

## 6.1 Eliashberg function in rigid muffin-tin approximation

To start with, the definition of the Eliashberg function as given by McMillan [McM68] reads

$$\alpha^2(\omega)F(\omega) = \frac{1}{(2\pi)^6 \pi N d(\epsilon_F)} \int d\mathbf{k} \int d\mathbf{k}' \sum_j \left| M_{\mathbf{k}\mathbf{k}'}^j \right|^2 \delta(\hbar\omega - \hbar\omega_{\mathbf{q}}^j) \times \delta(E_{\mathbf{k}} - \epsilon_F) \delta(E_{\mathbf{k}'} - \epsilon_F) \quad (6.17)$$

where  $M_{\mathbf{k}\mathbf{k}'}^j$  is the probability amplitude of a phonon of band index  $j$  for scattering an electron  $\mathbf{k}$  into the state  $\mathbf{k}'$  and  $N$  denotes the number of unit cells. The frequency of this phonon is  $\omega_{\mathbf{q}}^j$  with  $\mathbf{q} = \mathbf{k} - \mathbf{k}'$ . The main problem in the determination of this function lies in the calculation of the matrix elements which have already been used in Eq. (2.16). Gaspari and Gyorffy [GG72] showed how the strength of the electron-phonon interaction can be calculated using only the phase shifts obtained from multiple scattering calculations. Later the theory was applied to a rigid muffin-tin electronic band structure method [GG74], which allowed to calculate the coupling parameter using the electronic band structure obtained using multiple scattering theory and the phonon band structure from experimental measurements. This formulation can readily be applied for use with the KKR method. In the above formulation, the matrix elements have been classified by the band index  $j$  for convenience. This band index is equivalent to a combination of polarization index  $\alpha$  and site index  $s$  of a displaced ion within the unit cell. Within this notation, an electron-phonon matrix element can be written as

$$\left| M_{\mathbf{k}\mathbf{k}'} \right|^2 = \left\langle \mathbf{k} \left| \frac{\partial v_{\text{eff}}^s}{\partial u_{\alpha}(s)} \right| \mathbf{k}' \right\rangle \left\langle \mathbf{k}' \left| \frac{\partial v_{\text{eff}}^{s'}}{\partial u_{\beta}(s')} \right| \mathbf{k} \right\rangle \quad (6.18)$$

$$= \int d\mathbf{r} \psi_{\mathbf{k}}^*(\mathbf{r}) \frac{\partial v_{\text{eff}}^s(\mathbf{r})}{\partial u_{\alpha}(s)} \psi_{\mathbf{k}'}(\mathbf{r}) \int d\mathbf{r}' \psi_{\mathbf{k}'}^*(\mathbf{r}') \frac{\partial v_{\text{eff}}^{s'}(\mathbf{r}')}{\partial u_{\beta}(s')} \psi_{\mathbf{k}}(\mathbf{r}'), \quad (6.19)$$

where  $v_{\text{eff}}^s$  is the effective single-particle potential within the muffin-tin sphere of ion  $s$ . Within the rigid muffin-tin scheme it is assumed that the ion moves rigidly with the associated potential, allowing for the the approximation

$$\frac{\partial v_{\text{eff}}^s(\mathbf{r})}{\partial u_{\alpha}(s)} \approx \frac{\partial v_{\text{eff}}^s(\mathbf{r})}{\partial r_{\alpha}}. \quad (6.20)$$

To further rearrange Eq. (6.19), it is useful to replace the phonon dynamical matrix by the so-called phonon Green function. As the name suggests, it can be derived in analogy to the electronic Green function by starting with the secular equation (2.32) of the harmonic approximation [Gon00],

$$\sum_{j\beta} \left[ D_{\alpha\beta}^{ij}(\mathbf{q}) - \omega^2 \delta_{\alpha\beta} \delta_{ij} \right] A_{\beta}(j, \mathbf{q}) = 0. \quad (6.21)$$

Here,  $D$  denotes the dynamical matrix of the system,  $s$  and  $s'$  identify lattice sites and greek letters represent directions of displacements. In a supermatrix notation, using the combined

indices  $\mu = (s, \alpha)$  and  $\nu = (s', \beta)$ , it can be rewritten as

$$\sum_{\nu} [D_{\mu\nu}(\mathbf{q}) - \omega^2 \delta_{\mu\nu}] A_{\nu}(\mathbf{q}) = 0 \quad (6.22)$$

or

$$[D(\mathbf{q}) - \omega^2 I] A(\mathbf{q}) = 0, \quad (6.23)$$

where  $I$  is a unit In analogy to electronic systems (see sect. 4.1), instead of calculating the eigenvalues of the dynamical matrix  $D(\mathbf{q})$ , the equation can be solved with help of a Green function, given by

$$\mathcal{D}(\mathbf{q}, \omega) = \lim_{\eta \rightarrow 0} [D(\mathbf{q}) - (\omega^2 + i\eta)I]^{-1} \quad (6.24)$$

with matrix elements

$$[\mathcal{D}(\mathbf{q}, \omega)]_{\mu\nu} = \mathcal{D}_{\alpha\beta}^{ss'}(\mathbf{q}, \omega). \quad (6.25)$$

Using the above definitions, the Eliashberg function can be written as

$$\begin{aligned} \alpha^2(\omega)F(\omega) &= \frac{1}{(2\pi)^6 \pi N d(\epsilon_F)} \sum_{ss'} \sum_{\alpha\beta} \int d\mathbf{k} \int d\mathbf{k}' \operatorname{Im} \left\{ \mathcal{D}_{\alpha\beta}^{ss'}(\mathbf{k} - \mathbf{k}'; \omega) \right\} \times \\ &\times \left\langle \mathbf{k} \left| \frac{\partial v_s(\mathbf{r})}{\partial \mathbf{r}_{\alpha}} \right| \mathbf{k}' \right\rangle \left\langle \mathbf{k}' \left| \frac{\partial v_{s'}(\mathbf{r}')}{\partial \mathbf{r}'_{\beta}} \right| \mathbf{k} \right\rangle \delta(E_{\mathbf{k}} - \epsilon_F) \delta(E_{\mathbf{k}'} - \epsilon_F). \end{aligned} \quad (6.26)$$

By using the Fourier transformation

$$\mathcal{D}_{\alpha\beta}^{ss'}(\mathbf{q}; \omega) = \frac{1}{N^2} \sum_{ll'} \mathcal{D}_{\alpha\beta}^{sl, s'l'}(\omega) e^{-i\mathbf{q} \cdot \mathbf{R}_{ll'}}, \quad (6.27)$$

with  $\mathbf{R}_{ll'} = \mathbf{R}_l - \mathbf{R}_{l'}$ , the above equation can be written in terms of the real-space phonon green function,

$$\begin{aligned} \alpha^2(\omega)F(\omega) &= \frac{1}{(2\pi)^6 \pi N^3 d(\epsilon_F)} \sum_{ss'} \sum_{ll'} \sum_{\alpha\beta} \int d\mathbf{k} \int d\mathbf{k}' e^{-i(\mathbf{k}-\mathbf{k}') \cdot \mathbf{R}_{ll'}} \operatorname{Im} \mathcal{D}_{\alpha\beta}^{sl, s'l'}(\omega) \times \\ &\times \left\langle \mathbf{k} \left| \frac{\partial v_s(\mathbf{r})}{\partial \mathbf{r}_{\alpha}} \right| \mathbf{k}' \right\rangle \left\langle \mathbf{k}' \left| \frac{\partial v_{s'}(\mathbf{r}')}{\partial \mathbf{r}'_{\beta}} \right| \mathbf{k} \right\rangle \delta(E_{\mathbf{k}} - \epsilon_F) \delta(E_{\mathbf{k}'} - \epsilon_F). \end{aligned} \quad (6.28)$$

In real space representation, the electron-phonon matrix elements used so far can be written as

$$\left\langle \mathbf{k} \left| \frac{\partial v_s(\mathbf{r})}{\partial \mathbf{r}_{\alpha}} \right| \mathbf{k}' \right\rangle = \int d\mathbf{r} \psi_{\mathbf{k}}(\mathbf{r}) \frac{\partial v_s(\mathbf{r})}{\partial \mathbf{r}'_{\beta}} \psi_{\mathbf{k}'}^*(\mathbf{r}). \quad (6.29)$$

For periodic boundary conditions one has

$$\int d\mathbf{k} \rightarrow \frac{V_{\text{UC}}}{(2\pi)^3} \int_{\text{BZ}} d\mathbf{k}, \quad (6.30)$$

where  $V$  is the unit cell volume.

By using the definition of the real-space electronic Green function

$$\operatorname{Im} G(\mathbf{r}_{ls}, \mathbf{r}'_{l's'}; E) = -\pi \frac{1}{N(2\pi)^3} \int d^3\mathbf{k} \psi_{\mathbf{k}}^*(\mathbf{r}_{ls}) \psi_{\mathbf{k}}(\mathbf{r}'_{l's'}) \delta(E_{\mathbf{k}} - E), \quad (6.31)$$

with  $\mathbf{r}_{ls} = \mathbf{R}_l + \tau_s + \mathbf{r}$ , and using Bloch's theorem

$$\psi_{\mathbf{k}}(\mathbf{r}_{ls}) = \psi_{\mathbf{k}}(\mathbf{r} - \mathbf{R}_l - \tau_s) = e^{-i\mathbf{k} \cdot \mathbf{R}_l} \psi_{\mathbf{k}}(\mathbf{r}_s), \quad (6.32)$$

the Eliashberg function can be represented in terms of Green functions as

$$\begin{aligned} \alpha^2(\omega)F(\omega) &= \frac{1}{N(2\pi)^3 n(\epsilon_F)} \sum_{ss'} \sum_{l'} \sum_{\alpha\beta} \int d\mathbf{r}_{l_s} \int d\mathbf{r}'_{l'_s} \text{Im} G(\mathbf{r}_{l_s}, \mathbf{r}'_{l'_s}; \epsilon_F) \times \\ &\times \frac{\partial v(\mathbf{r}_{l_s})}{\partial(\mathbf{r}_{l_s})_\alpha} \text{Im} \mathcal{D}_{\alpha\beta}^{ls, l's'}(\omega) \frac{\partial v(\mathbf{r}'_{l'_s})}{\partial(\mathbf{r}'_{l'_s})_\beta} \text{Im} G(\mathbf{r}'_{l'_s}, \mathbf{r}_{l_s}; \epsilon_F). \end{aligned} \quad (6.33)$$

Here,  $\int d\mathbf{r}_{l_s}$  denotes integration over the muffin-tin sphere of the  $s^{\text{th}}$  ion within the  $l^{\text{th}}$  unit cell. This formulation is ready to be used with the KKR method.

One form of the Green function, as it is used within the KKR, was given in chapter 4 as

$$G(\mathbf{r}_{l_s}, \mathbf{r}'_{l'_s}; E) = \sum_{L_1 L_2} R_{L_1}^{ls}(\mathbf{r}; E) G_{L_1 L_2}^{ls, l's'}(E) R_{L_2}^{l's'+}(\mathbf{r}'; E) \quad (6.34)$$

$$- \sqrt{E} \sum_L \delta_{ll'} \delta_{ss'} R_L^{ls}(\mathbf{r}_{<}; E) H_L^{ls+}(\mathbf{r}_{>}; E). \quad (6.35)$$

It is an expansion in terms of spherical harmonics using the regular and irregular solutions  $R_L(\mathbf{r}, E)$  and  $H_L(\mathbf{r}, E)$  together with the structure constants  $G_{L_1 L_2}^{ls, l's'}(E)$  of the crystal. Alternatively, a similar expansion can be constructed using the scattering path operator  $\tau$ , reading

$$G(\mathbf{r}_{l_s}, \mathbf{r}'_{l'_s}; E) = \sum_{L_1 L_2} Z_{L_1}^{ls}(\mathbf{r}; E) \tau_{L_1 L_2}^{ls, l's'}(E) Z_{L_2}^{l's'+}(\mathbf{r}'; E) \quad (6.36)$$

$$- \sum_L \delta_{ll'} \delta_{ss'} Z_L^{ls}(\mathbf{r}_{<}; E) J_L^{ls+}(\mathbf{r}_{>}; E). \quad (6.37)$$

$Z_L(\mathbf{r}, E)$  and  $J_L(\mathbf{r}, E)$  are the so-called regular and irregular scattering solutions of the radial Schrödinger equation and are related to the 'normal' solutions via the single-site  $t$ -matrix (see [Zab+05]). Using Eq. (6.36) can substantially simplify the evaluation of the spectral function (6.33), since the radial functions are real and the imaginary part of the last term in Eq. (6.36) for real energies vanishes. Thus, the Eliashberg function can be expressed by

$$\begin{aligned} \alpha^2(\omega)F(\omega) &= \frac{1}{N(2\pi)^3 d(\epsilon_F)} \sum_{l'} \sum_{ss'} \sum_{\alpha\beta} \text{Im} \mathcal{D}_{\alpha\beta}^{ls, l's'}(\omega) \sum_{\substack{L_1 L_2 \\ L_3 L_4}} \text{Im} \tau_{L_1 L_2}^{ls, l's'}(\epsilon_F) \text{Im} \tau_{L_3 L_4}^{l's', ls}(\epsilon_F) \times \\ &\times \left\{ \int d^3 \mathbf{r}_{l_s} Z_{L_1}^s(\mathbf{r}_{l_s}; \epsilon_F) \frac{\partial v_\mu(\mathbf{r}_{l_s})}{\partial(\mathbf{r}_{l_s})_\alpha} Z_{L_4}^{s+}(\mathbf{r}_{l_s}; \epsilon_F) \right\} \times \\ &\times \left\{ \int d^3 \mathbf{r}'_{l'_s} Z_{L_2}^{s'+}(\mathbf{r}'_{l'_s}; \epsilon_F) \frac{\partial v_\nu(\mathbf{r}'_{l'_s})}{\partial(\mathbf{r}'_{l'_s})_\beta} Z_{L_3}^{s'}(\mathbf{r}'_{l'_s}; \epsilon_F) \right\}. \end{aligned} \quad (6.38)$$

Introducing the short form

$$A_{LL'}^{ls}(\epsilon_F) = \int d\mathbf{r}_{l_s} Z_L^s(\mathbf{r}_{l_s}; \epsilon_F) \frac{\partial v_\mu(\mathbf{r}_{l_s})}{\partial(\mathbf{r}_{l_s})_\alpha} Z_{L'}^{s+}(\mathbf{r}_{l_s}; \epsilon_F), \quad (6.39)$$

the spectral function becomes

$$\begin{aligned} \alpha^2(\omega)F(\omega) &= \frac{1}{N(2\pi)^3 d(\epsilon_F)} \sum_{l'} \sum_{ss'} \sum_{\alpha\beta} \text{Im} \mathcal{D}_{\alpha\beta}^{ls, l's'}(\omega) \times \\ &\times \sum_{\substack{L_1 L_2 \\ L_3 L_4}} \text{Im} \left\{ \tau_{L_1 L_2}^{ls, l's'}(\epsilon_F) \right\} \text{Im} \left\{ \tau_{L_3 L_4}^{l's', ls}(\epsilon_F) \right\} \times \\ &\times A_{L_1 L_4}^{ls}(\epsilon_F) A_{L_2 L_3}^{l's'}(\epsilon_F). \end{aligned} \quad (6.40)$$

This is the final formula for the Eliashberg function in the real space representation and can be directly implemented into the KKR code. From this expression, it is easy to derive the spectral function for a single atom ( $ls$ ):

$$\begin{aligned} \alpha^2(\omega)F(\omega)_i^s &= \frac{1}{N(2\pi)^3d(\epsilon_F)} \sum_{l'} \sum_{s'} \sum_{\alpha\beta} \text{Im} \mathcal{D}_{\alpha\beta}^{ls,l's'}(\omega) \times \\ &\times \sum_{\substack{L_1L_2 \\ L_3L_4}} \text{Im} \left\{ \tau_{L_1L_2}^{ls,l's'}(\epsilon_F) \right\} \text{Im} \left\{ \tau_{L_3L_4}^{l's',ls}(\epsilon_F) \right\} \times \\ &\times A_{L_1L_4}^{ls}(\epsilon_F) A_{L_2L_3}^{l's'}(\epsilon_F). \end{aligned} \quad (6.41)$$

This real-space representation serves as a starting point for various useful reciprocal-space representations. Using the lattice Fourier transform of the scattering path operator,

$$\tau_{LL'}^{ls,l's'}(E) = \sum_{\mathbf{k}} \tau_{LL'}^{ss'}(\mathbf{k}; E) e^{i\mathbf{k}\cdot\mathbf{R}_{l'}} \quad (6.42)$$

as well as the inverse transform of the phonon Green function (6.27), one has

$$\begin{aligned} \alpha^2(\omega)F(\omega) &= \frac{1}{N(2\pi)^3d(\epsilon_F)} \sum_{l'l''} \sum_{ss'} \sum_{\alpha\beta} \sum_{\substack{\mathbf{q} \\ \mathbf{k}\mathbf{k}'}} e^{i\mathbf{R}_{ij}\cdot(\mathbf{q}+\mathbf{k}-\mathbf{k}')} \text{Im} \mathcal{D}_{\alpha\beta}^{ss'}(\mathbf{q}; \omega) \times \\ &\times \sum_{\substack{L_1L_2 \\ L_3L_4}} \text{Im} \left\{ \tau_{L_1L_2}^{ss'}(\mathbf{k}; \epsilon_F) \right\} \text{Im} \left\{ \tau_{L_3L_4}^{s's}(\mathbf{k}'; \epsilon_F) \right\} \times \\ &\times A_{L_1L_4}^s(\epsilon_F) A_{L_2L_3}^{s'}(\epsilon_F) \end{aligned} \quad (6.43)$$

and due to the lattice identity

$$\frac{1}{N} \sum_l e^{i\mathbf{k}\cdot\mathbf{R}_l} = \delta_{\mathbf{k},0} \quad (6.44)$$

the  $\mathbf{k}$ -averaged Eliashberg spectral function

$$\begin{aligned} \alpha^2(\omega)F(\omega) &= \frac{1}{(2\pi)^3d(\epsilon_F)} \sum_{ss'} \sum_{\alpha\beta} \sum_{\mathbf{q},\mathbf{k}} \text{Im} \mathcal{D}_{\alpha\beta}^{ss'}(\mathbf{q}; \omega) \times \\ &\times \sum_{\substack{L_1L_2 \\ L_3L_4}} \text{Im} \left\{ \tau_{L_1L_2}^{ss'}(\mathbf{k}; \epsilon_F) \right\} \text{Im} \left\{ \tau_{L_3L_4}^{s's}(\mathbf{q} + \mathbf{k}; \epsilon_F) \right\} \times \\ &\times A_{L_1L_4}^s(\epsilon_F) A_{L_2L_3}^{s'}(\epsilon_F) \end{aligned} \quad (6.45)$$

From this formulation, the  $\mathbf{k}$ -dependent Eliashberg function follows straightforwardly as

$$\begin{aligned} \alpha_{\mathbf{k}}^2(\omega)F(\omega) &= \frac{1}{(2\pi)^3d(\epsilon_F)} \sum_{ss'} \sum_{\alpha\beta} \sum_{\mathbf{q}} \text{Im} \mathcal{D}_{\alpha\beta}^{ss'}(\mathbf{q}; \omega) \times \\ &\times \sum_{\substack{L_1L_2 \\ L_3L_4}} \text{Im} \left\{ \tau_{L_1L_2}^{ss'}(\mathbf{k}; \epsilon_F) \right\} \text{Im} \left\{ \tau_{L_3L_4}^{s's}(\mathbf{q} + \mathbf{k}; \epsilon_F) \right\} \times \\ &\times A_{L_1L_4}^s(\epsilon_F) A_{L_2L_3}^{s'}(\epsilon_F). \end{aligned} \quad (6.46)$$

The above formula can also be adapted for the description of Systems with reduced symmetry, such as surfaces. The latter are only periodic in directions parallel to the surface, such that a Fourier transform is only properly defined for these directions. An example for a possible surface structure is shown in Fig. 6.2, where every layer is identified by an index

$p$ . The two-dimensional lattice within each layer is spanned by primitive lattice vectors  $\mathbf{a}_1$  and  $\mathbf{a}_2$ . Every lattice point  $\mathbf{T}_h$  within a layer can be described by a linear combination of these two vectors. A summation over all possible lattice points, including all layers is thus rewritten as

$$\sum_l \mathbf{R}_l \longrightarrow \sum_p \sum_h (\mathbf{T}_h + \mathbf{N}_p) \quad (6.47)$$

Here,  $\mathbf{N}_p$  is a vector perpendicular to the surface whose length is defined as the distance of the  $p$ th layer from the top layer. In the case of complex materials, it is possible that a three-dimensional unit cell contains several layers. The 3D site vectors  $\tau_s$ , denoting the positions of ions within the cell, can be expressed as vectors  $\mathbf{t}_{\zeta(p)}$  parallel to the layers. Now  $\zeta$  is an index which denotes the ions within each layer  $p$ . Thus, a sum over the positions of all ions within the crystal is written as

$$\sum_l \sum_s (\mathbf{R}_l + \tau_s) \longrightarrow \sum_p \sum_h \sum_{\zeta(p)} (\mathbf{T}_h + \mathbf{t}_{\zeta} + \mathbf{N}_p). \quad (6.48)$$

Using this convention, an Eliashberg function for surfaces can be formulated. In order to

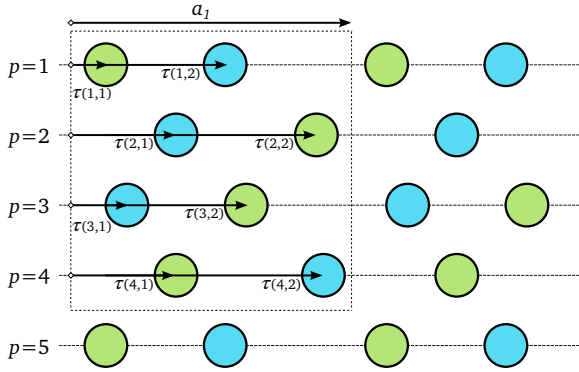


**Figure 6.2:** Notation scheme for sites in a layered system with two-dimensional periodicity. Index  $p$  denotes the layer and  $\tau$  indicates individual sites within the layers. In this illustration, the system is periodic from left to right, but aperiodic from top to bottom

define it analogously to the bulk case, one introduces a two-dimensional Fourier transform of the Green functions, which for phonons reads

$$\mathcal{D}_{\alpha\beta}^{p\zeta, q\eta}(\mathbf{q}_{\parallel}; \omega) = \frac{1}{\mathcal{N}^2} \sum_{hh'} D_{\alpha\beta}^{ls, l's'}(\omega) e^{-i\mathbf{q}_{\parallel} \cdot \mathbf{T}_{hh'}}. \quad (6.49)$$

Here, all 3D lattice indices on the right side are functions of the layer ( $l = l(p, m)$ ,  $l' = l'(q, n)$ ,  $s = s(p, \zeta)$  and  $s' = s'(q, \eta)$  and  $\mathcal{N}$  denotes the number of 2D lattice points.  $\mathbf{q}_{\parallel}$  is an arbitrary vector within the first two-dimensional Brillouin zone.

Then, the equation (6.40) can be rewritten as

$$\begin{aligned} \alpha^2(\omega)F(\omega) &= \frac{1}{(2\pi)^3 d(\epsilon_F)} \sum_{\zeta\eta} \sum_{\alpha\beta} \sum_{p,q} \sum_{\mathbf{q}_{\parallel}, \mathbf{k}_{\parallel}} \text{Im} D_{\alpha\beta}^{p\zeta, q\eta}(\mathbf{q}_{\parallel}; \omega) \times \\ &\times \sum_{\substack{L_1 L_2 \\ L_3 L_4}} \text{Im} \{ \tau_{L_1 L_2}^{p\zeta, q\eta}(\mathbf{k}_{\parallel}; \epsilon_F) \} \text{Im} \{ \tau_{L_3 L_4}^{q\eta, p\zeta}(\mathbf{q}_{\parallel} + \mathbf{k}_{\parallel}; \epsilon_F) \} \times \\ &\times A_{L_1 L_4}^{p\zeta}(\epsilon_F) A_{L_2 L_3}^{q\eta}(\epsilon_F). \end{aligned} \quad (6.50)$$

Again, for an atom in the layer  $p$  and position  $\zeta$  at the wave vector  $\mathbf{k}_{\parallel}$  the Eliashberg function

is given by

$$\begin{aligned}
\left\{ \alpha_{\mathbf{k}_{\parallel}}^2(\omega) F(\omega) \right\}_p^{\zeta} &= \frac{1}{(2\pi)^3 d(\epsilon_F)} \sum_{\eta} \sum_{\alpha\beta} \sum_q \sum_{\mathbf{q}_{\parallel}} \text{Im} D_{\alpha\beta}^{p\zeta, q\eta}(\mathbf{q}_{\parallel}; \omega) \times \\
&\times \sum_{\substack{L_1 L_2 \\ L_3 L_4}} \text{Im} \{ \tau_{L_1 L_2}^{p\zeta, q\eta}(\mathbf{k}_{\parallel}; \epsilon_F) \} \text{Im} \{ \tau_{L_3 L_4}^{q\eta, p\zeta}(\mathbf{q}_{\parallel} + \mathbf{k}_{\parallel}; \epsilon_F) \} \times \\
&\times A_{L_1 L_4}^{p\zeta}(\epsilon_F) A_{L_2 L_3}^{q\eta}(\epsilon_F).
\end{aligned} \tag{6.51}$$

The following section shows the application of this formalism to thin Pb films on Cu(111).

## 6.2 Application to Pb/Cu(111) islands

While the density of phonon modes is accessible via neutron scattering experiments, the Eliashberg spectral function  $\alpha^2 F(\omega)$  is not, since the electron-phonon coupling has no direct influence on the scattering behaviour of neutrons, which interact with atomic nuclei. The spectral function can be measured indirectly by tunneling measurements of the electronic density of states of a superconductor when using the inverse gap equations [MR65]. Since several superconducting gaps may exist, this procedure is prone to failure. A direct access to  $\alpha^2 F(\omega)$  can be achieved by inelastic tunnelling spectroscopy. This can be done by using a scanning tunneling microscope (STM), which additionally allows measurements with high spatial resolution [Bin+82]. In order to probe the electronic DOS of the sample, the tip-to-sample bias  $U$  is varied in a range of several eV while the tunnelling conductance,  $dI/dU$  is recorded. In Tersoff-Hamann theory of the STM [TH85], under the assumption that the DOS of the tip is constant, this value is directly proportional to the DOS at the sample as long as the bias is smaller than the work function of the surface [Wie94]. In this spectroscopy mode, only elastic tunnelling processes are of importance. Opposed to this, the measurement of phonon excitations requires the detection of inelastic tunnelling. Since these processes typically contribute by a few percent to the  $dI/dU$ -curve, a lock-in amplifier is used to record the second derivative  $d^2 I/dU^2$  of the tunnelling current. Small excitations due to electron-phonon interaction appear as peaks at the voltage corresponding to the phonon energy.

These kind of measurements have been realized for the first time by [Sch+15; Sch14] for Pb islands on a Cu(111) surface. Lead is a prototype for strong-coupling superconductors [Hei+10] with a bulk coupling constant of  $\lambda = 1.55$  [DK10; DS75]. However, the formation of the superconducting gap below  $T_C$  often causes quasiparticle peaks which dominate the  $d^2 I/dU^2$ -spectra. Therefore, Pb/Cu(111) is an ideal system to study electron-phonon effects because due to the proximity effect, Pb stays in the normal conducting phase.

It is well known that the vertical confinement of electronic degrees of freedom in thin Lead films causes the forming of quantum well states (QWS), which have a strong influence on the growth characteristics of such films under ultra-high vacuum conditions. At room temperature, the growth mode of Pb on Cu(111) is of Stranski-Krastanov type [Sch14], meaning that after a complete wetting layer has been deposited, islands start to grow. The thickness distribution of the latter is non-statistical: When QWS occur near the Fermi level, the redistribution of electronic states makes such layer numbers energetically unfavourable. The growing behaviour and its interference with QWS was studied in [OVM02]. This work and the corresponding experimental study [Sch14; Sch+15] aim to investigate the influence of the QWS on the electron-phonon coupling.

### 6.2.1 Quantum well states

Since the smallest wave lengths of Bloch electrons in metals (Fermi wavelength,  $\lambda_F = h/\sqrt{2m_e E_F}$ ) are of the same order of magnitude as the lattice constant, a confinement of the material to very thin films can lead to a discretisation of electronic states with wave vectors parallel to the film normal. The most simple model for the description of those states is one of the oldest in quantum mechanics, the particle in a box.

Instead of this potential well with infinite walls, a real system is bound by potential barriers of finite energy which allow for tunneling and result in slightly different energy levels compared to the box model.

In case of Pb on Cu(111) the depth of the potential well is given by the available electronic states at the metal-metal interface as well as the work function of the Pb surface ( $W = 4.25$  eV [Tha75]). Fig. 6.3 shows the electronic band structure of both metals in (111) direction. In Lead, an sp-type band crosses the Fermi level. Electrons from these states can only enter the Cu substrate if there are available states, which is not the case between -1 eV and 3.8 eV. This potential barrier of 4.8 eV is of roughly the same height as the work function at the Pb surface. Ignoring this finite potential barrier and applying the box model, the possible wave vectors due to the boundary condition of impenetrable potential walls are determined by the Pb film thickness  $L \cdot d_{ML}$  where  $L$  is the number of layers and  $d_{ML} = 2.86$  Å [Klu46] is the distance between neighbouring Pb(111) layers. The resulting wave numbers are

$$k_{ln} = \frac{n\pi}{Ld_{ML}}, \quad n \in \mathbb{Z} \quad (6.52)$$

with a main quantum number  $n$ . Assuming a quadratic dispersion of the quasi-free band in (111)-direction and  $k_F = 1.585$  Å<sup>-1</sup> [Sch14], the resulting energy levels read

$$E_{ln} = \frac{\hbar^2}{2m_e} (k_{ln}^2 - k_F^2). \quad (6.53)$$

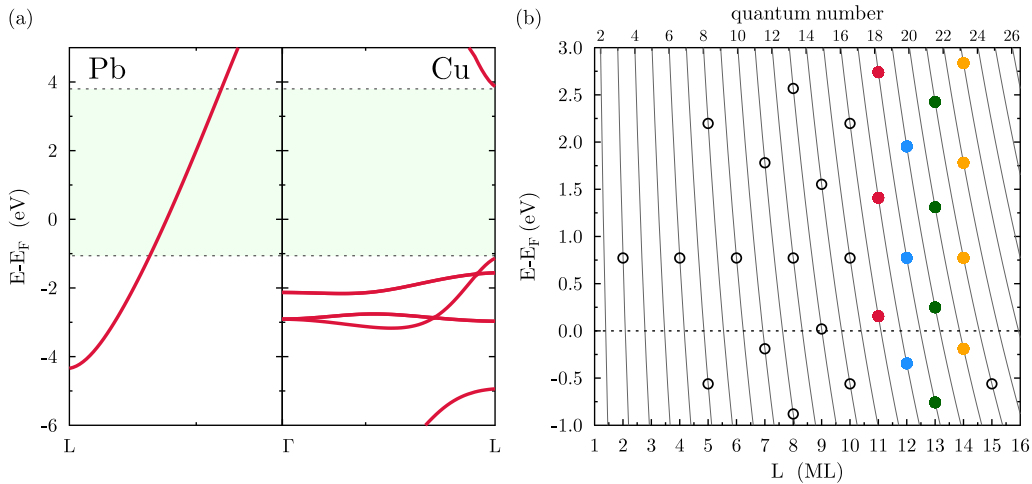


**Figure 6.3:** (a) Electronic states of bulk Pb and Cu in (111) direction. States from the s-like band in Pb cannot propagate into the band gap of Cu (shaded in green) and experience an effective potential barrier. (b) Energy of the QWS (grey lines) for different quantum numbers plotted with respect to the width of the potential well. Every curve corresponds to the quantum number where it intersects with the upper x-axis. Circles mark the energies where the width of the potential well is an integer multiple of the layer distance  $d_L$ . The colours of filled circles refer to the states emerging at the experimentally probed layer heights. Figures adapted from [OVM02].

Fig. 6.3 (b) shows all possible QWS for layers up to  $L = 16$  ML thickness and all quantum numbers within an energy range from -1 eV to +3 eV around the Fermi level. Grey lines show the energy-curves with respect to film thickness for all quantum numbers, whereas circles mark the energies occurring at integral layer numbers. The coloured points refer to the film thicknesses probed in the experiments.

Instead of this potential well with infinite walls, the real system is bound by potential barriers of finite energy which allow for tunneling and result in slightly different energy levels compared to the box model. However, it was shown that the particle-in-a-box model is very well applicable for Pb/Cu, at least in the energy range of 1 eV around the Fermi level [OVM02]. For instance, the QWS at  $E = 0.774$  eV, which is constant in energy for all even layer numbers, was found only 0.1 eV below [OVM02; Sch+15; Sch14].

## 6.2.2 Phonon dispersion/Bulk calculations

In order to calculate the Eliashberg function using the above presented formalism, the phonon Green function of Pb was needed on a dense mesh of  $k$ -points within the first Brillouin zone. Since at that time it was not possible to calculate the phonon dispersion within the KKR scheme, the direct method by Kresse et al. [KFH95] (see p. 17) was used. The force matrix (Eq. (2.45)) has been generated using the pseudopotential Code VASP (Vienna Ab initio Simulation Package [KH93; KH94; KF96a; KF96b]) in the following way: Due to the long-range interactions in Pb, a supercell of  $7 \times 7 \times 7$  bulk unit cells of fcc Pb ( $a = 4.9508$  Å) was constructed, in which one atom has been displaced from its equilibrium position in direction of its next neighbour by  $\approx 0.05$  Å. Then a self-consistent total-energy calculation has been performed using PAW (Projector-Augmented Wave method [Blö94; KJ99; Höl10]) pseudopotentials for the description of the ion potentials and the LDA [PZ81] as approximation of the exchange-correlation potential. The semicore d-states were treated as valence electrons. Due to the size of the supercell, the  $k$ -point mesh for the Brillouin-zone integration consisted only of  $4 \times 4 \times 4$  Monkhorst-Pack special points [MP76]. This is possible because of the small Brillouin Zone and preferable considering the computational resources needed for an accurate calculation with 343 atoms. After convergence of the self-consistent cycle, the forces exerted by the displaced atom on all other atoms within the supercell have been calculated via the Hellmann-Feynman theorem. The convergence of this force matrix was tested with respect to the maximum energy of the plane waves used to describe the wave functions. It was found that  $E_{\max} = 250$  eV was sufficient to provide a well-converged set of force constants for further processing into a dynamical matrix (see p. 17). This step was done using the open source PHON-code [Alf09], which provides the required symmetry operations and Fourier transformations.

Fig. 6.4 shows the resulting phonon dispersion on selected high-symmetry lines of the fcc Brillouin zone. Red lines represent the calculated modes and black dots plot experimental frequencies from [Ste+67]. In contrast to other elemental superconductors, DFT calculations for Pb often failed to reproduce the strong coupling due to the prominent anomalies in its phonon dispersion. In the present case, the theoretical curves resemble the main features which are typical for Pb, such as the local minima (a) of both longitudinal and transverse modes at X as well as the shoulder (b) of the longitudinal mode between  $\Gamma$  and X. Both are Kohn anomalies [Koh59; Dal08] and reflect the strong electron-phonon interaction at the Fermi surface. At the same time, the Kohn anomalies near L are not reproduced by the calculation, the frequencies of the transverse branches near the zone boundary are too high and the longitudinal modes tend to lower frequencies than experimentally measured. This behaviour is due to several reasons: The correct reproduction of Kohn anomalies is only possible when the Fermi surface is sampled with high resolution, with a dense  $k$ -mesh and a carefully chosen smearing parameter [Dal08]. Since they are

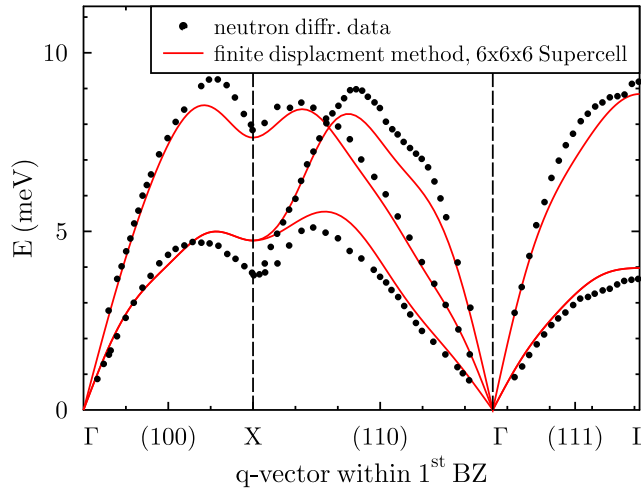


**Figure 6.4:** Phonon frequencies ( $E = \hbar\omega$ ) of Pb on high-symmetry lines of the fcc Brillouin zone. Circles denote experimental data from [Ste+67], measured via neutron scattering at 80 K. The lines show the results of the present supercell calculation.

so prominent in Pb, this element needs more  $k$ -points than most other metals to calculate accurate phonon frequencies. Due to the high atomic number of Pb, the general agreement between theory and experiment can be improved by including spin-orbit coupling [Hei+10; Ver+08; Dal08] using semi- or fully relativistic approaches.

The influence of SOC on the electron-phonon coupling strength was studied by Chulkov [Hei+10]. Neglecting the influence of SOC on the electronic density of states at the Fermi surface and the electron-phonon matrix elements, they found an increase of  $\lambda$  by 25% alone due to the renormalization of the phonon dispersion due to the inclusion of SOC, compared to a non-relativistic calculation. One has to note that their phonon frequencies without SOC are appr. 8–15% higher than the experimental values and including SOC caused a softening such that the renormalized frequencies agreed well with experiment. In our case, high-frequency-modes are too low (mainly longitudinal), whereas the lower-lying transverse modes are mostly too high. Thus, an inclusion of SOC would probably lead to a cancellation of errors and would have a smaller impact on the coupling strength.

Fig. 6.5 shows the phonon density of states (PDOS) as well as  $\alpha^2 F(\omega)$  of bulk Pb. The black line represents the PDOS calculated from the theoretical phonon dispersion by making use of the tetrahedron integration method [JA71; LT72]. The green line shows the

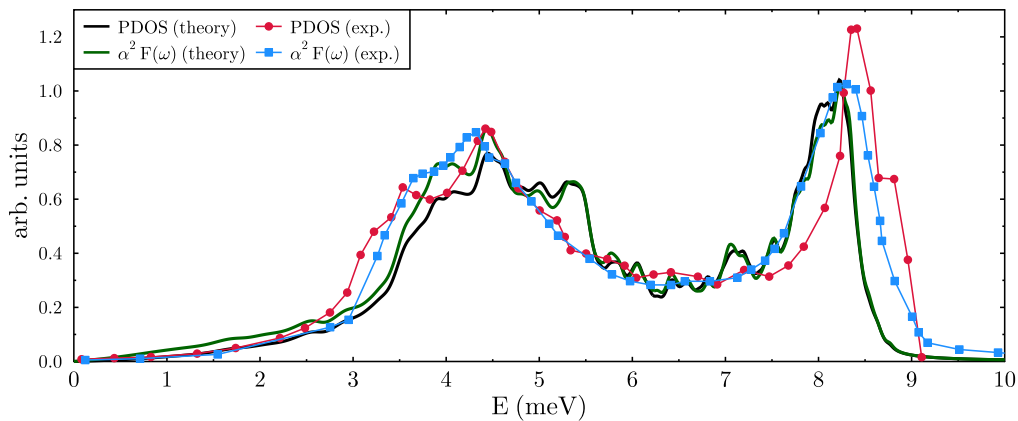


**Figure 6.5:** Phonon density of states and Eliashberg function of bulk Pb from theory and experiment. The measured PDOS is taken from neutron scattering data [SAN67], whereas  $\alpha^2 F(\omega)$  is obtained from tunneling measurements [DK10]. The curves are normalized for the sake of better comparability.

integrated Eliashberg function, computed via Eq. (6.45) from the phonon Green function as well as electronic Green function and electron-phonon matrix elements from self-consistent KKR calculations, and is basically a slightly renormalized version of the PDOS.

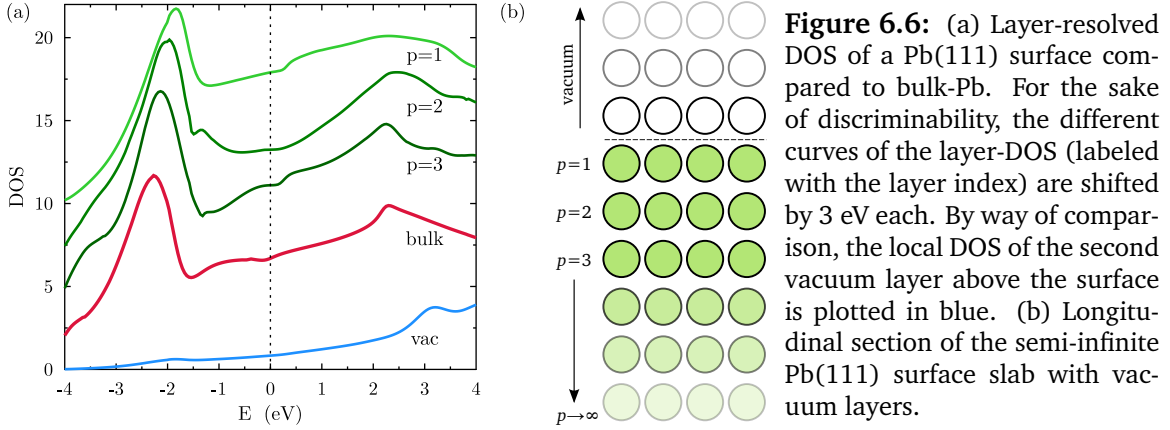
In contrast, the experimental PDOS is shown as red circles (data taken from neutron scattering experiments [SAN67], lines are guide to the eye) and the Eliashberg function measured via tunneling currents [DK10] is plotted as blue squares. The overall agreement between theory and experiment is good. The maximum of the lower transverse modes is shifted to higher frequencies and broadened, compared to the experimental data and the second peak, which is mainly due to the high-frequency longitudinal modes, is shifted to lower frequencies. This corresponds to the differences in experimental and calculated phonon dispersions. The deviations lead to a reduced contribution of the transverse modes to the overall coupling strength and an increased contribution of the longitudinal modes. The resulting coupling strength for bulk Pb is  $\lambda = 1.08$ , whereas the experimental result is  $\lambda = 1.55$  [DR75]. The large difference can not only be explained by the differences in the phonon dispersions, but also originates in the neglect of SOC in the electron-phonon matrix elements due to the differences in the electronic band structure and Fermi surface caused by SOC. Another important influence is given by the RMTA used here, which does not allow the redistribution of the electron gas due to moving atoms, but rather restricts its changes to a rigid shift of the electronic wave functions within the MT sphere of the atom. Still, this work aims to emphasize the effects of quantum well states on the electron-phonon coupling instead of reproducing the exact experimental value.

### 6.2.3 Surface and film calculations

To investigate whether pure surface states have an influence on the electronic DOS near the Fermi level, a calculation for a Pb(111) surface with a semi-infinite slab construction was set up first. For this purpose, a KKR formalism specially designed for surfaces and interfaces was used, which is able to efficiently treat two-dimensional periodic and semi-infinite surface structures by means of a screening transformation [Szu+94; Ern07; Lüd+01]. The unit cell for this calculation is a slab of 23 monolayers of Pb(111) and 4 layers of empty spheres on top, as sketched in Fig. 6.6 (b). For the calculation of the structure constants, the bottom of the slab is terminated with a Pb substrate with bulk  $\hat{T}$ -matrix to simulate the scattering behaviour of a real semi-infinite surface. In the same sense, the top side is terminated by a semiinfinite vacuum matrix. This kind of calculation can only be done properly with two-dimensional periodicity. 3d-calculations work with alternating slabs of vacuum and substrate, both of finite thickness. In this case, the potential within the vacuum region is treated wrongly and effects the correct representation of surface states. In the same way, artificial states due to the vertical confinement of the material may occur.

Fig. 6.6 (a) shows the resulting local DOS of the three layers closest to the surface (green) as well as the second vacuum layer (blue) which is the region in which the real system is probed by the STM tip. In comparison, the red curve shows the Pb-bulk DOS. As expected, the LDOS converges to the bulk run with increasing layer index. The vacuum curve is naturally of lower amplitude and shows less features since only weakly localized states propagate into the vacuum. All spectra have in common that there are no prominent features close to the Fermi level.

DFT-calculations of Pb(111) on Cu are a difficult task due to the incommensurable lattices of the metals ( $a_{\text{Cu}} = 3.61\text{\AA}$ ,  $a_{\text{Pb}} = 4.95\text{\AA}$ ). To maintain the two-dimensional periodicity, a very large supercell of  $8 \times 8$  Pb unit cells (and  $11 \times 11$  Cu unit cells) parallel to the surface and a reasonable number of layers would be necessary, and even in this case the lattices would be subject to strain. Hence, it was decided to simulate the Pb islands as freestanding



layers with two-dimensional periodicity and semi-infinite vacuum parts above and below the Pb slabs.

The calculations have been performed for island thicknesses of  $L = 11 \dots 14$  ML since these showed the strongest enhancement of electron-phonon coupling in the experiments. The results are condensed in Fig. 6.7: Panel (a) shows  $dI/dU$  tunneling spectra for different numbers of Pb layers. These measurements have been performed with tip-to-surface separations of a few  $d_{\text{ML}}$  and can, if no significant scattering processes occur, be interpreted as mapping of the local electronic DOS above the Pb surface [TH85].

In contrast, panel (b) shows the calculated local electronic DOS of the second vacuum layer above the Pb slab. The qualitative agreement with the measurements is remarkably good. The four main peaks above the Fermi level are comparable in both datasets and can be identified as quantum well states  $P_1 \dots P_4$  in Fig. 6.3 (b). Both experimental and theoretical peak positions differ slightly from the predictions of the particle-in-a-box model, since the potential well is not infinitely deep. The differences between DFT and experiment are most likely due to the effective potential wall positions: The calculation did not consider that the layer distances near the surface differ from their respective bulk values due to surface relaxations. Additionally, the description of the charge density above the surface is not accurate within the framework of LDA, which is designed for the description of slowly varying densities and tends to underestimate the drop of the charge density with increasing distance from the surface. Both effects may have an influence on the width of the appro-

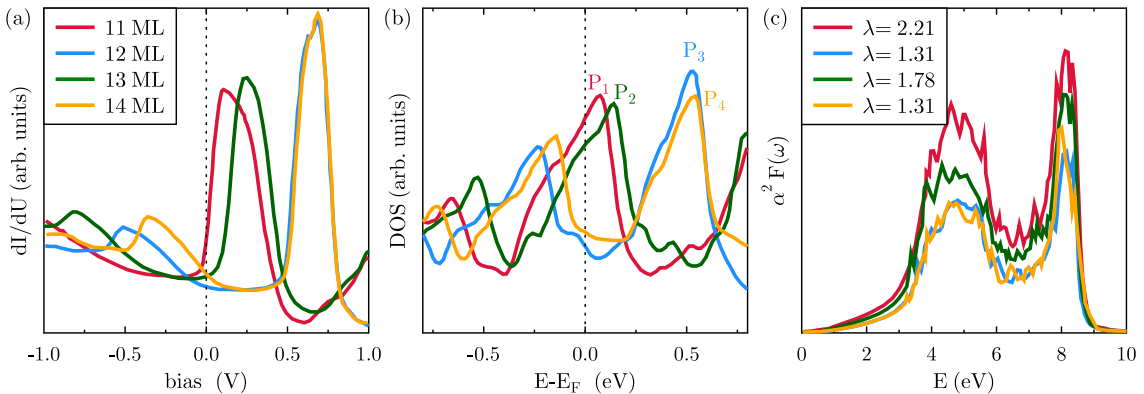


**Figure 6.7:** Measured and theoretical QWS for different layer numbers of Pb. (a)  $dI/dU$ -spectra of the tunneling current for Pb islands of 11 to 14 ML thickness. (b) Local DOS of the second vacuum layer near the Fermi energy, calculated for the same layer numbers. (c) Calculated Eliashberg functions as well as coupling parameters for the same systems.

priate model potential well in an order of magnitude of 1%, which is enough to cause a substantial shift of the QWS. However, the qualitative agreement with experiment is quite well and also the QWS below  $\epsilon_F$  fit in this scheme.

Fig. 6.3 (c) shows the calculated Eliashberg functions of the layer system together with the resulting coupling parameters. These spectral functions have been obtained by making use of the Fourier transform 6.49 and the layer-sum 6.50. In agreement with the experimental findings, the spectral functions and the resulting coupling parameters are scaled in proportion with the peak height at the Fermi level. Whereas  $\lambda$  is increased by 21% for  $L = 12$  ML and  $L = 14$  ML compared to the bulk value of  $\lambda = 1.08$ , a layer thickness of  $L = 13$  ML leads to an increase of 65% and for the case of  $L = 11$  ML a more than doubled coupling strength is observed.

The qualitative agreement between experiment and theory shows that the spectra shown in Fig. 6.3 (a) can indeed be interpreted as mappings of the electronic DOS. This proportionality of  $\lambda$  and  $d(E_F)$  was also predicted by [Bru+09] and shows that the enhancement of the coupling in thin Pb layers is a purely electronic effect, since in all cases the Fourier-transformed phonon green function of bulk Pb was used. This result was also supported experimentally:  $d^2I/dU^2$ -spectra which measured  $\alpha^2F(\omega)$  showed the same peak positions and thus the same van-Hoove singularities in the phonon spectrum for all layer thicknesses [Sch14].

The observed enhancement of the electron-phonon coupling strikingly shows the close connection between the coupling parameter  $\lambda$ , the DOS at Fermi level and the effective mass of the electrons involved in the interaction (Eq. (6.2)). A QWS is strongly located and thus has a flat dispersion, giving rise to a peak in the DOS. The curvature of such a flat band is smaller than the curvature of the nearly-free-electron-like sp band in Pb, giving rise to a higher effective mass. If a QWS is located close to the Fermi level, due to Eq. (6.16) this results in an increased DOS at  $\epsilon_F$  and an increased electron-phonon coupling. The experimentally measured enhancement of  $\lambda$  was 2–3 times higher than predicted by the calculations. The  $dI/dU$ -spectra show QWS of lower width than the theoretical DOS. This leads to higher effective masses and higher electron-phonon coupling.

## 6.2.4 Summary and Outlook

It was shown that the Tersoff-Hamann interpretation of the  $dI/dU$ -spectra as well as the ab-initio calculations lead to commensurable results and that the local density of states near the Fermi energy is dominated by quantum well states originating from the spatial confinement of sp-like electrons in thin Pb films. The enhancement of the electron-phonon coupling due to the QWS measured by  $d^2I/dU^2$  spectroscopy was confirmed theoretically and could be ascribed to changes of the electronic states as a consequence of the appearance of QWS.

The applied method was well suited for the analysis of the experimental data and to reproduce the relative changes of the coupling parameter  $\lambda$ . Still, the used Rigid-Muffin-Tin approximation offers only a simplified solution of the electron-phonon problem since the change of the charge density induced by the shift of an atom is not self-consistently calculated. Therefore, in many cases and also here, it delivers values for  $\lambda$  which are too small. Among many improved methods (see e.g. [Win81] for a short review), the linear response method of Winter [Win81] appears to be best-suited to be made use of in the formalism presented above, because it uses a similar approach as described in Chap. 5



## Conclusion

The main goal of the work at hand was to improve the description of lattice vibrations in the context of Korringa-Kohn-Rostoker (KKR) multiple scattering theory. At this, priority was given to the development of a linear response theory for the parameter-free prediction of phonon spectra of crystals, where the focus was on metals. Furthermore, the numerical description of electron-phonon interactions was a substantial part of this work.

In order to point towards general concepts and problems associated with the numerical treatment of lattice vibrations, Chap. 5.17 introduced the harmonic approximation as well as established techniques for ab-initio calculations of force constants. Chap. 3 aimed to introduce the reader to the basics of both linear response theory and as density functional theory whereof the latter is the foundational principle of the ab-initio calculations discussed in this thesis. Moreover, with time-dependent density functional theory a method was presented which elegantly allows to combine both concepts. With multiple scattering theory, Chap. 4 detailed a numerical principle which is, despite its age, a powerful implementation of density functional theory and is renowned for allowing accurate total energy and band structure calculations. At this, the formulation of the KKR method as a Green-function approach was stressed, having established it as an efficient and versatile tool.

After these foundational parts, Chap. 5 first elaborated on recent developments in the description of lattice dynamics based on KKR. So far, those have been limited to the direct method, computing real space force constants via supercell calculations, and the required numerical effort is high due to the large number of atoms within the unit cell or cluster and because of the necessary full-potential (FP) treatment of the scattering sites. To begin with, a rigid-ion model of lattice dynamics was derived which is suitable for the use with the KKR. This led to a formulation of the dynamical matrix based on the Hellmann-Feynman theorem. The most interesting input quantity for these equations is the differential variation of the charge density upon an oscillatory distortion of the crystal lattice. In order to compute this function  $\mathcal{K}(\mathbf{q})$  self-consistently, a linear response approach was developed, starting from the KKR Green function of the electronic ground state of the system under concern. Afterwards, details of the implementation of the algorithm into the KKR code HUTSEPOT applying the atomic sphere approximation were presented. The test calculations revealed a good convergence behaviour of  $\mathcal{K}$  with respect to numerical parameters. Nevertheless, the charge density variations differed quantitatively from expected results, strongly influencing the predicted phonon dispersions.

The last chapter, however, dealt with low-temperature superconductivity and the underlying electron-phonon interaction. The purpose of this part of the work was the implementation of the rigid muffin tin approximation to the Eliashberg spectral function for low-dimensional systems and for use in the HUTSEPOT code. After a detailed derivation of the formalism, the latter was applied to the interpretation of elastic and inelastic tunnelling measurements of Pb islands on a Cu(111) surface. It was possible to show how the emergence of quantum well states can influence the strength of electron-phonon coupling and thus  $T_C$  due to changes of the electronic density of states at the Fermi level.

Summarising, it was possible to show that the method developed in Chap. 5 delivers promising results, the quality of which was limited by restrictions of the atomic sphere approximation. The latter uses a spherically symmetric representation of the charge density as well as the ionic potential, giving rise to large errors in the Hellmann-Feynman forces. A substantial improvement requires the application of a full potential or full charge density

approximation. Fortunately, the formalism is designed such that it can be adjusted to support these varieties of KKR. This extension of the code is planned for the near future and is expected to allow a linear-response treatment of lattice dynamics with KKR. Although there are numerically less expensive techniques for the computation of lattice-dynamical properties, such as pseudopotential methods, advantages of a treatment within KKR lie in the high precision of this all-electron method as well as the ability to deal with disordered and low-dimensional systems.

The rigid muffin tin approximation used in Chap. 6 for the description of electron-phonon interactions was able to explain the relative heights of  $\alpha^2 F(\omega)$  due to varying density of states at the Fermi energy, but has its weaknesses when it comes to the prediction of absolute values of  $\lambda$  and  $T_C$ , depending on the element. This is caused by the simplified description of the change of the valence charge density induced by the displacement of ions due to lattice waves. This aspect can be greatly improved by implementing the methods developed in Chap. 5, allowing for a self-consistent calculation of electron-phonon matrix elements with linear response theory. This approach is planned to be advanced in the future to enhance the versatility of HUTSEPOT in respect of the description of superconductors.

## Coulomb potential

### A.1 Ewald summation technique

An important problem in solid state physics is the evaluation of sums over charges in an infinite crystal lattice. The prototypical lattice sum appears in the expression for the total electrostatic energy of a lattice of point charges

$$\mathcal{U} = \frac{1}{2} \sum_s \sum_{s'} \sum_l \frac{Z_s Z_{s'}}{|\boldsymbol{\tau}_s - \boldsymbol{\tau}_{s'} + \mathbf{R}_l|}, \quad (\text{A.1})$$

where  $s$  and  $s'$  denote sites within a unit cell and  $l$  indicates the position of the unit cell with respect to the point of origin. Because of the long-ranging coulomb interaction the evaluation of this sum is tricky: It is conditionally convergent, meaning that the value of its partial sums strongly depends on the order of summation. An elegant solution to this problem was pointed out by P. P. Ewald [Ewa21]. Without going into details of its derivation, Ewald, in principle, used a replacement of the kind

$$\frac{1}{r} = \frac{f(r)}{r} + \frac{1 - f(r)}{r}, \quad (\text{A.2})$$

where  $f(r) = \text{erfc}(\alpha r)$ , to split the sum into two rapidly converging sums over real and reciprocal lattice vectors, resulting in

$$\mathcal{U} = \mathcal{U}_r + \mathcal{U}_k + \mathcal{U}_{\text{self}} + \mathcal{U}_{\text{dipol}}. \quad (\text{A.3})$$

The real space term reads

$$\mathcal{U}_r = \frac{1}{2} \sum_{ss'} \sum_l Z_s Z_{s'} \frac{\text{erfc}(\alpha |\boldsymbol{\tau}_s - \boldsymbol{\tau}_{s'} + \mathbf{R}_l|)}{|\boldsymbol{\tau}_s - \boldsymbol{\tau}_{s'} + \mathbf{R}_l|}, \quad (\text{A.4})$$

in which the self-interaction term with  $\boldsymbol{\tau}_s - \boldsymbol{\tau}_{s'} + \mathbf{R}_l = 0$  is omitted. Opposed to this, the reciprocal contribution is given by

$$\mathcal{U}_k = \frac{2\pi}{\Omega_{\text{WS}}} \sum_n \frac{e^{-\mathbf{G}_n^2/4\alpha^2}}{\mathbf{G}_n^2} \sum_{ss'} Z_s Z_{s'} e^{-i\mathbf{G}_n \cdot (\boldsymbol{\tau}_s - \boldsymbol{\tau}_{s'})}. \quad (\text{A.5})$$

Since the self-interaction was omitted in the real space term, it is taken account of via the remaining two terms,

$$\begin{aligned} \mathcal{U}_{\text{self}} &= -\frac{\alpha}{\sqrt{\pi}} \sum_s Z_s^2 \\ \mathcal{U}_{\text{dipol}} &= \frac{2\pi}{3\Omega_{\text{WS}}} \left( \sum_s Z_s \boldsymbol{\tau}_s \right)^2. \end{aligned}$$

This expression is independent of the Ewald parameter  $\alpha$ , the value of which should be chosen such that real and reciprocal sum converge most rapidly. The Ewald method can

also be used to calculate the potential at a point  $\mathbf{r}$  within a crystal of point ions which, omitting the constant self-energy contribution, results in

$$\begin{aligned} V^{\text{ext}}(\mathbf{r}) &= \sum_s \sum_l \frac{Z_s}{|\mathbf{R}_l + \boldsymbol{\tau}_s - \mathbf{r}|} \\ &= \sum_s \sum_l Z_s \frac{\text{erfc}(\alpha |\mathbf{R}_l + \boldsymbol{\tau}_s - \mathbf{r}|)}{|\mathbf{R}_l + \boldsymbol{\tau}_s - \mathbf{r}|} + \frac{4\pi}{\Omega_{\text{BZ}}} \sum_n \frac{e^{-\mathbf{G}_n^2/4\alpha^2}}{\mathbf{G}_n^2} \sum_s Z_s e^{i\mathbf{G}_n \cdot (\mathbf{r} - \boldsymbol{\tau}_s)}. \end{aligned} \quad (\text{A.6})$$

## A.2 Fourier transform of the Coulomb potential

An important part of the susceptibility Dyson equation is the Bloch-Fourier transform of the Coulomb denominator, for which an angular momentum representation is needed. In atomic rydberg units, the Coulomb potential is given as

$$V(\mathbf{x}, \mathbf{x}') = \frac{2}{|\mathbf{x} - \mathbf{x}'|} = V_{nn'}^{ss'}(\mathbf{r}, \mathbf{r}') = \frac{2}{|\mathbf{r} + \boldsymbol{\tau}_s + \mathbf{R}_n - \mathbf{r}' - \boldsymbol{\tau}_{s'} - \mathbf{R}_{n'}|} \quad (\text{A.7})$$

and its Fourier representation is defined as

$$V^{ss'}(\mathbf{r}, \mathbf{r}', \mathbf{q}) = 2 \sum_n \frac{e^{i\mathbf{q} \cdot \mathbf{R}_n}}{|\mathbf{r} + \boldsymbol{\tau}_s + \mathbf{R}_n - \mathbf{r}' - \boldsymbol{\tau}_{s'}|}. \quad (\text{A.8})$$

Using the same procedure which leads to Eq. (A.6), this potential can be expressed as the Ewald sum [Zim92]

$$\begin{aligned} V^{ss'}(\mathbf{r}, \mathbf{r}', \mathbf{q}) &= 2 \sum_{\mathbf{R}} \frac{\text{erfc}(\eta |\mathbf{r} - \mathbf{r}' + \boldsymbol{\tau}_s - \boldsymbol{\tau}_{s'} - \mathbf{R}|)}{|\mathbf{r} - \mathbf{r}' + \boldsymbol{\tau}_s - \boldsymbol{\tau}_{s'} - \mathbf{R}|} e^{i\mathbf{q} \cdot \mathbf{R}} \\ &\quad + \frac{8\pi}{\Omega_{\text{UC}}} \sum_{\mathbf{G}} \frac{e^{|\mathbf{G} + \mathbf{q}|/4\eta^2}}{|\mathbf{G} + \mathbf{q}|^2} e^{i(\mathbf{G} + \mathbf{q}) \cdot (\mathbf{r} - \mathbf{r}' + \boldsymbol{\tau}_s - \boldsymbol{\tau}_{s'})}. \end{aligned} \quad (\text{A.9})$$

Nevertheless, a numerical quadrature of this expression in order to obtain coefficients for an expansion in terms of spherical harmonics is computationally very demanding. An alternative approach can be constructed [Buc12b] starting from the Green function of free space, which is given by

$$\mathcal{G}_f(\mathbf{x}, \mathbf{x}', E) = -\frac{1}{4\pi} \frac{e^{ik|\mathbf{x} - \mathbf{x}'|}}{|\mathbf{x} - \mathbf{x}'|}, \quad k = \sqrt{E} \quad (\text{A.10})$$

and is related to the Coulomb potential via

$$V(\mathbf{x}, \mathbf{x}') = -8\pi \lim_{E \rightarrow 0} \mathcal{G}_f(\mathbf{x}', \mathbf{x}', E). \quad (\text{A.11})$$

The angular momentum representation of the free particle propagator in real space can be written as

$$\begin{aligned} \mathcal{G}_{f,nn'}^{ss'}(\mathbf{r}, \mathbf{r}', E) &= -\delta_{nn'} \delta_{ss'} i k \sum_L Y_L(\hat{\mathbf{r}}_{ns}) j_\ell(kr_{ns<}) h_\ell(kr_{ns>}) Y_L(\hat{\mathbf{r}}'_{ns}) \\ &\quad + (1 - \delta_{nn'} \delta_{ss'}) \sum_{LL'} Y_L(\hat{\mathbf{r}}_{ns}) j_\ell(kr_{ns}) g_{f,LL'}^{ss'}(E) j_{\ell'}(kr'_{n's'}) Y_{L'}(\hat{\mathbf{r}}'_{n's'}) \end{aligned} \quad (\text{A.12})$$

where  $s$  and  $s'$  are basis site indices and the factor  $(1 - \delta_{nn'} \delta_{ss'})$  has been taken out of the structure constants, compared to Eq. (4.45) and the definition  $\mathbf{r}_{ns} = \mathbf{x} - \mathbf{R}_n - \boldsymbol{\tau}_s$  was used.

The spherical Hankel functions are defined as  $h_\ell(x) = j_\ell(x) + in_\ell(x)$ . In the limit of small arguments, the spherical Bessel and Neumann functions are given by

$$j_\ell(x) \approx \sqrt{\frac{\pi}{2x}} \left(\frac{x}{2}\right)^{\ell+\frac{1}{2}} \frac{1}{\Gamma(\ell + \frac{3}{2})} \quad (\text{A.13})$$

$$n_\ell(x) \approx \sqrt{\frac{1}{2\pi x}} \left(\frac{2}{x}\right)^{\ell+\frac{1}{2}} \Gamma\left(\ell + \frac{1}{2}\right), \quad (\text{A.14})$$

using the Euler gamma function  $\Gamma$ . Using the Legendre duplication formula [Leg09]

$$\Gamma\left(\ell + \frac{1}{2}\right) = 2^{1-2\ell} \sqrt{\pi} \frac{\Gamma(2\ell)}{\Gamma(\ell)}, \quad (\text{A.15})$$

the single-site part of the Green function in the zero energy limit reads

$$- \delta_{nn'} \delta_{ss'} i \sum_L \frac{r_{ns}^\ell}{r_{ns}^{\ell+1}} \frac{1}{2\ell+1} Y_L(\hat{\mathbf{r}}_{ns}) Y_L(\hat{\mathbf{r}}'_{ns}). \quad (\text{A.16})$$

In the same limit, the product of two spherical Bessel functions appearing in the multiple scattering part of Eq. (A.12) can be expressed as

$$\frac{(r)^\ell (r')^{\ell'}}{\tilde{\Gamma}(\ell+1) \tilde{\Gamma}(\ell'+1)} k^{\ell+\ell'} \quad (\text{A.17})$$

where the modified Euler function reads

$$\tilde{\Gamma}(\ell) = \frac{2^\ell}{\sqrt{\pi}} \Gamma\left(\ell + \frac{1}{2}\right) = 2^{1-2\ell} \frac{(2\ell-1)!}{(\ell-1)!}. \quad (\text{A.18})$$

The structure constants of free space are given as

$$g_{LL',nn'}^{ss'}(E) = -4\pi i \sum_{L''} i^{-\ell+\ell'-\ell''} h_{\ell''}(\sqrt{z} |\mathbf{R}_{nn'} + \boldsymbol{\tau}_s - \boldsymbol{\tau}_{s'}|) Y_{L''}(\widehat{\mathbf{R}_{nn'} + \boldsymbol{\tau}_s - \boldsymbol{\tau}_{s'}}) C_{LL'}^{L''} \quad (\text{A.19})$$

and in the limit of vanishing energy one has

$$h_\ell(kr) = -i \tilde{\Gamma}(\ell) (kr)^{-\ell-1}. \quad (\text{A.20})$$

The selection rule of the Gaunt coefficients  $\ell'' \leq \ell + \ell'$  causes a cancellation of the above divergence for  $k \rightarrow 0$  in the multiple scattering part of the green function. Furthermore, only terms with  $\ell'' = \ell + \ell'$  survive the limit. As a consequence, the structure constants can be simplified to

$$g_{LL'}(\mathbf{R}^{ss'}, E) = -4\pi k^{\ell''} \tilde{\Gamma}(\ell'') i^{-\ell+\ell'-\ell''} \sum_{m''=-\ell''}^{\ell''} \frac{Y_{L''}(\hat{\mathbf{R}}^{ss'})}{|\mathbf{R}^{ss'}|^{\ell''+1}} C_{LL'}^{L''}, \quad \ell'' = \ell + \ell', \quad (\text{A.21})$$

where  $\mathbf{R}$  is an arbitrary lattice vector, replacing the former  $\mathbf{R}_{nn'} = \mathbf{R}_n - \mathbf{R}_{n'}$ , and  $\mathbf{R}^{ss'} = \mathbf{R} + \boldsymbol{\tau}_s - \boldsymbol{\tau}_{s'}$  was defined. To construct the lattice Fourier transform of the Coulomb potential, Eq. (A.8), only the part of the Green function which depends on a lattice vector enters the lattice sum. Thus, the Fourier-transformed structure constants read

$$g_{LL'}^{ss'}(\mathbf{q}, E) = -4\pi k^{\ell''} \tilde{\Gamma}(\ell'') i^{-\ell+\ell'-\ell''} \sum_{m''=-\ell''}^{\ell''} D_{LL'}^{ss'}(\mathbf{q}) C_{LL'}^{L''}, \quad \ell'' = \ell + \ell', \quad (\text{A.22})$$

using

$$D_{L'L''}^{ss'}(\mathbf{q}) = \sum_{\mathbf{R}, \mathbf{R}^{ss'} \neq 0} \frac{Y_{L''}(\hat{\mathbf{R}}^{ss'})}{|\mathbf{R}^{ss'}|^{\ell''+1}} e^{i\mathbf{q}\cdot\mathbf{R}}. \quad (\text{A.23})$$

Using the following definition, in which the diverging powers of  $k$  are omitted,

$$A_{LL'}^{ss'}(\mathbf{q}) = -4\pi\tilde{\Gamma}(\ell'')i^{-\ell+\ell'-\ell''} \sum_{m''=-\ell''}^{\ell''} D_{L'L''}^{ss'}(\mathbf{q})C_{LL'}^{L''}, \quad \ell'' = \ell + \ell', \quad (\text{A.24})$$

the Fourier transform of the Coulomb potential can be constructed via the following set of equations:

$$V^{ss'}(\mathbf{r}, \mathbf{r}', \mathbf{q}) = \sum_{LL'} Y_L(\hat{\mathbf{r}})V_{LL'}^{ss'}(r, r', \mathbf{q})Y_{L'}(\hat{\mathbf{r}}') \quad (\text{A.25})$$

$$V_{LL'}^{ss'}(r, r', \mathbf{q}) = 8\pi \left( \delta_{ss'}\delta_{LL'} \frac{-1}{2\ell+1} \frac{r_{<}^{\ell}}{r_{>}^{\ell+1}} - A_{LL'}^{ss'}(\mathbf{q}) \frac{(r)^{\ell}(r')^{\ell'}}{\tilde{\Gamma}(\ell+1)\tilde{\Gamma}(\ell'+1)} k^{\ell+\ell'} \right). \quad (\text{A.26})$$

### A.3 Derivatives

Several expressions in this work contain derivatives of the Fourier-transformed lattice potential, such as the dynamical Matrix Eq. (5.21). As already mentioned above, the Fourier transform can be obtained in the same way as Eq. (A.6), giving

$$\begin{aligned} \mathring{V}_{0l}^{ss'}(0, \mathbf{r}, \mathbf{q}) &= \sum_l \frac{e^{i\mathbf{q}\cdot\mathbf{R}_l}}{|\mathbf{R}_l + \boldsymbol{\tau}_{s'} - \boldsymbol{\tau}_s + \mathbf{r}|} \\ &= \sum_l e^{i\mathbf{q}\cdot\mathbf{R}_l} \frac{\text{erfc}(\eta|\mathbf{R}_l + \boldsymbol{\tau}_{s'} - \boldsymbol{\tau}_s + \mathbf{r}|)}{|\mathbf{R}_l + \boldsymbol{\tau}_{s'} - \boldsymbol{\tau}_s + \mathbf{r}|} \\ &\quad + \frac{4\pi}{\Omega_{\text{BZ}}} \sum_n \frac{e^{-(\mathbf{G}_n + \mathbf{q})^2/4\eta^2}}{|\mathbf{G}_n + \mathbf{q}|^2} e^{i(\mathbf{G}_n + \mathbf{q})\cdot(\boldsymbol{\tau}_s - \boldsymbol{\tau}_{s'} - \mathbf{r})}. \end{aligned} \quad (\text{A.27})$$

Due to the uniform convergence of the Ewald series [Cam63], the derivative with respect to the  $\alpha$ th component of the local spatial coordinate  $\mathbf{r}$ ,

$$\mathcal{C}_{\alpha}^{ss'}(\mathbf{r}, \mathbf{q}) = \frac{\partial}{\partial r_{\alpha}} \mathring{V}_{0l}^{ss'}(0, \mathbf{r}, \mathbf{q}) \quad (\text{A.28})$$

can now directly be calculated and leads to the result

$$\begin{aligned} \mathcal{C}_{\alpha}^{ss'}(\mathbf{r}, \mathbf{q}) &= \sum_l e^{i\mathbf{q}\cdot\mathbf{R}_l} \frac{(\mathbf{R}_{lss'}(\mathbf{r}))_{\alpha}}{|\mathbf{R}_{lss'}(\mathbf{r})|^3} \left[ \frac{2}{\sqrt{\pi}} e^{-\eta^2|\mathbf{R}_{lss'}(\mathbf{r})|^2} |\mathbf{R}_{lss'}(\mathbf{r})| \eta + \text{erfc}(\eta|\mathbf{R}_{lss'}(\mathbf{r})|) \right] \\ &\quad - i \frac{4\pi}{\Omega_{\text{WS}}} \sum_G \frac{(\mathbf{G} + \mathbf{q})_{\alpha}}{|\mathbf{G} + \mathbf{q}|^2} e^{-|\mathbf{G} + \mathbf{q}|^2/4\eta} e^{i(\mathbf{G} + \mathbf{q})\cdot(\boldsymbol{\tau}_s - \boldsymbol{\tau}_{s'} - \mathbf{r})} \end{aligned} \quad (\text{A.29})$$

with  $\mathbf{R}_{lss'}(\mathbf{x}) = \mathbf{R}_l + \boldsymbol{\tau}_{s'} - \boldsymbol{\tau}_s + \mathbf{x}$ .  $\mathcal{C}_{\alpha}^{ss'}(\mathbf{r}, \mathbf{q})$  can be efficiently expanded in spherical harmonics to separate radial and angular coordinates using Lebedev quadrature (see App. B).

## Numerical Quadrature

### B.1 One-dimensional integration

For all radial integrations a Gauss-Legendre quadrature [Bro+01] has been used. This method approximates an integral of a function  $f(x)$  over an interval  $[a, b]$  as

$$\int_a^b dx f(x) = \frac{b-a}{2} \int_{-1}^1 dz f\left(\frac{b-a}{2}z + \frac{a+b}{2}\right) \quad (\text{B.1})$$

$$\approx \sum_{i=1}^n w_i f\left(\frac{b-a}{2}z_i + \frac{a+b}{2}\right) = \sum_{i=1}^n w_i f(x_i). \quad (\text{B.2})$$

The integration weights are given as

$$w_i = \frac{b-a}{(1-z_i^2)P'_n(z_i)^2} \quad (\text{B.3})$$

with the associated Legendre polynomials  $P'_n(z_i)$ . The  $z_i$  are the  $i^{\text{th}}$  roots of the respective polynomials and define the radial mesh by means of

$$x_i = \frac{b-a}{2}z_i + \frac{a+b}{2}. \quad (\text{B.4})$$

The benefit of this procedure is that the integration weights have to be calculated only once since all quantities with spatial dependence use the same radial mesh. Additionally, the distribution of mesh points is advantageous for the functions used here. The Gaussian mesh is most dense at radii near the origin, where potentials change most rapidly and near the cell boundary, where the contribution of the integrand is largest.

### B.2 Angular integration

In cases where the angular part of volume integrals can not be reduced to sums over angular momentum indices by utilizing the orthogonality relations of spherical harmonics, a numerical treatment is necessary. Here, the method of Lebedev and Laikov has been used. They developed a highly efficient mesh of quadrature points and weights  $w_i$  for angular integration on a sphere by using the symmetry properties of the octahedral point group [LL99; Leb75; Leb76], resulting in the quadrature formula

$$\int d\hat{r} f(\hat{r}) = \int_0^{2\pi} d\theta \int_0^\pi d\phi f(\theta, \phi) \sin\theta = \sum_{i=1}^{N_{\hat{r}}} w_{i,\hat{r}} f(\hat{r}_i). \quad (\text{B.5})$$



# Bibliography

- [AJ84] **O. K. Andersen** and **O. Jepsen**. “Explicit, First-Principles Tight-Binding Theory”. In: *Phys. Rev. Lett.* 53.27 (1984), pp. 2571–2574. DOI: 10.1103/PhysRevLett.53.2571 (cit. on p. 40).
- [Alf09] **D. Alfè**. “PHON: A program to calculate phonons using the small displacement method”. In: *Comp. Phys. Comm.* 180 (2009), pp. 2622–2633. DOI: 10.1016/j.cpc.2009.03.010 (cit. on p. 85).
- [AM05] **N. W. Ashcroft** and **N. D. Mermin**. *Festkörperphysik*. 2nd ed. Oldenbourg, 2005 (cit. on p. 44).
- [And75] **O. K. Andersen**. “Linear methods in band theory”. In: *Phys. Rev. B* 12.8 (1975), pp. 3060–3083. DOI: 10.1103/PhysRevB.12.3060 (cit. on p. 40).
- [And77] **T. Ando**. “Inter-subband optical absorption in space-charge layers on semiconductor surfaces”. In: *Z. Phys. B* 26.3 (1977), pp. 263–272. DOI: 10.1007/BF01312933 (cit. on p. 32).
- [Ang+90] **E. Angerson** et al. “LAPACK: a portable linear algebra library for high-performance computers”. In: *Proceedings of Supercomputing '90*. New York: IEEE Computer Society / ACM, Nov. 1990, pp. 2–11. DOI: 10.1109/SUPERC.1990.129995 (cit. on p. 65).
- [AS72] **M. Abramowitz** and **I. A. Stegun**, eds. *Handbook of Mathematical Functions with Formulas, Graphs, and Mathematical Tables*. 10. print, Dec. 1972, with corr. United States Department of Commerce, 1972, p. 882 (cit. on p. 67).
- [Asa+99] **M. Asato** et al. “Full-potential KKR calculations for metals and semiconductors”. In: *Phys. Rev. B* 60.8 (1999), pp. 5202–5210. DOI: 10.1103/PhysRevB.60.5202 (cit. on pp. 49, 74).
- [AT79] **T. Asada** and **K. Terakura**. “A Calculation of the Electronic Structure of Palladium Containing an Impurity–Spin Paramagnetic Susceptibility”. In: *J. Phys. Soc. Japan* 47.5 (1979), pp. 1495–1502. DOI: 10.1143/JPSJ.47.1495 (cit. on p. 65).
- [BCS57] **J. Bardeen**, **L. N. Cooper**, and **J. R. Schrieffer**. “Theory of Superconductivity”. In: *Phys. Rev.* 108 (1957), pp. 1175–1204. DOI: 10.1103/PhysRev.108.1175 (cit. on p. 75).
- [Bec93] **A. D. Becke**. “Density Functional Thermochemistry. III The Role of Exact Exchange”. In: *J. Chem. Phys.* 98 (1993), pp. 5648–5652 (cit. on p. 32).
- [Bee64] **J. L. Beeby**. “Electronic Structure of Alloys”. In: *Phys. Rev.* 135 (1964), A130–A143. DOI: 10.1103/PhysRev.135.A130 (cit. on p. 40).
- [Bee67] **J. L. Beeby**. “The density of electrons in a perfect or imperfect lattice”. In: *Proc. R. Soc. London A* 302 (1967), pp. 113–136. URL: <http://rspa.royalsocietypublishing.org/content/302/1468/113.abstract> (cit. on p. 40).
- [BF04] **H. Bruus** and **K. Flensberg**. *Many-body Quantum Theory in Condensed Matter Physics*. Oxford University Press, 2004. ISBN: 978-0-19-856633-5 (cit. on pp. 25, 35).

- [BGD01] **S. Baroni, S. de Gironcoli, and A. Dal Corso.** “Phonons and related crystal properties from density-functional perturbation theory”. In: *Rev. Mod. Phys.* 73.2 (2001), pp. 515–562. DOI: 10.1103/RevModPhys.73.515 (cit. on pp. 19, 73).
- [BGT87] **S. Baroni, P. Giannozzi, and A. Testa.** “Green’s-Function Approach to Linear Response in Solids”. In: *Phys. Rev. Lett.* 58.18 (1987), pp. 1861–1864. DOI: 10.1103/PhysRevLett.58.1861 (cit. on p. 19).
- [BH72] **U. von Barth and L. Hedin.** “A local exchange-correlation potential for the spin polarized case. i”. In: *J. Phys. C* 5.13 (1972), pp. 1629–1642. DOI: 10.1088/0022-3719/5/13/012 (cit. on p. 31).
- [Bin+82] **G. Binnig et al.** “Surface Studies by Scanning Tunneling Microscopy”. In: *Phys. Rev. Lett.* 49.1 (1982), pp. 57–61. DOI: 10.1103/PhysRevLett.49.57 (cit. on p. 83).
- [BK09] **S. K. Bose and J. Kortus.** “Electron-phonon coupling in metallic solids from density functional theory”. In: *Vibronic interactions and Electron-Phonon Interactions and Their Role in Modern Chemistry and Physics*. Ed. by **T. Kato**. Transworld Research Network, 2009. ISBN: 978-81-7895-336-6 (cit. on p. 75).
- [BK12] **M. Born and T. von Kármán.** “Über Schwingungen in Raumgittern”. In: *Phys. Zeitschrift* 13.8 (1912), pp. 297–309 (cit. on pp. 7, 12, 14).
- [BK13] **M. Born and T. von Kármán.** “Über die Verteilung der Eigenschwingungen von Punktgittern”. In: *Phys. Zeitschrift* 14 (1913), pp. 65–71 (cit. on pp. 7, 12, 14).
- [BL94] **P.J. Braspenning and A. Lodder.** “Generalized multiple-scattering theory”. In: *Phys. Rev. B* 49.15 (1994), pp. 10222–10230. DOI: 10.1103/PhysRevB.49.10222 (cit. on p. 40).
- [Blo29] **F. Bloch.** “Über die Quantenmechanik der Elektronen in Kristallgittern”. In: *Zeitschrift für Physik* 52.7–8 (1929), pp. 555–600. DOI: 10.1007/BF01339455 (cit. on p. 14).
- [Blö94] **P. E. Blöchl.** “Projector augmented-wave method”. In: *Phys. Rev. B* 50.24 (1994), pp. 17953–17979. DOI: 10.1103/PhysRevB.50.17953 (cit. on p. 85).
- [Blü06] **S. Blügel.** “Density Functional Theory in Practice”. In: *Computational Condensed Matter Physics: Lecture Manuscripts of the 37th Spring School of the Institute of Solid State Research. Reihe Materie und Material*. Ed. by **S. Blügel** et al. Vol. 32. Forschungszentrum Jülich GmbH, 2006, A.8.14–A.1.16. ISBN: 3-89336-430-7 (cit. on p. 37).
- [BO27] **M. Born and R. Oppenheimer.** “Zur Quantentheorie der Molekeln”. In: *Ann. Phys.* 20.4 (1927), pp. 457–484. DOI: 10.1002/andp.19273892002 (cit. on p. 10).
- [Bro+01] **I. N. Bronstein et al.** *Taschenbuch der Mathematik*. 5th ed. Verlag Harry Deutsch, 2001. ISBN: 3-8171-2005-2 (cit. on pp. 22, 97).
- [Bro65] **C. G. Broyden.** “A class of methods for solving nonlinear simultaneous equations”. In: *Math. Comp* 19 (1965), pp. 577–593. DOI: 10.1090/S0025-5718-1965-0198670-6 (cit. on p. 47).
- [Bru+09] **C. Brun et al.** “Reduction of the Superconducting Gap of Ultrathin Pb Islands Grown on Si(111)”. In: *Phys. Rev. Lett.* 102.20 (2009), pp. 207002-1–207002-4. DOI: 10.1103/PhysRevLett.102.207002 (cit. on p. 89).

- [Brü82] **P. Brüesch**. *Phonons: Theory and Experiments I*. Ed. by **M. Cardona**, **P. Fulde**, and **H.-J. Queisser**. Berlin Heidelberg New York: Springer-Verlag, 1982. DOI: 10.1007/978-3-642-81781-6 (cit. on p. 22).
- [Buc+09] **P. Buczek** et al. “Energies and Lifetimes of Magnons in Complex Ferromagnets: A First-Principle Study of Heusler Alloys”. In: *Phys. Rev. Lett.* 102.24 (2009), p. 247206. DOI: 10.1103/PhysRevLett.102.247206 (cit. on p. 62).
- [Buc09] **P. A. Buczek**. “Spindynamik komplexer itineranter Magnete”. PhD thesis. Martin-Luther-Universität Halle-Wittenberg, 2009 (cit. on p. 35).
- [Buc12a] **P. A. Buczek**. *personal communication*. 2012 (cit. on pp. 60, 65).
- [Buc12b] **P. A. Buczek**. *personal communication*. 2012 (cit. on p. 94).
- [CA80] **D. M. Ceperley** and **B. J. Alder**. “Ground State of the Electron Gas by a Stochastic Method”. In: *Phys. Rev. Lett.* 45 (1980), pp. 566–569. DOI: 10.1103/PhysRevLett.45.566 (cit. on p. 32).
- [Cam63] **E. S. Campbell**. “Existence of a well defined specific energy for an ionic crystal; Justification of Ewald’s formulae and of their use to deduce equations for multipole lattices”. In: *J. Phys. Chem. Solids* 24 (1963), pp. 197–208 (cit. on p. 96).
- [Car90] **J. P. Carbotte**. “Properties of boson-exchange superconductors”. In: 62.4 (1990), p. 1046. DOI: 10.1103/RevModPhys.62.1027 (cit. on p. 77).
- [Coo56] **L. N. Cooper**. “Bound Electron Pairs in a Degenerate Fermi Gas”. In: *Phys. Rev.* 104 (1956), pp. 1189–1190. DOI: 10.1103/PhysRev.104.1189 (cit. on p. 75).
- [Dal08] **A. Dal Corso**. “Ab initio phonon dispersions of face centered cubic Pb: effects of spin–orbit coupling”. In: *J. Phys.: Condens. Matter* 20 (2008), pp. 445202-1–445202-6. DOI: 10.1088/0953-8984/20/44/445202 (cit. on pp. 85, 86).
- [Deb12] **P. Debye**. “Zur Theorie der spezifischen Wärme”. In: *Ann. Phys.* 344.14 (1912), pp. 789–839. DOI: 10.1002/andp.19123441404 (cit. on p. 7).
- [Ded+91] **P. H. Dederichs** et al. “Total-energy calculations for point defects in metals”. In: *Physica B: Condensed Matter* 172.1–2 (1991), pp. 203–209. DOI: 10.1016/0921-4526(91)90432-E (cit. on pp. 40, 49).
- [DJ69] **P. D. De Cicco** and **F. A. Johnson**. “The Quantum Theory of Lattice Dynamics. IV”. In: *Proc. R. Soc. London A* 310.1500 (1969), pp. 111–119. DOI: 10.1098/rspa.1969.0066 (cit. on p. 19).
- [DK10] **D. van Delft** and **P. Kes**. “The discovery of superconductivity”. In: *Physics Today* 63.9 (2010), pp. 38–43. DOI: 10.1063/1.3490499 (cit. on pp. 75, 83, 86, 87).
- [DLZ06] **P. H. Dederichs**, **S. Lounis**, and **R. Zeller**. “The Korringa-Kohn-Rostoker (KKR) Green Function Method II. Impurities and Clusters in the Bulk and on Surfaces The Korringa-Kohn-Rostoker (KKR) Green Function Method II. Impurities and Clusters in the Bulk and on Surfaces The Korringa-Kohn-Rostoker (KKR) Green Function Method – II. Impurities and Clusters in the Bulk and on Surfaces”. In: *Computational Nanoscience: Do it Yourself*. Ed. by **J. Grotenhorst**, **S. Blügel**, and **D. Marx**. Vol. 31. John von Neumann Institute for Computing, 2006, pp. 279–298. ISBN: 3-00-017350-1. URL: <http://webarchiv.fz-juelich.de/nic-series//volume31/volume31.html> (cit. on p. 40).
- [DR75] **R. C. Dynes** and **J. M. Rowell**. “Influence of electrons-per-atom ratio and phonon frequencies on the superconducting transition temperature of Lead alloys”. In: *Phys. Rev. B* 11.5 (1975), pp. 1884–1894. DOI: 10.1103/PhysRevB.11.1884 (cit. on p. 87).

- [Dri91] **B. H. Dritler**. “KKR-Greensche Funktionsmethode für das volle Zellpotential”. PhD thesis. Forschungszentrum Jülich, 1991 (cit. on pp. 40, 49).
- [DS75] **B. J. Dalrymple** and **P. Santhanam**. “Approximating the electron-phonon coupling constant in superconductors from thermodynamic data”. In: *Journal of Low Temperature Physics* 57.3–4 (1975), pp. 349–357. DOI: 10.1007/BF00681198 (cit. on p. 83).
- [Dys49] **F. J. Dyson**. “The S Matrix in Quantum Electrodynamics”. In: *Phys. Rev.* 75 (1949), pp. 1736–1755. DOI: 10.1103/PhysRev.75.1736 (cit. on p. 38).
- [Ein07] **A. Einstein**. “Die Plancksche Theorie der Strahlung und die Theorie der spezifischen Wärme”. In: *Ann. Phys.* 22 (1907), pp. 180–190 (cit. on p. 7).
- [Éli60] **G. M. Éliashberg**. “Interactions Between Electrons And Lattice Vibrations In A Superconductor”. In: *Soviet Physics JETP* 11.3 (1960), pp. 696–702 (cit. on p. 75).
- [Éli61] **G. M. Éliashberg**. “Temperature Greens function for electrons in a superconductor”. In: *Soviet Physics JETP* 12.5 (1961), pp. 1000–10002 (cit. on p. 75).
- [Éli62] **G. M. Éliashberg**. “Transport equation for a degenerate system of fermi particles”. In: *Soviet Physics JETP* 14.4 (1962) (cit. on p. 75).
- [Ern07] **A. Ernst**. “Multiple-scattering theory: new developments and applications”. Habilitationsschrift. Martin-Luther-Universität Halle-Wittenberg, 2007. URL: <http://nbn-resolving.de/urn/resolver.pl?urn=nbn:de:gbv:3-000012928> (cit. on p. 87).
- [Ewa21] **P. P. Ewald**. “Die Berechnung optischer und elektrostatischer Gitterpotentiale”. In: *Ann. Phys.* 369.3 (1921), pp. 253–287. DOI: 10.1002/andp.19213690304 (cit. on pp. 22, 93).
- [Ewa38] **P. P. Ewald**. “Elektrostatische und optische Potentiale im Kristallraum und im Fourierraum”. In: *Nachrichten von der Gesellschaft der Wissenschaften zu Göttingen : Mathematisch-physikalische Klasse ; Fachgr. 2* 3.4 (1938), pp. 55–64 (cit. on p. 22).
- [Fer28] **E. Fermi**. “Eine statistische Methode zur Bestimmung einiger Eigenschaften des Atoms und ihre Anwendung auf die Theorie des periodischen Systems der Elemente”. In: *Zeitschrift für Physik* 48.1–2 (1928), pp. 73–79. DOI: 10.1007/BF01351576 (cit. on p. 29).
- [Fey39] **R. P. Feynman**. “Forces in Molecules”. In: *Phys. Rev.* 56.4 (1939), pp. 340–343. DOI: 10.1103/PhysRev.56.340 (cit. on p. 15).
- [FH08] **G. E. Farin** and **D. Hansford**. *Mathematical principles for scientific computing and visualization*. A K Peters/CRC Press, 2008. ISBN: 978-1568813219 (cit. on p. 43).
- [Fin03] **M. Finnis**. *Interatomic Forces in Condensed Matter*. Oxford University Press, 2003. DOI: 10.1093/acprof:oso/9780198509776.001.0001 (cit. on pp. 14, 16).
- [FW71] **A. L. Fetter** and **J. D. Walecka**. *Quantum Theory of Many-Particle Systems*. International series in pure and applied physics. McGraw-Hill Book Company, 1971. ISBN: 0-07-020653-8 (cit. on pp. 27, 35).
- [GG53] **M. Gell-Mann** and **M. L. Goldberger**. “The Formal Theory of Scattering”. In: *Phys. Rev.* 91.2 (1953), p. 398. DOI: 10.1103/PhysRev.91.398 (cit. on p. 38).

- [GG72] **G. D. Gaspari** and **B. L. Gyorffy**. “Electron-Phonon Interactions, d Resonances, and Superconductivity in Transition Metals”. In: *Phys. Rev. Lett.* 28.3 (1972), p. 802. DOI: 10.1103/PhysRevLett.28.801 (cit. on p. 78).
- [GG74] **I. R. Gomersall** and **B. L. Gyorffy**. “A simple theory of the electron-phonon mass enhancement in transition metal compounds”. In: *J. Phys. F* 4 (1974), pp. 1204–1221. DOI: 10.1088/0305-4608/4/8/015 (cit. on p. 78).
- [GK85] **E. K. U. Gross** and **W. Kohn**. “Local density-functional theory of frequency-dependent linear response”. In: *Phys. Rev. Lett.* 55.26 (1985), pp. 2850–2852. DOI: 10.1103/PhysRevLett.55.2850 (cit. on p. 34).
- [GK86] **E. K. U. Gross** and **W. Kohn**. “Erratum: Local Density-Functional Theory of Frequency-Dependent Linear Response”. In: *Phys. Rev. Lett.* 57.7 (1986), pp. 923–923. DOI: 10.1103/PhysRevLett.57.923.2 (cit. on p. 34).
- [GM12] **E. K. U. Gross** and **N. T. Maitra**. “Introduction to TDDFT”. In: *Fundamentals of Time-Dependent Density Functional Theory*. Ed. by **M. A. L. Marques** et al. Springer, 2012. DOI: 10.1007/978-3-642-23518-4 (cit. on p. 29, 35).
- [Gon00] **A. Gonis**. *Theoretical Materials Science*. Materials Research Society, 2000. ISBN: 978-1-55899-540-6 (cit. on pp. 12, 29, 41, 57, 58, 73, 76, 78).
- [Gon92] **A. Gonis**. *Green Functions for Ordered and Disordered Systems*. New York: North-Holland, 1992. ISBN: 0444889868 (cit. on p. 41).
- [Gon94] **X. Gonze**. “Perturbation expansion of variational principles at arbitrary order”. In: *Phys. Rev. A* 52.2 (1994), pp. 1086–1095. DOI: <http://dx.doi.org/10.1103/PhysRevA.52.1086> (cit. on p. 19).
- [Gon95] **X. Gonze**. “Adiabatic density-functional perturbation theory”. In: *Phys. Rev. A* 52.2 (1995), pp. 1096–1114. DOI: 10.1103/PhysRevA.52.1096 (cit. on p. 19).
- [Gre28] **G. Green**. “An Essay on the Application of mathematical Analysis to the theories of Electricity and Magnetism”. In: *Nottingham* (1928). URL: <http://arxiv.org/abs/0807.0088> (cit. on p. 37).
- [GZN88] **A. Gonis**, **X.-G. Zhang**, and **D. M. Nicholson**. “Electronic-structure method for general space-filling cell potentials”. In: *Phys. Rev. B* 38.5 (1988), pp. 3564–3567. DOI: 10.1103/PhysRevB.38.3564 (cit. on p. 49).
- [Hei+10] **R. Heid** et al. “Effect of spin-orbit coupling on the electron-phonon interaction of the superconductors Pb and Tl”. In: *Phys. Rev. B* 81.17 (2010), pp. 174527-1–174527-6. DOI: 10.1103/PhysRevB.81.174527 (cit. on p. 83, 86).
- [Hel37] **H. Hellmann**. *Einführung in die Quantenchemie*. Leipzig Wien: Franz Deuticke, 1937. URL: <http://d-nb.info/361489242> (cit. on p. 15).
- [HK64] **P. Hohenberg** and **W. Kohn**. “Inhomogeneous Electron Gas”. In: *Phys. Rev. B* 136.3 (1964), pp. 864–871. DOI: 10.1103/PhysRev.136.B864 (cit. on p. 29).
- [Höl10] **M. Hölzer**. “Magnetoelektrische Kopplung an multiferroischen Grenzflächen”. Diplomarbeit. Martin-Luther-Universität Halle-Wittenberg, 2010 (cit. on p. 85).
- [HSC79] **D. R. Hamann**, **M. Schlüter**, and **C. Chiang**. “Norm-Conserving Pseudopotentials”. In: *Phys. Rev. Lett.* 43.20 (1979), pp. 1494–1497. DOI: 10.1103/PhysRevLett.43.1494 (cit. on p. 37).

- [Hug+07] **I. D. Hughes** et al. “Lanthanide contraction and magnetism in the heavy rare earth elements Lanthanide contraction and magnetism in the heavy rare earth elements Lanthanide contraction and magnetism in the heavy rare earth elements”. In: *Nature* 446 (2007), pp. 650–653. DOI: 10.1038/nature05668 (cit. on p. 62).
- [Hyl30] **E. A. Hylleraas**. “Über den Grundterm der Zweielektronenprobleme von  $H^-$ , He,  $Li^+$ ,  $Be^{++}$  usw.” In: *Zeitschrift für Physik* 65.3–4 (1930), pp. 209–225. DOI: 10.1007/BF01397032 (cit. on p. 19).
- [JA71] **O. Jepsen** and **O. K. Anderson**. “The electronic structure of h.c.p. Ytterbium”. In: *Solid State Communications* 9.20 (1971), pp. 1763–1767. DOI: 10.1016/0038-1098(71)90313-9 (cit. on p. 86).
- [JG89] **R. O. Jones** and **O. Gunnarsson**. “The density functional formalism, its applications and prospects”. In: *Rev. Mod. Phys.* 61.3 (1989), pp. 689–746. DOI: 10.1103/RevModPhys.61.689 (cit. on p. 32).
- [Käl52] **G. Källén**. “On the Definition of the Renormalization Constants in Quantum Electrodynamics”. In: *Helvetica Physica Acta* 25 (1952), p. 417. DOI: 10.5169/seals-112316 (cit. on p. 28).
- [Kel40] **E. W. Kellermann**. “Theory of the Vibrations of the Sodium Chloride Lattice”. In: *Phil. Trans. R. Soc. Lond. A* 238 (1940), pp. 513–548. DOI: 10.1098/rsta.1940.0005 (cit. on pp. 15, 22).
- [Kel65] **J. V. Keldysh**. “Diagram Technique for Nonequilibrium Processes”. In: *Soviet Physics JETP* 20.4 (1965) (cit. on p. 33).
- [KF96a] **G. Kresse** and **J. Furthmüller**. “Efficiency of ab-initio total energy calculations for metals and semiconductors using a plane-wave basis set”. In: *Comp. Mat. Science* 6.1 (1996), pp. 15–50. DOI: 10.1016/0927-0256(96)00008-0 (cit. on p. 85).
- [KF96b] **G. Kresse** and **J. Furthmüller**. “Efficient iterative schemes for ab initio total-energy calculations using a plane-wave basis set”. In: *Phys. Rev. B* 54.16 (1996), pp. 11169–11186. DOI: 10.1103/PhysRevB.54.11169 (cit. on p. 85).
- [KFH95] **G. Kresse**, **J. Furthmüller**, and **J. Hafner**. “Ab initio Force Constant Approach to Phonon Dispersion Relations of Diamond and Graphite”. In: *Europhys. Lett.* 32 (1995), p. 729. DOI: 10.1209/0295-5075/32/9/005 (cit. on pp. 17, 85).
- [KH93] **G. Kresse** and **J. Hafner**. “Ab initio molecular dynamics for liquid metals”. In: *Phys. Rev. B* 47.1 (1993), pp. 558–561. DOI: 10.1103/PhysRevB.47.558 (cit. on p. 85).
- [KH94] **G. Kresse** and **J. Hafner**. “Ab initio molecular-dynamics simulation of the liquid-metal–amorphous-semiconductor transition in germanium”. In: *Phys. Rev. B* 49.20 (1994), pp. 14251–14269. DOI: 10.1103/PhysRevB.49.14251 (cit. on p. 85).
- [Kha+09] **M. Khalid** et al. “Defect-induced magnetic order in pure ZnO films”. In: *Phys. Rev. B* 80.3 (2009), p. 035331. DOI: 10.1103/PhysRevB.80.035331 (cit. on p. 62).
- [Kha13] **A. A. Khaledi**. “Correlated Electron-Nuclear Dynamics”. PhD thesis. Freie Universität Berlin, 2013. URL: [http://www.diss.fu-berlin.de/diss/receive/FUDISS\\_thesis\\_000000096878](http://www.diss.fu-berlin.de/diss/receive/FUDISS_thesis_000000096878) (cit. on p. 10).

- [KJ99] **G. Kresse** and **D. Joubert**. “From ultrasoft pseudopotentials to the projector augmented-wave method”. In: *Phys. Rev. B* 59.3 (1999), pp. 1758–1775. DOI: 10.1103/PhysRevB.59.1758 (cit. on p. 85).
- [Klu46] **H. P. Klug**. “A.Redetermination of the Lattice Constant of Lead A.Redetermination of the Lattice Constant of Lead”. In: *J. Am. Chem. Soc.* 68.8 (1946), pp. 1493–1494. DOI: 10.1021/ja01212a032 (cit. on p. 84).
- [KM82] **K. Kunc** and **R. M. Martin**. “Ab Initio Force Constants of GaAs: A New Approach to Calculation of Phonons and Dielectric Properties”. In: *Phys. Rev. Lett.* 48.6 (1982), p. 406. DOI: 10.1103/PhysRevLett.48.406 (cit. on p. 17).
- [KMG12] **A. A. Khaledi**, **N. T. Maitra**, and **E. K. U. Gross**. “Correlated electron-nuclear dynamics: Exact factorization of the molecular wavefunction”. In: *The Journal of Chemical Physics* 137.22 (2012), A530. DOI: 10.1063/1.4745836 (cit. on p. 10).
- [Koh59] **W. Kohn**. “Image of the Fermi Surface in the Vibration Spectrum of a Metal”. In: *Phys. Rev. Lett.* 2.9 (1959), pp. 393–394. DOI: 10.1103/PhysRevLett.2.393 (cit. on p. 85).
- [Kor47] **J. Koringa**. “On the calculation of the energy of a Bloch wave in a metal”. In: *Physica* 13.6–7 (1947), pp. 392–400. DOI: 10.1016/0031-8914(47)90013-X (cit. on p. 40).
- [Kor58] **J. Koringa**. “Dispersion theory for electrons in a random lattice with applications to the electronic structure of alloys”. In: *J. Phys. Chem. Solids* 7.2–3 (1958), pp. 252–258. DOI: 10.1016/0022-3697(58)90270-1 (cit. on p. 40).
- [KR54] **W. Kohn** and **N. Rostoker**. “Solution of the Schrödinger Equation in Periodic Lattices with an Application to Metallic Lithium”. In: *Phys. Rev.* 94.5 (1954), pp. 1111–1120. DOI: 10.1103/PhysRev.94.1111 (cit. on p. 40).
- [KS65] **W. Kohn** and **L. J. Sham**. “Self-Consistent Equations Including Exchange and Correlation Effects”. In: *Phys. Rev. A* 140.4 (1965), pp. 1133–1138. DOI: 10.1103/PhysRev.140.A1133 (cit. on p. 30).
- [Kub57] **R. Kubo**. “Statistical-Mechanical Theory of Irreversible Processes. I. General Theory and Simple Applications to Magnetic and Conduction Problems”. In: *J. Phys. Soc. Japan* 12 (1957), p. 570. DOI: 10.1143/JPSJ.12.570 (cit. on p. 25).
- [Kub66] **R. Kubo**. “The fluctuation-dissipation theorem”. In: *Reports on Progress in Physics* 29 (1966). DOI: doi:10.1088/0034-4885/29/1/306 (cit. on p. 25).
- [Laa+91] **K. Laasonen** et al. “Implementation of ultrasoft pseudopotentials in ab initio molecular dynamics”. In: *Phys. Rev. B* 43.8 (1991), pp. 6796–6799. DOI: 10.1103/PhysRevB.43.6796 (cit. on p. 37).
- [Leb75] **V. I. Lebedev**. “Values of the nodes and weights of ninth to seventeenth order Gauss-Markov quadrature formulae invariant under the octahedron group with inversion”. In: *Computational Mathematics and Mathematical Physics* 15.1 (1975), pp. 44–51. DOI: 10.1016/0041-5553(75)90133-0 (cit. on p. 97).
- [Leb76] **V. I. Lebedev**. “Quadratures on a sphere”. In: *Computational Mathematics and Mathematical Physics* 16.2 (1976), pp. 10–24. DOI: 10.1016/0041-5553(76)90100-2 (cit. on p. 97).
- [Lee98] **R. van Leeuwen**. “Causality and Symmetry in Time-Dependent Density-Functional Theory”. In: *Phys. Rev. Lett.* 80.6 (1998), pp. 1280–1283. DOI: 10.1103/PhysRevLett.80.1280 (cit. on p. 33).

- [Leg09] **A.-M. Legendre**. “Recherches sur diverses sortes d’intégrales définies”. In: *Mémoires de la classe des sciences mathématiques et physiques de l’Institut de France* 10 (1809), p. 485 (cit. on p. 95).
- [Leh54] **H. Lehmann**. “Über die Eigenschaften von Ausbreitungsfunktionen und Renormierungskonstanten quantisierter Felder”. In: *Nuovo Cimento* 11.4 (1954), pp. 342–357 (cit. on p. 28).
- [Lev96] **M. Levy**. “Recent Developments and Applications of Modern Density Functional Theory”. In: ed. by **J. M. Seminario**. Elsevier, 1996. Chap. Elementary concepts in density functional theory (cit. on p. 32).
- [LL99] **V. I. Lebedev** and **D. N. Laikov**. “a quadrature formula for the sphere of the 131st Algebraic Order of Accuracy”. In: *Doklady Mathematics* 59.3 (1999), pp. 477–481 (cit. on p. 97).
- [LS50] **B. A. Lippmann** and **J. Schwinger**. “Variational Principles for Scattering Processes. I”. In: *Phys. Rev.* 79.3 (1950), p. 469. DOI: 10.1103/PhysRev.79.469 (cit. on p. 38).
- [LT72] **G. Lehmann** and **M. Taut**. “On the Numerical Calculation of the Density of States and Related Properties”. In: *Phys. Stat. Solidi B* 54.2 (1972), pp. 469–477. DOI: 10.1002/pssb.2220540211 (cit. on p. 86).
- [Lüd+01] **M. Lüders** et al. “Ab initio angle-resolved photoemission in multiple-scattering formulation”. In: *J. Phys.: Condens. Matter* 13.38 (2001), pp. 8587–8606. DOI: 10.1088/0953-8984/13/38/305 (cit. on pp. 62, 87).
- [Lüd+05] **M. Lüders** et al. “Self-interaction correction in multiple scattering theory”. In: *Phys. Rev. B* 71.20 (2005), p. 205109. DOI: 10.1103/PhysRevB.71.205109 (cit. on p. 62).
- [LV89] **K.-L. Liu** and **S. H. Vosko**. “A time-dependent spin density functional theory for the dynamical spin susceptibility”. In: *Can. J. Phys.* 67 (1989), p. 1015. DOI: 10.1139/p89-178 (cit. on p. 33).
- [Mah80] **G. D. Mahan**. “Modified Sternheimer equation for polarizability”. In: *Phys. Rev. A* 22.5 (1980), pp. 1780–1785. DOI: 10.1103/PhysRevA.22.1780 (cit. on p. 19).
- [Mat02] **A. E. Mattsson**. “In Pursuit of the “Divine” Functional”. In: *Science* 298.5594 (2002), pp. 759–760. DOI: 10.1126/science.1077710 (cit. on p. 32).
- [McM68] **W. L. McMillan**. “Transition Temperature of Strong-Coupled Superconductors”. In: *Phys. Rev.* 167.2 (1968), p. 334. DOI: 10.1103/PhysRev.167.331 (cit. on p. 78).
- [MG03] **M. A. L. Marques** and **E. K. U. Gross**. “Time-Dependent Density Functional Theory”. In: *A Primer in Density Functional Theory*. Ed. by **C. Fiolhais**, **F. Nogueira**, and **M. Marques**. Berlin Heidelberg New York: Springer, 2003. DOI: 10.1007/3-540-37072-2 (cit. on p. 33).
- [MG04] **M. Marques** and **E. K. U. Gross**. “Time-Dependent Density Functional Theory”. In: *Annu. Rev. Phys. Chem.* 55 (2004), pp. 427–455. DOI: 10.1146/annurev.physchem.55.091602.094449 (cit. on p. 33).

- [MP06] **P. Mavropoulos** and **N. Papanikolaou**. “The Korringa-Kohn-Rostoker (KKR) Green Function Method – I. Electronic Structure of periodic Systems”. In: *Computational Nanoscience: Do it Yourself*. Ed. by **J. Grotenhorst**, **S. Blügel**, and **D. Marx**. Vol. 31. John von Neumann Institute for Computing, 2006, pp. 131–158. ISBN: 3-00-017350-1. URL: <http://webarchiv.fz-juelich.de/nic-series//volume31/volume31.html> (cit. on pp. 48, 61).
- [MP76] **H. J. Monkhorst** and **J. D. Pack**. “Special points for Brillouin-zone integrations”. In: *Phys. Rev. B* 13.12 (1976), pp. 5188–5192. DOI: 10.1103/PhysRevB.13.5188 (cit. on p. 85).
- [MR65] **W. L. McMillan** and **J. M. Rowell**. “Lead Phonon Spectrum Calculated from Superconducting Density of States”. In: *Phys. Rev. Lett.* 14.4 (1965), pp. 108–112. DOI: 10.1103/PhysRevLett.14.108 (cit. on p. 83).
- [MSN67] **V. J. Minkiewicz**, **G. Shirane**, and **R. Nathans**. “Phonon Dispersion Relation for Iron”. In: *Phys. Rev.* 162.3 (1967), pp. 528–531. DOI: 10.1103/PhysRev.162.528 (cit. on p. 72).
- [MTN12] **P. J. Mohr**, **B. N. Taylor**, and **D. B. Newell**. “CODATA recommended values of the fundamental physical constants: 2010”. In: *Rev. Mod. Phys.* 84 (2012), p. 1533. DOI: 10.1103/RevModPhys.84.1527 (cit. on p. 10).
- [Nic+67] **R. M. Nicklow** et al. “Phonon Frequencies in Copper at 49 and 298 °K”. In: *Phys. Rev.* 164.3 (1967), p. 924. DOI: 10.1103/PhysRev.164.922 (cit. on p. 24).
- [Nol06] **W. Nolting**. *Grundkurs Theoretische Physik 5/2: Quantenmechanik – Methoden und Anwendungen*. 6th ed. Berlin Heidelberg: Springer-Verlag, 2006. ISBN: 3-540-26035-8 (cit. on p. 30).
- [OG88] **L. N. Oliveira** and **E. K. U. Gross**. “Density-Functional Theory for Superconductors Density-Functional Theory for Superconductors Density-Functional Theory for Superconductors Density-Functional Theory for Superconductors”. In: *Phys. Rev. Lett.* 60.23 (1988), pp. 2430–2433. DOI: 10.1103/PhysRevLett.60.2430 (cit. on p. 78).
- [OVM02] **R. Otero**, **A. L. Vázquez**, and **R. Miranda**. “Observation of preferred heights in Pb nanoislands: A quantum size effect”. In: *Phys. Rev. B* 66.11 (2002), pp. 115401-1–115401-6. DOI: 10.1103/PhysRevB.66.115401 (cit. on pp. 83–85).
- [PBE96] **J. P. Perdew**, **K. Burke**, and **M. Ernzerhof**. “Generalized Gradient Approximation Made Simple”. In: *Phys. Rev. Lett.* 77.18 (1996), pp. 3865–3868. DOI: 10.1103/PhysRevLett.77.3865 (cit. on p. 32).
- [PBE97] **J. P. Perdew**, **K. Burke**, and **M. Ernzerhof**. “Erratum: Generalized Gradient Approximation Made Simple”. In: *Phys. Rev. Lett.* 78.7 (1997), pp. 1396–1396. DOI: 10.1103/PhysRevLett.78.1396 (cit. on p. 32).
- [PCM70] **R. M. Pick**, **M. H. Cohen**, and **R. M. Martin**. “Microscopic Theory of Force Constants in the Adiabatic Approximation”. In: *Phys. Rev. B* 1.2 (1970), pp. 910–920. DOI: 10.1103/PhysRevB.1.910 (cit. on p. 19).
- [PGG96] **M. Petersilka**, **U. J. Gossmann**, and **E. K. U. Gross**. “Excitation Energies from Time-Dependent Density-Functional Theory”. In: *Phys. Rev. Lett.* 76.8 (1996). DOI: 10.1103/PhysRevLett.76.1212 (cit. on p. 34).

- [PK03] **J. P. Perdew** and **S. Kurth**. “Density Functionals for Non-relativistic Coulomb Systems in the New Century”. In: *A Primer in Density Functional Theory*. Ed. by **C. Fiolhais**, **F. Nogueira**, and **M. Marques**. Berlin Heidelberg New York: Springer, 2003. DOI: 10.1007/3-540-37072-2 (cit. on p. 31).
- [Pla00] **M. Planck**. “Zur Theorie des Gesetzes der Energieverteilung im Normalspectrum”. In: *Verhandlungen der Deutschen physikalischen Gesellschaft* 2.17 (1900), pp. 237–245 (cit. on p. 7).
- [PS01] **J. P. Perdew** and **K. Schmidt**. “Jacob’s ladder of density functional approximations for the exchange-correlation energy”. In: *AIP Conf. Proc.* Ed. by **V. Van Doren et al.** Vol. 577. 2001. DOI: 10.1063/1.1390175 (cit. on p. 32).
- [PW86] **J. P. Perdew** and **Y. Wang**. “Accurate and simple density functional for the electronic exchange energy: Generalized gradient approximation”. In: *Phys. Rev. B* 33.12 (1986), pp. 8800–8802. DOI: 10.1103/PhysRevB.33.8800 (cit. on p. 32).
- [PW89] **J. P. Perdew** and **Y. Wang**. “Erratum: Accurate and simple density functional for the electronic exchange energy: Generalized gradient approximation”. In: *Phys. Rev. B* 40.5 (1989), pp. 3399–3399. DOI: 10.1103/PhysRevB.40.3399 (cit. on p. 32).
- [PW92] **J. P. Perdew** and **Y. Wang**. “Accurate and simple analytic representation of the electron-gas correlation energy”. In: *Phys. Rev. B* 45.23 (1992), pp. 13244–13249. DOI: 10.1103/PhysRevB.45.13244 (cit. on p. 32).
- [PZ81] **J. P. Perdew** and **A. Zunger**. “Self-interaction correction to density-functional approximations for many-electron systems”. In: *Phys. Rev. B* 23.10 (1981), pp. 5048–5079. DOI: 10.1103/PhysRevB.23.5048 (cit. on p. 85).
- [PZD02] **N. Papanikolaou**, **R. Zeller**, and **P. H. Dederichs**. “Conceptual improvements of the KKR method”. In: *J. Phys. C* 14.11 (2002), pp. 2799–2823. DOI: 10.1088/0953-8984/14/11/304 (cit. on p. 49).
- [RG84] **E. Runge** and **E. K. U. Gross**. “Density-Functional Theory for Time-Dependent Systems”. In: *Phys. Rev. Lett.* 52.12 (1984), pp. 997–1000. DOI: 10.1103/PhysRevLett.52.997 (cit. on p. 33).
- [SAN67] **R. Stedman**, **L. Almqvist**, and **G. Nilsson**. “Phonon-Frequency Distributions and Heat Capacities of Aluminum and Lead”. In: *Phys. Rev. Lett.* 162.3 (1967), pp. 549–557. DOI: 10.1103/PhysRev.162.549 (cit. on pp. 86, 87).
- [Sca69] **D. J. Scalapino**. “The Electron-Phonon Interaction and Strong-Coupling Superconductors”. In: *Superconductivity*. Ed. by **R.D. Parks**. New York: Marcel Dekker, Inc., 1969. ISBN: 978-0824715205 (cit. on p. 76).
- [Sch+15] **M. Schackert** et al. “Local Measurement of the Eliashberg Function of Pb Islands: Enhancement of Electron-Phonon Coupling by Quantum Well States”. In: *Phys. Rev. Lett.* 114.4 (2015), p. 047002. DOI: 10.1103/PhysRevLett.114.047002 (cit. on pp. 83, 85).
- [Sch14] **M. P. Schackert**. “Scanning Tunneling Spectroscopy on Electron-Boson Interactions in Superconductors”. Dissertation. Karlsruhe Institut für Technologie, June 2014. URL: <http://nbn-resolving.org/urn:nbn:de:swb:90-416899> (cit. on pp. 83–85, 89).
- [Sha69] **L. J. Sham**. “Electronic Contribution to Lattice Dynamics in Insulating Crystals”. In: *Phys. Rev.* 188.3 (1969), pp. 1431–1439. DOI: 10.1103/PhysRev.188.1431 (cit. on p. 15).

- [Sha74] **L. J. Sham.** *Dynamical Properties of Solids*. Ed. by **G. K. Horton** and **A. A. Maradudin**. North-Holland, 1974. ISBN: 9780720402780 (cit. on p. 15).
- [Sin69] **S. K. Sinha.** “Derivation of the Shell Model of Lattice Dynamics and its Relation to the Theory of the Dielectric Constant”. In: *Phys. Rev.* 177.3 (1969). DOI: 10.1103/PhysRev.177.1256 (cit. on p. 15).
- [Sla53] **J. C. Slater.** “An Augmented Plane Wave Method for the Periodic Potential Problem”. In: *Phys. Rev.* 92.3 (1953). DOI: 10.1103/PhysRev.92.603 (cit. on p. 43).
- [Sól07] **J. Sólyom.** *Fundamentals of the Physics of Solids, Volume 1: Structure and Dynamics*. Springer-Verlag, 2007. ISBN: 978-3-540-72600-5. URL: <http://www.springer.com/materials/book/978-3-540-72599-2> (cit. on p. 12).
- [Sól09] **J. Sólyom.** *Fundamentals of the Physics of Solids, Volume 2: Electronic Properties*. Berlin Heidelberg New York: Springer-Verlag, 2009. ISBN: 978-3-540-85316-9. DOI: <http://www.springer.com/materials/book/978-3-540-85315-2> (cit. on p. 11).
- [Sov67] **P. Soven.** “Coherent-Potential Model of Substitutional Disordered Alloys”. In: *Phys. Rev.* 156 (1967), pp. 809–813. DOI: 10.1103/PhysRev.156.809 (cit. on p. 40).
- [Sri90] **G. P. Srivastava.** *The Physics of Phonons*. Philadelphia and New York: Adam Hilger, 1990. ISBN: 0-85274-153-7 (cit. on pp. 12, 14, 16, 17).
- [SS05] **G. E. Scuseria** and **V. N. Staroverov.** “Progress in the development of exchange-correlation functionals”. In: *Theory and Applications of Computational Chemistry*. Ed. by **C. E. Dykstra** et al. Elsevier, 2005, pp. 669–724. ISBN: 978-0-444-51719-7 (cit. on p. 32).
- [SS06] **M. Shubin** and **T. Sunada.** “Geometric Theory of Lattice Vibrations and Specific Heat”. In: *Pure and Applied Mathematics Quarterly* 2.3 (2006), pp. 745–777 (cit. on p. 7).
- [Ste+67] **R. Stedman** et al. “Dispersion Relations for Phonons in Lead at 80 and 300 °K”. In: *Phys. Rev. Lett.* 162.3 (1967), pp. 545–548. DOI: 10.1103/PhysRev.162.545 (cit. on pp. 85, 86).
- [Ste54] **R. M. Sternheimer.** “Electronic Polarizabilities of Ions from the Hartree-Fock Wave Functions”. In: *Phys. Rev.* 96.4 (1954), p. 951. DOI: 10.1103/PhysRev.96.951 (cit. on p. 19).
- [Str+12] **D. A. Strubbe** et al. “Response Functions in TDDFT”. In: *Fundamentals of Time-Dependent Density Functional Theory*. Ed. by **M. A. L. Marques** et al. Springer, 2012. DOI: 10.1007/978-3-642-23518-4 (cit. on p. 34).
- [SW85] **E. Stenzel** and **H. Winter.** “A real-space method for the evaluation of the dynamic spin susceptibility of paramagnetic metals with application to palladium”. In: *J. Phys. F* 15.7 (1985), pp. 1571–1594. DOI: 10.1088/0305-4608/15/7/016 (cit. on p. 65).
- [SZ80] **M. J. Stott** and **E. Zaremba.** “Linear-response theory within the density-functional formalism: Application to atomic polarizabilities”. In: *Phys. Rev. A* 21.1 (1980), pp. 12–23. DOI: 10.1103/PhysRevA.21.12 (cit. on p. 19).
- [Szu+94] **L. Szunyogh** et al. “Self-consistent localized KKR scheme for surfaces and interfaces”. In: *Phys. Rev. B* 49.4 (1994), pp. 2721–2729. DOI: 10.1103/PhysRevB.49.2721 (cit. on pp. 40, 87).

- [Tay67] **D. W. Taylor.** “Vibrational Properties of Imperfect Crystals with Large Defect Concentrations”. In: *Phys. Rev.* 156 (1967), pp. 1017–1029. DOI: 10.1103/PhysRev.156.1017 (cit. on p. 40).
- [Ter+82] **K. Terakura et al.** “Local and non-local spin susceptibilities of transition metals”. In: *J. Phys. F* 12.8 (1982), pp. 1661–1678. DOI: 10.1088/0305-4608/12/8/012 (cit. on p. 65).
- [TH85] **J. Tersoff and D. R. Hamann.** “Theory of the scanning tunneling microscope”. In: *Phys. Rev. B* 31.2 (1985), pp. 805–813. DOI: 10.1103/PhysRevB.31.805 (cit. on pp. 83, 88).
- [Tha75] **A. Thanailakis.** “Contacts between simple metals and atomically clean silicon”. In: *J. Phys. C* 8.5 (1975), pp. 655–668. DOI: 10.1088/0022-3719/8/5/012 (cit. on p. 84).
- [Tho27] **L. H. Thomas.** “The calculation of atomic fields”. In: *Mathematical Proceedings of the Cambridge Philosophical Society* 23.5 (1927), pp. 542–548. DOI: 10.1017/S0305004100011683 (cit. on p. 29).
- [Van90] **D. Vanderbilt.** “Soft self-consistent pseudopotentials in a generalized eigenvalue formalism”. In: *Phys. Rev. B* 41.11 (1990), pp. 7892–7895. DOI: 10.1103/PhysRevB.41.7892 (cit. on p. 37).
- [Ver+08] **M. J. Verstraete et al.** “Density functional perturbation theory with spin-orbit coupling: Phonon band structure of Lead”. In: *Phys. Rev. B* 78.4 (2008), pp. 45119–45119-9. DOI: 10.1103/PhysRevB.78.045119 (cit. on p. 86).
- [VKS97] **L. Vitos, J. Kollár, and H. L. Skriver.** “Full charge-density scheme with a kinetic-energy correction: Application to ground-state properties of the 4d metals”. In: *Phys. Rev. B* 55.20 (1997), pp. 13521–13527. DOI: 10.1103/PhysRevB.55.13521 (cit. on p. 74).
- [Wie94] **R. Wiesendanger.** *Scanning Probe Microscopy and Spectroscopy: Methods and Applications.* Cambridge University Press, 1994. ISBN: 0-521-41810-0 0-521-41810-0 0-521-41810-0 (cit. on p. 83).
- [Win13] **H. Winter.** *personal communication.* 2013 (cit. on p. 60).
- [Win81] **H. Winter.** “Application of linear response theory to electron-phonon coupling”. In: *J. Phys. F* 11.11 (1981), pp. 2283–2300. DOI: 10.1088/0305-4608/11/11/011 (cit. on p. 89).
- [WM78] **H. Wendel and R. M. Martin.** “Charge Density and Structural Properties of Covalent Semiconductors”. In: *Phys. Rev. Lett.* 40.14 (1978), p. 950. DOI: 10.1103/PhysRevLett.40.950 (cit. on p. 16).
- [WM79] **H. Wendel and R. M. Martin.** “Theory of structural properties of covalent semiconductors”. In: *Phys. Rev. B* 19.10 (1979), p. 5251. DOI: 10.1103/PhysRevB.19.5251 (cit. on p. 16).
- [Zab+05] **J. Zabloudil et al.** *Electron Scattering in Solid Matter.* Berlin Heidelberg New York: Springer, 2005. ISBN: 3-540-22524-2 (cit. on pp. 59, 80).
- [Zec01] **C. Zecha.** “Treatment of structural disorder in crystalline solids and hyperfine fields of light interstitials in ferromagnetic metals”. PhD thesis. Ludwig-Maximilians-Universität München, 2001 (cit. on pp. 51, 73).
- [Zei84] **E. N. Zein.** “Density functional calculations of elastic moduli and phonon spectra of crystals”. In: *Fiz. Tverd. Tela (Leningrad)* 26 (1984), pp. 3028–3034 (cit. on p. 19).

- 
- [Zel+98] **R. Zeller** et al. “Total-energy calculations with the full-potential KKR method”. In: *Phil. Mag. B* 78.5–6 (1998), pp. 417–422. DOI: 10.1080/13642819808206739 (cit. on p. 49).
- [Zel06] **R. Zeller**. “Introduction to Density-Functional Theory”. In: *Computational Condensed Matter Physics*. Ed. by **S. Blügel et al.** Vol. 37. Forschungszentrum Jülich GmbH, 2006, A.1.1–A.1.19. ISBN: 3-89336-430-7 (cit. on p. 32).
- [Zel87] **R. Zeller**. “Multiple-scattering solution of Schrodinger’s equation for potentials of general shape”. In: *J. Phys. C* 20.16 (1987), pp. 2347–2360. DOI: 10.1088/0022-3719/20/16/010 (cit. on pp. 40, 49).
- [Zim92] **J. M. Ziman**. *Prinzipien der Festkörpertheorie*. Verlag Harry Deutsch, 1992. DOI: 10.1002/piuz.19760070213 (cit. on pp. 12, 22, 24, 94).
- [ZS80] **A. Zangwill** and **P. Soven**. “Density-functional approach to local-field effects in finite systems: Photoabsorption in the rare gases”. In: *Phys. Rev. A* 21.5 (1980). DOI: 10.1103/PhysRevA.21.1561 (cit. on pp. 19, 32).



# *Eidesstattliche Versicherung*

Hiermit erkläre ich gemäß §5 Abs. 2b der Promotionsordnung der Naturwissenschaftlichen Fakultät II – Chemie und Physik der Martin-Luther-Universität Halle-Wittenberg vom 13.06.2012, dass ich die vorliegende Arbeit

## LATTICE DYNAMICS FROM FIRST PRINCIPLES

selbstständig und ohne fremde Hilfe verfasst, keine anderen als die von mir angegebenen Quellen und Hilfsmittel benutzt und die den verwendeten Werken wörtlich oder inhaltlich entnommenen Stellen als solche kenntlich gemacht habe. Ich erkläre, die Angaben wahrheitsgemäß gemacht und keine Dissertation zur Erlangung eines akademischen Grades an einer anderen wissenschaftlichen Einrichtung eingereicht zu haben.

Halle (Saale), 6. Mai 2015



# *Danksagung*

An dieser Stelle möchte ich allen Kollegen, Mitstreitern, Freunden und lieben Menschen, die zur Fertigstellung dieser Arbeit beigetragen haben, danken.

Ich danke Dr. Arthur Ernst für die herzliche Aufnahme in seiner kleinen Gruppe am Institut und für die Anregung dieses Projekts. Die nicht nur wissenschaftlichen Diskussionen mit ihm bei unzähligen Tassen Tee sorgten immer wieder für Inspiration und ohne sein Talent, Programmierfehler zu finden, wäre diese Arbeit zum Scheitern verurteilt gewesen.

Weiterhin bin ich Dr. Hermann Winter zu tiefem Dank verpflichtet. Seine bereits langjährige Beschäftigung mit dem Thema und sein tiefes Verständnis der KKR, aus welchem ich bei zahlreichen Gastaufenthalten schöpfen konnte, waren für mich von unschätzbarem Wert. Seine Leidenschaft für das Klavier hat mich zuletzt sogar musikalisch beim Schreiben der Arbeit unterstützt.

Dr. Pawel Buczek danke ich für seine Hilfe bei der Einfindung in die Wirren des KKR-Formalismus und für seine ehrgeizige Beschäftigung mit meinen Fragen. Sein Talent, komplexe Probleme schnell zu erfassen sowie seine mathematischen Fähigkeiten waren eine große Hilfe und haben mich, zum Glück, oftmals zur Sorgfalt ermahnt. Das gleiche gilt für seine konstruktive Kritik am Manuskript dieser Arbeit.

Ich möchte Prof. Dr. Ingrid Mertig dafür danken, dass sie mein Interesse an der theoretischen Physik geweckt hat und es mir ermöglichte, meine Diplomarbeit in ihrer Arbeitsgruppe anzufertigen. Ich danke allen aktuellen und ehemaligen Mitgliedern dieser Gruppe für die freundliche Aufnahme und die stets offenen Türen auch nach meiner Diplomzeit, darunter Dr. Steven Achilles, Dr. Stephan Borek, Dr. Peter Bose, Dr. Michael Fechner, Markus Flieger und Dr. Peter Zahn. Mein besonderer Dank gilt dem feinen Geist Dr. Nicki Hinsche für philosophische Diskussionen, fotografische Eskapaden auf den Spuren von Henri Cartier-Bresson und Eric Hosking, sowie seiner Fähigkeit für neue und alte Themen zu begeistern.

Ich danke meinen Bürogenossen Dr. Danny Thonig, Martin Hoffmann und Dr. Guntram Fischer für deren Hilfsbereitschaft und die angenehme Atmosphäre, in der immer Raum für konzentriertes Arbeiten und erholsame Ablenkung war.

Weiterhin bin ich Udo Schmidt für seine stete Hilfsbereitschaft bei meinen nicht funktionierenden Rechnungen zu Dank verpflichtet, wie auch Ina Goffin, die mit ihrer angenehm entspannten Art die Theorie-Abteilung des Instituts in einem dynamischen Gleichgewicht zu halten vermag.

Nicht zuletzt möchte ich meiner Familie danken, die mich auf meinem Bildungsweg immer unterstützt hat sowie Freunden, die trotz großer räumlicher Distanzen stets zu mir gehalten haben.

Mein finaler Dank gilt meiner wunderbaren Frau Jana, die mir in all den Jahren immer mit ihrem Scharfsinn, ihrer tiefen Menschenkenntnis, ihrem Gespür für die wichtigen Dinge des Lebens und ihrer Liebe beigestanden hat, obwohl die Zeit des Schreibens teilweise eine sehr nervenaufreibende war.

Danke!



# *Curriculum vitae*

## Personal information

Name	Martin Hölzer
Address	Puschkinstr. 18, 06108 Halle (Saale), Germany
Date and place of birth	7th September 1984, Halle (Saale)
Academical Grade	Diplom-Physiker

## Education

since 3/2010	PhD studies at Martin-Luther Universität Halle-Wittenberg and Max-Planck-Institut für Mikrostrukturphysik, Halle (Saale)
10/2004–2/2010	Studies of physics at Martin-Luther Universität Halle-Wittenberg, Halle (Saale). Diploma thesis "Magneto-electric coupling at multiferroic interfaces", supervised by Dr. Michael Fechner
9/1995–7/2004	Grammar school "Gymnasium Landsberg"
9/1991-7/1995	Elementary school "Bergschule Landsberg"

## Academic career

since 3/2010	Research assistant at Max-Planck-Institut für Mikrostrukturphysik, Halle (Saale), group of Dr. habil. Arthur Ernst
10/2008–2/2010	Student assistant at Martin-Luther Universität Halle-Wittenberg, Halle (Saale), research group 'Quantum Theory of the Solid State' under Prof. Dr. Ingrid Mertig

## List of Publications

**M. Hölzer, M. Fechner, S. Ostanin, I. Mertig**, *Effect of interfacial Cr on magnetoelectricity of  $Fe_2/CrO_2/BaTiO_3(001)$* , Phys. Rev. B 81.8 (2010), p. 214428, DOI:10.1103/PhysRevB.81.214428

**M. Hölzer, M. Fechner, S. Ostanin, I. Mertig**, *Ab initio study of magnetoelectricity in  $Fe/BaTiO_3$ : the effects of n-doped perovskite interfaces*, Journal of Physics: Condensed Matter 23.45 (2011), p. 455902, DOI:10.1088/0953-8984/23/45/455902

**A. Höfer, M. Fechner, K. Duncker, M. Hölzer, I. Mertig, and W. Widdra**, *Persistence of Surface Domain Structures for a Bulk Ferroelectric above  $T_C$* , Phys. Rev. Lett. 108.8 (2012), p. 087602, DOI:10.1103/PhysRevLett.108.087602

**M. Schackert, T. Märkl, J. Jandke, M. Hölzer, S. Ostanin, E. K. U. Gross, and W. Wulfhekel**, *Local Measurement of the Eliashberg Function of Pb Islands: Enhancement of Electron-Phonon Coupling by Quantum Well States*, Phys. Rev. Lett. 114.4 (2015), p. 047002, DOI:10.1103/PhysRevLett.114.047002

**N. Hinsche, M. Hölzer, A. Ernst, I. Mertig, P. Zahn**, *Ab Initio Description of Transport Properties Based on the Boltzmann Transport Theory*, in: 'Thermoelectric  $Bi_2Te_3$  Nanomaterials'. Ed. by O. Eibl, K. Nielsch, N. Peranio and F. Völklein. Wiley 2015, ISBN: 978-3-527-33489-6